



Norwegian University of Life Sciences
Faculty of Science and Technology

Philosophiae Doctor (PhD)
Thesis 2019:83

Flux Enhancers in Biofilm Membrane Bioreactors: Insight into Fouling Control

Kjemikaler for fluksforbedringer i biofilm
membran bioreaktorer: Innsikt i kontroll
av gjentetting av membraner

Olga Kulesha

Flux Enhancers in Biofilm Membrane Bioreactors: Insight into Fouling Control

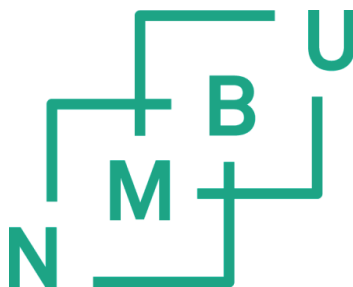
Kjemikaler for fluksforbedringer i biofilm membran bioreaktorer:
Innsikt i kontroll av gjentetting av membraner

Philosophiae Doctor (PhD) Thesis

Olga Kulesha

Norwegian University of Life Sciences
Faculty of Science and Technology

Ås (2019)



Supervisory team

Harsha Ratnaweera (the main supervisor)

Professor, Faculty of Science and Technology (REALTEK),
Norwegian University of Life Sciences (NMBU)

Arve Heistad (co-supervisor)

Professor, Faculty of Science and Technology (REALTEK),
Norwegian University of Life Sciences (NMBU)

Zakhar Maletskyi (co-supervisor)

Postdoctoral Fellow, Faculty of Science and Technology (REALTEK),
Norwegian University of Life Sciences (NMBU)

© Olga Kulesha, 2019

All rights reserved. No part of this publication may be reproduced or transmitted, in any form or by any means, without permission.

Abstract

Conventional wastewater treatment technologies are not able to keep up with the population growth and new challenges and restrictions, induced by climate change. Membrane bioreactor (MBR) technology has a high potential to become a solution of choice when implementing the concepts of minimal/zero liquid discharge and 100% recycling. However, membrane fouling highly inhibits the expansion of MBR technology.

Among the variety of methods to fouling mitigation, the integration of the biofilm membrane bioreactor technology (BF-MBR), which is the advancement of the MBR, with the coagulation approach into a concept of flux enhancement has been showing high potential. Due to the complexity of the fouling phenomenon and underlying mechanisms of its mitigation, process control in coagulant-assisted BF-MBR remains a major gap in its investigation. The development of the universal strategy for real-time fouling control and prediction in coagulant-assisted BF-MBR requires the comprehension of the membrane fouling patterns, determination of the underlying mechanisms of coagulant action, and system optimisation.

According to the analysis of the latest studies, performed in **Paper I**, membrane fouling phenomenon is primarily caused by floc-bound extracellular polymeric substances (EPSs) and soluble microbial products (SMPs), whose accumulation causes pore blockage and cake and gel layer formation, resulting in reversible, irreversible and irrecoverable fouling. Polysaccharides of the SMPs were identified as the primary foulants in MBR. Among the most efficient approaches to flux enhancement, the use of coagulants was recognized as one of the most promising directions. The outlined mechanisms of fouling mitigation during chemical flux enhancement in MBR became the instrument of “navigation” in the development of an advanced fouling mitigation strategy with regard to BF-MBR at the further stages of the present research.

Paper II was focused on the identification of membrane fouling patterns in the BF-MBR. During 114 days of system performance, a large representative, with regard to the application of the variety of operational conditions in BF-MBR, data array was analysed. One of the main contributions of this work was the development of the multivariate chemometric approach to fouling monitoring and control in BF-MBR based on the interrelation between the characteristics of the mixed liquor fouling propensity, membrane fouling indicators, and operational conditions. The introduction of the term “critical solids retention time” (SRT) allowed for determining SRT operational window with regard to the absence of severe

fouling, which was less than 31 days for the investigated BF-MBR. The automated monitoring of the MLSS concentration in the moving bed biofilm (MBBR) and the separation chambers was implemented. The developed partial least squares (PLS) models were used to adjust the operational conditions (SRT, permeate flux, and sludge recirculation intensity) according to the characteristic of mixed liquor, which enabled the system to work below the critical fouling levels.

In **Paper III**, the comparative analysis of the prepolymerized and non-prepolymerized coagulants with regard to flux enhancement in BF-MBR revealed that the extent of chemical flux enhancement via floc-bound EPSs removal highly correlated with the intrinsic charge concentration of the coagulants and their basicity. pH correction was shown to have a tremendous influence on fouling mitigating performance of every coagulant. The operational settings in the pilot system, which was the source of mixed liquor, were kept at the optimum levels, determined in **Paper II**. **Paper III** addresses one of the main concepts of the thesis, i.e., the development of the core model for the soft sensor for fouling control and prediction based on the electrostatic mechanism of the floc-bound EPSs removal during coagulation. The optimisation analysis applying the most effective coagulant revealed the significance of mixed liquor suspended solids (MLSS), coagulant dose, temperature, pH, and the interaction factors in the filtration processes. The derived optimisation models allow for minimising the adverse effects of low temperatures on the membrane filtration process by adjusting the operational conditions in BF-MBR.

Paper III allowed for the determination of the most efficient coagulant with respect to flux enhancement and the optimum pH of its performance in BF-MBR. Based on these findings and according to the literature analysis, conducted in **Paper IV**, the active hydrolysis species of the optimum coagulant (i.e., Al_{13}^{2+} complex of the prepolymerized aluminium chloride with medium basicity) and the dominant carbohydrates in the structure of SMPs in MBR and BF-MBR systems were identified. By applying the quantum chemical and thermodynamic calculations, and multivariate chemometric analysis, the other main concept of the thesis was addressed, i.e., the deriving of the core model for the soft sensor for membrane fouling estimation and prediction based on the chemical coordination of the carbohydrates of SMPs to the Al_{13}^{2+} complex. In **Paper IV**, a two-stage supervised classifier was developed based on data mining and cluster analysis of the PLS Y-scores. The results of this study served as a basis for developing an unsupervised hierarchical classifier for online monitoring of the reduction of the mixed liquor fouling propensity during coagulation in BF-MBR based on the thermodynamic parameters of the system.

Sammendrag

Konvensjonelle teknologier for rensing av avløpsvann klarer ikke å følge med befolkningsveksten og nye utfordringer og restriksjoner, drevet frem av klimaendringer. Membran-bioreaktor (MBR) - teknologi har et stort potensial til å bli den foretrukne løsningen når man skal oppnå minimale/null utslipp av avløpsvann og 100% resirkulering. Gjentetting av membraner hindrer imidlertid utbredelsen av MBR-teknologien.

Kombinasjonen av biofilm-membran-bioreaktor (BF-MBR) – teknologi, som er en videreutvikling av MBR, og koagulering i et konsept for fluksforbedring har vist et stort potensial blant de mange metodene for å begrense gjentetting av membraner. På grunn av kompleksiteten i gjentettingssfenomenet og de underliggende mekanismene for å forebygge gjentetting, utgjør prosesskontroll i koagulant-assistert BF-MBR fortsatt et kunnskapshull. Utvikling av en universell strategi for sanntids kontroll og prediksjon av gjentetting i koagulant-assistert BF-MBR krever forståelse av gjentettingsmønstre, klarlegging av de underliggende mekanismene for koagulantenes virkning samt systemoptimalisering.

I følge en gjennomgang av de nyeste studiene, gjennomført i **Artikkel I**, er membrangjentettingsfenomenet primært forårsaket av fnokkbundne ekstracellulære polymere stoffer (EPS) og løselige mikrobielle produkter (SMP), hvis akkumulering forårsaker blokkering av porene og dannelse av slamkake og gel, noe som resulterer i reversibel, irreversibel og uopprettelig gjentetting. Polysakkarider av SMPene ble identifisert som de viktigste stoffene som bidrar til gjentetting i MBR. Blant de mest effektive tilnærmingene til fluksforbedring ble bruken av koagulanter anerkjent som en av de mest lovende retningene. De skisserte mekanismene for forebygging av membrangjentetting ved kjemisk fluksforbedring i MBR utgjorde veikartet for de videre stadier av denne avhandlingen i utviklingen av en avansert strategi for forebygging av gjentetting ved BF-MBR.

Artikkel II fokuserte på identifisering av gjentettingsmønstre for membraner ved BF-MBR. Med 114 dagers driftstid ble en stor representativ datasamling – med hensyn til forskjellige driftsforhold i BF-MBR – analysert. Et av hovedbidragene i dette arbeidet var utviklingen av en multivariat kjemometrisk tilnærming til overvåkning og kontroll av membrangjentetting i BF-MBR, basert på sammenhengen mellom egenskapene til slamsuspensjonen og dens gjentettingspotensiale, gjentettingsindikatorer for membranen samt driftsforhold. Innføringen av begrepet "kritisk slamalder" (SRT) tillot å bestemme et driftsvindu for SRT med hensyn til fravær av alvorlig gjentetting, som var mindre enn 31 dager for den undersøkte BF-MBR. Automatisert overvåkning av slam-konsentrasjonen i

"moving bed" bioreaktoren (MBBR) – og separasjonskamrene ble implementert. De utviklede PLS-modellene (PLS er delvis minste kvadraters metode) ble brukt til å justere driftsforholdene (SRT, permeatfluks og slamresirkuleringsintensitet) i henhold til egenskapene til slamsuspensjonen, noe som gjorde det mulig for systemet å holde seg under kritiske nivåer for gjentetting.

I **Artikkel III** avdekket en sammenlignende analyse av de prepolymeriserte og ikke-prepolymeriserte koagulantene med hensyn til fluksforbedring i BF-MBR at graden av kjemisk fluksforbedring via fjerning av fnokkbundet EPS korrelerte sterkt med ladningskonsentrasjonen til koagulantene og deres basisitet. Korrigering av pH viste seg å ha en enorm innflytelse på evnen til å forebygge gjentetting for hver koagulant. Driftsinnstillingene for pilotsystemet som var kilden til slamsuspensjonen, ble holdt på optimale nivåer bestemt i **Artikkel II**. **Artikkel III** tar for seg en av hovedideene i avhandlingen, nemlig utviklingen av selve modellen for en virtuell sensor for kontroll og prediksjon av gjentetting basert på den elektrostatiske mekanismen for fjerning av EPS-fnokker ved koagulering. En optimaliseringsanalyse der den mest effektive koagulant ble brukt, avslørte betydningen av slamkonsentrasjon (MLSS), koagulantdose, temperatur, pH og samvirkingseffekter i filtreringsprosessene. De avledede optimaliseringsmodellene gjør det mulig å minimere ugunstige effekter av lave temperaturer på membranfiltreringsprosessen ved å justere driftsforholdene i BF-MBR.

I **Artikkel III** ble den mest effektive koagulant identifisert med hensyn til fluksforbedring og dens optimale pH i BF-MBR. Basert på disse funnene og i henhold til litteraturgjennomgangen utført i **Artikkel IV**, ble den aktive hydrolyserte formen av den optimale koagulant (dvs. Al_{13}^{2+} -komplekset av prepolymerisert aluminiumklorid med middels basisitet) og de dominerende karbohydratene i strukturen til SMP-er i MBR- og BF-MBR-systemer identifisert. Ved å anvende kvantekjemiske og termodynamiske beregninger og den multivariate kjemometriske analysen, ble den andre hovedideen i avhandlingen behandlet, det vil si utviklingen av selve modellen for den virtuelle sensoren for estimering og prediksjon av membrangjentetting basert på den kjemiske koordineringen av karbohydrater i SMP til Al_{13}^{2+} -komplekset. I **Artikkel IV** ble en to-trinns overvåket klassifikator utviklet basert på data mining og clusteranalyse av PLS Y-scoreverdier. Resultatene fra denne studien utgjorde et grunnlag for å utvikle en ikke-overvåket hierarkisk klassifikator for online overvåking av reduksjonen i gjentettingspotensialet til slamsuspensjonen ved koagulering i BF-MBR basert på de termodynamiske parametrene til systemet.

To the memory of my grandparents, Olga and Gregory

Acknowledgements

*Men se, Gud er min hjelper,
det er Herren
som holder meg oppe.*

(Salme 54:6)

There are a lot of people who deserve acknowledgments and my gratitude. First and foremost I would like to express my deepest gratitude to my main supervisor Professor Harsha Ratnaweera for giving me the opportunity to become a member of the Water, Environment, Sanitation and Health (WESH) team, his guidance throughout my entire research, funding acquisition, and his kind assistance in all administrative matters. Thank you, Harsha, for the insightful discussions with regard to my research, helpful advice, and sharing of your colossal scientific knowledge and experience with me.

I am deeply grateful to Professor Knut Kvaal for the great help in comprehension of the multivariate statistics and image analysis, fruitful discussions, and immense support and encouragement in the pursuit of my scientific ideas.

I would like to thank Doctor Zakhar Maletskyi for his guidance on the subject of membrane filtration and fouling, unique scientific ideas, help in conceiving and designing the experiments, and project administration activities.

Special thanks to Professor Arve Heistad for his support and confidence in my work.

I am appreciative of being a PhD candidate at the Faculty of Science and Technology at the Norwegian University of Life Sciences (NMBU). NMBU provided me with the ideal working environment, where I enjoyed studying and working; and funds to publish the results of my research in the peer-reviewed open access journals, buy scientific literature, participate in the international conferences, and use the required software packages and equipment.

I appreciate the financial support from Norwegian State Educational Loan Fund, Lånekassen, which made it possible for me to stay in this amazing country, and the help of Vilma Veronica Bischof during the preparation of the necessary documentation in this regard.

I also want to thank Doctor Daniel Todt from Ecomotive AS for facilitating pilot plant studies and insightful comments during the discussions on the pilot system performance.

I was lucky to have the chance to work with Doctor Xiaodong Wang, Doctor Vegard Nilsen, Doctor Nataliia Sivchenko, Doctor Melesse Moges, Doctor Fasil Eregno, Duo Zhang, Marta Litynska, Abhilash Nair, and Sven Andreas Högfeldt. Thank you, guys, for helping me every time I needed it. Dinindu Ratnaweera, thank you for arranging PhD social clubs with

the cosy atmosphere, board games, and quizzes. I want to thank Elisabeth Hoff for her efforts during the organisation of the trip to IFAT 2018 in Munich. Vegard Nilsen and Aleksander Hykkerud, thank you for arranging the WESH meetings. Vegard, I appreciate your help every time I asked to review my Norwegian.

I owe my heartfelt gratitude to my alma mater, National Technical University of Ukraine “Igor Sikorsky Kyiv Polytechnic Institute” for giving me the required knowledge on physical and formal sciences, ecology, engineering, and water and wastewater treatment, used during the presented research.

I am deeply thankful to my fiancée, Martinius, and my mom, Tetiana, for their love, support, endless patience, and believing in me.

Ås, September, 2019

Olga Kulesha

Table of Contents

Abstract.....	iii
Sammendrag	v
Acknowledgements.....	ix
Table of Contents.....	xi
List of Figures.....	xiii
List of Tables.....	xv
List of Acronyms	xvi
List of Publications	xix
1. Introduction.....	1
2. Objectives and Scopes of the Study, Thesis Structure.....	5
2.1 Objective of this research.....	5
2.2 Structure of the research and thesis.....	6
3. Methods and materials	7
3.1 Study objects.....	7
3.2 Jar tests.....	8
3.3 Membrane filtration experiments.....	8
3.3.1 BF-MBR pilot system.....	9
3.3.2 Total recycle test in the laboratory MBR system.....	10
3.4 Applied analytical techniques.....	11
3.4.1 Mixed liquor analysis.....	11
3.4.2 Methods for determination of the intrinsic characteristics of the coagulants.....	11
3.5 Statistical mining of the investigated relationships.....	14
3.5.1 Multivariate statistics.....	14
3.5.2 Cluster analysis.....	19
3.5.3 Two-level fractional factorial design of the experiment.....	20
3.6 Image acquisition, analysis, and particle size distribution.....	21

3.7 Quantum chemical and thermodynamic calculations.....	23
4. Results and discussion	25
4.1 State of the art of membrane flux enhancement in a membrane bioreactor: Paper I.....	25
4.2 Identification of membrane fouling patterns in Biofilm Ceramic Membrane Bioreactor applying multivariate chemometric analysis: Paper II.....	32
Discussion.....	41
4.3 The concept of the chemical flux enhancement based on the comparative mechanistic assessment of the Al- and Fe-based coagulants, multivariate chemometric approach, and optimisation analysis: Paper III.....	42
Discussion.....	58
4.4 Development of the model for continuous classification of thermodynamically stable and less stable complexes after coagulant dosing in BF-MBR: Paper IV.....	62
Discussion.....	72
5. Conclusions and Outlook	76
References.....	80
Appendix A.....	91
Synopsis of the appended papers	93
Appendix B.....	97

List of Figures

Figure 2.1 The structure of the doctoral thesis.....	6
Figure 3.1 The BF-MBR pilot plant: Schematic diagram and the photo of installation.....	9
Figure 3.2 The total recycle test system.....	10
Figure 3.3 The form of the curve typical for the streaming current titration, using strong poly-base as the titrant and strong poly-acid as the titrated solution.....	12
Figure 3.4 The principle of the dimension reduction into principal components, scores, and loadings.....	14
Figure 3.5 The idea behind the PLS technique.....	17
Figure 3.6 Determination of the particle size by image processing and analysis.....	22
Figure 3.7 Cumulative distribution plot of the sizes of suspended solids in the analysed mixed liquor sample.....	22
Figure 4.1. The role of the different SMP fractions in membrane fouling.....	27
Figure 4.2 The formation of organic/inorganic solid complexes by the interaction of aluminium coagulants; iron (III) coagulants with the amino acid residues of the bound EPSs.....	30
Figure 4.3 Results of PLS of the data from the period A of the filtration performance monitoring..	34
Figure 4.4 Results of PLS of the data from the period B of the filtration performance monitoring..	36
Figure 4.5 Results of PLS of the data from the period C of the filtration performance monitoring..	37
Figure 4.6 Prediction results for the new data from Period C for four factors using the derived PLS model for the relevant period.....	38
Figure 4.7. Results of PLSs of the data from all the periods of the filtration performance monitoring, including SRT.....	39
Figure 4.8 The correlation curves between the MLSS values in the MBBR chamber obtained through the sensor and experimentally determined MLSS values in the MBBR chamber and separation chamber.....	41
Figure 4.9 A negative correlation between capillary suction time and relative hydrophobicity earlier obtained for BF-MBR mixed liquor.....	43
Figure 4.10 The stepwise strategy for the assessment of the selected flux enhancers.....	44
Figure 4.11 Determination of the optimum pH with regard to flux enhancement at fixed coagulant dose during the jar tests.....	45
Figure 4.12 Influence of the coagulant dose on the monitored parameters at fixed pH during the TRT.....	46
Figure 4.13. Relationship between the coagulant dose and the filtration performance at fixed pH during the TRT.....	48

Figure 4.14. Influence of the coagulant dose on the monitored parameters at fixed pH during the TRT.....	50
Figure 4.15 The results of the potentiometric titration experiments.....	51
Figure 4.16 Results of PLS of the data from the TRT - regression overview.....	52
Figure 4.17 Results of PLS for the tested membrane flux enhancers – scores plot with the sample grouping according to the monitored parameters.....	54
Figure 4.18 Model graphs (cube plots) of the analysed factorial designs ($k=3$, $D=1.5 \mu\text{molAl/mgSS}$).....	57
Figure 4.19 The applied concentrations of non-prepolymerized Fe and Al coagulants during TRT (regions, coloured in red) at the angle of the equilibrium-solubility domains.....	59
Figure 4.20 Molecular structure of β -D-glucopyranose with the numerated carbon atoms (based on their position in the structure), mapped onto an isosurface of total electron density of 0.13 e/a_0^3 ...	63
Figure 4.21 Molecular structure of the Al_{13}^{2+} complex.....	64
Figure 4.22 The development of the Gibbs energy change of formation of Al_{13} -monosaccharide complex depending on the active centres of the solvated Al_{13}^{2+} complex and monosaccharide for the double-O-ligand coordination of the selected monosaccharides.....	66
Figure 4.23 Results of the partial least squares analysis (PLS) using the results as the quantum chemical and thermodynamic calculations.....	69
Figure 4.24 Dendrogram plot acquired during the cluster analysis based on the scores of PLS.....	71
Figure 4.25 Flowchart of the development of a classification model for the continuous online discrimination of the thermodynamically stable and less stable species as a result of the chemical flux enhancement in BF-MBR.....	73

List of Tables

Table 3.1 Properties of the tested flux enhancers.....	7
Table 4.1 Types of membrane pore blocking in terms of Hermia's pore blocking models, characteristic pore-blocking patterns for the typical foulants, and the corresponding fouling types in membrane systems, MBR, and BF-MBR.....	28
Table 4.2 Intrinsic mechanisms of coagulant action with regard to membrane flux enhancement in MBR.....	31
Table 4.3 Parameters of mixed liquor in the separation chamber.....	33
Table 4.4 Model inputs.....	33
Table 4.5 Mixed liquor characteristics and fouling indicators during period C (new data).....	38
Table 4.6 Optimum dosages with respect to flux enhancement obtained at the corrected pH values applying tested coagulants during the jar tests.....	46
Table 4.7 Prevailing mechanisms of action for the tested coagulants.....	51
Table 4.8 Factors and levels for two-level alternative factorial design.....	55
Table 4.9 Layout for a designed experiment.....	56
Table 4.10 The final equations in terms of coded and actual factors used for the optimization of the selected response functions.....	56

List of Acronyms

MBR	membrane bioreactor technology
USD	United States Dollar
SMPs	soluble microbial products
EPSs	extracellular polymeric substances
BF-MBR	biofilm membrane bioreactor
MBBR	moving bed biofilm reactor
PACl	prepolymerized aluminium chloride
Me-based	metal-based
Al-based	aluminium-based
SMP _c	the carbohydrate fraction of soluble microbial products
PLC	programmable logic controller
COD _{dis}	chemical oxygen demand of dissolved organics
SRT	solids retention time
MLSS, SS	mixed liquor suspended solids
PO ₄ -P	orthophosphates
RAS	return activated sludge
SiC	silicon carbide
TMP	transmembrane pressure
LMH	liter/(m ² ·hour)
ML	mixed liquor
TMP _{in}	initial transmembrane pressure (TMP at the beginning of filtration)
CST	capillary suction time
TTF	Time-to-Filter
DSVI	diluted sludge volume index
ζ-potential	electrokinetic potential
MATH	microbial adherence to hydrocarbons method
MGC	methyl glycol chitosan

PVSK	potassium polyvinyl sulphate
F_{pH}	correction factor for the calculation of charge concentration
SEC	size exclusion chromatography
PCA	principal component analysis
PCR	principal component regression
PLS	projection to latent structures (also known as partial least squares method)
PC1/PC2	first/second principal component
$_{av}P_n, _{av}P_N$	average normalized permeability
$_{av}P_n/dt, _{av}P_N/dt,$	average normalized permeability slope
ANOVA	analysis of variance
TL–BF	transmitted light–bright field contrast technique
D10/D50/D90	the diameters where 10%/50%/90% of the sample’s population lie below this value
D[4,3]	volume/mass moment mean (the De Brouckere mean diameter)
D[3,2]	surface area moment mean (the Sauter mean diameter)
$\Delta H^\circ_f/S^\circ_f/\Delta G^\circ_f$	standard enthalpy change/standard entropy/standard Gibbs energy change of the formation of the individual reactants and the relevant complexes
PM3	Parameterized Model number 3
NDDO	neglect of diatomic differential overlap
$\Delta H^\circ/\Delta S^\circ/\Delta G^\circ$	standard enthalpy change/standard entropy change/standard Gibbs energy change of the investigated process (formation of Al ₁₃ -monosaccharide complex)
PVDF	polyvinylidene fluoride
SMP _p	protein fraction of soluble microbial products
CEB	chemically enhanced backwash
CIP	cleaning in place
CIA	cleaning in air
WWTP	wastewater treatment plant
Fe-based	iron-based
PFS	prepolymerized ferric sulphate
RH	relative hydrophobicity
$(dMLSS/dt)/(dDSVI/dt)/$ $(dRH/dt)/(dCOD_{dis}/dt)$	slope of mixed liquor suspended solids/diluted sludge volume index/relative hydrophobicity/chemical oxygen demand of dissolved organics

SDev	standardization based on the standard deviation
RMSEV	the Root Mean Square Error of Cross-Validation
SECV	the standard error of cross-validation
MLR	multiple linear regression
F	filtration time
MW	molecular weight
TRT	total recycle test
T	temperature
D	coagulant dose
Glc	glucopyranose
Gal	galactopyranose
Man	mannopyranose
GlcUA	glucopyranuronic acid
Rha	rhamnopyranose
Fuc	fucopyranose
Ara	arabinofuranose
GlcN	glucosamine
a_0	the first Bohr radius
e	electron charge
ANN	artificial neural network
CPV	cumulative percent variance

List of Publications

The present thesis is based on the following appended papers, which will be referred to by their Roman numerals throughout the text. All the papers are reproduced according to the Creative Commons Attribution License (CC BY 4.0).

Paper I

Kulesha, O.; Maletskyi, Z.; Ratnaweera, H. State-of-the-art of membrane flux enhancement in membrane bioreactor. *Cogent Eng.* **2018**, *5*, 1–30; DOI:10.1080/23311916.2018.1489700.

Paper II

Kulesha, O.; Maletskyi, Z.; Ratnaweera, H. Multivariate Chemometric Analysis of Membrane Fouling Patterns in Biofilm Ceramic Membrane Bioreactor. *Water* **2018**, *10*, 982, 1–23; DOI:10.3390/w10080982.

Paper III

Kulesha, O.; Maletskyi, Z.; Kvaal, K.; Ratnaweera, H. Strategy for Flux Enhancement in Biofilm Ceramic Membrane Bioreactor Applying Prepolymerized and Non - Prepolymerized Inorganic Coagulants. *Water* **2019**, *11*, 446, 1–42; DOI:10.3390/w11030446.

Paper IV

Kulesha, O.; Ratnaweera, H. C. Computational Thermodynamic Analysis of the Interaction between Coagulants and Monosaccharides as a Tool to Quantify the Fouling Potential Reduction in the Biofilm Membrane Bioreactor. *Water* **2019**, *11*, 1275, 1–30; DOI:10.3390/w11061275.

1. Introduction

Nowadays water scarcity is no longer the probability but the reality for many regions in the world. Climate change with its detrimental environmental and economic consequences, along with demographic growth and economic development, is putting tremendous pressure on water resources. And by 2050, demand for water is expected to increase approximately by one-third [1–3]. In 2018, more than 2 billion people had limited access to safe drinking water and more than 4 billion people lacked access to safe sanitation [2]. According to the estimations, by 2050, at least 25% of the entire world population is likely to live in the area, affected by chronic or recurring shortages of fresh water [4].

Therefore, a substantial increase in water recycling and safe water reuse on a global scale by 2030 are among the main targets of the sustainable development goal 6, set by the United Nations [2,5]. As emphasized by the European Commission [6], wastewater treatment and reuse remain among the top priority areas in the strategic plans for sustainable water management. Besides, more attention is being paid to the concepts of minimal/zero liquid discharge and 100% recycling of wastewater as a new priority [7–10].

In light of increasing demand for water recycle and reuse and strengthening requirements for reclaimed water quality, a fast-emerging membrane bioreactor technology (MBR) is gaining momentum worldwide. MBR is a highly competitive technique when applied in water reuse systems. The expected growth of the MBR market is estimated to be around USD 8.27 billion by 2025 [11,12]. The main advantages of MBR, which contributed to its expansion are: compactness, complete retention of suspended solids, the absence of secondary clarifier, small footprint, consistency of the permeate quality independently of the fluctuations in the feed water characteristics, modular design with a potential for future expansion of the system, and disinfection capability with regard to retention of pathogenic bacteria [13–18].

Further expansion of MBR technology is, however, hampered due to the occurrence of unplanned high operating costs, decrease of system performance (permeate yield), compromising of the system operability, the use of the environmentally harmful aggressive compounds for chemical cleanings and the possible generation of the relevant by-products, and disturbance of the remote monitoring and control [19–22]. Membrane fouling poses to be the most serious challenge in this context. Membrane fouling is attributed to the deposition of such biopolymers of mixed liquor as soluble microbial products (SMPs) and extracellular polymeric substances (EPSs) on the membrane surface and its pores [20,23].

One of the potential ways to mitigate fouling is to modify the MBR design, which was achieved by introducing the moving bed biofilm process prior to membrane filtration. The developed system, called biofilm membrane bioreactor (BF-MBR), is an advanced innovation in the evolution of MBR technology. BF-MBR is characterised by reduced membrane fouling and the ability to work at higher operational fluxes [24,25]. Since the biomass on the suspended carriers in the moving bed biofilm (MBBR) part is primarily responsible for the biodegradation, much lower concentrations of the mixed liquor suspended solids are required in the membrane separation chamber. This feature brings such positive outcomes as the reduction of the mixed liquor fouling propensity and lower excess sludge production [19,26]. Meanwhile, the tendency of BF-MBR system to floc breakage, which is induced by the biofilm carriers and intense aeration, entails a higher content of submicron particles and SMPs in mixed liquor, responsible for more severe membrane fouling [19,27,28].

Therefore, membrane fouling remains a critical issue for BF-MBR, as is the case in MBR systems.

The absence of universal procedure/standard protocol for fouling monitoring in MBR and BF-MBR is among the main gaps in the investigation of these systems. Thus, the membrane fouling patterns are still being poorly investigated, especially in the case of the recently developed BF-MBR technology. In addition, according to Meng et al. [29], a more detailed study on the foulants is required to provide new insight into the membrane fouling issues and to illuminate the “black box”.

A different way to mitigate fouling is to combine BF-MBR with another approach to fouling alleviation, the modification of the mixed liquor characteristics by adding chemical flux enhancers, specifically the coagulants, which were proven to be highly effective with respect to fouling mitigation in MBR and BF-MBR systems [30–32]. Since the attached growth part is decoupled from the MBR chamber and there is a minimum demand on biomass recirculation in the BF-MBR system [31,33], the application of BF-MBR allows for using the chemical flux enhancement with no concern about reducing the potential of active microbial communities to biodegradation of the organic material.

Despite the advantages of prepolymerized aluminium coagulants, there is a controversy in the literature over their superior performance with regard to flux enhancement in MBR and BF-MBR systems in comparison to the non-prepolymerized coagulants. Better performance of the prepolymerized aluminium chloride (PACl) with respect to membrane flux enhancement was observed by different studies [32,34]. In contrast, other research works reported a superior flux enhancement potential of non-prepolymerized Me-based coagulants

in comparison to their prepolymerized counterparts [31,35]. The mechanisms behind the observed differences in coagulant performance are not well understood. There is a variety of PACl commercial products, with the variation in composition, depending on the supplier. It is essential to underline the governing mechanisms of membrane fouling mitigation by Me-based coagulants to select the optimum flux enhancer or compound basicity (in case PACl shows the highest fouling mitigation propensity). Besides, the lack of the optimization of the coagulant addition in BF-MBR makes it impossible to conduct a trustworthy comparative analysis of the coagulants with regard to their fouling mitigation efficiencies.

It is worth noting, that the traditional time- and resource-demanding experiments for coagulant testing are becoming quite outdated and are limiting the development of the flux enhancing strategy in MBR and BF-MBR. The search for a more effective alternative to reduce the amount of the required experiments should be conducted to bring the technology to the next level.

Another major gap in the investigation of the flux enhancement in BF-MBR is the lack of implementation of the automated process control in this system, despite the fact that it is a promising approach to reduce the operating costs [17]. This can be overcome by the application of the multivariate chemometric analysis resulting in the development of the validated models of the chemical flux enhancement, which allow for the assessment and prediction of the reduction of the mixed liquor fouling propensity. These models will serve as an early warning tool for fouling development, so that the operator can make an instant decision on the adjustment of the operating conditions, affecting fouling intensity in the coagulant-assisted BF-MBR, based on the membrane fouling indicators.

In order to develop an accurate model, which would be suitable for other BF-MBR systems, it is not enough to consider mixed liquor as a “black box”, due to the system complexity, but to conduct the mechanistic investigation of the underlying pathways of chemical flux enhancement applying the coagulants. This approach, however, has not yet been exploited for process control in coagulant-assisted BF-MBR.

Based on the study by Stumm and Morgan [36] and the evidence on the major role of the floc-bound (particulate) extracellular polymeric substances and soluble microbial products (solutes, macromolecular soles) in membrane fouling [12,20], both the electrostatic double-layer interactions and purely chemical coordination must be considered to comprehensively explain the coagulation processes occurring during the addition of the chemical flux enhancers in BF-MBR.

As briefly laid out below, the current thesis aims to contribute to filling the knowledge gaps with respect to (1) identification of the membrane fouling patterns, fouling prediction and control in BF-MBR; (2) identification of the predominant mechanisms of coagulant action during chemical flux enhancement in BF-MBR; (3) optimisation of the work of the coagulant-assisted BF-MBR system; (4) introduction of a more advanced way of assessment of the flux enhancing capacity of the coagulants in order to reduce the number of the required experiments; (5) development of the models for the prediction and control of chemical flux enhancement based on the mechanisms of removal of extracellular polymeric substances (EPSs) and soluble microbial products (SPMs) during the addition of coagulants as flux enhancers in BF-MBR. More details on each of these topics are provided in the respective chapters of this thesis.

2. Objectives and Scopes of the Study, Thesis Structure

2.1 Objective of this research

The overall objective of this work is to develop the multivariate models for membrane fouling assessment, control, and prediction, based on the mechanisms of flux enhancement in the coagulant-assisted BF-MBR system.

This was achieved through the interconnection of the multivariate chemometric analysis, quantum chemical modelling, thermodynamic analysis, cluster analysis, and experimental design techniques, which evolved into the development of the mechanistic-statistical approach to process control in BF-MBR systems.

A better understanding of the mechanisms of membrane flux enhancement will lead to a targeted fouling control, shifting the paradigm of the coagulant assessment with regard to its flux enhancing capacities in BF-MBR from the time- and resource-demanding experiments towards more accurate statistical and quantum chemical modelling.

The overall objective of the thesis is achieved through four sub-objectives, each of which is the focus of the relevant appended paper:

Paper I: identification of the potential flux enhancers and mechanisms of their action with regard to the removal of typical foulants in MBR.

Paper II: identification of membrane fouling patterns in the BF-MBR pilot system and their use for fouling prediction and control based on the validated mixed liquor parameters, fouling indicators, and operational conditions.

Paper III: development of the model for membrane fouling assessment, prediction, and control based on the electrostatic interactions between the floc-bound extracellular polymeric substances and the coagulant during the chemical flux enhancement in BF-MBR; optimization of membrane filtration.

Paper IV: development of the model for membrane fouling assessment and prediction based on the thermodynamic properties and mechanisms of the removal of the soluble microbial products (i.e, carbohydrates) by applying Al-based prepolymerized coagulant during chemical flux enhancement in the BF-MBR system.

Synopsis of the appended papers is provided in Appendix A, the post-print versions of the papers are given in Appendix B.

2.2 Structure of the research and thesis

The research was organized into four stages, presented by four papers published in the peer-reviewed journals. The interconnection between the appended papers and the relevant studied areas is illustrated in Figure 2.1.

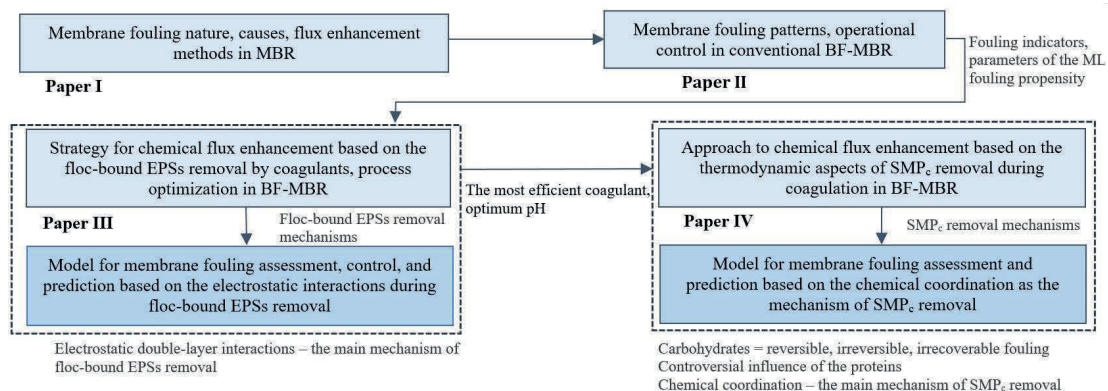


Figure 2.1 The structure of the doctoral thesis. (Notes: SMP_c is the carbohydrate fraction of soluble microbial products.).

The specific scopes of the research stages and the relevant publications are as follows:

Paper I: membrane fouling mechanisms, the main foulants, contemporary approaches to membrane flux enhancement in MBR and BF-MBR systems.

Paper II: interconnection between the characteristics of the mixed liquor fouling propensity, fouling indicators, and the operating conditions in the membrane separation chamber of the BF-MBR pilot-scale system with the submerged ceramic membrane elements.

Paper III: the comparative analysis of the inorganic prepolymerized and non-prepolymerized coagulants as membrane flux enhancers in the lab-scale MBR system using mixed liquor from the BF-MBR pilot plant, the optimum coagulant and conditions for flux enhancement; the mechanisms of removal of floc-bound EPSs during chemical flux enhancement in the coagulant-assisted BF-MBR.

Paper IV: a computational analysis (case study) on the thermodynamically favourable pathways of the formation of inorganic-organic complexes during the application of the optimum coagulant as a flux enhancer in BF-MBR; membrane fouling as a function of the standard Gibbs energy change; removal mechanisms of SMP_c (carbohydrate fraction of SMPs) during chemical flux enhancement in the coagulant-assisted BF-MBR.

3. Methods and materials

3.1 Study objects

Mixed liquor, analysed in **Paper II**, was collected from the aerobic submerged BF-MBR pilot system, which was operated under constant flux conditions, controlled through the programmable logic controller (PLC) (MoreControl, Aas, Norway).

The sampling from the constantly aerated MBBR and MBR chambers was performed through the relevant sampling valves mounted on the walls of the reactor. A sampling of mixed liquor, raw wastewater, and the permeate was organized on a daily basis. The subsequent analytical analysis was conducted within the first 6-8 hours after the sampling (**Paper II**).

The pilot BF-MBR system was fed with the wastewater, supplied at 0.3 m³/day through the screens to the equalization tank from the source-separated sewer network, keeping the ratio of black to grey water at 1:9. Black water was collected from the toilets and grey water from all other discharge points of the households around the pilot site. The influent quality was kept at 1–1.3 g/L by suspended solids and 100–350 mg-O₂/L by chemical oxygen demand of dissolved organics, COD_{dis}.

Initial biological activity in the system was provided by inoculation with activated sludge without the coagulant addition, which was obtained from the municipal wastewater treatment plant (BEVAS, Oslo, Norway).

The abovementioned BF-MBR pilot system was used as a source of mixed liquor for the jar tests and total recycle tests (the latter ones were conducted in the laboratory scale MBR) described in **Paper III**. The BF-MBR pilot system worked at solids retention time (SRT) 20 days. The feeding inlet was the mixture of black to grey wastewater at the ratio 1:9 (MLSS 0.4–1.31 g/L, COD_{dis} 142–262 mg-O₂/L, PO₄-P 6.08–10.28 ppm).

In **Paper III**, the following Al- and Fe-based flux enhancers were selected for the study: prepolymerized aluminium chloride with medium and high basicity and non-prepolymerized aluminium and iron (III) sulphate (Table 3.1). The applied coagulants are available from commercial suppliers by active compound name and metal content. Products of Kemira Chemicals AS (Helsinki, Finland) were used in this study.

Table 3.1 Properties of the tested flux enhancers.

Designation	Active compound	Metal content, %	Basicity (OH/Me)	Density (20°C), g/cm ³	pH
PAX18	[AlClOH] _n	9.0 ± 0.2%	42.0 ± 2% (1.3)	1.37 ± 0.03	0.6

Table 3.1 *Cont.*

PAXXL61	$\text{Al(OH)}_x\text{Cl}_{(3-x-2y)}(\text{SiO}_2)_y$	$5.4 \pm 0.3\%$	$68.0 \pm 5\% (1.9)$	1.26 ± 0.03	2.7
ALS	$\text{Al}_2(\text{SO}_4)_3$	$4.3 \pm 0.1\%$	- (0)	1.33 ± 0.01	1.8
PIX313	$\text{Fe}_2(\text{SO}_4)_3$	$11.6 \pm 0.4\%$	- (0)	1.52 ± 0.06	< 0.5

The correction of the pH values in mixed liquor before and during coagulation was performed with the aid of 0.01N NaOH in the case of aluminium coagulants, and 0.1 N NaOH when applying iron (III) sulphate due to the higher tendency of the system for pH decrease in the latter case.

The study objects of **Paper IV** are the modelled solvated molecules of the following compounds: the typical for MBR and BF-MBR monosaccharides, which are the building blocks of the major membrane foulants; the open structure $[\text{Al}_{13}\text{O}_4(\text{OH})_{29}]^{2+}$ complex, which was found to be the dominant hydrolysis species with regard to the prepolymerized aluminium chloride with medium basicity; and the relevant Al_{13} -monosaccharide complexes, which are the product of the interactions between the Al_{13}^{2+} complex and the selected foulants.

3.2 Jar tests

In **Paper III**, the adapted jar tests allowed for simulating the application of the selected prepolymerized and non-prepolymerized Me-based coagulants for the coagulation-flocculation in the separation chamber of the BF-MBR. One of the main advantages of this method is the acceleration and simplification of the determination of the optimum pH and dosages during the testing of coagulants. For this purpose, the Flocculator 2000 from Kemira Chemicals AS and 1 L beakers were used. The following mixing conditions were applied during coagulation: 1 min rapid mixing (400 RPM), 10 min slow mixing (30 RPM), followed by 20 min of sedimentation with no mixing.

3.3 Membrane filtration experiments

Prior to the membrane filtration experiments, described in **Paper II** and **Paper III**, the integrity of the membrane sheets was evaluated through the bubble point test and the vacuum decay test by following the procedures described by method F 316-03 (Reapproved 2011) and method D 6908-03, respectively, according to the American Society for Testing and Materials. Both tests are based on the determination of the diameter of the pore or defect calculated from its bubble point.

3.3.1 BF-MBR pilot system

The BF-MBR pilot plant, which was set up for the study described in **Paper II**, had a four-stage design and consisted of the equalization (I), MBBR (II), separation (III), and permeate (IV) compartments (Figure 3.1).

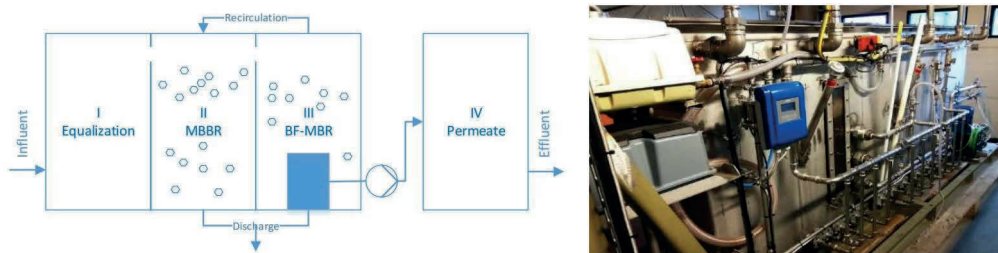


Figure 3.1 The BF-MBR pilot plant: Schematic diagram (left) and the photo of installation (right). Figure from **Paper II**.

As shown in Figure 3.1, compartments I, II and III were interconnected through the overflow. The submerged flat-sheet membrane modules were in contact with suspended biofilm carriers in the separation chamber III, where the separation process was driven by a reversible peristaltic pump (Verderflex, Castleford, UK), controlled from the PLC. A return activated sludge (RAS) line was incorporated into the system between chambers III and II, controlled by the adjustment of the RAS pumping intervals (i.e. pulse length and frequency).

Flat sheet silicon carbide (SiC) microfiltration membranes with 0.1 μm pore size (Cembrane, Lyngø, Denmark) were used in the separation chamber III, providing a total filtering area of 0.828 m^2 . Aeration was provided in chambers II and III by a MEDO LA-60E (Nitto Kohki®, Nitto Kohki Co., Ltd, Tokyo, Japan) air compressor at 60 L/min.

Plant operation data was continuously recorded every 3 s to the data-logger, in-built in the PLC. Flow in the permeate line and transmembrane pressure (TMP) were measured through the flow (Krohne OPTIFLUX 5100, Krohne Ltd., Duisburg, Germany) and pressure (Klay 8000 series, Klay Instruments B.V., Dwingeloo, Netherlands) sensors, respectively, and logged every second to the PLC together with filtration cycle settings. Values of system inflow, level in the separation chamber, TMP, and permeate flow were stored and recalculated further to analytical values.

The initial filtration settings were: 300 s of filtration at net-flux 8.2 LMH, 60 s relaxation, 15 s backwash with permeate at net-flux 180 LMH, and 120 s relaxation. Further changes were introduced into the plant operation resulting in 8 periods, characterised by different operational settings during the operation time of 114 days, described in **Paper II**.

In order to avoid a severe membrane fouling, entailed by permeate flux, all the operational fluxes were kept below the critical flux values 12–15 LMH, which were determined by the flux-step method, described by Miller et al. [37].

3.3.2 Total recycle test in the laboratory MBR system

In **Paper III**, total recycle tests (TRTs) were conducted in a plastic transparent 2.8 L MBR reactor, where the flat-sheet ceramic membrane was submerged with a provided cross-flow aeration (Figure 3.2).

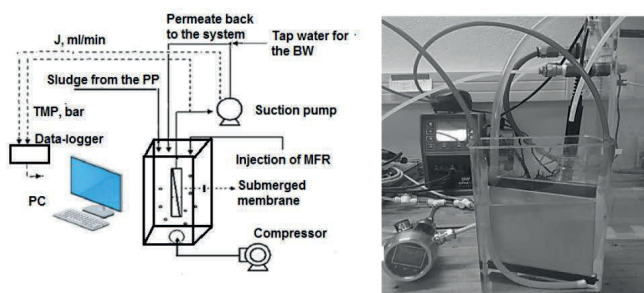


Figure 3.2 The total recycle test system, adapted from [38]. Figure from **Paper III**.

SiC microfiltration membrane sheets with 0.1 μm nominal pore size and surface area of 0.0355 m^2 were used for these studies (Cembrane, Lyngø, Denmark). The filtration was provided by the vacuum in the permeate line, applied to the submerged membrane using a peristaltic metering pump (Qdos30, Watson-Marlow, USA). The separation process was carried out under constant flux conditions (80 LMH) with the recycling of all the filtrate back to the mixed liquor container. The pressure in the vacuum line was measured with an electronic pressure transducer (Klay 8000 series, Klay Instruments B.V., Dwingeloo, Netherlands) and, together with the permeate flow values from the peristaltic metering pump, recorded into the laboratory data-logger.

Coagulants were added to mixed liquor (ML) before membrane filtration and intensively mixed, applying aeration during 30 s. After this time, the aeration was turned off and the membrane system remained in the relaxation mode for 90 s more. Then, the aeration was turned on and the filtration started. Ten minutes after the dosing of flux enhancer, the first sampling was performed in a quantity of 200 mL to keep the membrane fully submerged in the ML solution. 60 mL of this sample were used to measure MLSS, residual aluminium, $\text{PO}_4\text{-P}$, and the particle size parameters. The rest of the ML was used for the measurement of electrokinetic potential and turbidity.

When TMP increased to the level of $1.2 \cdot \text{TMP}_{\text{in}}$ (TMP_{in} is the initial TMP) and more than 1010 s elapsed after the dosing of flux enhancer, the filtration was stopped and the specimens for capillary suction time (CST) and Time-to-Filter (TTF) analyses were taken.

3.4 Applied analytical techniques

3.4.1 Mixed liquor analysis

Mixed liquor suspended solids (MLSS), capillary suction time (CST), Time-to-Filter (TTF), turbidity, COD_{dis} , orthophosphates ($\text{PO}_4\text{-P}$), residual aluminium, and diluted sludge volume index (DSVI) were determined according to the standard methods, specified in **Paper II** and **Paper III**.

Electrokinetic potential (ζ -potential) was determined through the measurement of electrophoretic mobility and the automatic derivation of ζ -potential according to Henry's equation under Zetasizer Nano-Z (Malvern™, Malvern Panalytical Ltd, Malvern, UK).

Prior to the measurement of turbidity and zeta potential, the supernatant of the mixed liquor samples was filtered through the quantitative cellulose filter paper with the pore size 8–12 μm (Grade MN 640 md, Macherey-Nagel™, MACHEREY-NAGEL GmbH & Co. KG, Düren, Germany).

Relative hydrophobicity (RH) was determined by the MATH (microbial adherence to hydrocarbons) method [39,40].

3.4.2 Methods for determination of the intrinsic characteristics of the coagulants

In **Paper III**, potentiometric back and direct titration and size exclusion chromatography were conducted in order to investigate the properties of the applied coagulants such as charge concentration and the dominant molecular weight fractions, respectively.

Potentiometric titration

The efficiency of the chemically enhanced membrane filtration is affected by intrinsic charges of the coagulants. The streaming current potential indicates the colloidal and net ionic charge in the stream of the analysed solution [41].

The work of the streaming current detector is based on the following principle: the analysed solution, which enters the contact cell, is drawn into the bore of a piston, which moves vertically in a reciprocating motion, during the upstroke, and is then expelled during the downstroke. Meanwhile, the ions and particles contained in the analyte solution get adsorbed on the surfaces of the piston and measurement cell. During the back and forth flow of the analysed solution, the ions and charged particles move past the electrodes in the wall

of the measurement cell, generating a small current, called the streaming current [42,43]. The schematic representation of the main components of the streaming current detector and the mathematical description of its work are provided by different studies [43–46].

During the potentiometric titration, the streaming current potential demonstrates the relative degree of neutralization as the oppositely charged titrant is added to the sample. The theoretical optimum endpoint is the point of zero charge (isoelectric point) (Figure 3.3).

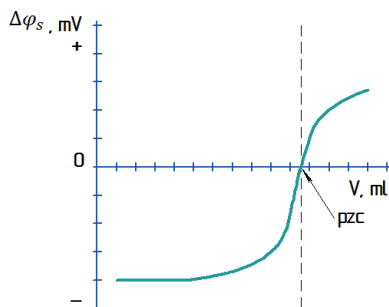


Figure 3.3 The form of the curve typical for the streaming current titration, using strong poly-base (for example, MGC) as the titrant and strong poly-acid (PVSK) as the titrated solution: $\Delta\varphi_s$ on the y-axis is a streaming potential, V on the x-axis stands for the volume of the titrant spent on the titration, adapted from Hubbe et al. [47] (Notes: “pzc” stands for the point of zero charge.).

Prior to the back titration, conducted in **Paper III**, the ratio factor of the selected polymers (potassium polyvinyl sulphate (PVSK) and methyl glycol chitosan (MGC)), i.e. the correction factor F_{pH} , was determined at pH 7 and the working pH values selected according to the intrinsic pH of the subsequently tested flux enhancers (Table 3.1) during the polyelectrolyte titration. PVSK was chosen to be a reference standard (titrant) and MGC concentration was adjusted to equate to PVSK at the selected pH. As a result of the polyelectrolyte titration, at pH 7, 2.7, and 2.12 the correction factor F_{pH} was equal to 1.0023, 1.0339, and 1.3266, respectively. Schematic representation of the polyelectrolyte complex, formed in the system of methyl glycol chitosan–polyvinyl sulphate is provided by Kikuchi and Kubota [48].

Then, back potentiometric titration of the coagulant samples was conducted using PVSK as a standard anionic polymer, which in the known volume was added to the coagulant sample; the extent of the PVSK, which did not react with the coagulant, was further back titrated with MGC — a standard cationic polymer, used as a titrant.

Based on the volume of the titrant of the known concentration, used for the titration until reaching the endpoint, and the correction factor at the relevant pH, the charge concentration of the analysed coagulants was calculated (Equation (2), **Paper III**).

In order to confirm the ranking trend among the studied coagulants with regard to their charge neutralization potential, potentiometric direct titration of mixed liquor, applying investigated coagulants as titrants, was performed using the specimens, sampled on the same day for all the coagulants. The selected coagulants were applied as titrants with no dilution.

During the determination of the correction factor, back titration of the coagulants, and direct titration of mixed liquor, a minimum of two parallel measurements were conducted for every sample.

Size Exclusion Chromatography

A comparative qualitative analysis of the investigated prepolymerized aluminium chloride (PACl) of the medium and high basicity with respect to the molecular weight distributions via size exclusion chromatography (SEC) was conducted in **Paper III**. The purpose of this analysis was to identify if the molecular weight difference was high enough to substantially influence the difference in charge concentration between two prepolymerized coagulants.

SEC is an analytical gel column chromatographic technique, which fractionates molecules according to their size in the solution. The size exclusion chromatography column is filled with the gel-like porous polymeric spheres of the rigid structure (stationary phase) and the mobile phase (solvent), where the latter transports the analysed sample solution through the column. The size fractionation occurs as a result of the repeated exchange of the solute molecules between the mobile phase and the stagnant liquid phase within the pores of the porous polymeric particles. The pore size of the beads, which make up the stationary phase, determine the molecular size range, within which exclusion takes place [49]. The polymeric constituents of the analysed solution, which have the higher molecular weight, due to their molecular size, occupy a smaller number of pores or a lower volume within a single pore than those of the lower size. As a result, the compounds of the highest molecular weight are eluted first from the column, whereas the smaller components are eluted later [50]. It is worth noting that, according to the study by Sun [51], during the separation of the linear and branched polymer molecules, their shape, expressed through the span dimension, should be considered as the influencing factor in addition to their radius.

In general, SEC is typically used for fractionation of the molecules of the polymeric sample according to the differences in their sizes, resulting in the acquisition of (1) the molecular weight averages; or (2) the molecular weight distribution of the polymeric substances [49].

Since the flow rates in the chromatography experiments are generally quite low (0.7 ml/min in the research described in **Paper III**), SEC is controlled by equilibrium thermodynamics, while the hydrodynamics has a little effect on the molecular fractionation; in particular, the retention in SEC is thought to be an entropy-governed size exclusion process [50–52].

The details on the SEC experimental setup and the conditions of the SEC fractionation were provided in **Paper III**.

3.5 Statistical mining of the investigated relationships

3.5.1 Multivariate statistics

In order to better comprehend the basics of the projection to latent structures (PLS) method, which was used in **Paper II**, **Paper III**, and **Paper IV**, it is essential to give details of the principal component analysis (PCA) and principal component regression (PCR) techniques.

It is worth noting that the PCA, PCR, and PLS analyses have one highly significant advantage in common: the orthogonality of the latent variables, which makes these techniques robust to the collinear variables.

According to CAMO Analytics AS [53], PCA is used for the exploratory data analysis (i.e. visual approaches to find the pattern in data), extraction of the necessary information and its separation from noise, and the reduction of the data dimensionality. It is particularly useful for the detection of the outliers, revealing of the hidden structures in the large sets of data, visual interpretation of the relationships between the samples and variables, and indicating of how the monitored variable causes the similarities or dissimilarities between the samples [54].

PCA is based on the principle of finding the directions in the space of samples, called principal components, along which the dispersion of the data points is the highest [54] (Figure 3.4).

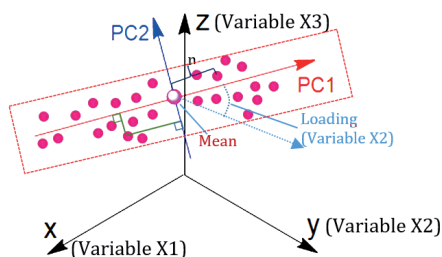


Figure 3.4 The principle of the dimension reduction into principal components, scores, and loadings, adapted from CAMO [54] and Torgersen [55].

Figure 3.4 represents the principles of projection applied in PCA for the dataset with three variables. The axes x , y , and z stand for variable 1, variable 2, and variable 3. The purple points designate the samples. PC1 and PC2 stand for the first and second principal component, respectively. The distance n from the mean value to the sample along the relevant PC is called the score. Samples with the close scores are similar with regard to the corresponding variable. Meanwhile, the loadings provide the link between the real and latent variables and describe the data with regard to variable contribution and correlations [54,56]. In geometrical terms, the loading is the cosine of the angle between the original variable and the selected latent variable: the decrease of this angle entails the increase of the correlation between the original and latent variable, expressed by the larger loading value. Principal components are the loading-score pairs, where each loading and score are mutually associated [54,56].

Generally, the number of variables is greater than three shown in Figure 3.4. For the dataset in the form of matrix $X^{m \times k}$, with m rows and k variables, PCA provides the smaller set with n latent variables ($n < k$), which thoroughly explains the variance of the original dataset.

According to PCA, an array of the predictors can be expressed by the empirical mathematical model, as specified by Equation (3.1).

$$X = T_k \cdot P_k^T + E \quad (3.1)$$

where X is the original data matrix; T_k is the principal component scores matrix of the size $n \times k$, whose columns are mutually orthogonal, P_k the matrix of eigenvectors – loadings, E is the error matrix, which contains unexplained variance.

The first column of scores and the first eigenvector (column in the matrix of loadings P) correspond to the first principal component. The first eigenvector corresponds to the one with the largest eigenvalue, and hence explains the maximum amount of variance in the original dataset. The second principal component (PC2) carries the maximum proportion of the residual variance [57].

Hence, the data matrix can be partitioned in a sum of k “rank one” $n \times m$ data matrices:

$$X = t_1 \cdot p_1^T + t_2 \cdot p_2^T + \dots + t_k \cdot p_k^T + E \quad (3.2)$$

where the outer vector, $t_1 \cdot p_1^T$, is the variance explained by the first principal component.

In order to perform the PCA, it is necessary to complete a set of eigenvectors, P , and eigenvalues, D , that diagonalize the square symmetric variance-covariance matrix, C [57].

The calculation of the covariance matrix is conducted according to:

$$C_{m \times m} = X^T \cdot X \quad (3.3)$$

where T is the transpose of the matrix X .

The computation of the eigenvectors and eigenvalues of the covariance matrix is conducted according to Equation (3.4).

$$P^T \cdot C \cdot P = D \quad (3.4)$$

where D is the diagonal matrix of eigenvalues of C , λ_i ($i = 1 \dots k$), along the diagonal; P is the matrix of eigenvectors, which diagonalizes the covariance matrix C .

The defining of the P_k and T_k , where P_k contains the selected k columns from the matrix P , enables the construction of the model defined by Equation (3.1):

$$P_k = [p_1 | p_2 | \dots | p_{k-1} | p_k] \quad (3.5)$$

$$T_k = X \cdot P_k \quad (3.6)$$

The variance, explained by the principal component model, which encompasses $PC_1 \dots PC_j$, —cumulative variance, can be expressed as [57,58]:

$$CPV_j = \frac{\sum_{i=1}^j \lambda_i}{\sum_{i=1}^l \lambda_i} \quad (3.7)$$

where CPV stands for the cumulative percent variance; $l = \min(n, m)$.

Principle component regression is a two-stage procedure. First, it conducts the principal component analysis on the original X variables to reduce the dimensionality of the data and to take into account their structure. Then, PCR uses the principal component scores from PCA, which are orthogonal, instead of the original X -variables, as predictors in the multiple linear regression model, i.e. relates the principal components to the response function, Y . The obtained model is stable and can be used when the X -variables are characterised by a large amount of correlation, or collinearity [54,59]. The mathematical description of PCR can be found in the work by Gemperline [57]. The disadvantage of PCR lies in the fact that it employs the latent variables that are response-independent [56].

This weakness is overcome by PLS analysis (projection to latent structures), which applies the PCA on both the predictor variables, X , and the response functions, Y [59]. PLS simultaneously models the matrices of the predictor variables and responses to find the hidden variables in X that will predict the latent variables in Y ; i.e. the latent variables are response-dependent, in contrast to PCR. Collinearity and noise are eliminated through the creation of new predictor variables and responses that are weighted combinations of the raw variables [40,54,60], which is accomplished through the steps, demonstrated in Figure 3.5.

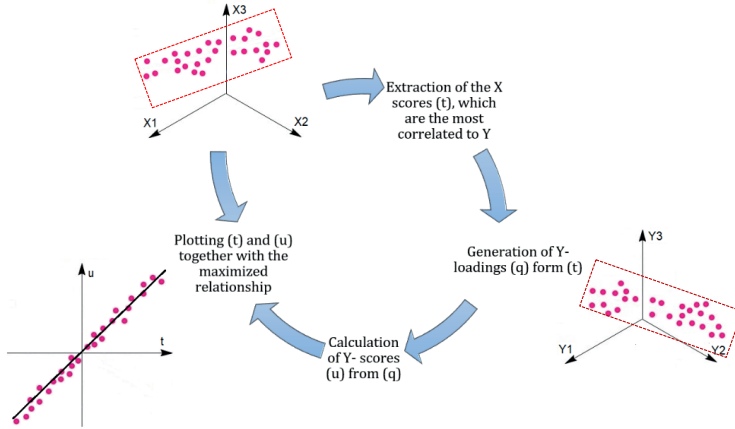


Figure 3.5 The idea behind the PLS technique, adapted from CAMO [54].

According to Figure 3.5, the original dataset of predictor variables, X , is regressed into t -scores (T), which are the most correlated to the response function, Y . The t -scores, T , in turn, are used to predict the Y -scores, U . Eventually, the u -scores, U , are used to predict the response function, Y . The process of decomposition of the X and Y matrices into the matrices of scores and loadings is finalized, when the linear combination of the predictors attains its maximum covariance with the response functions [55]. Hence, PLS generates orthogonal score vectors by maximizing the covariance between different sets of variables [61].

The scores T and U contain the information about the samples, their similarities, and dissimilarities with regard to the model. The model also contains the weights, which give the interpretation of the scores, thus contributing to the understanding of which predictor variables are significant [62].

In general, in PLS, the matrix of the predictor variables (X) consists of the components, which are similar to those in PCA, being characterized by the matrix of scores, T , loadings, P , and the error component, E . The response function undergoes similar analysis, as shown in Figure 3.4, thus it also contains the matrix of scores U , loadings Q , and the matrix of unexplained variance, E [57]:

$$X = T \cdot P^T + E \quad (3.8)$$

$$Y = U \cdot Q^T + E \quad (3.9)$$

In comparison to multiple linear regression (MLR), PLS has such advantages as: more accurate calibration models and analytical predictions, lower influence of noise, higher sensitivity, orthogonality of the scores, visualization of the relationship among the samples

and variables, toleration of the moderate amount of the missing data with respect to both the predictor and response variables [56,62].

PLS uses simultaneous information from the predictor and the response variables, which makes it a more complex technique than PCR. As a result, the regression vectors, which are more harmonious with respect to the bias/variance balance, are generated. In contrast to PCR, PLS employs the analyte-specific latent variables, which are more adapted to the requirements of each analyte of interest; and typically provides lower root mean square errors of calibration. In addition, PLS uses fewer factors than PCR, which results in the generation of the less complex model [57].

There are two versions of PLS — PLS-1 and PLS-2. The principal difference between PLS-1 and PLS-2 is that PLS-1 employs the modelling of one response function at a time — the building of specific models adapted for the needs of each response function; whereas PLS-2 provides the simultaneous modelling of all response functions. During PLS-1, in the calibration phase, the correlation of the X -data matrix with the vector of the response function is conducted. Meanwhile, PLS-2 correlates the X data matrix with all the calibration matrices Y . At the regression stage, PLS-2 replaces Y by a Y -scores matrix [56]. The principles of PLS-1 and PLS-2 are described in a more detailed way by Brereton [63] and Olivieri [56].

Paper II and **Paper III** applied PLS-2 as the multivariate chemometric tool for fouling prediction and control in the BF-MBR without the chemical dosing and the coagulant-assistant BF-MBR, respectively. In these cases, PLS-2 was used in order to analyse all the response functions, i.e., their relationships with each other and the predictors, at the same time. In addition, in **Paper II**, there was a positive correlation between the response functions, average normalized permeability ($_{av}P_n$) and average normalized permeability slope ($_{av}P_n/dt$), therefore the use of the PLS-2, which uses the orthogonal Y -scores, alleviating the correlation issues, is more preferable [56].

On the contrary, **Paper IV** used PLS-1 in the statistical analysis for the distinguishing of the thermodynamic patterns of the interactions between the Al_{13}^{2+} complex and selected monosaccharides of SMP_c , where a single response function, Gibbs energy change, was in the focus of interest.

In all the models, the Kernel PLS algorithm was used for the model calibration, which is beneficial when the number of observations substantially differs from the number of variables. Kernel PLS algorithm is characterised by computation and implementation simplicity and capability of modelling complex non-linear aspects of measured data [61,62]. The

comparative analysis of the PLS algorithms is provided by Andersson [64] and Björck and Indahl [65].

3.5.2 Cluster analysis

Cluster analysis was used in **Paper IV** in order to understand the structure of the complex multivariate dataset, which was generated during the quantum chemical, thermodynamic, and the PLS analyses. The complexity of the analysed dataset was indicated during the PLS sample grouping, which revealed no distinctive clusters, i.e. the scattered nature of the scores, which can be explained by a peculiarity of every investigated process of formation of the individual Al₁₃-monosaccharide complexes.

Apart from the advantages of using preprocessed data (PLS scores) rather than the raw dataset, underlined in **Paper IV**, the application of the PLS analysis prior to cluster analysis helped to comprehend the nature of the generated clusters, giving the necessary preliminary knowledge about the problem and the pursued goals. This outcome was essential due to the intuitiveness of the process of cluster definition [57].

The idea of the cluster analysis is the inverse relation of the distances between the samples and the degree of their affinity.

Hierarchical clustering method, which was used in **Paper IV**, is the most widespread clustering method. The computation of the similarity matrix, formed by calculating the distances between all pairs of points in the dataset, converting them into similarity values (Equation (3.10)), and arranging the similarity values into the matrix, is the starting point for hierarchical clustering method [57].

$$s_{ik} = 1 - \frac{d_{ik}}{d_{max}} \quad (3.10)$$

where s_{ik} is the similarity between the samples i and k , $0 \leq s_{ik} \leq 1$; d_{ik} is the Euclidean distance between these samples; and d_{max} is the distance between two the most diverse samples, which is the largest distance in the dataset.

The similarity matrix undergoes scanning for the largest value, which corresponds to the most similar point pair. Two samples from the original dataset, which make up this point pair, are then combined into the new point, located in the middle between them. This process continues until there are no pairs of samples left from the original dataset. Then, the symmetry matrix is updated to include the information about the similarity between the new point and every other point in the dataset. The matrix is scanned and recomputed again according to the same principle, which is repeated until all points are linked [57]. Consequently, a diagram,

i.e. dendrogram, is generated, which visually represents the relationships between the sample points. The procedure for hierarchical cluster analysis is described in detail by Wang [66]. The iteration procedure, applied during the hierarchical clustering, can be carried out using any programming language [66], thus it can be easily implemented in any PLC.

Euclidean distance is the most useful and common for defining the distances between the samples. In the case of using the PCA/PLS scores, the distance between the samples X_i and X_k with scores t_i and t_k , respectively, is defined according to [67]:

$$d_{ik} = \sqrt{(t_i - t_k) \cdot (t_i - t_k)^T} \quad (3.11)$$

where t_i and t_k are the vectors, which contain the scores on all latent variables of the model for the samples X_i and X_k .

In **Paper IV**, the squared Euclidean distance was used, which is useful in cases, where some variables may dominate the distance between groups, serving as a tool for data normalization [54].

The complete linkage, which is characterised by more compact and rounded clusters than the analogues [54], was used in **Paper IV**. The principle of computation of the complete linkage method, as well as the other linkage methods of the hierarchical cluster analysis, is represented by Gemperline [57] and King [68].

3.5.3 Two-level fractional factorial design of the experiment

A factorial design was defined as the method of designing the profile of the experiment by generating all possible combinations of levels [69].

Full factorial designs of the type 2^k , where k is the number of factors, are characterised by the exponential increase of the number of experiments with the increase of the number of factors. For example, for 9-factor design at two levels, 512 experiments are required. The extra experiments are usually wasteful with regard to time and resources since they do not typically result in useful or interesting extra information. In other words, there is a large redundancy, which can be omitted by running the fractional designs [63,70].

The fractional design merely employs a special carefully chosen subset of the experimental conditions from the complete factorial design, which are required to estimate the results, based on the assumptions, being followed. It is focused on the reduction of the number of experiments with the simultaneous maintaining of orthogonality of the levels and the estimates [69,71]. Orthogonality assures that the effect of one factor or factor interaction is estimated separately from the effect of any other factor or factor interaction in the model [72].

The following peculiarities of the fractional design makes it an attractive option for the researchers: (1) in the presence of several variables, the process, which is designed, can be controlled by some of the main effects and low-order interactions; (2) the ability to be projected into larger designs; (3) the possibility of a combination of runs of several fractional designs to estimate the effects and interactions of interest [73].

One of the examples of the fractional designs is the design based on the one-half fraction of the 2^k design, i.e., 2^{4-1} , which was used in **Paper III**. It described the experiment with four factors, of two levels each. The design contained eight treatment combinations and two replicates of each experiment. This design belongs to the resolution IV designs, where two-factor interactions are aliased with each other, while no main effect is aliased with any other main effect or with any two-factor interaction [71,73]. Resolution indicates how clearly the sample points can be separated in a design.

After selecting the factors and their levels and building the layout for the designed experiment based on the performed experiments at the relevant conditions, the development of the factorial design consisted of the following stages, described in **Paper III**: (1) preliminary analysis of effects through the correlation grid and the scattered plots; (2) analysis of the results (selection of the transformation and significant effects to the model, analysis of variance (ANOVA), diagnostics, interaction graphs); (3) numerical optimization (criteria and solutions); and (4) post analysis (point prediction and confirmation).

3.6 Image acquisition, analysis, and particle size distribution

Image acquisition and analysis were applied for characterization of the particle size distribution conducted in **Paper III**. First, the acquisition of the images under a light microscope (Leica DM 6B) was performed with the camera Leica DMC4500 (90× magnification) at exposure time 70 ms, gain 2.2–2.3, and intensity 54–55. The contrast technique, transmitted light–bright field (TL–BF), was applied, using the objective HC¹ PL FLUOTAR 10×/0.32 Dry: magnification 10×/numerical aperture 0.32 (objective class—Semi-Apochromats, for applications in the visual spectral range with higher specifications [74]). The acquired at 90× magnification images (Figure 3.6a) were transmitted from the camera to the computer.

For every image, the original scale in pixels was converted to microns (~ 3 pixels/micron), followed by the cropping of the 2544 × 1816 pixel area after its manual

¹ HC-objective is included into harmonic compound system

investigation, and conversion of the image into the 8-bit type (Figure 3.6b). Then, the threshold was adjusted applying black foreground and white background (Figure 3.6c). Subsequently, analysis of the particles was conducted, which resulted in the generation of the image, which contained the numbered outlines of the measured particles (Figure 3.6d), and the table of the measured particle areas in microns. ImageJ software [75] was used throughout image analysis.

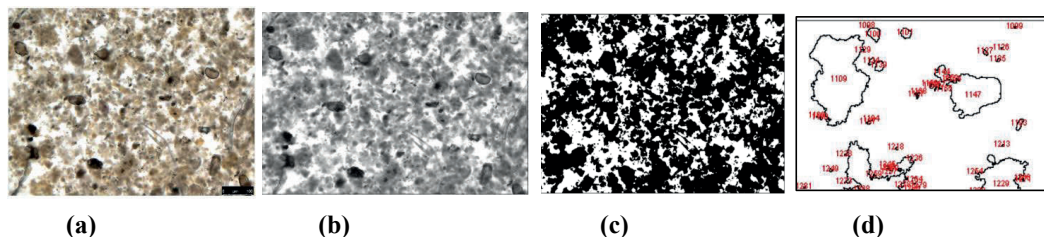


Figure 3.6 Determination of the particle size by image processing and analysis: (a) the original sample image, acquired under the light microscope; (b) the cropped image with the scale in microns converted to the 8-bit type; (c) the sample image after the adjusted threshold; (d) 150% magnified area in the image after particle analysis.

The acquired areas of every recognized particle were recalculated to the diameters, which were used as the basis for the pivot table in Excel. The pivot table consisted of the columns of particle size ranges, frequency of their occurrence, and the percentage of these sizes out of total. Then, the percentage of each size out of total was recalculated to the cumulative probabilities (in decimals) with regard to the upper limit of every particle size range. Based on this data, the cumulative distribution plot was built (Figure 3.7).

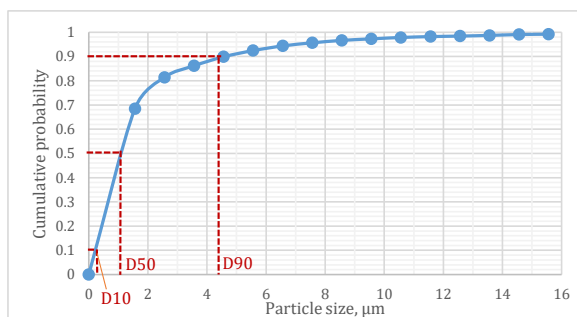


Figure 3.7 Cumulative distribution plot of the sizes of suspended solids in the analysed mixed liquor sample.

As demonstrated in Figure 3.7, based on the cumulative distribution plot, D10, D50, D90, the diameters where 10%, 50%, and 90% of the sample's population lie below this value, respectively, were determined. D10, D50, D90 were used to calculate volume/mass moment mean (the De Brouckere mean diameter), $D[4,3]$; surface area moment mean (the Sauter mean diameter), $D[3,2]$; and span (the distribution width) according to the formulas provided in

Paper III. The volume mean diameter, $D[4,3]$, expresses the weighted average volume diameter, whereas the surface area mean, $D[3,2]$, is the weighted average surface diameter of the sphere, which has the same physical properties as the actual particle, i.e., $D[4,3]/D[3,2]$ is calculated under the assumption that spherical particles are of the same volume/surface area as the actual particles [76,77]. $D[4,3]$ and $D[3,2]$ helped to quantify and interpret the image analysis data and were further used for the PLS analysis and characterization of the flocculation mechanism of the membrane flux enhancement by studied coagulants in **Paper III**.

In addition to the above-mentioned characteristics, the uniformity parameter was also added as the predictor variable to the PLS model. Uniformity was determined as the absolute deviation from the median, using the whole spectrum of particle sizes for every sample.

3.7 Quantum chemical and thermodynamic calculations

In **Paper IV**, the assessment of the spontaneity of the potential interactions between the selected monosaccharides of SMP_c and Al_{13}^{2+} complex was performed through two steps. First, the series of quantum chemical simulations were conducted, focused on the determination of the thermodynamic parameters of the formation of the individual reactants and the relevant complexes — standard enthalpy change (ΔH°_i), standard entropy (S°_i), and standard Gibbs energy change (ΔG°_i), applying the semi-empirical quantum-mechanical computational molecular orbital method — Parameterized Model number 3 (PM3). The quantum chemical calculations were performed using HyperChemTM 8.0.6 software (Hypercube Inc., Waterloo, Canada).

By applying certain approximations, semi-empirical calculations solve the partial differential Schrödinger equation, which describes the wave function $\psi(q, t)$ (where q is the set of coordinates, necessary to describe the system; t is time) of a quantum-mechanical system:

$$\mathcal{H}_i \cdot \psi_i = E_i \cdot \psi_i, \quad (3.12)$$

where \mathcal{H} is the Hamiltonian operator; E is a scalar quantity (constant), which corresponds to the energy of the system; ψ is the wave function, which is called the eigenfunction of the Hamiltonian operator; E is called the eigenvalue; i is the subscript related to the analysed unit [78].

$$\mathcal{H} = -\frac{\hbar}{2m} \cdot \left(\frac{\partial^2}{\partial x^2} + \frac{\partial^2}{\partial y^2} + \frac{\partial^2}{\partial z^2} \right) + U(x, y, z) = -\frac{\hbar}{2m} \cdot \nabla^2 + U(x, y, z) \quad (3.13)$$

where $\hbar = \frac{h}{2\pi}$ is the reduced Planck's constant; ∇^2 is the Laplacian; m is mass of the subatomic particle; $-\frac{\hbar}{2m} \cdot \left(\frac{\partial^2}{\partial x^2} + \frac{\partial^2}{\partial y^2} + \frac{\partial^2}{\partial z^2} \right) = -\frac{\hbar}{2m} \cdot \nabla^2$ is the kinetic energy; $U(x, y, z)$ is the potential energy [78].

The Schrödinger equation and its derivatives describe the behaviour of electrons and nuclei, and thus the behaviour of atoms and molecules. Hence, semi-empirical calculations describe the electronic properties of atoms and molecules. Semi-empirical calculations employ the simplification of the described calculations to speed them up by addressing only the valence electrons in the Schrödinger equation, neglecting the integrals for certain interactions, and by using standard electron orbital basis functions and experimentally derived parameters. The application of the empirical data helps to reduce certain calculations and to avoid the error correction of some approximations [79]. More details on the quantum mechanics and mathematical description of the semi-empirical methods are provided in different studies [78,80,81].

PM3 is based on the neglect of diatomic differential overlap (NDDO) approximation. PM3 is used for describing the elements of the main group in the periodic table (s-block and p-block elements), particularly the organic molecules (C, H, N, O). Among the parameters, determined through the PM3 parametrization procedure, the following ones can be singled out: the enthalpies of formation, dipole moments, ionization potentials, and molecular geometries [79,82]. Besides, PM3 enables the option of including solvation effects of the molecules in the analysis [83]. The settings for the PM3 calculations, which were used in the present study, and the accuracy of this method with regard to the enthalpies of formation were provided in **Paper IV**.

Then, the calculation of the main thermodynamic parameters of the reaction between the selected monosaccharides of SMP_c and Al₁₃²⁺ complex, i.e. the process of formation of Al₁₃-monosaccharide complex, — standard enthalpy change (ΔH^0), standard entropy change (ΔS^0), and standard Gibbs energy change (ΔG^0) was performed according to Hess's law (Equation (3.14)), its extension to entropy (Equation (3.15)) and Gibbs energy (Equation (3.16)), and the Gibbs-Helmholtz equation (Equation (3.17)).

$$\Delta H^0 = \sum (n_i \cdot \Delta H_{f,i}^0)_{products} - \sum (n \cdot \Delta H_{f,i}^0)_{reactants} \quad (3.14)$$

$$\Delta S^0 = \sum (n_i \cdot S_{f,i}^0)_{products} - \sum (n \cdot S_{f,i}^0)_{reactants} \quad (3.15)$$

$$\Delta G^0 = \sum (n_i \cdot \Delta G_{f,i}^0)_{products} - \sum (n \cdot \Delta G_{f,i}^0)_{reactants} \quad (3.16)$$

$$\Delta G^0 = \Delta H^0 - T \cdot \Delta S^0 \quad (3.17)$$

4. Results and discussion

4.1 State of the art of membrane flux enhancement in a membrane bioreactor: Paper I

Membrane bioreactor is a highly competitive technology, however, membrane fouling restrains the MBR expansion. The same problem is relevant to the advanced innovation in the development of MBR, i.e., biofilm membrane bioreactor (BF-MBR) technology.

According to the literature findings [15,84,85], membrane fouling occurs through membrane pore blockage and cake and gel layer formation, caused by soluble microbial products (SMPs) and floc-bound extracellular polymeric substances (EPSs). The accumulation of the solutes and colloids in the membrane pores and on the membrane surface is primarily responsible for membrane pore blockage, which comprises complete, internal, and intermediate pore blocking mechanisms. Membrane pore blockage, altogether with the cake filtration during the dead-end membrane filtration, was comprehensively described by Hermia's pore-blocking models. Hermia's pore-blocking models are the fundamental unified analytical description of the blocking mechanisms, which were formulated with regard to power-law non-Newtonian (further extended to Newtonian) fluids [86–89].

Concerning the cake layer, its formation is entailed by the deposition of suspended solids onto the sealed pores with a subsequent stacking. The gel layer is the matrix, which consists of highly concentrated solutes and macromolecular species, deposited at the membrane surface. This gel layer is usually incorporated into the cake matrix, therefore it is highly complicated to distinguish either of them [90]. The formation of the cake layer and the gel matrix at the membrane surface are governed by the pressure-driven convective flow from the bulk mixed liquor solution to the membrane during filtration [15,90,91].

Polysaccharides were identified as the primary foulants in MBR and BF-MBR systems [92–95]. Apart from their prime role in the formation of the gel and cake layer on the membrane surface (**Paper I**), polysaccharides are principally responsible for complete, intermediate, and internal pore-blocking [29,96,97].

The second important group of foulants is the proteins, which contribute to membrane fouling mainly through the interactions with the polysaccharides [98,99]. In the studies by Choi and Ng [100] and Zhou et al. [101], the proteins exhibited high fouling propensity in the submerged MBR. In the studies by Bowen et al. [89] and Soler-Cabezas et al. [102], the proteins were responsible for the complete, internal, and intermediate pore blocking, as well as for cake filtration. Miyoshi et al. [103] indicated the dominance of proteins in the foulant

deposits inside the membrane fibers (irreversible fouling), extracted from the membrane of the MBR, and identified the amino acid sequences of the relevant proteins. In contrast, other studies [20,95,104–106] pointed out that the proteins demonstrated occasional or no quantitative relationship with the fouling extent, while the carbohydrates were found to be responsible for the reversible, irreversible, and irrecoverable fouling in MBR and BF-MBR. Hence, the role of the proteins in membrane fouling still remains controversial and needs further investigations.

Humic substances is another organic component of mixed liquor, which is associated with membrane fouling [107]. As reported by Kimura et al. [108], humic substances are hydrophobic small molecules in contrast to the polysaccharides, which are the hydrophilic macromolecules. The same team reported two-stage fouling for the hydrophobic polyvinylidene fluoride (PVDF) membranes: adsorption of the humic substances on the membrane surface followed by the gradual accumulation of polysaccharide molecules. However, in the case of ceramic silicon carbide (SiC) membranes, used in the present research, the adsorption of humic substances is less likely to occur due to the hydrophilic nature of the applied membranes.

Among all of these foulants, carbohydrates (polysaccharides) were found to be the major contributor to SMPs in mixed liquor, which was characterised by elevated fouling propensity, whereas the fractions of proteins and humic substances were relatively low [20,109]. According to the recent study by Gkotsis and Zouboulis [110], the content of the carbohydrate (polysaccharide) fraction of SMPs (SMP_c) is the main contributor to membrane fouling in contrast to the protein fraction of SMPs (SMP_p), which was explained by the hydrophilic nature and the gelling properties of the polysaccharides. These conclusions, together with the results of the study by Ivanovic and Leiknes [95], suggest that the dominant role of SMPs in membrane fouling in MBR and BF-MBR is primarily attributed to their polysaccharide fraction (SMP_c).

Based on all aforementioned and on the finding by Jørgensen et al. [20] and Neeman et al. [98], the role of the components of the soluble microbial products in the membrane fouling in MBR and BF-MBR and the characteristic fouling types, presented in **Paper I**, were reconsidered accordingly and are summarised in Figure 4.1 and Table 4.1.

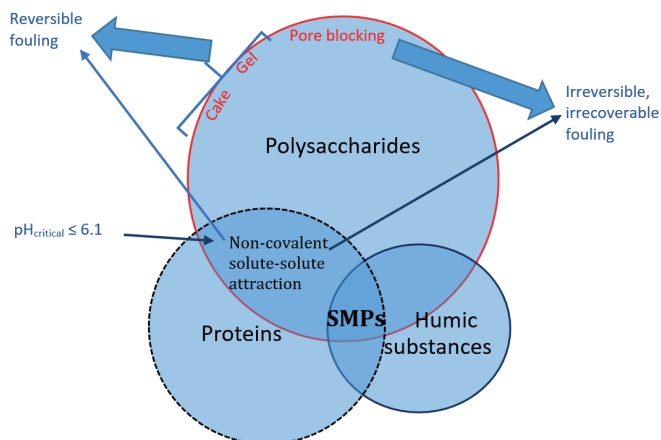
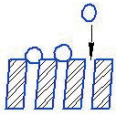
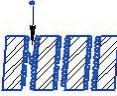
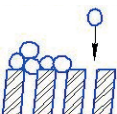
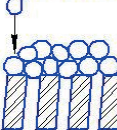


Figure 4.1. The role of the different SMP fractions in membrane fouling. Adapted from **Paper I**.

As previously mentioned, floc-bound extracellular polymeric substances (EPSs) also play an important role in membrane fouling in MBR and BF-MBR [19,111]. EPSs primarily contribute to the formation of the cake layer, by “triggering the process of colonization and biofilm development” on the membrane surface [112], and are responsible for the excretion of the SMPs into the bulk mixed liquor [84,113,114].

Fouling types can be categorized with regard to membrane permeability recovery as reversible, irreversible, and irrecoverable fouling. Reversible fouling is caused by deposition of the foulants on the membrane surface, leading to the formation of the cake layer and gel matrix. It can be removed by physical cleaning (back-flushing, air injection, relaxation, the addition of the biomass carriers). However, irreversible and irrecoverable fouling are associated with internal pore blockage. Irreversible membrane fouling can be removed by a more aggressive cleaning method — chemically enhanced backwash (CEB), applying NaOCl, NaOH, H₂O₂, and biocides; cleaning in place (CIP) or “cleaning in air” (CIA) via soaking the membranes in NaOCl and NaOH solutions. On the contrary, no techniques that could cope with the irrecoverable fouling have been developed [16,115–118].

Table 4.1 Types of membrane pore blocking in terms of Hermia's pore blocking models, characteristic pore-blocking patterns for the typical foulants, and the corresponding fouling types in membrane systems, MBR, and BF-MBR [21,24,87,89,119–123]. Adapted from **Paper I**.

Pore blocking model	Schematic illustration	Relation to the pore size	Physical concept	Foulants	Fouling type, References
Complete pore blocking		$d_{\text{foulant}} > d_{\text{pore}}$	the sealing of the membrane pores, no superimposing with other particles		Irreversible [124]
Standard (internal) pore blocking or pore constriction		$d_{\text{foulant}} < d_{\text{pore}}$	deposition onto the internal pore walls, the pore volume decreases proportionally to the volume of deposited particles	Polysaccharides, Proteins	Irreversible and irrecoverable [49,50]
Intermediate pore blocking		$d_{\text{foulant}} \approx d_{\text{pore}}$	pore sealing and deposition on other particles accumulated on the surface (formation of multilayers)		Irreversible [87]
Cake formation		$d_{\text{foulant}} > d_{\text{pore}}$	accumulation of the foulant on the surface/sealed pores with the subsequent stacking		Reversible, irreversible [123–125]

Among all the strategies to flux enhancement via the modification of the mixed liquor characteristics, described in **Paper I**, coagulation is one of the most promising techniques.

According to the report by Ratnaweera [126], more than 70% of the whole volume of wastewater, produced in Norway, is treated by coagulation applying Al- and Fe-based salts in the municipal wastewater treatment plants (WWTPs). For example, the wastewater treatment plant in Oslo, BEVAS, seasonally applies prepolymerized aluminium chloride of medium basicity and iron (III) sulphate for the removal of suspended solids and phosphorus [127]. Therefore, the advancement of the existing WWTP plants by the incorporation of the membranes with the coagulant dosing will not disturb the operation and maintenance routine, omitting the need for the new dosing equipment and search for the new suppliers of reagents.

Membrane flux enhancement via coagulation can be performed by using prepolymerized and non-prepolymerized inorganic coagulants. A positive effect of prepolymerized coagulants such as prepolymerized aluminium chloride (PACl) and prepolymerized ferric sulphate (PFS) on fouling reduction in MBR due to their higher intrinsic charges and greater flocculating ability than of their non-prepolymerized counterparts was admitted by different studies [30,34]. Prepolymerized ferric coagulants will not be investigated at the further stages of the

present research since it is very difficult to produce stable prepolymerized coagulant based on iron, therefore these coagulants are rarely marketed [128].

However, according to other studies, non-prepolymerized flux enhancers, particularly iron-based coagulants, also exhibited high efficiency with regard to fouling mitigation in MBR and BF-MBR systems [31,95,129], which was further explained in **Paper III** of the present research. As a result of comparative analysis of non-prepolymerized aluminium and iron coagulants, Song et al. [130] concluded that the Al-based coagulant was more advantageous than its Fe-based counterpart due to a less drastic pH decrease, which was also elucidated in **Paper III**.

The mechanisms of interaction between the coagulants and the foulants in MBR and BF-MBR systems are the key to the prediction and intelligent optimization of the membrane filtration performance, which still remains poorly studied.

According to the study by Malamis and Andreadakis [109], polysaccharides were found to be the dominant species in the soluble microbial products (SMPs), while the proteins were found to be the major component of the extracellular polymeric substances (EPSs). It is necessary to differentiate that EPSs are in the form of the floc-bound/particulate matter, whereas SMPs are soluble, being the product of the dissolution of EPSs [109].

According to the evidence, presented by Bratby [131] and Stumm and Morgan [36], bacterial solid surfaces contain readily ionizable functional groups, such as: $-\text{OH}$, $-\text{COOH}$, $-\text{OPO}_3\text{H}_2$, and $-\text{NH}_2$. However, the amine groups/the protonated amine groups are typically characteristic for the amino acids, the building blocks of proteins, which generally bear a positive charge at acidic pH. Therefore, the structure of the bacterial surfaces depending on pH conditions, presented in **Paper I**, is rather relevant for the description of proteins than carbohydrates/polysaccharides (except for glucosamine). Therefore, due to the dominance of the carbohydrates/polysaccharides in the SMPs and their major role in membrane fouling, the functional groups of SMPs should be illustrated as $R - \text{COOH}$ ($\text{pH} < 5$) \leftrightarrow $R - \text{COO}^-$ ($\text{pH} 5-7$); whereas, due to the prevalence of proteins, and thus amino acids in the EPSs, the bacterial surface of EPSs at different pH is described as $R < \overset{\text{COOH}}{\text{NH}_3^+}$ ($\text{pH} < 4.0$) \leftrightarrow $R < \overset{\text{COO}^-}{\text{NH}_3^+}$ ($\text{pH} 4.0-5.5$) \leftrightarrow $R < \overset{\text{COO}^-}{\text{NH}_2}$ ($\text{pH} > 5.5$) (the information on the isoelectric point of the proteins is provided in subchapter 4.4 of this work).

According to Zhou et al. [101], the SMP proteins have the isoelectric point at pH 5.5–7, while the EPS proteins — at pH 4.0–5.5. Zhang at el. [132] discovered, that the majority of the identified proteins in the aerobic sludge have the isoelectric point of pH 5–6, which agrees with the findings reported by Rijnaarts et al. [133]. According to the latter team, COO^- and

PO_4^{3-} groups determine the anionic nature of polysaccharides. Meanwhile, as reported by She et al. [134], during the colloidal and organic fouling, polysaccharides generally bear negative charge at pH 5–8, while proteins are characterised by the isoelectric point of pH 5–11. Even at pH 7, activated sludge with the higher ratio of polysaccharides to proteins has a higher negative charge concentration than the one with the higher protein fraction [135]. Therefore, in **Paper III**, the zeta-potential values of the filtrates with no coagulant addition or pH adjustment equal to $-14.01 - (-11.5)$ mV at acidic/neutral pH_{raw} 5.1– 7.0 and temperature 17.1– 23.1°C can be attributed to the dominance of polysaccharides in the SMPs, apart from the hypotheses on the origin of the negative charge, suggested earlier.

According to Stumm and Morgan [36], the fixation of the multivalent cations onto the deprotonated group of macromolecular sol (carbohydrates, proteins, and their derivatives), is an electrostatic or chemical interaction. This fixation is accompanied by the charge neutralizing process.

Since the isoelectric point of the floc-bound/particulate proteins, which originate from EPSs, was found to be at pH 4.0–5.5 [101], at $\text{pH} > 5.5$ the charge of the amino acid residues of the floc-bound EPS can be neutralized by the micelles, formed during the hydrolysis of coagulant, via the electrostatic interaction, resulting in the formation of organic-inorganic solid complexes according to the theories of double layer and electrostatic interactions (Figure 4.2).

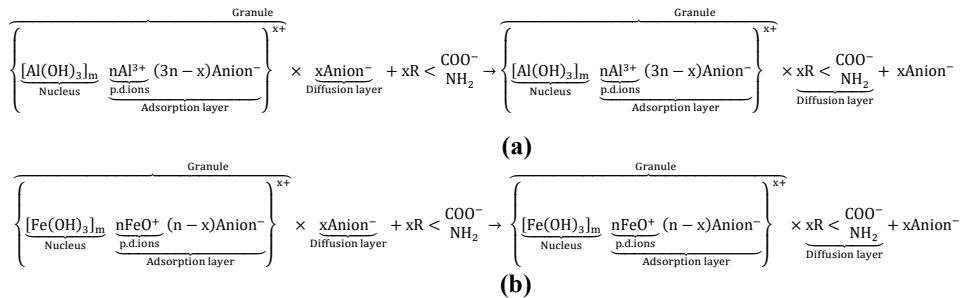


Figure 4.2 The formation of organic/inorganic solid complexes by the interaction of: **(a)** aluminium coagulants; **(b)** iron (III) coagulants with the amino acid residues of the bound EPSs. From **Paper I**.

Meanwhile, the process of SMPs removal can be described by the chemical coordination of the polysaccharides of SMPs (i.e., SMP_c) to the soluble $\text{Al}_{13}^{\text{nt}}$ complexes, which was investigated in **Paper IV**.

Due to the gap in process control approaches for the application of the chemical flux enhancement in MBR and BF-MBR systems, there is a need for the development of the models for membrane fouling assessment, prediction, and control.

According to the above-mentioned findings, the development of the fundamental models of the two soft sensors: one, which can describe/predict the removal of floc-bound EPSs by the Me-based micelles (investigated in **Paper III**); and the other one, which is based on the chemical interaction of the SMP_c to the Al₁₃ⁿ⁺ complex (a research focus of **Paper IV**) should be considered to fill the existing gap.

The intrinsic mechanisms of coagulant performance with regard to fouling mitigation in the MBR (Table 4.2) allow for selecting the representative characteristics of the mixed liquor fouling propensity (COD_{dis}, relative hydrophobicity/capillary suction time, particle size distribution parameters, zeta potential), which were validated in relation to the advanced BF-MBR technology in **Paper III**.

Table 4.2 Intrinsic mechanisms of coagulant action with regard to membrane flux enhancement in MBR [30,34,130,136–140]. Fragment of the table from **Paper I**.

Mechanisms of membrane flux enhancement in MBR	Non-prepolymerized coagulants		Prepolymerized coagulants	
	FeCl ₃	Al ₂ (SO ₄) ₃ ·xH ₂ O	Polymeric ferric sulfate (PFS)	Polyaluminium chloride (PACl)
The reduction of SMP level in mixed liquor	+ ¹	+	+	+
Increasing mean sludge floc size, drop fractal dimension	+	+	+	+
Enhancing charge neutralization	+		+	+
Increasing sludge relative hydrophobicity	+	+	+	+
Lowering gel layer formation, cake porosity increase, specific cake resistance reduction	+	+	+	+

Notes: ¹ “+” stands for the presence of the selected mechanism during flux enhancement action of the particular coagulant.

Besides, the addition of the flocculants/bio-flocculants can be considered in order to enhance fouling mitigation by the application of the coagulant-flocculant pairs. In this case, the selection of the appropriate flocculant/bio-flocculant can be conducted based on the assessment of its mechanisms according to Table 7 in **Paper I**, extended to the organic flocculants and bio-flocculants, to provide the combination of flocculant’s fouling reduction pathways with those of the validated optimum coagulant (Table 4.2).

The statement in **Paper I**, on the uncertainty, whether the cost of coagulants is justified by membrane fouling decrease, was refuted in **Paper III**, which proved that that the use of the most efficient coagulant under the optimum conditions resulted in a tenfold increase in filtration time of the membrane separation cycle and 30.0–56.0% higher net flux (depending on the operational period) in the BF-MBR pilot system, in comparison to this system without the coagulant dosing. The obtained flux enhancement will reduce the frequency of the regular backwashes by ten times and the number of resource-demanding chemical cleanings, and

hence the operational costs. In addition, as shown in **Paper III**, coagulant dosing allows the studied system to cope with the requirements on phosphorus discharge, which biological treatment alone couldn't achieve.

4.2 Identification of membrane fouling patterns in Biofilm Ceramic Membrane Bioreactor applying multivariate chemometric analysis: Paper II

Understanding, detection, and control of membrane fouling via advanced statistics and mathematical modelling represents a significant potential for improvement of the cost-efficiency of the BF-MBR process and provides the instruments for dynamic and real-time process control. Their implementation requires the determination of the representative variables, which could accurately indicate the mixed liquor fouling propensity, and the instruments of influencing it; and the response functions, which would precisely and quickly indicate fouling intensity for the effective and well-timed process control. However, in the case of BF-MBR systems, this subject still needs holistic investigation.

In the research, reported by **Paper II**, the BF-MBR pilot plant was monitored during 114 days, when transmembrane pressure and average normalized permeability were selected as the membrane fouling indicators, while MLSS, diluted sludge volume index (DSVI), floc relative hydrophobicity (RH), and COD_{dis} were the monitored parameters of mixed liquor. The acquired operation profile, which demonstrates the development of the monitored parameters in the system, is represented in **Paper II**.

The operating conditions in BF-MBR underwent considerable changes throughout the whole filtration period (114 days) in order to acquire a large representative (with regard to the application of the variety of operational modes) data array. Since these changes influenced both the mixed liquor parameters and the membrane fouling indicators, it was decided to split the whole data range into its characteristic phases and statistically analyse them separately from each other, excluding the data, which covered the chemical cleanings and TMP jumps. In general, three basic periods were established: period A (days 3–34), period B (days 49–77), and period C (days 86–114).

Period A encompassed biological adaptation and biomass development and the subsequent steady fouling. The biological adaptation and biomass development was characterized by moderate growth of biomass up to MLSS-III 5–6 g/L and increased biodegradation of organics in the range of 67–81%, together with a steep TMP growth and a respective decrease of permeability at a relatively high rate of 0.35–0.47 LMH/bar/s. This

state can be identified as conditioning fouling. After reaching the conditionally critical value of 1.7 times permeability decrease, the return of suspended solids from separation chamber (III) to MBBR chamber (II) (Figure 3.1) was doubled, leading to stabilization of permeability and MLSS-III (MLSS in the separation chamber) in the next sub-period (21–34 days) and decreasing the membrane fouling rate to 0.25–0.27 LMH/bar/s by permeability, which is considered as steady fouling. Fouling stages in the MBR, operated at a constant flux (i.e., conditioning fouling, steady fouling, and TMP jump), are described by Judd [15].

Period B covers the filtration phase after the increase of the permeate flux, prolongation of the backwash and relaxation, and the subsequent chemical cleaning. This period is characterised by another steady fouling state. It reproduced the same trends from the period A (21–34 days), except for a more stable COD degradation due to well-developed biofilms in the MBBR part and on the carriers in the separation chamber (III).

Period C (86–114 days) of system operation, which followed the chemical cleaning after period B, is a control period, which is characterized by both conditional and steady fouling in the permeability pattern.

The mixed liquor characteristics and membrane filtration performance in the separation chamber and their variation over time in the investigated system were monitored and statistically processed to gain a deeper understanding of their role in the studied BF-MBR. The ranges of the variation of the mixed liquor parameters are represented in Table 4.3.

Table 4.3 Parameters of mixed liquor in the separation chamber.

Parameter	Value
MLSS, g/L	5–6.5
dMLSS/dt, (g/L)/day	–0.61–2.06
DSVI, mL/g	118–272
dDSVI/dt, (mL/g)/day	–91–57
RH, %	20.5–61.5
dRH/dt, %/day	–27–35
COD _{dis} , mgO ₂ /L	38–134
dCOD _{dis} /dt, mgO ₂ /L/day	–35–27.5

PLS analysis was used as a multivariate statistical tool to model the relations between the predictor variables (the parameters of mixed liquor) and response functions (membrane fouling indicators) within every selected period (Table 4.4).

Table 4.4 Model inputs.

Period	Predictors	Responses
A	MLSS, dMLSS/dt, DSVI dDSVI/dt, RH, dRH/dt, COD _{dis} , dCOD _{dis} /dt	TMP, Pn, dPn/dt ²
B	MLSS, dMLSS/dt, DSVI dDSVI/dt, COD _{dis} , dCOD _{dis} /dt	TMP, Pn, dPn/dt
C	MLSS, dMLSS/dt, DSVI dDSVI/dt, COD _{dis} , dCOD _{dis} /dt	TMP, Pn, dPn/dt

² Hereafter, in this sub-chapter, dPn/dt stands for the average dPn/dt

In order to give all variables the same variance, the weighting option $1/(SDev)$, which is called standardization, was used during the analysis. This option provides all variables with the same influence on the estimation of the components, and is used if the variables are measured with different units; have different ranges; are of different types [54].

After the weighting, the models obtained for period A and B underwent random cross-validation in PLS, during which the dataset was divided into 20 and 15 segments, respectively, with 1–2 samples per segment. With regard to the model, which describes period C, it underwent full cross-validation so as to further apply the model for the prediction of the new data. Certain samples were taken out of analysis since they were indicated as potential outliers. The number of PLS factors was chosen according to the explained variance.

The results of the performed analyses of the data from period A of the system performance (biological adaptation, biomass development, and steady fouling) are shown below (Figure 4.3).

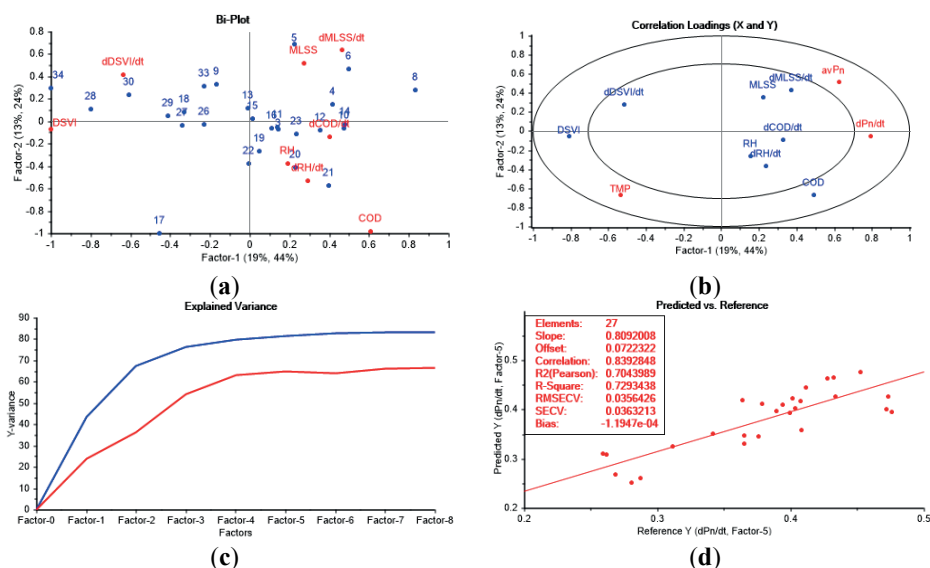


Figure 4.3 Results of PLS of the data from the period A of the filtration performance monitoring: (a) Bi-plot; (b) correlation loadings plot; (c) explained variance plot; (d) fouling intensity prediction model. From **Paper II**.

The analysis of the scores and correlation loadings plot and the bi-plot demonstrates that the samples from days 1–23 are mostly characterized by higher RH, dRH/dt , MLSS, $dMLSS/dt$, COD^3 , and $dCOD/dt$, while the samples taken during the period 26–34 day have higher DSVI and $dDSVI/dt$ values.

³ Hereafter, in this sub-chapter, COD stands for COD_{dis}

According to the correlation loadings plot, Factor-1 clearly describes DSVI, dDSVI/dt, TMP, COD, dMLSS/dt, dCOD/dt, average normalized permeability ($_{av}P_n$), and its slope (dP_n/dt). Meanwhile, MLSS, RH/dt, and dRH/dt mainly contribute to Factor-2. According to the PLS correlation loadings plot, COD and DSVI explain more than 50% of the variance and are apparently the most important variables. The rest of the variables explain less than 50% of the explained variance; however, it was decided to keep them to make the model more reliable.

DSVI has a negative correlation with both permeability parameters ($_{av}P_n$ and dP_n/dt) but is positively linked to TMP along Factor-1. COD has a negative correlation with the variables DSVI, dDSVI/dt, MLSS, and dMLSS/dt and is negatively linked to the average normalized permeability ($_{av}P_n$). This means, that the increase in DSVI and COD over time triggers fouling development.

As demonstrated by the graph of explained variance (Figure 4.3c), it is preferable to use five latent variables in the model since this number gives a higher explained variance.

According to the validation plot in Figure 4.3d, the R-squared of the developed model is 0.73, which indicates its linearity. The model is characterised by a reasonable fit to the majority of data: Slope = 0.81, offset 0.07 with the dispersion of the validation samples around the regression line (Root Mean Square Error of Cross-Validation–RMSEV) and the standard error of cross-validation (SECV) of approximately 0.036. Consequently, the model is reliable and can be used for future predictions for the defined number of factors under the operational conditions applied during period A.

It was decided to exclude RH and dRH/dt from further monitoring and analysis due to their low significance in the model, described in **Paper II**, and time- and effort-consuming determination procedure.

The results of the PLS analysis of Period B, which encompasses another steady fouling state but at increased permeate flux (18% higher than during days 1–20, and 47% higher than during the days 21–34) and prolonged backwash and relaxation, are represented below (Figure 4.4).

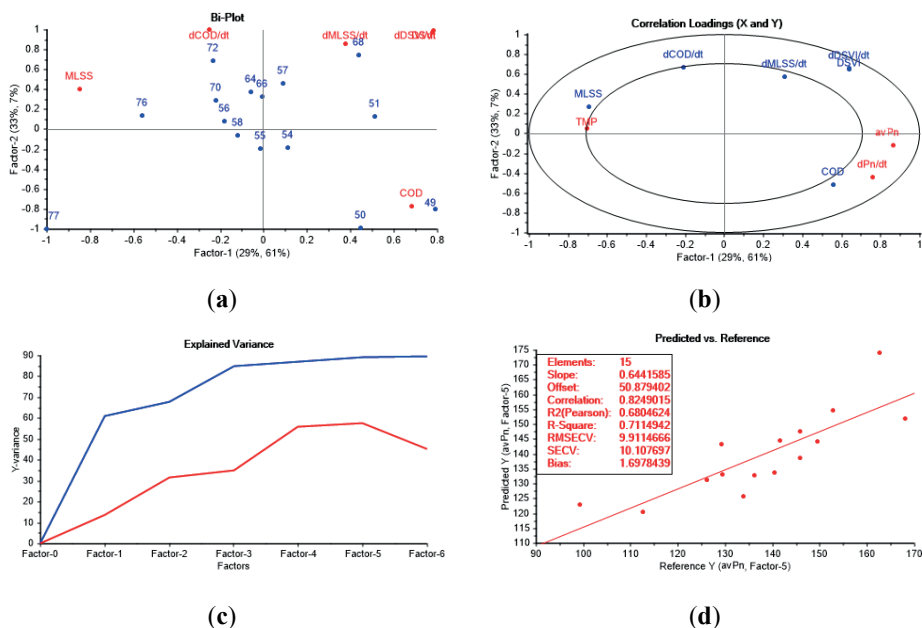


Figure 4.4 Results of PLS of the data from the period B of the filtration performance monitoring: (a) Bi-plot; (b) correlation loadings plot; (c) explained variance plot; (d) fouling intensity prediction model. From **Paper II**.

According to the bi-plot (Figure 4.4b), the majority of the samples within period B are characterized by higher dCOD/dt values. Meanwhile, the samples taken on days 49–50 are characterized by higher COD values; on days 51, 57 and 68 by relatively high dMLSS/dt, DSVI, and dDSVI/dt values; on day 72 by comparatively high dCOD/dt values; and on days 76 and 77 by more significant MLSS values.

According to the correlation loadings plot, Factor-1 clearly describes TMP, MLSS, COD, average permeability (avP_n), dP_n/dt , DSVI and dDSVI/dt. Factor-2 is related to dCOD/dt and dMLSS/dt. All the variables were marked as significant according to the plot of correlation loadings, even though the dMLSS/dt variable gives slightly less than 50% of the explained variance. MLSS and dCOD/dt are positively linked to the TMP response. dMLSS/dt, DSVI, and dDSVI/dt have a negative correlation with TMP and the permeability slope (dP_n/dt). The COD variable has a high positive correlation with dP_n/dt and is positively linked to the average permeability (avP_n), which might be entailed by the presence of SMP proteins with increased hydrophobicity (higher positive charge of the amino acid residues), which facilitate flocculation in mixed liquor [20] (pH in the separation chamber was equal to 3.9–4.5). Meanwhile, the rate of COD_{dis} change (dCOD/dt) positively correlates with fouling intensity.

Figure 4.4 demonstrates that the optimum number of factors is five, which provides 57.4% of the explained Y-variance.

An analysis of the validation plot shows that the resulting cross-validation R-squared was 0.71 and with a good fit to the majority of data (i.e., slope = 0.64). RMSEV and SECV were approximately 10. R-squared (Pearson) is close to R-squared correlation (0.68 vs. 0.82), which indicates the reliability of the model. A relatively low bias (1.70 LMH/bar) shows that the model has a low tendency to over- or underestimation of the validation values. Consequently, a good prediction is attained, which proves that the model is reliable and can be used during further stages when the operating conditions applied in period B are replicated.

Figure 4.5 demonstrates the results of the PLS analysis of the data from the last monitored period, characterised by both conditional and steady fouling (Period C), acquired after the second CIP (86–114 days).

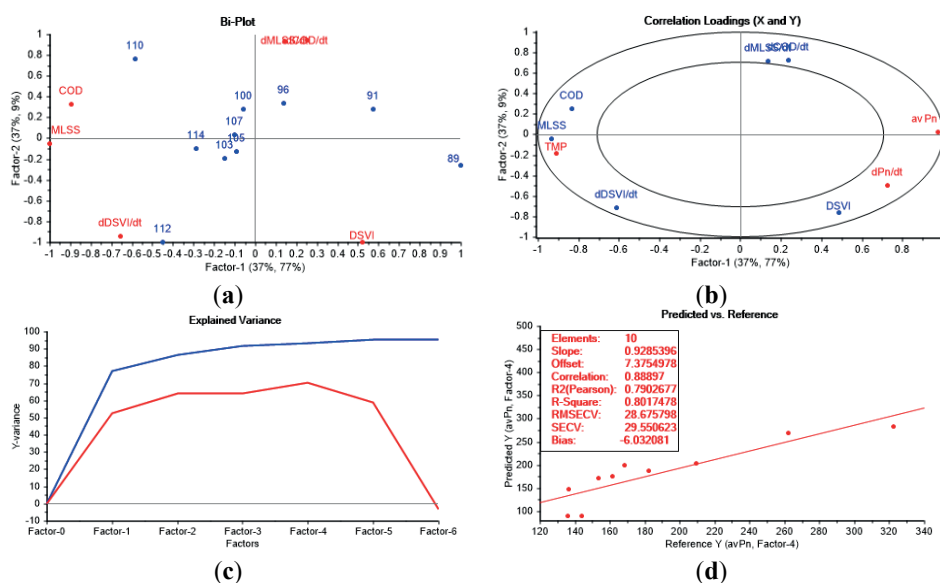


Figure 4.5 Results of PLS of the data from the period C of the filtration performance monitoring: (a) Bi-plot; (b) correlation loadings plot; (c) explained variance plot; (d) fouling intensity prediction model. From **Paper II**.

According to the obtained bi-plot (Figure 4.5a), the samples from day 89 are characterised by a higher DSVI value, while the days no 91 and 96 have a higher dMLSS/dt and dCOD/dt. Days 100, 107, and 110 are characterized by higher COD content, whereas days 103, 105, and 114 have higher MLSS values. Day 112 is characterized by a higher dDSVI/dt.

The correlation loadings plot (Figure 4.5b) shows, that COD, MLSS, TMP, dDSVI/dt, DSVI, avP_n , and dP_n/dt contribute to Factor-1, while Factor-2 accounts for dMLSS/dt and dCOD/dt. All the specified variables explain more than 50% of the variance, and thus have high importance in relation to Factor-1 and Factor-2. MLSS, COD, and dDSVI/dt are positively linked to TMP and have a negative correlation with the permeability indicators,

avP_n , and dP_n/dt , meaning, that the increase in $dDSVI/dt$, COD, and MLSS causes more intense fouling. DSVI is positively correlated to dP_n/dt , while $dMLSS/dt$ and $dCOD/dt$ have a negative correlation with the permeability slope.

The explained variance plot (Figure 4.5c) indicates that the optimum number of factors is four, which provides more than 70% of explained Y-variance.

The validation graph in Figure 4.5d has a linear trend (R -squared = 0.8), having a good fit to the majority of data (slope = 0.93). R -squared (Pearson) is close to R -squared correlation (0.79 vs. 0.89), which indicates the reliability of the model. RMSEV and SECV are 28.7 and 29.6, respectively.

The last model was also tested for the prediction of the new data (Table 4.5) in order to check its applicability in the real-life conditions.

Table 4.5. Mixed liquor characteristics and fouling indicators during period C (new data).
From **Paper II**.

	TMP _{av} ¹ , bar	av dP_n/dt ²	av P_n ³ , LMH/bar	DSVI ⁴ , mL/g	dDSVI/dt ⁵	MLSS ⁶ , g/L	dMLSS/dt ⁷	COD _{dis} ⁸ , mgO ₂ /L	dCOD _{dis} /dt ⁹
max.	266.16	0.26	125.45	185.41	5.52	5.74	0.35	69.80	5.00
min.	232.30	0.23	112.98	142.60	-7.79	5.32	-0.17	45.40	-3.83
average	249.26	0.24	120.66	166.56	-1.96	5.48	0.02	55.52	-0.44

Notes: ¹ Average transmembrane pressure; ² Average normalized permeability slope; ³ Average normalized permeability; ⁴ Diluted sludge volume index; ⁵ Diluted sludge volume index slope; ⁶ Mixed liquor suspended solids; ⁷ Mixed liquor suspended solids slope; ⁸ Chemical oxygen demand (filtered); ⁹ Chemical oxygen demand slope.

Full prediction with the identification of outliers was used. The X-matrix included DSVI, MLSS, COD, and their slopes; whereas the response Y was the rate of the average normalized permeability change. The following results were obtained (Figure 4.6).

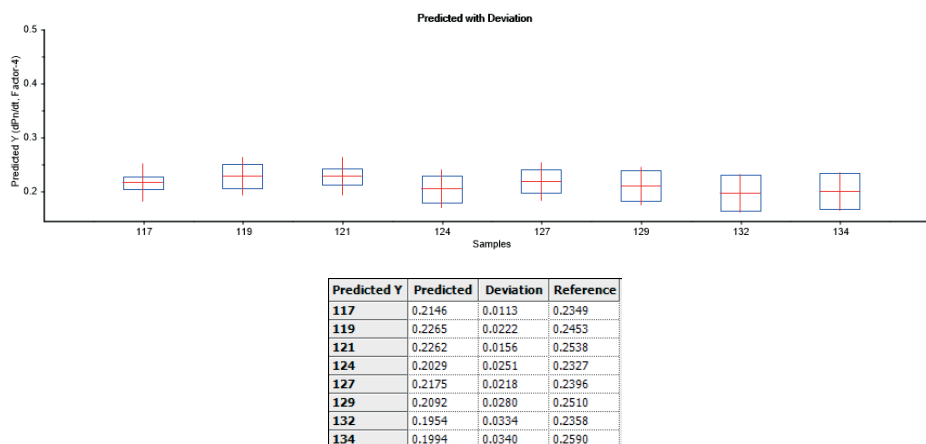


Figure 4.6 Prediction results for the new data from Period C for four factors using the derived PLS model for the relevant period. From **Paper II**.

The deviation between the predicted and the reference values is in the range 0.01–0.034, which demonstrates a good prediction ability of the developed model and its reliability under the operating conditions, that were applied during period C.

The multiple linear regression (MLR) analysis was also performed for the obtained dataset, however, due to the superiority of the PLS method, the first one was excluded from further consideration. More details on this topic were provided in **Paper II**.

Solids retention time (SRT) was found to be among the key operational parameters, which control membrane fouling in the MBR and BF-MBR systems [23,141,142]. In order to estimate the influence of SRT on the analysed BF-MBR pilot system, this parameter was included as a predictor variable into the models, which describe every one of the investigated periods (Figure 4.7).

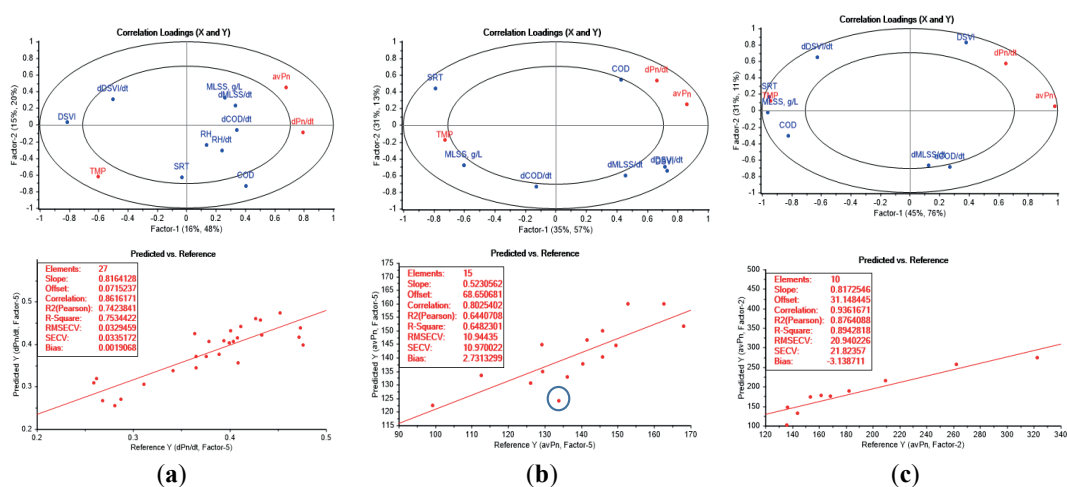


Figure 4.7. Results of PLSs of the data from all the periods of the filtration performance monitoring, including SRT: (a) period A (SRT = 20 days); (b) period B (SRT = 31 days); (c) period C (SRT = ∞). (Notes: SRT is the solids retention time in the relevant period, ∞ stands for no sludge discharge.). From **Paper II**.

According to the correlation loadings plot related to period A (Figure 4.7a), SRT explains less than 50% of the variance, and thus has relatively lower significance. SRT exhibits an independent variation in relation to other variables, except for COD and TMP. COD has a weak positive link with SRT along Factor-2, whereas SRT exhibits a slight positive correlation with TMP.

The results related to period B (Figure 4.7b) demonstrate that for the system at the applied operation settings, SRT is a significant variable, which explains more than 50% of the variance in the dataset. It has a strong negative correlation with COD and the normalized permeability and its slope along Factor-1. In addition, SRT is positively correlated with MLSS

and TMP along Factor-1. The negative correlation between SRT and COD during this period can be attributed to the higher treatment performance of the biomass, which becomes well-developed at SRT up to 40 days, and thus is capable of a more efficient biodegradation of organic contaminants, reduced microbial death, and less production of SMP_e (polysaccharides), causing the decrease of COD values [143]. Meanwhile, the increase in SRT promotes the development of higher MLSS concentrations and the increase in TMP, hence indicating fouling triggering through the increase of MLSS at higher SRTs.

Concerning the validation plots for the models, which describe period A and period B (Figure 4.7a,b), the introduction of the new variable did not entail any significant improvement; moreover, it slightly weakened the prediction accuracy of the selected models, which was reported in detail in **Paper II**.

The PLS analysis of the dataset from period C demonstrates the SRT variable explains more than 50% of the variance, and thus is significant (Figure 4.7c). SRT is highly positively correlated with MLSS, dDSVI/dt, COD, and TMP and is negatively linked to normalized permeability and its slope. Thus, the increase in SRT to the infinite values (no sludge discharge) promotes the development of higher MLSS and COD, and worsens biofloculation (expressed through dDSVI/dt) [142], hence inducing membrane fouling.

Based on the developed PLS models, starting from 31 days of SRT, a high negative correlation between SRT and the permeability indicators and high positive link between SRT and TMP were observed (Figure 4.7b,c). Hence, SRT equal to 31 days was found to be the critical SRT, which designated the phase of the severe membrane fouling, whereas SRT of 20 days was identified as optimum for the stable work of the studied system. Apart from SRT, the permeate net flux was kept below its critical value (12–15 LMH). The return activated sludge (RAS) pumping intensity was also adjusted to control MLSS and to assure the sufficient level of COD and NH₄⁺ removal. More details on the control of operational conditions in the studied system are provided in **Paper II**.

In order to automate the monitoring of the MLSS concentration, it was decided to establish the correlation between the experimental measurements of MLSS according to the dry residue test 2540 D [144] in the membrane separation (which were used for development of the PLS models) and MBBR chambers (MLSS-II); and the values obtained using the suspended solids/turbidity sensor Ponsel MES5 (AQUALABO, France) mounted in the MBBR chamber. After excluding the outliers, the correlations, represented in Figure 4.8, were obtained.

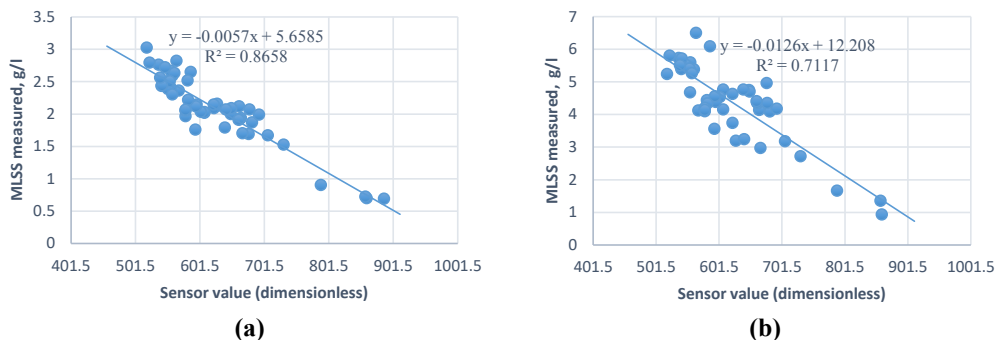


Figure 4.8 The correlation curves between the MLSS values in the MBBR chamber obtained through the sensor and experimentally determined MLSS values in: (a) MBBR chamber, (b) separation chamber.

According to the obtained correlation models, the measurements of the sensor for the detection of the MLSS in the MBBR chamber are the most reliable in the range 1.5–3 g/L (Figure 4.8a), whereas the indication of the MLSS values in the separation chamber is the most accurate in the range of MLSS 2.7–5.8 g/L (Figure 4.8b) since there is a sufficient amount of data in the selected areas. These models were further used for the automated monitoring of the MLSS levels in the MBBR and MBR chambers of the BF-MBR pilot system based on the measurements of the sensor Ponsel MES5, using the query in MS Access, established by Dr. Daniel Todt.

Discussion

By using multivariate chemometric analysis, the current work encapsulates the relationship between the mixed liquor characteristics, membrane fouling indicators, and the operational conditions in the BF-MBR pilot system with ceramic modules, and thus provides a comprehensive analysis of the system performance and the mechanisms for influencing it. It is worth noting that no precedent in literature with regard to this type of approach to the investigation of fouling mitigation in the BF-MBR system was found.

COD, MLSS, and SVI were identified as the representative parameters of mixed liquor fouling propensity, while the relative hydrophobicity parameter should be replaced with a more accurate and less time-/recourse demanding alternative. The average normalized permeability was identified as the most reliable membrane fouling indicator. The validated mixed liquor parameters, except for DSVI, and membrane fouling indicator were used at the further stages of this research to assess and predict biomass fouling propensity and membrane fouling extent in the BF-MBR system with chemical flux enhancement.

The introduction of SRT to the models helped to understand its influence on the mixed liquor fouling propensity. A positive correlation between SRT and MLSS in the models for

period B and period C agrees with the previous findings by Le-Clech et al. [145], Van den Broeck et al. [142], Yigit et al. [146]. During period C, the positive link between SRT and COD can be attributed to the release of small microbial SMPs, i.e., polysaccharides (SMP_c), at high SRTs (>31 days) [109,114,146]. The value of the optimum SRT of 20 days agrees with the previous studies [109,143].

The automation of the MLSS measurements in both MBBR and separation chambers helped to advance the monitoring process of suspended solids concentration.

The obtained results allowed for adjusting the operational parameters of the BF-MBR pilot system according to the characteristics of biomass, keeping the system running below critical transmembrane pressure (500 mbar), with 67–90% removal of chemical oxygen demand, 100% retention of suspended solids, and permeate turbidity 0.1–1.1 NTU. Besides, a good recovery of membrane permeability, and thus efficient removal of irreversible fouling, was attained after chemical cleanings.

4.3 The concept of the chemical flux enhancement based on the comparative mechanistic assessment of the Al- and Fe-based coagulants, multivariate chemometric approach, and optimisation analysis: Paper III

The main motivation to conduct this study was a huge potential of BF-MBR technology coupled with chemical flux enhancement, which still remained beyond the comprehensive investigation due to the complexity of the underlying processes. In order to develop a stable and robust system, the prediction of the reduction of the mixed liquor fouling propensity and optimization of the coagulant dosing were required. This could be achieved only after the identification of the mechanisms of the fouling mitigation by the applied coagulants. The parameters of mixed liquor, which are representative with regard to the demonstration of its fouling propensity (MLSS, COD_{dis}), as well as the most reliable fouling indicator (average normalized permeability), identified in **Paper II**, were used in the current study. Besides, the BF-MBR pilot system, which was used as the source of mixed liquor for the current study, was operated at the levels of the operational parameters (SRT, permeate flux, the intensity of sludge recirculation), which facilitate lower fouling intensity, adjusted according to the results of **Paper II**.

During the investigation, conducted in **Paper II**, the floc relative hydrophobicity (RH) parameter, determined through the MATH method, was considered as time- and effort-demanding procedure. And according to PLS analysis, RH appeared to be a weak indicator of the mixed liquor fouling propensity, explaining less than 50% of the variance in the dataset,

in contrast to the evidence of the tight link between the relative hydrophobicity of the flocs and membrane fouling from the literature. During the analysis of the data acquired from the investigated in **Paper II** BF-MBR pilot plant, the study in **Paper III** identified, that CST parameter, except for its link to dewaterability of the sludge flocs, is characterised by high negative correlation with their relative hydrophobicity (the loadings plot in Figure 4.9).

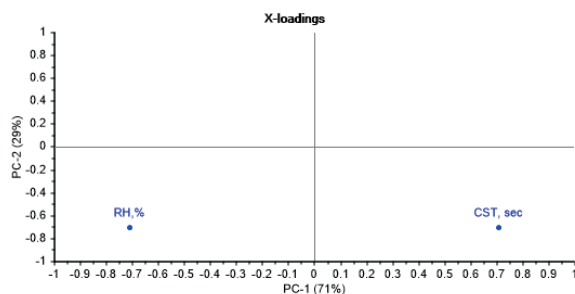


Figure 4.9 A negative correlation between capillary suction time (CST) and relative hydrophobicity (RH) earlier obtained for BF-MBR mixed liquor studied in **Paper II**. From supplementary material of **Paper III**.

This additional valuable property of CST allowed for using this parameter as the indicator of the relative hydrophobicity of flocs in **Paper III**.

In **Paper III**, the following sequential strategy was developed to conduct a holistic assessment of the Al- and Fe-based coagulants as membrane flux enhancers for the BF-MBR system (Figure 4.10).

First, the jar tests were conducted to identify the optimum pH for every coagulant with regard to flux enhancement and then the optimum dosage range. The jar tests were followed by the total recycle test with pH correction, in order to identify the most efficient coagulant with regard to flux enhancement and to determine its concrete optimum dose. Then, the total recycle tests without the pH adjustment were performed so as to compare the obtained results with the pH-controlled process and justify/refute the need for the pH control during chemical flux enhancement. The results of both stages of total recycle test were used as the raw dataset for the PLS analysis, which helped to identify the significant variables, build the model for the prediction of fouling mitigation, and determine the governing mechanisms of action of every studied flux enhancer. The reasons for the observed performance of flux enhancers were explained by the determination of their intrinsic properties. Eventually, the most efficient flux enhancer was selected and used for the two-level factorial design of experiment for the identification of the factors with the most significant effects, the tendencies in their interactions, and optimization of the filtration process. The whole procedure is described in a more detailed way in **Paper III**.

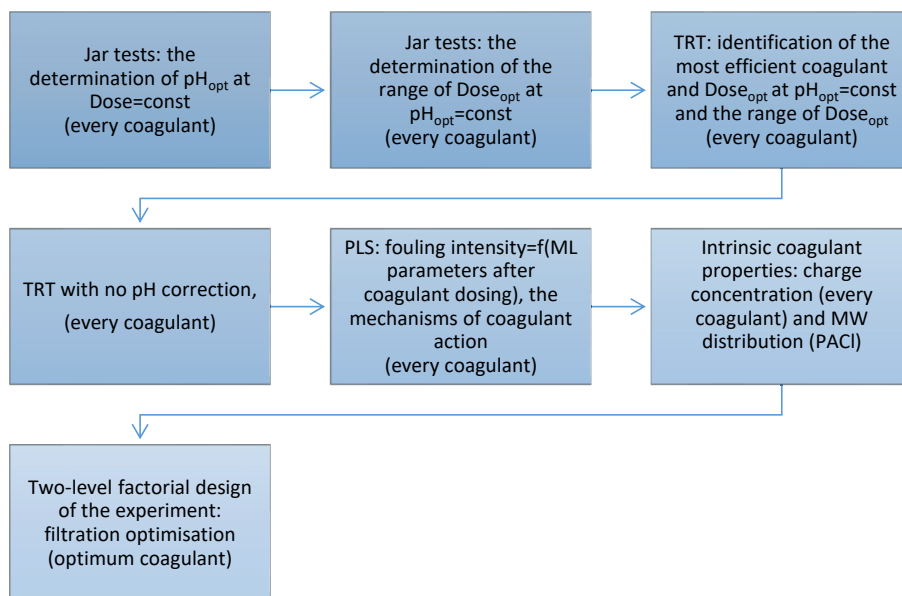


Figure 4.10 The stepwise strategy for the assessment of the selected flux enhancers (Notes: “Dose” stands for coagulant dose, the subscript “opt” means optimum, “MW” stands for molecular weight, TRT means total recycle test, PACl is prepolymerized aluminium chloride.).

Based on the literature findings, reported in **Paper III**, it was decided to choose zeta potential, turbidity, capillary suction time as the indicator of relative hydrophobicity of the flocs, and the mean particle size (expressed through the volume moment mean) as the basic indicators for the mixed liquor fouling propensity during the jar tests. Meanwhile, these parameters, altogether with the parameters of wastewater treatment quality and the auxiliary time-to-filter indicator, were used for a more comprehensive assessment of the coagulant performance during the targeting total recycle tests.

Coagulant action is pH dependent, therefore the determination of the optimum pH of every tested coagulant with regard to flux enhancement is required prior to the comparative analysis. The relevant analysis was conducted by varying the pH conditions while applying a constant dose of the coagulant — $0.4 \mu\text{molAl}/\text{mgSS}$ for the Al-based coagulants and $0.9 \mu\text{molFe}/\text{mgSS}$ for the non-prepolymerized iron (III) sulphate at MLSS of the raw mixed liquor 5.9–6.2 g/L (Figure 4.11).

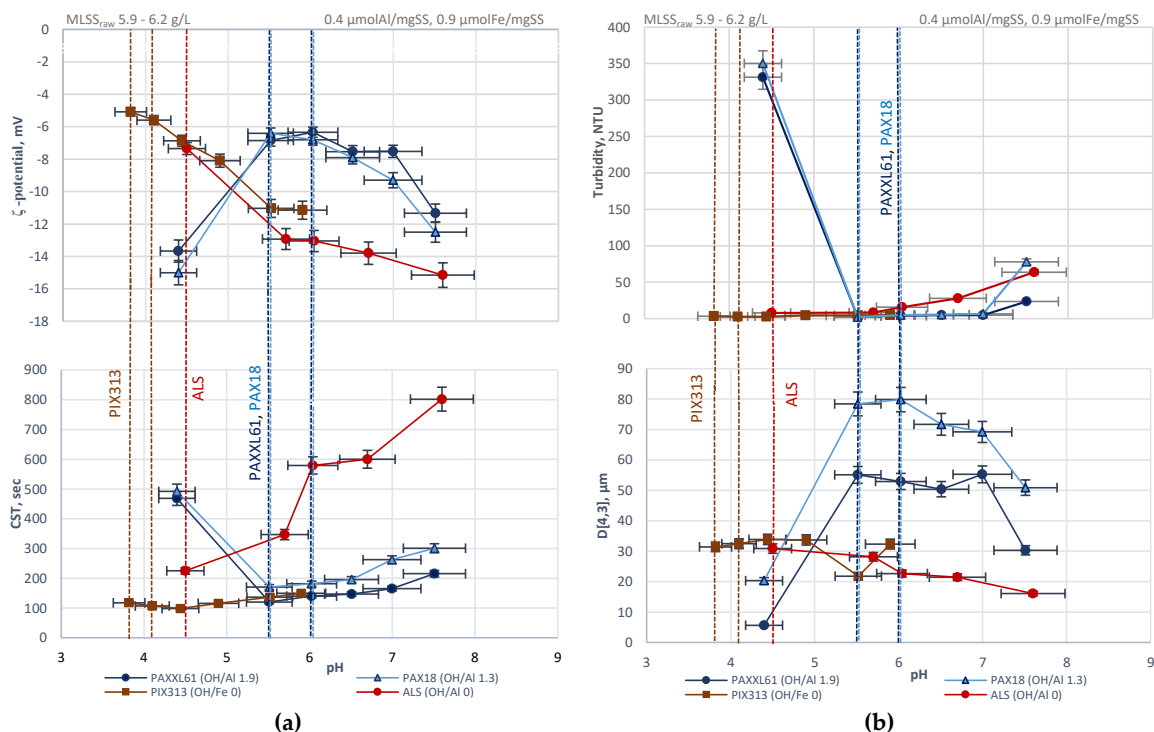


Figure 4.11 Determination of the optimum pH with regard to flux enhancement at fixed coagulant dose during the jar tests according to: (a) zeta potential, CST; (b) turbidity, the volume moment mean. From **Paper III**.

According to the obtained graphs, the optimum pH values with regard to flux enhancement (those, which resulted in the lowest residual turbidity, highest floc relative hydrophobicity (lowest CST), the maximum reduction of the absolute zeta potential values, and the highest increase of the mean particle size ($D[4,3]$)) were the following (marked with the dashed lines in Figure 4.11 for every flux enhancer): pH 5.5 – 6.0 for two prepolymersed aluminium chloride coagulants; pH 4.5 for aluminium sulphate; and pH 3.8 – 4.1 for iron (III) sulphate.

Then, the determination of the optimum dosage range for flux enhancement at the constant optimum pH levels with regard to every coagulant was performed. The results are presented in Table 4.6.

According to the obtained results (Table 4.6), prepolymersed aluminium coagulants were characterised by broader dosing ranges, higher degree of charge neutralization, less turbid effluents, and relatively higher degree of flocculation than their non-prepolymersed counterparts.

Table 4.6 Optimum dosages with respect to flux enhancement obtained at the corrected pH values applying tested coagulants during the jar tests (MLSS_{raw} 5.8-6.2 g/L). From supplementary material of **Paper III**.

Chemical	Maintained pH	Parameters				Optimum dosage ranges, $\mu\text{mole Me/mgSS}$
		CST, sec	Zeta potential, mV	Turbidity, NTU	D [4,3]	
PAXXL61 (OH/Al 1.9)	5.5 – 6.2	45.8 – 60.7	-1.1 – 3.7	0.5 – 1.8	25.6 – 32.6	1.1 – 2.6
PAX18 (OH/Al 1.3)	5.5 – 6.0	75.1 – 77.7	-3.7 – (-2.5)	0.5 – 1.1	37.5 – 67.4	1.3 – 2.6
ALS (OH/Al 0)	4.4 – 4.5	81.2 – 103.0	-4.6 – (-3.7)	1.8 – 2.5	21.0 – 34.3	0.5 – 1.2
PIX313 (OH/Fe 0)	4.0 – 4.1	130.0 – 150.0	-3.9 – (-3.5)	2.0 – 2.6	16.4 – 24.9	2.2 – 3.2

In order to avoid under- or overdosing, which can deteriorate the treatment efficiency, the determined ranges of optimum dosages were further applied during the TRT experiments. The results of the monitoring of wastewater treatment quality during the TRT are represented in Figure 4.12.

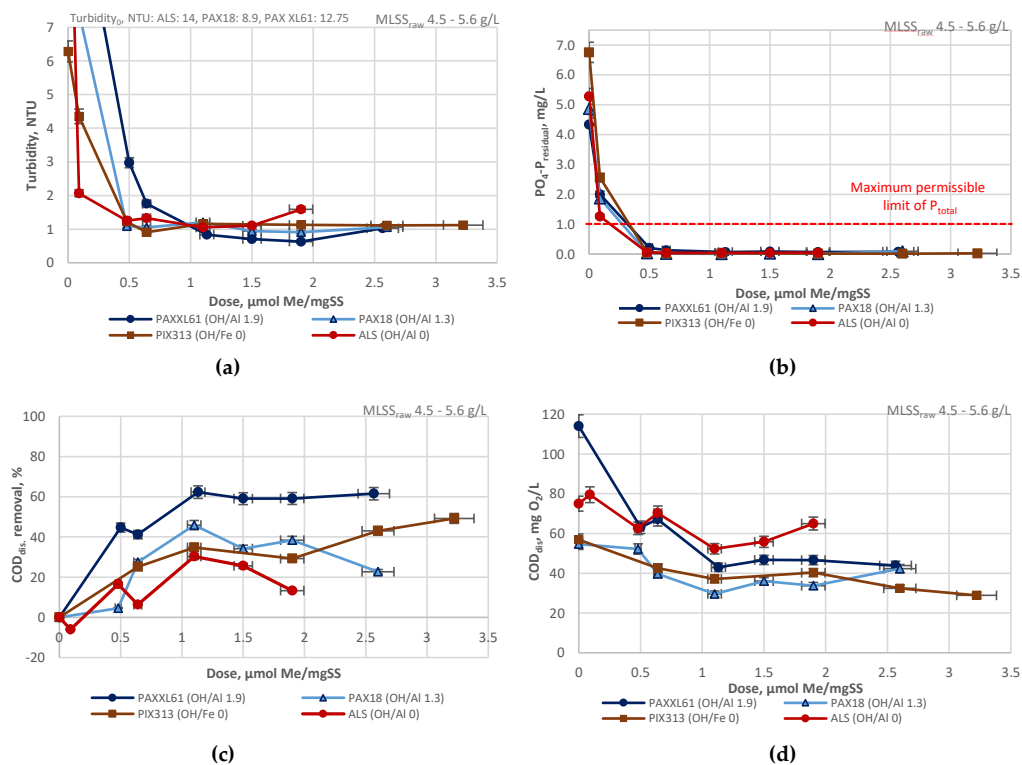


Figure 4.12 Influence of the coagulant dose on the monitored parameters at fixed pH during the TRT: (a) turbidity; (b) residual orthophosphates; (c) COD_{dis} removal, (d) COD_{dis} . From **Paper III**.

The graphs, represented above, demonstrate, that with respect to the wastewater treatment quality, the use of coagulants provides the compliance of the system with the regulations on the residual phosphorus and COD_{dis} . It is worth noting that COD_{dis} in the raw mixed liquor was the residual COD_{dis} concentration after the biological treatment at the MBBR stage of the

BF-MBR pilot system when the latter one provided the treatment efficiencies in terms of COD_{dis} removal equal to 67.0–92.0%. The detailed description and analysis of the represented plots (Figure 4.12) are provided in **Paper III**.

Another valuable property of COD_{dis} parameter in relation to MBR and BF-MBR is that it is an indicator of the SMPs content in mixed liquor based on the literature, represented in **Paper II** and **Paper III**. Hence, COD_{dis} also indicates the fouling propensity of mixed liquor, and with regard to chemical flux enhancement, the ability of the coagulants to reduce fouling intensity. According to obtained results (Figure 4.12c), the ranking trend among the studied coagulants in decreasing order of dominance of SMPs removal mechanism based on COD_{dis} removal, can be classified as: PAXXL61 > PAX18 = PIX313 > ALS, which corresponds to the findings of the previous works [128,136,147]. A more detailed description of the manual data-driven sample grouping regarding COD_{dis} removal is provided in **Paper III**.

In addition to the results, demonstrated above, the experiments on the residual aluminium concentration after using Al-based coagulants were performed (not shown here). According to the obtained results (described in **Paper III**), the use of aluminium sulphate at the dosages, higher than 0.5 µmolAl/mgSS, as well as the use of the prepolymerized aluminium chloride of the medium basicity in the overdosing region (2.6 µmolAl/mgSS), generates supernatant, whose characteristics do not comply with the regulations on the permissible aluminium in the drinking water and the criteria for water reuse [144,148–150]. Thus, the discharge of this supernatant is undesirable from the environmental point of view. The best results, which were below the regulatory limits, were provided by both prepolymerized aluminium coagulants in the range 0.5–1.9 µmolAl/mgSS.

The detailed description of the determination of the membrane fouling indicators (average normalized permeability, $_{av}P_N$, and filtration time, F) during TRT is provided in **Paper III**.

The development of fouling intensity depending on the coagulant type and dose at the fixed pH (optimum for every coagulant) is demonstrated below (Figure 4.13).

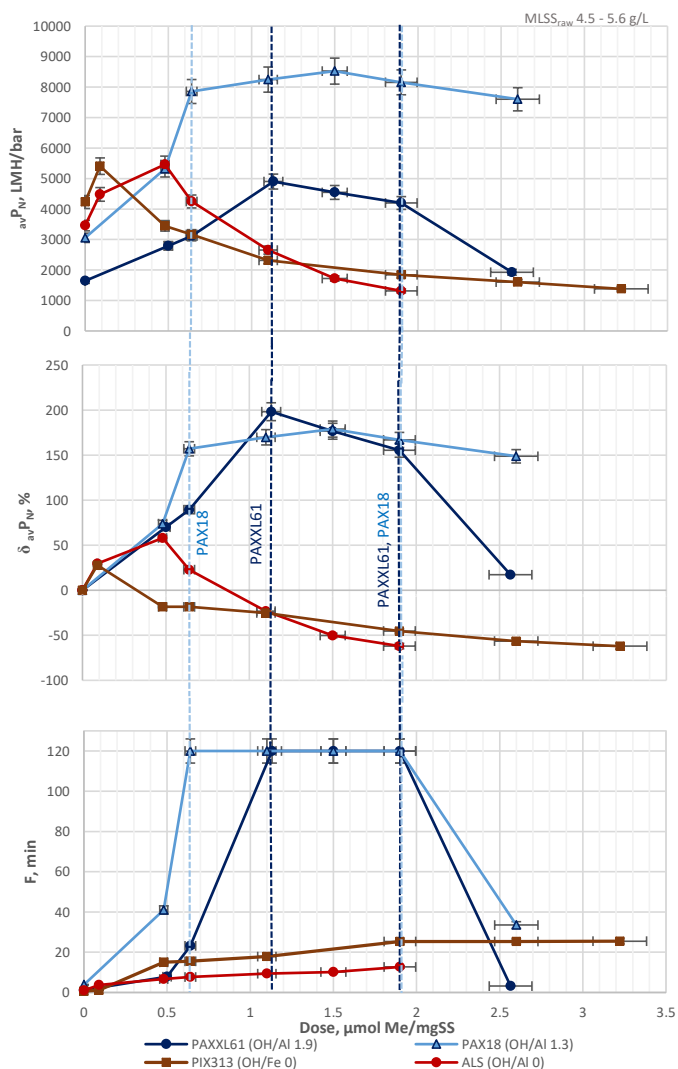


Figure 4.13 Relationship between the coagulant dose and the filtration performance according to normalized permeability, normalized permeability change, and filtration time at fixed pH during the TRT. From **Paper III**.

According to the graphs above (Figure 4.13), the prepolymerized aluminium coagulants provided the greatest extent of fouling mitigation among the studied flux enhancers: the maximum filtration time (F) equal to 120 min and the maximum increase of average normalized permeability ($\delta_{av}P_N$) by 155.0–198.0%. In relation to the BF-MBR pilot system, these results correspond to a tenfold increase in filtration time of the membrane separation cycle and 30.0–56.0% higher net flux (depending on the operational period), in comparison to the net flux in this system without the PACl dosing.

The broader range of optimum dosages and a lower dose, required to reach the region with maximum values of the response functions (Figure 4.13), indicated that prepolymerized aluminium chloride with medium basicity (PAX18) is superior with respect to fouling mitigation than its counterpart with high basicity (PAXXL61). Therefore, it was decided to use prepolymerized aluminium chloride with medium basicity for the two-level factorial design of the experiment and at the further stages of this research.

The demonstrated in Figure 4.12 results suggest that with regard to removal of COD_{dis} , orthophosphates, and turbidity, — the parameters, which are commonly considered as the basic monitored parameters at the wastewater treatment plants and during the standard procedure of the jar tests, all four coagulants provide a sufficient quality of wastewater treatment. However, during the comparison of the above-mentioned results of wastewater treatment quality with the fouling mitigation capacity of every coagulant (Figure 4.13), it is apparent that merely the first ones are not sufficient for the comprehensive evaluation of the coagulants as flux enhancers. Therefore, there was a need to identify and monitor the reliable parameters of the mixed liquor fouling propensity.

The highest efficiency of the prepolymerized aluminium chloride with medium basicity during the filtration experiments is predominantly attributed to a greater adsorption/charge neutralization potential of this species over its counterpart with high basicity, expressed through a more rapid increase of zeta potential in the overdosing region (Figure 4.14a); and enhanced flocculation, which was indicated by the mean particle size profile (Figure 4.14d).

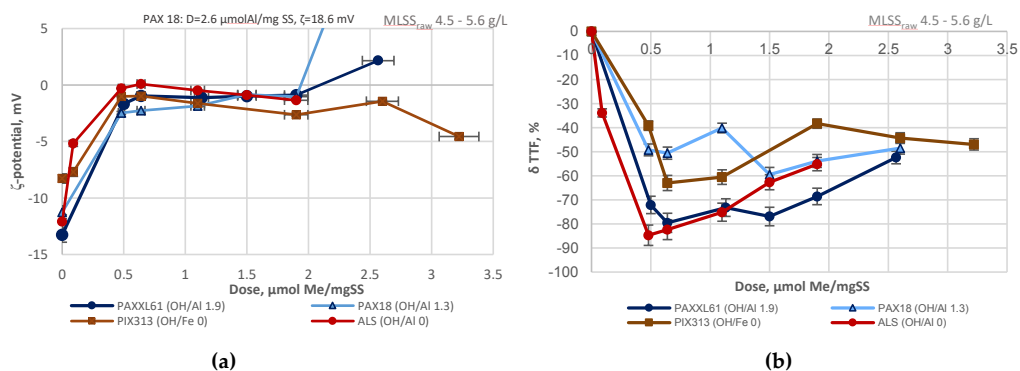


Figure 4.14. Cont.

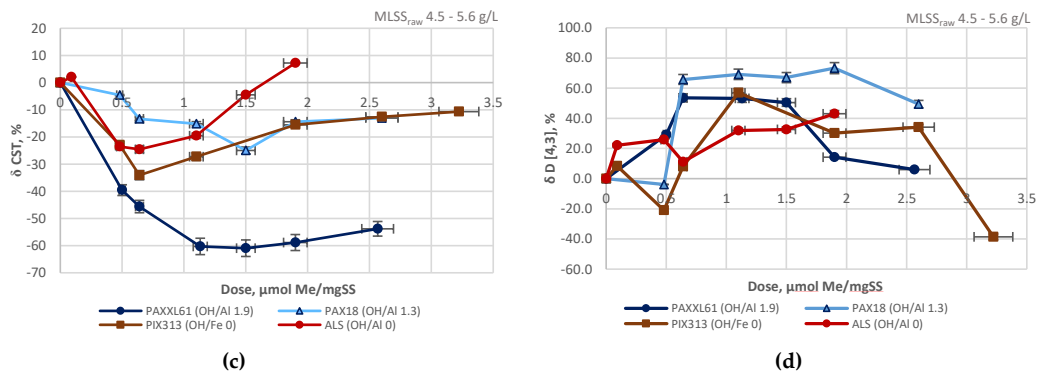


Figure 4.14. Influence of the coagulant dose on the monitored parameters at fixed pH during the TRT: (a) zeta potential; (b) TRT change, (c) CST change; (d) volume moment mean change. From **Paper III**.

According to Figure 4.14b, prepolymerized aluminium chloride with high basicity (PAXXL61) as well as the non-prepolymerized aluminium sulphate (ALS), exhibited the highest potential for improving mixed liquor filterability, expressed through the TTF parameter.

With regard to the increase of the mixed liquor relative hydrophobicity, expressed via the decrease of the capillary suction time (Figure 4.14c), prepolymerized aluminium chloride of high basicity provided the most significant changes.

The TRT experiments without pH correction resulted in higher coagulant doses, required for the achievement of the optimum filtration; and relatively low improvement of membrane filtration, in comparison to the results of TRT with pH correction. Higher coagulant dosages entail higher operational costs and excess sludge production. Consequently, pH adjustment is considered a valuable tool in the optimization of the fouling mitigation in BF-MBR based on the addition of coagulants as flux enhancers.

A more thorough analysis of all acquired plots, as well as the comparison of the results of TRT applying pH control with TRT with non-corrected pH, is given in **Paper III**.

The investigation of the coagulant characteristics, i.e., charge concentration and molecular weight distribution, was performed in order to identify the prerequisites for the dominance of charge neutralization mechanism in studied coagulants. The results of the potentiometric back titration of the studied coagulants and potentiometric direct titration of mixed liquor are represented below (Figure 4.15).

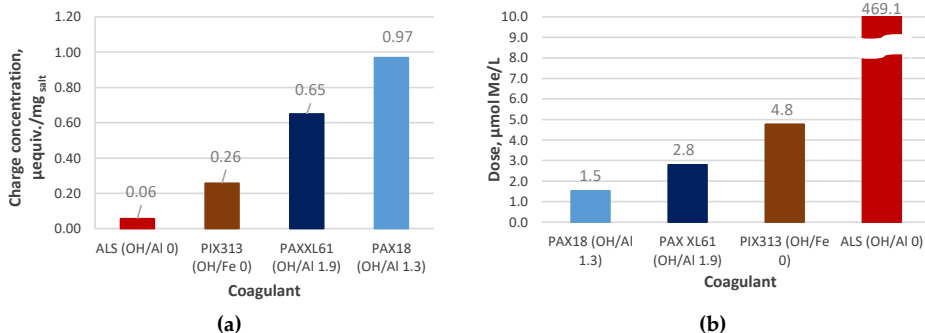


Figure 4.15 The results of the potentiometric titration experiments: (a) charge concentrations of the studied coagulants determined during their back titration; (b) coagulant dose, required for reaching the endpoint during the direct titration of mixed liquor. From **Paper III**.

According to the acquired charts (Figure 4.15), prepolymerized aluminium chloride coagulants have the highest charge concentrations, which correspond to their high efficiency regarding the increase in average normalized permeability and filtration time (Figure 4.13). Meanwhile, the charge concentration of prepolymerized aluminium chloride with medium basicity (PAX18) is higher than the charge concentration of its counterpart with high basicity (PAXXL61). This effect can be entailed by the incorporation of SiO_2 group in the skeleton of prepolymerized aluminium chloride with high basicity. Due to its neutrality, silica group potentially decrements the coagulant charge concentration and results in the reduced content of the active polymeric $\text{Al}_{13}^{\text{nt}}$ component and increased concentration of monomeric octahedral Al_1 species in the coagulant structure, which decreases its adsorption/charge neutralization potential [151–154].

The charge concentrations of the non-prepolymerized coagulants were significantly lower, in comparison to the prepolymerized coagulants, which correlates with the character of the fouling mitigation profiles of the selected coagulants according to Figure 4.13.

With regard to the molecular weight distributions of the collected fractions of the studied prepolymerized aluminium coagulants, the relevant size exclusion chromatograms are represented and analysed in detail in **Paper III**. According to the obtained chromatography profiles, high MW isolate of the prepolymerized aluminium chloride (PACl) with high basicity was obtained 36 min earlier than the respective isolate of its counterpart with the medium basicity, (i.e., the first coagulant had higher MW fractions in comparison to the latter one). Nevertheless, high MW isolates constituted less than half of the total Al concentration in the prepolymerized aluminium chloride with high basicity, which suggests they might not be the predominant contributor to the overall MW, and hence to the charge concentration of the relevant compound. Meanwhile, the constituents with the low molecular weight constitute

35% of the total aluminium in the structure of PACl with high basicity. This evidence confirms the hypothesis on the elevated concentration of the monomeric Al_1 species in the structure of PACl with high basicity, and hence its lower adsorption/charge neutralization potential. This effect potentially results from the partial hindering of the formation of the active polycation Al_{13}^{n+} in the coagulant structure by SiO_2 groups during its prepolymerization phase, which should be the subject of further investigations.

The partial least squares analysis was performed based on the data from the total recycle tests with and without pH correction. The variable dataset consisted of the information on the MLSS of mixed liquor before the chemical dosing ($MLSS_{in}$), pH, zeta potential, coagulant dose (Dose), turbidity, CST, and the parameters of the particle size distribution (i.e., $D[4,3]$, $D[3,2]$, span, uniformity). The average normalized permeability (avP_N) and filtration time (F) were selected as the responses in the model. The obtained model was validated by applying random cross-validation in PLS. During the cross-validation, the dataset was divided into 20 segments. Some elements were taken out of analysis since they were indicated as potential outliers. The number of PLS components (factors) was chosen according to the explained variance. The obtained results are demonstrated below (Figure 4.16).

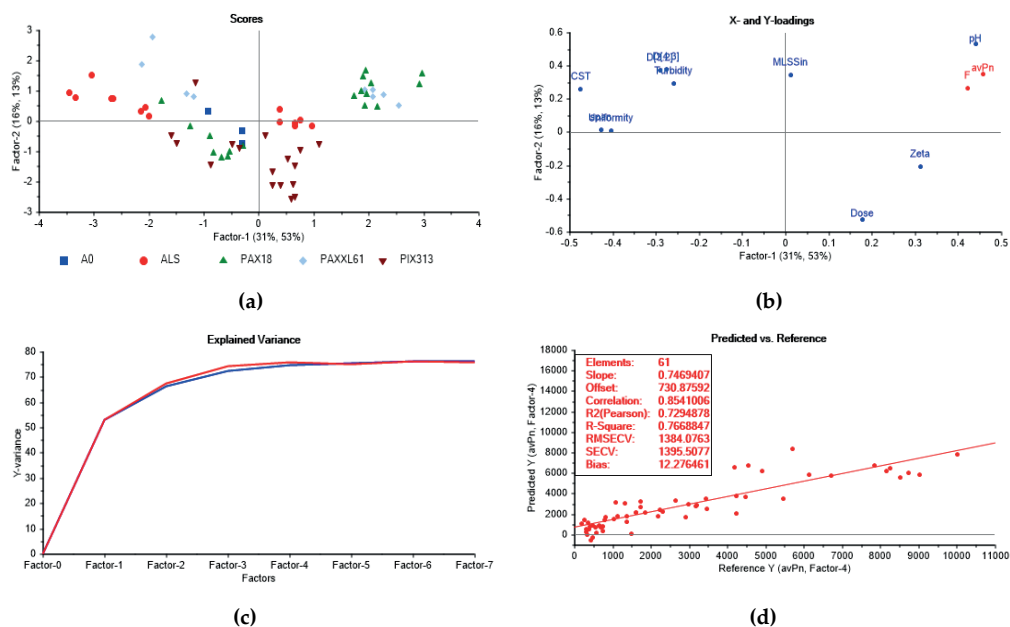


Figure 4.16 Results of PLS of the data from the TRT - regression overview: (a) scores plot; (b) loadings plot; (c) total residual variance plot; (d) fouling intensity prediction model. From **Paper III**. (Notes: PAX18 and PAXXL61 stand for the prepolymerized aluminium chloride with medium and high basicity, respectively; A0 stands for the raw mixed liquor samples without coagulant dosing; PIX313 is iron (III) sulphate; ALS is aluminium sulphate.)

The scores plot revealed four distinctive clusters: the mixed liquor samples treated with the prepolymerized aluminium chloride of medium (PAX18) and high (PAXXL61) basicity, non-prepolymerized aluminium (ALS) and iron (III) sulphate (PIX313). Samples within a cluster contained similar samples. The difference between the clusters is explained by Factor-1 and Factor-2. According to the PLS loadings plot (Figure 4.16b), Factor-1 clearly describes span, uniformity, CST, zeta potential, pH, filtration time (F), and the average normalized permeability ($_{av}P_N$). Factor-2 apparently accounts for D[4,3], D[3,2], turbidity, MLSS_{in}, and coagulant dose.

From the loadings plot, all the variables appeared to be significant. Span, uniformity D[4,3], D[3,2], CST, and turbidity are positively correlated with each other. These correlations give a promising prospect of the future CST determination via the soft sensor based on the automated monitoring of particle size distribution parameters (which can be measured online using laser diffraction particle size analyzer) and turbidity. Meanwhile, span, uniformity D[4,3], D[3,2], CST, and turbidity exhibit a negative correlation to zeta potential, coagulation dose, pH, and the response functions along Factor-1 and Factor-2. The coagulant dose is positively correlated with zeta potential, whereas pH is positively linked to the response functions.

According to the total explained variance plot (Figure 4.16c), the highest explained Y-variance (76%) is attained while applying four factors and then reaches a plateau.

The validation plot (Figure 4.16d) indicates the linearity of the developed model (i.e., R-squared value of 0.77) and its good fit for the majority of data (i.e., slope = 0.75). The developed model has a relatively low bias equal to 12.3 LMH/bar, indicating that it has a low tendency to over- or underestimate the validation values, which is highly essential during the further implementation of the model. If the model had high bias, the overestimation of the response functions would cause severe fouling development (which is detrimental for the equipment since the BF-MBR pilot system works at constant permeate flux); whereas the underestimation of the response functions would result in the unnecessary increase of coagulant dosing (entailing the shift of the system to the overdosing region). Hence, the developed model demonstrates a good prediction of the bound EPSs removal during the addition of the selected flux enhancers. The obtained results prove reliability and high potential of this model to be used during further stages when the operating conditions applied in this work are replicated.

The data-driven sample grouping, focused on the determination of the prevailing mechanisms of the floc-bound EPSs removal, which govern the behaviour of every coagulant,

was automatically performed by equally dividing the band of the targeted parameter values in the whole range between the upper and lower limits into five groups. As a result, the relevant ranges were generated (Figure 4.17).

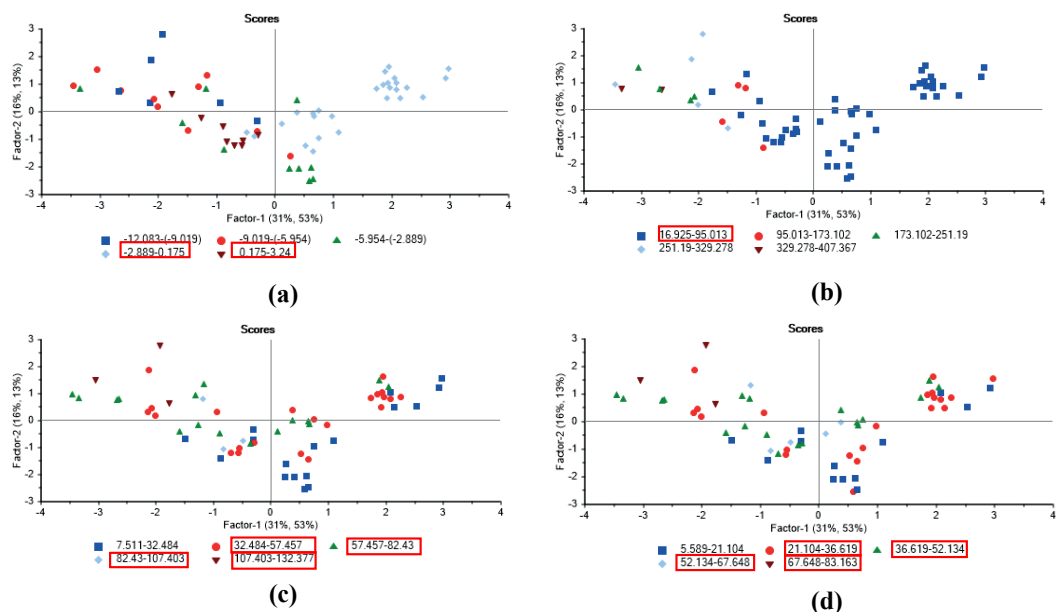


Figure 4.17 Results of PLS for the tested membrane flux enhancers – scores plot with the sample grouping according to: (a) zeta potential; (b) CST; (c) D[4,3]; (d) D[3,2]. From **Paper III**.

The selection of the targeted levels of interest (marked with the red rectangles in the legends in Figure 4.17) was congruent with the main mechanisms of fouling control: adsorption/charge neutralization (preferential decrease of zeta potential absolute value), the increase of relative hydrophobicity of the flocs (the decrease of dewaterability), and the increase of the mean particle size. According to the obtained PLS scores plot (Figure 4.17), the ranking trend among the studied coagulants, in decreasing order of dominance of each particular fouling mitigation mechanism, can be classified as:

- enhanced adsorption/charge neutralization (zeta potential -2.9 – 3.2 mV): PAX18 (100% of all PAX18 samples) > PAXXL61 (55.6%) > PIX313 (41.0%) > ALS (36.0%);
- the increase of relative hydrophobicity of the flocs (CST 17 – 95 sec): PAX18 (100%) > PIX313 (82.0 %) > PAXXL61 (56.0%) > ALS (43.0%);
- the increase in particle size (D[4,3] 32.5–132 μm /D[3,2] 21–83 μm): ALS (100%/100%) > PAX18 (78.0%/94.0%) > PAXXL61 (78.0%/78.0%) > PIX313 (41.0%/53.0%).

It was decided to denominate the mechanism of fouling inhibition as dominant if 55.0 % or more of a total number of the samples of every coagulant is characterized by the above-

mentioned ranges of the monitored parameters. As determined earlier (during the analysis of the TRT with pH correction), based on Figure 4.12c, the highest level of COD_{dis} removal (which is linked to the reduction of the SMPs content) was observed for the majority of samples of prepolymerized aluminium coagulants (PAXXL61 and PAX18) and iron (III) sulphate (PIX313). Consequently, the principal mechanism differs depending on the nature of flux enhancer (Table 4.7).

Table 4.7 Prevailing mechanisms of action for the tested coagulants. From **Paper III**.

Mechanism of action	Enhanced adsorption/charge neutralization	The increase in relative hydrophobicity of the flocs	The increase in particle size	The reduction of the SMPs level
PAX18 (OH/Al 1.3)	+	+	+	+
PAXXL61 (OH/Al 1.9)	+	+	+	+
PIX313 (OH/Fe 0)		+		+
ALS (OH/Al 0)			+	

Notes: 1 “+” stands for the dominance of the selected mechanism during flux enhancement action of the particular coagulant.

The optimisation analysis was performed applying the prepolymerized aluminium chloride with medium basicity, which was the most effective flux enhancer among the studied compounds. Two two-level fractional factorial designs of the experiments were built with respect to the average permeability and filtration time as a response function. The main purpose was to determine the optimum combination of factor levels, that simultaneously satisfy the criteria of the maximum average permeability or filtration time for the chosen coagulant (i.e., optimisation of flux enhancement in BF-MBR). In addition, the analysis, of the factorial design of the experiment allows for the identification of how the selected factors interacted and individually affected the flux enhancement process.

To study the possible options of maximization of the average permeability and filtration time systematically, two separate two-level fractional factorial designs were set up on the key factors: pH, temperature, MLSS, and coagulant dose with two replicates (Tables 4.8 and 4.9).

Table 4.8 Factors and levels for two-level alternative factorial design. From **Paper III**.

Factor	Units	Low level	High level
pH	-	5.5	6.5
Temperature	°C	20	25
MLSS	g/L	4.0	6.0
D	μmolAl/mgSS	1.1	1.9

Table 4.9 Layout for a designed experiment. Adapted from **Paper III**.

	Factor 1	Factor 2	Factor 3	Factor 4	Response 1	Response 2
Run	A:pH	B:Temperature, C	C:MLSS, g/L	D:D, $\mu\text{molAl/mgSS}$	avP, LMH/bar	F, min
1	5.5	20	4.0	1.1	8725.6	120
2	6.5	25	6.0	1.9	6614.1	120
3	6.5	20	6.0	1.1	2055.5	120
4	5.5	20	4.0	1.1	8698.6	120
5	5.5	25	4.0	1.9	12204.9	120
6	5.5	25	6.0	1.1	7146.1	23.33
7	6.5	20	4.0	1.9	10020.4	15.2
8	6.5	25	6.0	1.9	6578.7	120
9	6.5	20	4.0	1.9	10046.9	16.4
10	6.5	25	4.0	1.1	11168.8	5
11	6.5	20	6.0	1.1	2024.6	120
12	6.5	25	4.0	1.1	11196.9	5.5
13	5.5	20	6.0	1.9	6827.6	25.5
14	5.5	25	6.0	1.1	7169.4	22.5
15	5.5	20	6.0	1.9	6859.4	26.3
16	5.5	25	4.0	1.9	12233.0	120

The preliminary analysis of the influence of the selected factors on the response functions was followed by the detection of the important effects among the variables and their interactions via a half-normal plot and Pareto chart. Then, the inspection of the ANOVA (analysis of variance) results was conducted and the following significant models were derived (Table 4.10).

Table 4.10 The final equations in terms of coded and actual factors used for the optimization of the selected response functions.

Response function	Model
	Coded factors ¹
avP, LMH/bar	$(avP)^{1.61} = 2.100 \cdot 10^6 - 1.779 \cdot 10^5 \cdot A + 4.292 \cdot 10^5 \cdot B - 9.187 \cdot 10^5 \cdot C + 2.691 \cdot 10^5 \cdot D - 1.923 \cdot 10^5 \cdot AC - 1.021 \cdot 10^5 \cdot AD$
F, min	$(F)^3 = 8.682 \cdot 10^5 - 3165.47 \cdot A - 1144.71 \cdot B + 3165.47 \cdot C + 1144.71 \cdot D + 8.598 \cdot 10^5 \cdot AC$
	Actual factors ²
avP, LMH/bar	$(avP)^{1.61} = -1.21741 \cdot 10^7 + 2.33256 \cdot 10^6 \cdot \text{pH} + 1.71694 \cdot 10^5 \cdot \text{Temperature} + 1.38853 \cdot 10^6 \cdot \text{MLSS} + 3.73531 \cdot 10^6 \cdot D - 3.84539 \cdot 10^5 \cdot \text{pH} \cdot \text{MLSS} - 5.10408 \cdot 10^5 \cdot \text{pH} \cdot D,$
F, min	$(F)^3 = 5.24848 \cdot 10^7 - 8.60441 \cdot 10^6 \cdot \text{pH} - 457.88285 \cdot \text{Temperature} - 1.03145 \cdot 10^7 \cdot \text{MLSS} + 2861.76781 \cdot D + 1.71962 \cdot 10^6 \cdot \text{pH} \cdot \text{MLSS}$

Notes: ¹ A is a coded value for pH, B is a coded value for temperature, C is a coded value for MLSS, D is a coded value for the coagulant dose, AC is a coded value for pH·MLSS, and AD is a coded value for pH·coagulant dose; ² D is a coagulant dose; avP stands for the average permeability; F is the filtration time required for reaching 1.2·TMP_{in}.

According to the obtained model for the prediction of the average permeability expressed through the coded factors, pH, MLSS, temperature, and coagulant dose (D) have the highest

impact on the average permeability. With regard to the model for the prediction of the filtration time, the interaction factor pH·MLSS has the highest influence on the response function, whereas the other factors have relatively identical impacts. It is worth noting that the equations expressed through the actual factors are only valid for making the predictions, while being not applicable for the determination of the relative impact of each factor since the coefficients are scaled to correspond to the units of each factor and the intercept is not at the centre of the design space [155].

Regression diagnostics, described in **Paper III**, was further performed to validate the derived models.

The interpretation of the derived models can be made by analysing the model graphs (Figure 4.18).

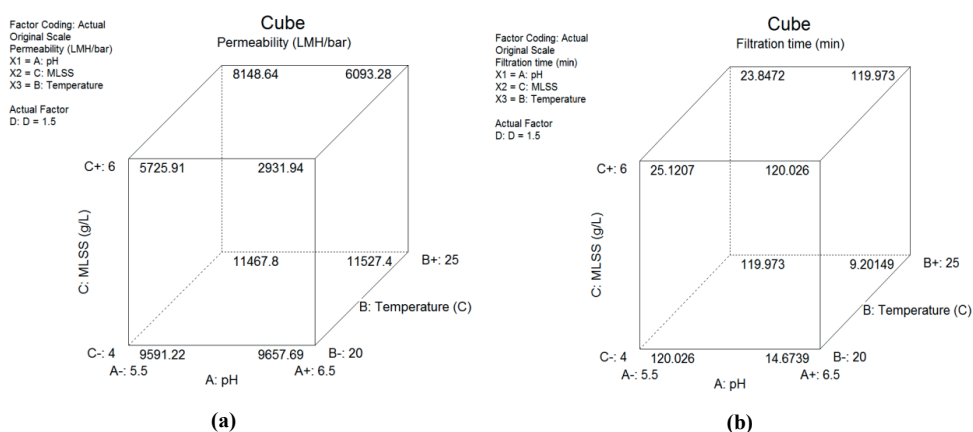


Figure 4.18 Model graphs (cube plots) of the analysed factorial designs ($k=3$, $D=1.5 \mu\text{molAl/mgSS}$) for the estimation of: (a) the average permeability, (b) the filtration time.

The cube plots (Figure 4.18) demonstrate the average predicted values of the response functions superimposed on the eight corners of the cube at the combinations of high and low levels of the three factors, that have significant effects: MLSS, pH, and temperature at the selected actual value of the coagulant dose ($1.5 \mu\text{molAl/mgSS}$ in the represented plots) [73,155].

With respect to the average permeability (Figure 4.18a), its highest levels 11467.8–11527.4 LMH/bar can be attained at the low level of MLSS (4 g/L) and high level of temperature (25 °C) (values calculated at $D = 1.5 \mu\text{molAl/mgSS}$). Meanwhile, pH has a minor positive effect on average permeability at the low level of MLSS and an adverse effect at a high MLSS level.

Concerning the filtration time (Figure 4.18b), an ambiguous effect of pH on the response function, which highly depends on the MLSS, was observed. At the low MLSS level (4 g/L), the increase of pH from 5.5 to 6.5 drastically reduces the filtration time from 120 to 9–15 min, whereas at the high MLSS level—6 g/L, the pH increase exhibits the opposite effect: the increase of filtration time from 23.8–25.1 to 120 min. In addition, a minor negative impact of temperature on the filtration time can be observed. According to the represented cube plot, the filtration time is maximum (120 min) in two scenarios (at the coagulant dose $D = 1.5 \mu\text{molAl/mgSS}$): (1) pH 6.5, $T = 20\text{--}25 \text{ }^\circ\text{C}$, MLSS 6 g/L; (2) pH 5.5, temperature (T) = 20–25 °C, MLSS 4 g/L.

The results of the numeric optimization, point prediction and confirmation are represented in **Paper III**.

Hence, the developed models can be used to determine the optimum conditions of the application of the prepolymerized aluminium chloride with medium basicity, which provide the highest yield of the average permeability and filtration time in accordance with the desired factor settings.

Discussion

The current part of the research demonstrates a great flux enhancing potential of the coagulants in the biofilm membrane bioreactor (BF-MBR).

The research was focused on the development of the concept of chemical flux enhancement in BF-MBR based on adsorption/charge neutralization mechanism, revealed from the comparative study of prepolymerized and non-prepolymerized inorganic coagulants through the chemometric approach to membrane fouling control and optimization of membrane filtration.

In the present study, the pH-controlled flux enhancement allowed for attaining efficient fouling mitigation with regard to the development of filtration indicators, i.e., average normalized permeability and filtration time (time, which is required for reaching $1.2 \cdot \text{TMP}_{\text{in}}$). Besides, in the system with pH adjustment, the optimum values of the filtration indicators were obtained at lower coagulant dosages in comparison to those, which were obtained during TRT with no pH correction (Table 5 in the supplementary material for **Paper III**). The following pH levels were identified as optimum with regard to flux enhancement during coagulant addition in BF-MBR: 5.5 – 6.0 for prepolymerized aluminium chloride coagulants, 4.5 for aluminium sulphate and 3.8 – 4.1 for iron (III) sulphate.

The investigation of the flux enhancing efficiency of aluminium sulphate in the BF-MBR without pH correction was also conducted by Maletskyi et al. [156] (who, however, expressed

their results with regard to filtration time required for reaching $1.5 \cdot \text{TMP}_{\text{in}}$). In the range of dosages, $0.95\text{--}1.5 \mu\text{molAl/mgSS}$, the recalculated filtration time required for reaching $1.2 \cdot \text{TMP}_{\text{in}}$ was equal to $3.17\text{--}3.83 \text{ min}$ [156]. These values are almost three times lower than the corresponding filtration times in the system with pH correction obtained in the current research — $9.33\text{--}10.17 \text{ min}$ (dosage range $1.1\text{--}1.5 \mu\text{molAl/mgSS}$ for ALS in Figure 4.13), which also supports the aforementioned conclusions on the beneficial impact of pH control on the chemical flux enhancement in BF-MBR.

In general, the results of the current research substantiate the need for pH-controlled flux enhancement in BF-MBR depending on coagulant type to provide a more complete coagulation according to Le Chatelier's principle, which influences charge, hydrophobicity, and size of flocs, the organic content of the system, and hence the filtration performance.

According to the calculations, the application of the non-prepolymerized aluminium and iron (III) coagulants during the total recycle tests in the present work was in the area of pH and coagulant dose (regions, coloured in red in Figure 4.19), where the system is oversaturated with regard to metal hydroxide [157].

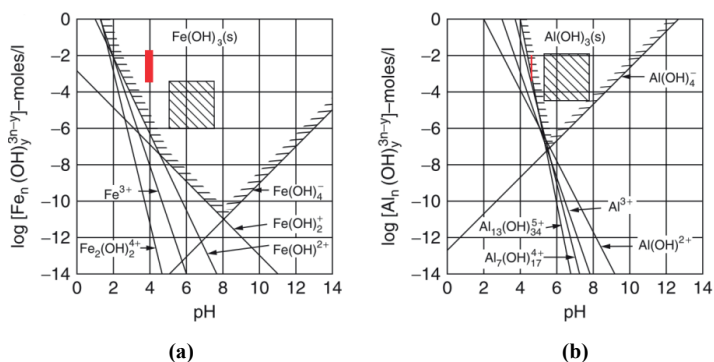


Figure 4.19 The applied concentrations of non-prepolymerized Fe and Al coagulants during TRT (regions, coloured in red) at the angle of the equilibrium-solubility domains with regard to: a) iron hydroxide, (b) aluminum hydroxide in water, as a result of hydrolysis of $\text{Fe}(\text{H}_2\text{O})_6^{3+}$ and $\text{Al}(\text{H}_2\text{O})_6^{3+}$ (Notes: shaded areas show the operational conditions, which are typically applied in practice during water and wastewater treatment.). From Bratby [131], Stumm and O'Melia [157] (with the permission).

In addition, the represented diagrams (Figure 4.19) justify the application of the lower down limit of pH values for the iron (III) sulphate, in comparison to that of the aluminium sulphate used in **Paper III**, since the iron (III) hydroxo- and polyhydroxy complexes are formed at lower pH values and wider pH range compared to their aluminium-based counterparts.

Partial least squares analysis allowed for selecting the significant variables with regard to the prediction of membrane fouling and interpreting their interrelationship. However, the

main outcome of the PLS analysis is the development and validation (via cross-validation) of the model for the assessment, prediction, and control of membrane fouling in the coagulant-assisted BF-MBR based on the theories of double layer and electrostatic interactions as the mechanism of the floc-bound EPSs removal during the application of the selected flux enhancers. This PLS model is the core of a soft sensor, which can be used for the prediction tasks [158].

The current research demonstrated that the general mechanisms of fouling mitigation in BF-MBR were almost the same as in MBR systems outlined in our earlier study, which were described in **Paper I**, thus the observations on MBR systems could be continued for BF-MBR systems, and the mechanisms of processes were studied and explained in this work. The dominant mechanisms of flux enhancement with regard to the studied coagulants were revealed from the automatic data-driven sample grouping in the obtained scores plot of the derived PLS model and during the analysis of the profiles of the monitored mixed liquor parameters in the coagulant-assisted BF-MBR system.

In contrast to the non-prepolymerized coagulants, prepolymerized aluminium coagulants were much more efficient with respect to flux enhancement. This observation was primarily attributed to the dominance of complex adsorption/charge neutralization mechanism in membrane flux enhancement in BF-MBR. The prepolymerized aluminium chloride of medium basicity demonstrated the greatest extent of membrane flux enhancement, which can be explained by its highest bearing charge, and hence the highest potential to neutralize the oppositely charged foulants.

The observations of the superior performance of prepolymerized coagulants as flux enhancers in the current research are in agreement with the studies by Wu et al. [34] and Chen and Liu [32], however, contradict to the conclusions by Ivanovic and Leiknes [31,95]. The latter team reported that membrane flux enhancement occurs merely through the increase of the particle size and reduction of the content of submicron particles with practically no role of charge neutralization mechanism. These conclusions by Ivanovic and Leiknes [31,95] cannot be supported without going into the conflict. However, their results might be explained by the applied pH of coagulation, which apparently was below the optimum levels, resulting in the incomplete hydrolysis of $\text{Fe}(\text{H}_2\text{O})_6^{3+}$ and prepolymerized aluminium species ($\text{Al}_{13}\text{O}_4(\text{OH})^{7+}$), and hence the incomplete destabilization of the disperse system. As shown in Figure 4.19 and **Paper III**, Fe-based coagulants can work at a more acidic pH than Al-based coagulants, and therefore can provide better coagulation and fouling mitigation, which apparently was the reason for the observations obtained in the mentioned studies [31,95].

In addition, prepolymerized aluminium chloride of medium basicity alleviated fouling by the increase of floc relative hydrophobicity, reduction of the concentration of soluble microbial products (SMPs), and the increase of the size of particulate matter. In **Paper III**, its efficiency was mainly attributed to the dominance of a complex adsorption/charge neutralization mechanism since in case of non-prepolymerized aluminium or iron (III) sulphate, neither the increase of the particle size nor the combination of the SMPs removal with the increase of floc relative hydrophobicity alone could provide a sufficient level of flux enhancement.

However, the role of the mechanism of removal of SMPs, particularly SMP_c , still remains unclear since SMP_c are the dominant foulants in MBR and BF-MBR systems, which were found to contribute to the membrane fouling more than the colloidal matter or the SMP_p (protein fraction of SMPs) [104]. The obtained in the current study results might be caused by the inability of the “mixed liquor as the substrate” approach to comprehensively and accurately describe the mechanism of SMPs (i.e., SMP_c) removal, and hence estimate its importance in the fouling prediction. Besides, the electrostatic phenomena, described by the theories of double layer and electrostatic interactions, are not applicable to the explanation of the interactions between the solutes/macromolecular sols and the soluble hydrolyzed coagulant species. Consequently, in further studies, it is necessary to focus on the composition of mixed liquor, its fouling potential, and interaction of the foulants with the coagulant active species. Therefore, further mechanistic investigations of the SMP_c removal are necessary.

Hence, as mentioned above, the obtained results are the basis for development of a soft sensor based on the electrostatic interactions as the main mechanism of the floc-bound EPSs removal by coagulation in BF-MBR; while the development of the model for a soft sensor, which considers the mechanisms of the SMP_c removal in coagulant-assisted BF-MBR, still requires further investigation, which was conducted in **Paper IV**.

The application of prepolymerized aluminium chloride with medium basicity in the dosage range 0.5 – 1.9 $\mu\text{molAl/mgSS}$ provided the residual aluminium concentration below the detectable limits ($< 0.01 \text{ mg Al/L}$), which suggest that it can be used for fouling mitigation not merely in the BF-MBR, treating domestic/municipal wastewater, but also in the MBR/BF-MBR systems for dairy wastewater treatment and recycle [32].

The optimization analysis revealed the significance of MLSS, coagulant dose, temperature, pH, and the interaction factors in the filtration processes. It is noteworthy that the developed optimization approach can be applied to predict the filtration performance, specifying the factorial levels for a single variable outside the defined factorial settings since

the valid range for coded values is $-5 - +5$. This feature can be practically useful during the operational routine, taking into account the fluctuations in the characteristics of the incoming wastewater. While wastewater temperature is barely controllable in practice and mostly varies with the season (warm/cold) [159] and the intensity/frequency of the storm events [160], its potential impact on the BF-MBR system can be predicted, applying the derived models. The adverse effect of the low influent sewage temperatures entailed by climate change [160] can be minimized by adjusting the levels of the other parameters in the membrane separation chamber of the BF-MBR system, according to the presented optimization analysis. As shown in **Paper II**, MLSS can be regulated by adjusting sludge retention time in the decentralized BF-MBR systems. Meanwhile, the coagulant dose and pH of mixed liquor are readily adjustable by changing the settings of the relevant dosing stations.

4.4 Development of the model for continuous classification of thermodynamically stable and less stable complexes after coagulant dosing in BF-MBR: Paper IV

The carbohydrates (polysaccharides) of SMPs, i.e., SMP_c, are the key foulants in MBR, demonstrated by different studies [29,110,161]. Monosaccharides (C_nH_{2n}O_n, n = 3–6) and their derivatives are the main building block molecules of polysaccharides, which determine the characteristics of the latter ones.

Based on the literature evidence on the composition of mixed liquor, gel and cake layer in MBRs, and the biofilms with respect to the monosaccharides [162–167] and according to the studies on the prevalence of the cyclic form of the selected monosaccharides and their characteristic anomeric forms, which were referred to in **Paper IV**, the following compounds are further considered as the targeted foulants in MBR and BF-MBR systems: β-D-glucopyranose (Glc), β-D-galactopyranose (Gal), β-D-mannopyranose (Man), α-D-glucopyranuronic acid (GlcUA), β-L-rhamnopyranose (Rha), β-L-fucopyranose (Fuc), α-L-arabinofuranose (Ara), and β-D-glucosamine (GlcN). In addition, in **Paper III**, the general mechanisms of fouling mitigation in BF-MBR were proven to be almost the same as in MBR systems, reported in **Paper I**, which in **Paper IV** also allowed for assuming that the above-mentioned targeted foulants in MBR are also valid for the BF-MBR.

Monosaccharides in the cyclic form are characterised by an active centre, which is called the glycosidic hydroxyl group. The higher reactivity of glycosidic hydroxyl group can be explained by the influence of the ether-type oxygen atom (between C₁ and C₅) (Figure 4.20a), which partially shifts the electrons from the contiguous C—O bond (in the C₁ position) to its

own orbitals. Hence, the shift of electron density increases the polarity between the C₁ carbon and the OH group, making this hydroxyl group more chemically active [168].

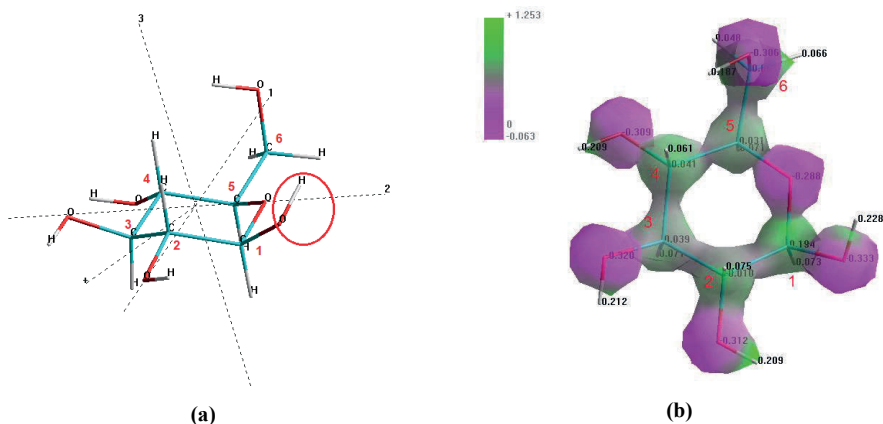


Figure 4.20 Molecular structure of β -D-glucopyranose with the numerated carbon atoms (based on their position in the structure): **(a)** the glycosidic hydroxyl group located at C₁ atom (marked with the red oval); **(b)** electrostatic potential (e/a_0), mapped onto an isosurface of total electron density of $0.13 e/a_0^3$ (Notes: ¹ the numerator stands for the electron charge “e” (1.6022×10^{-19} coulombs), and the denominator is the first Bohr radius “ a_0 ” (5.62918×10^{-11} m)). From **Paper IV**.

Figure 4.20b demonstrates the computationally generated electrostatic potential map of the β -D-glucopyranose molecule, which visualises the charge/electron density distribution within the molecule represented as the isosurface. The bright and dark green colours indicate the areas with low electron density, and hence net positive charge and positive electrostatic potential (the hydrogen and carbon atoms); whereas, the deep purple colour shows the regions of high electron density, and thus net negative charge and negative electrostatic potential (the oxygen atoms). According to Figure 4.20b, the shift of the electrons from the carbon atom in position 1 (atom C₁) to the ether-type oxygen atom in the structure of β -D-glucopyranose is clearly indicated by the area of the relatively higher electrostatic potential (around $1.25 e/a_0$) and increased net positive charge of C₁ ($+0.194$) in comparison to the other present carbon atoms.

The electrostatic potential map (Figure 4.20b) indicates a significant part of intermediary electrostatic potential regions, whose colours are not completely green or completely purple, in the structure of the investigated molecule. This effect is explained by the nature of observed bonds in the structure of β -D-glucopyranose as well as in the structure of the other selected monosaccharides, which is covalent polar. Meanwhile, the polarity of the O—H bonds is higher than the polarity of C—O bonds $-\Delta\chi_{\text{OH}} = 1.4 > \Delta\chi_{\text{CO}} = 1.0$.

The total dipole moment of the β -D-glucopyranose molecule is 1.639 D, with the highest contribution from the X and Z vector components (Figure 4.20a).

The electrostatic potential surfaces of the other investigated monosaccharides have the character similar to the one of β -D-glucopyranose and are demonstrated in the supplementary material of **Paper IV**.

With regard to the coagulant, according to **Paper III**, prepolymerized aluminium chloride with the medium basicity (OH/Al 1.3) exhibited the best potential to mitigate fouling in BF-MBR system at the optimum pH range 5.5–6, which was mainly attributed to the highest bearing charge concentration among the studied species.

Based on the discoveries by Sarpola [169,170] and the findings of different research teams [171–176], described in detail in **Paper IV**, the present study assumed that during coagulation applying the prepolymerized aluminium chloride with medium basicity the open structure of Al_{13} complex in the form of $[Al_{13}O_4(OH)_{29}]^{2+}$ plays the most crucial role in the reactions with the oppositely charged foulants.

The planar open structure of the Al_{13}^{3+} complex, introduced by Sarpola [169], was taken as the basis for building Al_{13}^{2+} . Meanwhile, the geometry optimisation analysis conducted in the present work indicated, that the minimum of potential energy can only be reached if the molecule has a non-planar conformation, as represented in Figure 4.21.

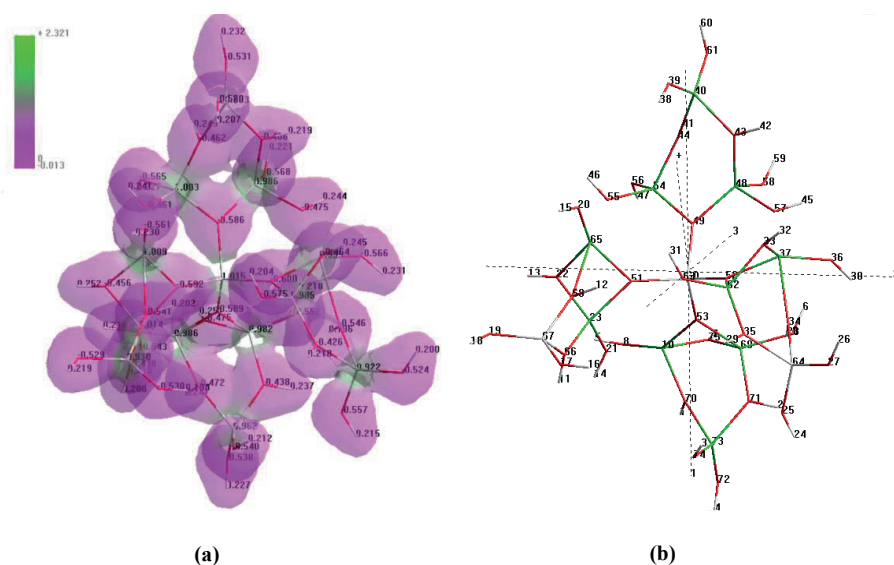


Figure 4.21 Molecular structure of the Al_{13}^{2+} complex: **(a)** electrostatic potential (e/a_0), mapped onto an isosurface of total electron density of $0.018 e/a_0^3$; **(b)** the marked aluminium atoms and their corresponding numbers, which were chosen for the simulations. From **Paper IV**.

According to the electrostatic potential map, represented as the isosurface of the Al_{13} complex (Figure 4.21a), the bright green colour indicates the regions of low electron density, net positive charge, and positive electrostatic potential (the aluminium atoms); whereas the bright purple colour points to the areas of high electron density, and thus net negative charge and negative electrostatic potential (the oxygen atoms). The entirely green and entirely purple regions, with no regions of intermediary electrostatic potential on the electrostatic potential map, indicate a significant differences in the electron density at the aluminium and oxygen atoms, and hence the ionic nature of observed bonds in the structure of Al_{13} complex, which is confirmed by the polarity of the O—Al bonds ($\Delta\chi_{\text{AlO}}$) equal to 2 ($\chi_{\text{O}}=3.5$, $\chi_{\text{Al}}=1.5$ on the Pauling scale).

As shown in Figure 4.21a, all aluminium atoms, except for the central tetrameric aluminium, are the potential active centres during the interaction with the foulants. However, based on the charge balance calculations, Al no 64 (Figure 4.21b) has a slight net negative charge (-0.023), and Al no 67 has almost no charge (0.004); thus, both are less likely to participate in the reactions. Hence, the aluminium atoms, highlighted with the light green colour in Figure 4.21b, are the potential active centres of the Al_{13} complex.

The total dipole moment of the Al_{13} complex is 7.25 D. The analysis of the components of the total dipole moment demonstrates the maximum contribution from the Z vector component (Figure 4.21b).

It was decided to investigate the Al_{13} -monosaccharide complex formation through the double-O-ligand coordination since the formed structure would contain an additional ring system with the delocalised π -electrons, that would potentially contribute to its stabilisation. Based on the structural peculiarities of the selected monosaccharides, the formation of the Al_{13} -monosaccharide complexes can occur through the following pairs of the carbon atoms with the adjacent oxygen atoms:

- 1) C₁-C₂, C₁-C₆, C₄-C₆, C₁-C₃ for the aldoses and uronic acid (β -D-glucopyranose, β -D-galactopyranose, β -D-mannopyranose, and α -D-glucopyranuronic acid);
- 2) C₁-C₂, C₁-C₄, C₂-C₃, C₁-C₃ for the deoxy sugars (β -L-rhamnopyranose and β -L-fucopyranose);
- 3) C₁-C₂, C₂-C₃, C₃-C₅, C₁-C₃ for the pentose (α -L-arabinofuranose);
- 4) C₁-C₆, C₁-C₄, C₄-C₆, C₁-C₃ for the aminosugar (β -D-glucosamine).

The aluminium atoms in the Al_{13}^{2+} complex, which can potentially participate in the interaction with the listed active centres of monosaccharides, are marked in green in Figure 4.21b.

The Gibbs energy change is the main indicator of the spontaneity in chemical reactions, i.e., the criterion for the direction of the spontaneous processes, at constant pressure and temperature [177].

The thermodynamic parameters of formation of the individual monosaccharides, Al_{13}^{2+} complex, and the relevant products of the reaction between them (i.e., Al_{13} -monosaccharide complexes) — standard enthalpy change (ΔH_f°), standard entropy (S_f°), and standard Gibbs energy change (ΔG_f°) were determined through the series of quantum chemical calculations by using semi-empirical PM3 method. This analysis was followed by the calculation of the standard enthalpy change (ΔH°), standard entropy change (ΔS°), and standard Gibbs energy change (ΔG°) of the reaction between the selected monosaccharides and Al_{13}^{2+} complex, performed according to Equations (3.14)–(3.17). The obtained results with regard to the standard Gibbs energy change of the process are represented in Figure 4.22.

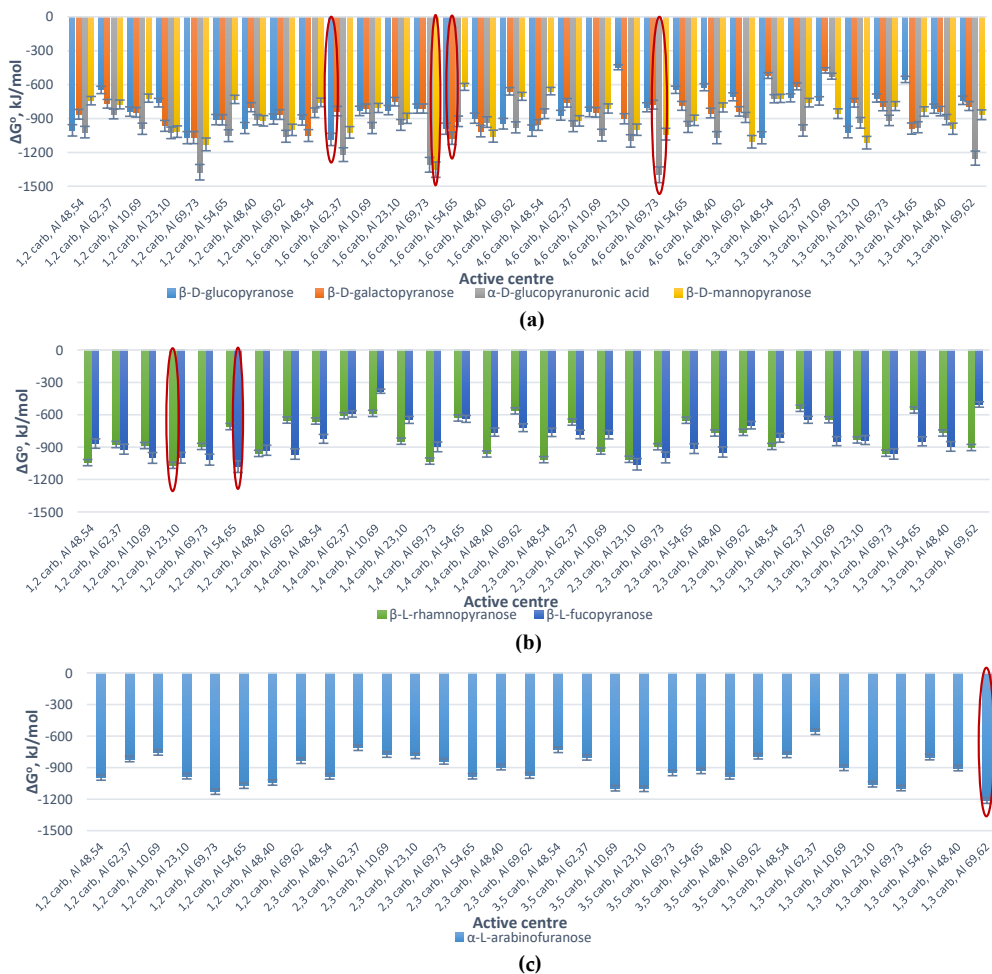


Figure 4.22 Cont.

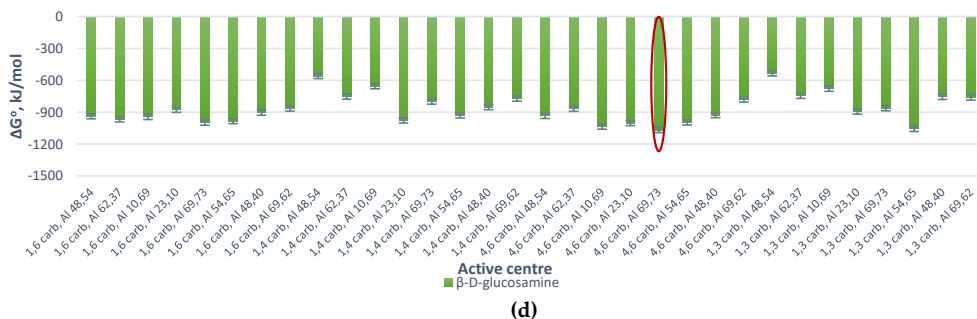


Figure 4.22 The development of the Gibbs energy change of formation of Al_{13}^{2+} complex and monosaccharide for the double-O-ligand coordination of the following monosaccharides: (a) β -D-glucopyranose, β -D-galactopyranose, α -D-glucopyranuronic acid, and β -D-mannopyranose; (b) β -L-rhamnopyranose and β -L-fucopyranose; (c) α -L-arabinofuranose; (d) β -D-glucosamine. (Notes: “carb” stands for carbohydrate; the first two numbers in the name of a complex are related to the pair of the carbon atoms with the adjacent oxygen atoms in the structure of the relevant monosaccharide, which participate in the coordination, and the second two numbers stand for the numbers of the aluminum atoms (active centers) of the Al_{13} complex, which interact with the above-mentioned oxygen centers of the monosaccharide.). From **Paper IV**.

The analysis of the acquired charts (Figure 4.22) demonstrates that all of the processes, which result in the formation of the suggested Al_{13} -monosaccharide complexes, have a negative standard Gibbs energy, which indicates that the processes of their formation are spontaneous, and hence thermodynamically favourable. Meanwhile, the extent of thermodynamic stability of the formed Al_{13} -monosaccharide complex highly depends on the active centres of the monosaccharides and the Al_{13}^{2+} complex, which participate in the chemical coordination process, and the nature of the monosaccharide. The following complexes (marked with the dark red ovals in Figure 4.22) were identified as the most thermodynamically stable since they exhibited the highest negative values (with regard to every considered monosaccharide as the reactant) of standard Gibbs energy change: 4,6 GlcUA, Al 69,73 ($\Delta G^\circ = -1398.87$ kJ/mol); 1,6 Glc, Al 62,37 ($\Delta G^\circ = -1085.82$ kJ/mol); 1,6 Gal, Al 54,65 ($\Delta G^\circ = -1075.71$ kJ/mol); 1,6 Man, Al 69,73 ($\Delta G^\circ = -1353.75$ kJ/mol); 1,2 Rha, Al 23,10 ($\Delta G^\circ = -1067.79$ kJ/mol); 1,2 Fuc, Al 54,65 ($\Delta G^\circ = -1080.55$ kJ/mol); 1,3 Ara, Al 69,62 ($\Delta G^\circ = -1215.10$ kJ/mol); 4,6 GlcN, Al 69,73 ($\Delta G^\circ = -1068.35$ kJ/mol).

The standard entropy change and enthalpy change of the processes resulting in the formation of the investigated Al_{13} -monosaccharide complexes are demonstrated in supplementary material in **Paper IV**.

According to Equation (3.17), the most favourable condition for the formation of any compound is established if $\Delta H < 0$ and $\Delta S > 0$, which indicates that this process of formation can occur spontaneously at any given temperature. As shown in **Paper IV**, ΔS° of the processes of formation of all of Al_{13} -monosaccharide complexes is negative, which can be

explained by the fact that the spontaneous association of such reactants as monosaccharide and the Al_{13}^{2+} complex gives the rise to a more compact/organised structure [177]; whereas the processes of their formation are highly exothermic ($\Delta H^\circ < 0$). In this case, there is a competition between the entropy (the level of disorder of the system) and enthalpy factors: the first parameter facilitates the reversible process (complex decomposition), while the latter one favours the forward reaction (complex formation) [178]. High negative values of ΔG° for all investigated processes (Figure 4.22) resulted from the dominance of the enthalpy factor at the standard temperature, meaning that this temperature ($T=298.15K$) is low enough to facilitate the formation of the Al_{13} -monosaccharide complex ($T < \Delta H^\circ/\Delta S^\circ$). However, at very high temperatures ($T > \Delta H^\circ/\Delta S^\circ$), the process of complex formation will not occur spontaneously.

Based on the above-mentioned findings, the mechanisms of the chemical coordination of the selected monosaccharides to the Al_{13} complex were established (demonstrated in **Paper IV**).

The potential factors, which facilitate the mechanisms of the interaction between the monosaccharides and Al_{13} complex by positively contributing to the stabilization of the Al_{13} -monosaccharide coordinated complexes, can be: The steric effects and the polarization of Al active centers towards the O_i-O_n atoms of the monosaccharide. However, the role of the stabilizing factors in the formation of Al_{13} -monosaccharide complexes should be the subject of further investigation.

The partial least squares analysis (PLS) of the obtained data was conducted, using the standard entropy change (ΔS°) and enthalpy change (ΔH°) of the investigated processes of formation of the Al_{13} -monosaccharide complexes as the predictors (X-variables) and the standard Gibbs energy change of these processes as the response function (Y-variable).

The obtained model underwent random cross-validation. The number of PLS factors was chosen according to the explained variance.

The results obtained during the PLS analysis are represented in Figure 4.23.

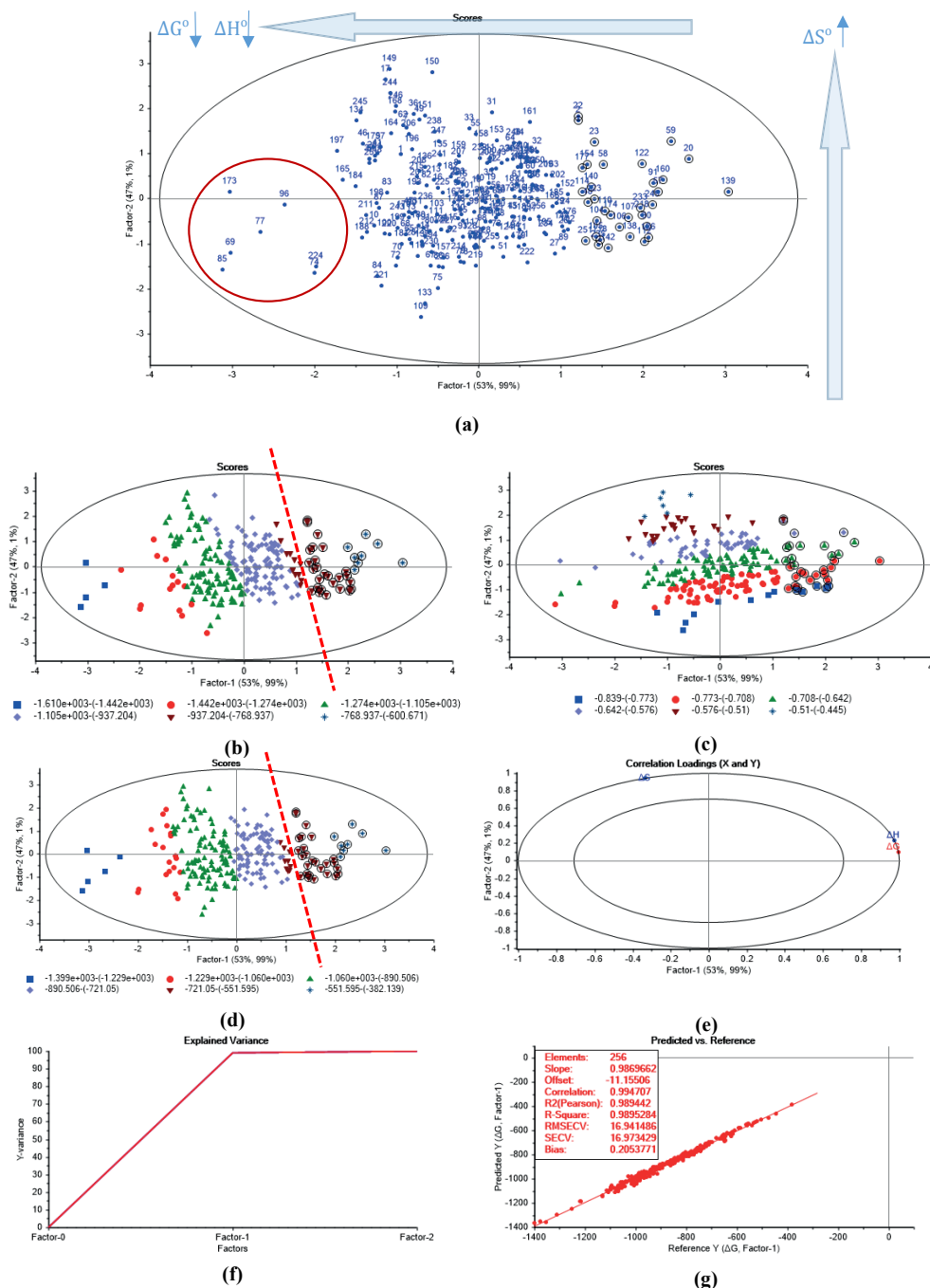


Figure 4.23 Results of the partial least squares analysis (PLS) using the results as the quantum chemical and thermodynamic calculations: **(a)** scores plot with no sample grouping; **(b)** scores plot with the sample grouping according to ΔH° ; **(c)** scores plot with the sample grouping according to ΔS° ; **(d)** scores plot with the sample grouping according to ΔG° ; **(e)** correlation loadings plot; **(f)** total explained variance plot; **(g)** standard Gibbs energy change prediction model (validation plot). From **Paper IV**.

As revealed during the analysis, the first two factors in total describe 100% of the variance in the dataset for x and y.

The scores plot demonstrates no clear clusters of similar samples as shown in supplementary material in **Paper IV**, which can be explained by a large number of categorical variables. Meanwhile, the samples marked with the dark red oval, which are located leftmost, in the third quadrant of the scores plot (Figure 4.23a), mostly exhibit the highest negative standard enthalpy change (ΔH°) and Gibbs energy change (ΔG°) — -1610–(-1442) kJ/mol and -1399–(-1229) kJ/mol, respectively, which was indicated by the results of the data-driven sample grouping (Figure 4.23b,d) and the correlation loadings plot (Figure 4.23e). These samples indicate the most thermodynamically stable complexes [177], the majority of which are formed by α -D-glucopyranuronic acid and the Al atoms no. 69, 73; 62, 37; and 69, 62 of the Al_{13}^{2+} complex (specified in detail in **Paper IV**). The data-driven sample grouping was automatically conducted by equally dividing the band of the values of the targeted thermodynamic parameters in the whole range between the upper and lower limits into six groups, shown in Figure 4.23b–d.

According to the PLS correlation loadings plot (Figure 4.23e), Factor-1 accounts for the standard enthalpy change (ΔH°) and the Gibbs energy change (ΔG°), while Factor-2 mainly describes the standard entropy change (ΔS°). All of the variables explain more than 50% of the variance, and hence have high importance in relation to Factor-1 and Factor-2. ΔH° has a high positive correlation with ΔG° and both are negatively correlated with ΔS° along Factor-1. The explained variance plot (Figure 4.23f) indicates that the optimum number of factors is one, which provides 98.9% of the explained Y-variance.

The analysis of the validation plot (Figure 4.23g) indicates that the developed model has a linear trend R -squared = 0.99, is reliable (R -squared (Pearson) = 0.989, the R -squared correlation = 0.995, the Root Mean Square Error of Cross-Validation (RMSECV) = 16.94 kJ/mol, and the standard error of cross-validation (SECV) = 16.97 kJ/mol), has a good fit for the majority of the data (slope = 0.987), and does not tend to over- or underestimate the validation values (bias 0.2).

The stability and applicability limits of the partial least squares (PLS) model were checked through the case scenarios based on the addition of the proportional and additive noise to both the predictors and response function, which was described in **Paper IV**. The results indicated that this model can be used, not merely for the computational results, but also for the experimentally-obtained data with the maximum noise, which affects the instrument amplification, 6%; and the maximum standard deviation for the noise, which

affects the measurement signal, equal to 14, imposed on all the investigated variables (ΔH° , ΔS° , ΔG°).

The cluster analysis was conducted based on the Y-scores for the latent variables, Factor-1 and Factor-2, acquired during the PLS analysis in order to screen out the noise of the raw data and use the prevailing differences of the most and least thermodynamically stable complexes. The classes were generated from the scores by applying a hierarchical complete-linkage clustering method and the squared Euclidean distance as the dissimilarity function. The obtained results are represented in Figure 4.24.

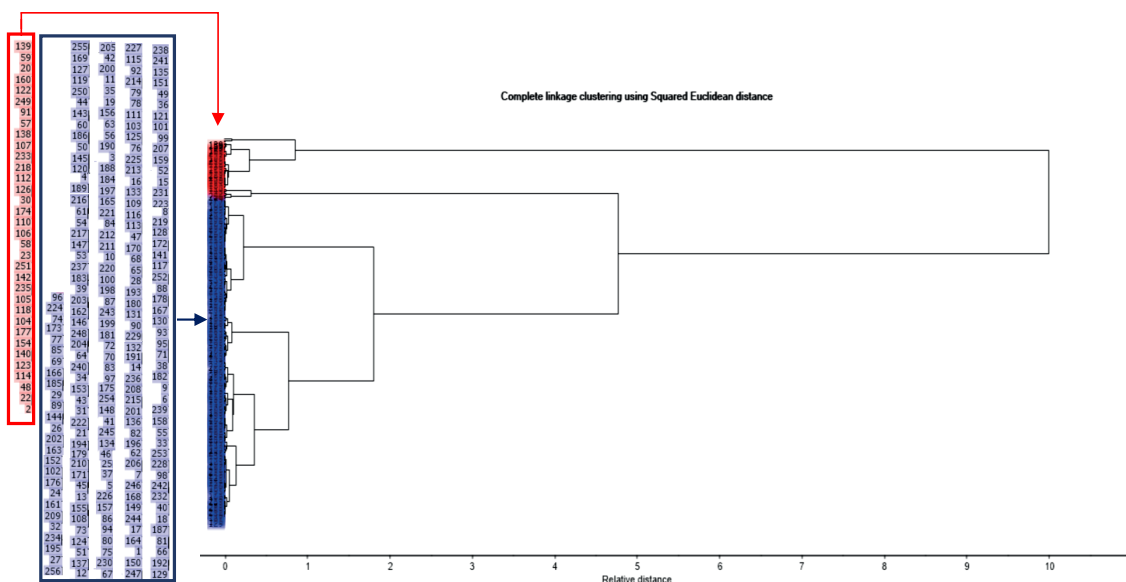


Figure 4.24 Dendrogram plot acquired during the cluster analysis based on the scores of PLS (the samples, highlighted with the red and blue rectangles, make up the red and blue clusters of the dendrogram, respectively; the samples are located on the y-axis of the dendrogram in the same order as in the columns in the rectangles). From **Paper IV**.

The acquired dendrogram visualizes the clustering (Figure 4.24), which corresponds to the Y-scores in the four quadrants of Figure 4.23a–d. Six classes can be identified at a higher resolution (a relative distance of around 0.8) (Figure 4.24), which correspond to the six groups of the standard Gibbs energy change in the scores plot, generated during the data-driven sample grouping (Figure 4.23d).

However, at a lower resolution (a relative distance of around 4.9), merely two classes can be identified (Figure 4.24). The red cluster is characterized by the samples with high values of Factor-1 and generally low values of Factor-2. The corresponding samples were marked with the black circles in Figure 4.23a–d. This position of these marked samples on the scores

plot indicates that they are characterized by the low negative values of the standard enthalpy change (ΔH°) and Gibbs energy change (ΔG°), and the predominantly high negative values of the standard entropy change (ΔS°). Hence, the complexes, which make up the red cluster, are less thermodynamically stable. The blue cluster represents the scores with low values of Factor-1, i.e., the corresponding samples are characterized by the relatively high negative values of ΔH° and ΔG° (all of the samples, which do not have the black-circle mark in Figure 4.23a–d). Hence, the complexes, which constitute the blue cluster, are more thermodynamically stable. The location of the scores of the certain sequence numbers, which make up each cluster shown in the dendrogram, can be found in the scores plot with no sample grouping (Figure 4.23a).

The described clusters, generated by cluster analysis, represented the Al-monosaccharide complexes, which are more or less liable to decompose during coagulation and can be assigned to the categories “Less stable” and “Stable”, respectively.

Discussion

Paper IV was focused on the development of the two-stage supervised classifier. The classifier is based on the following steps: (1) the PLS analysis on the raw thermodynamic characteristics of the formation of Al₁₃-monosaccharide complexes; (2) the subsequent use of the generated scores for the hierarchical cluster analysis (path (1) in Figure 4.25); and (3) the manual detection of the samples from each cluster in the scores plot with the sample grouping with respect to the response function, ΔG° (Figure 4.23d), and their analysis according to the correlation loadings plot of the PLS (Figure 4.23e) as demonstrated by path (2) in Figure 4.25. The last step results in classifying the samples according to the variables into two clear groups, i.e. defining the threshold in the scores plot between the thermodynamically stable and less stable species (the red dashed line in Figure 4.23b,d). In other words, the identification of the cluster's location in the scores plot and its analysis according to the location of the variables in the correlation loadings plot make it possible to understand, what the clusters, generated by cluster analysis, stand for.

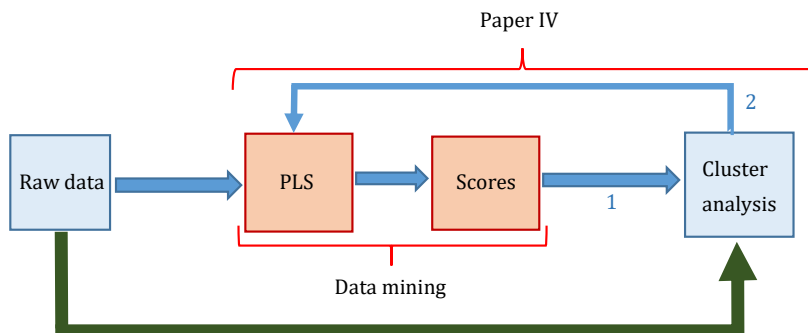


Figure 4.25 Flowchart of the development of a classification model for the continuous online discrimination of the thermodynamically stable and less stable species as a result of the chemical flux enhancement in BF-MBR.

In addition, the use of the Y-scores of the PLS for the cluster analysis helps to screen out the noise of the raw data, which, however, was not the issue in the present study due to the accurately determined thermodynamic parameters of the investigated system.

The other alternative to the two-stage calculation approach, described above, is PLS Discriminant Analysis (PLS-DA), applying the “winner-takes-all-strategy”, described by Torgersen [55]. However, this approach typically requires manual analysis, and thus is less favourable.

Validation of the PLS model was performed applying the following methods: (1) cross-validation, described in **Paper IV**; and (2) the test matrix validation by keeping the randomly chosen 1/3 of the data out of the model and running the model using 2/3 of the data with the subsequent prediction of the excluded 1/3 of the data (new data) based on the produced model. The cross-validation provides a reasonable estimation of the stability and accuracy of the model; whereas the prediction set provides the prediction of the new data (not included in the model) based on the generated model. Thus, the test matrix validation (prediction set) duplicates the real-life conditions, when the new data, generated in the filtration system, needs to be analysed. Eventually, the model mapped by 2/3 of the data provided the same results as the cross-validated model with the difference in values of R-squared, R-squared (Pearson), and R-squared correlation equal to 1% between two models. Hence, it can be concluded that the cross-validation and prediction sets give relatively the same results in the current study.

The analysis of the dendrogram, generated by the cluster analysis of the raw data (not shown in this work), indicated that at low resolutions (relative distance ≥ 5.1) the same classes with the same samples, as in the case of the classes from the cluster analysis on the PLS Y-scores at a relative distance ≥ 4.9 (Figure 4.24), were recognized. This observation means that the data mining based on PLS, which is followed by the cluster analysis of the Y-scores, can

be bypassed during the conventional monitoring in the automated system, and the classifier can be applied directly to the raw data (i.e., unsupervised hierarchical cluster analysis, marked with the green arrow in Figure 4.25). Nevertheless, the two-stage supervised classifier is still required in order to get feedback from the system to check if the model needs to be revised/adjusted with respect to the new incoming data via the PLS and cluster analysis of the Y-scores.

The present research provides the bridge from the chemometric multivariate analysis and supervised learning to machine learning, which is gaining momentum worldwide [179].

The implication of the findings

The developed PLS model is the core of the soft sensor for membrane fouling assessment and prediction based on the chemical coordination of the SMP_c to the Al_{13}^{2+} complex during the application of prepolymerized aluminium chloride of medium basicity as a chemical flux enhancer in BF-MBR.

By introducing the relationship—fouling as a function of Gibbs energy change, the developed in **Paper IV** strategy helps to partially computerize the stage of the coagulant testing with regard to their flux enhancement efficiency in BF-MBR, thus reducing the demand for time- and resource-consuming experiments.

The combination of the thermodynamic analysis with the unsupervised hierarchical cluster analysis (CA of the raw data) allows for the implementation of the online monitoring and prediction of the reduction of the mixed liquor fouling propensity based on the thermodynamic parameters of the system. After adding the flux enhancer, the thermodynamic parameters of the system can be determined by the differential scanning calorimeter and subsequently transferred to the unsupervised classifier for the continuous discrimination of the thermodynamically stable and less stable Al_{13} -monosaccharide complexes. As a result, depending on the percentage of the less thermodynamically stable species, the decision on adding the flocculant/adsorbent can be taken. Meanwhile, the two-stage supervised classifier will keep the model revised in terms of new incoming data, which will help to maintain a “smart” classification during the operational routine of the BF-MBR system.

With regard to the chemical coordination of the protein, i.e., O atoms in the COOH group of the amino acid strands in its skeleton, to the Al_{13}^{2+} complex, this process can potentially take place via donor-acceptor mechanism, but is less likely to occur due to the electrostatic repulsive effect of $-NH_3^+$ groups, which drastically weakens the strength of their complexation to Al (III) [180].

This evidence, together with the value of isoelectric point of the SMP proteins (pH 5.5–7), suggests that amino acids in the protein structure, and hence proteins of the SMPs, are less likely to interact with the Al_{13}^{2+} molecule in the pH range of 5.5–6. Therefore, amino acids/proteins of the SMPs, i.e. SMP_p , can be excluded as the influencing factor during the measurement of the thermodynamic properties of the analysed system after the dosing of prepolymerised aluminium chloride with medium basicity. Nevertheless, it is worth noting, that due to the complex nature of the wastewater, the chemical coordination of other compounds to the Al_{13}^{2+} complex might take place, which can slightly influence the obtained measurement. In this case, after the identification of such compounds and quantum chemical and thermodynamic calculations, the relevant data can be added to the two-stage supervised classifier to revise the employed model.

In the study by Fernandez de Canete et al. [181], PCA in combination with the adaptive neural network was successfully used for the online prediction of the effluent characteristics in the conventional activated sludge system. According to Choi and Park [182], the integration of the PCA with the artificial neural network into the hybrid model for the prediction of the influent wastewater parameters in the biological wastewater treatment system improved the prediction accuracy of the artificial neural network and mitigated its sensitivity to noise. Hence, further development of the data-driven sensor based on the partial least squares-artificial neural network (PLS-ANN) hybrid model using the PLS models, developed in **Paper III** and **Paper IV**, has the potential to advance process control in the coagulant-assisted BF-MBR.

5. Conclusions and Outlook

The current research integrated experimental design, data mining, quantum chemical and thermodynamic analysis, and cluster analysis into the mechanistic-statistical approach to optimization and process control of fouling mitigation in the coagulant-assisted biofilm membrane bioreactor (BF-MBR). This approach implies the development of the core models for membrane fouling assessment, prediction, and control based on the mechanisms of flux enhancement during the coagulant addition in BF-MBR⁴.

The analysis of the latest literature reports revealed that soluble microbial products (SMPs), particularly polysaccharides (SMP_c), and floc-bound extracellular polymeric substances (EPSs) play the key role in fouling development in the membrane bioreactor (MBR) and biofilm membrane bioreactor (BF-MBR) systems designed to treat domestic/municipal wastewater, and hence are the targeted foulants. The specified foulants cause the formation of gel, cake layers on the membrane surface and pore blockage, and thus are primarily responsible for the reversible, irreversible, and irrecoverable membrane fouling, suggesting, that the regular physical cleaning is not enough to completely recover permeability of the fouled membrane. The addition of coagulants was revealed to be among the most promising strategies for fouling mitigation. The following mechanisms of coagulant action with regard to flux enhancement in MBR were identified by the previous studies: enhancement of adsorption/charge neutralization, reduction of SMPs level in mixed liquor, increase of the mean floc size, increase of the mixed liquor relative hydrophobicity, and reduction of the specific cake/gel layer resistance. The outlined mechanisms of coagulant action can be the “navigator” for the selection of the representative parameters of the mixed liquor fouling propensity during chemical flux enhancement in BF-MBR systems, which was verified at the further stages of this research.

- The presented outline of the principal mechanisms of action of the selected chemical additives may guide future efforts to think up and apply the concept of flux enhancement based on the use of coagulant–flocculant pairs in MBR, which will act via the combination of the respective fouling reduction pathways.

BF-MBR system is the advancement of MBR technology with regard to fouling mitigation. The application of the PLS analysis of the membrane fouling patterns in the BF-MBR pilot system without coagulant addition allowed for the development of the fouling mitigation approach, which encapsulated the relationship between the significant mixed liquor

⁴ Recommendations for further research and practical implications are provided in bullet points

characteristics, membrane fouling indicators, and the operational conditions in BF-MBR. Thus, the developed approach allowed for assessment and prediction of the system performance with regard to fouling development and provided the tools for influencing it. The average normalized permeability was found to be the most reliable indicator of fouling intensity in the system. The developed PLS models along with the introduced critical SRT (31 days) allowed for the adjustment of the operational conditions of the BF-MBR system according to the mixed liquor characteristics. As a result, membrane filtration was kept outside the region of the critical fouling development with high recovery of membrane permeability after physical and chemical cleanings: 88–126% and 158–182%, respectively. Besides, stable treatment efficiency was provided independently from the fluctuations in the membrane separation part.

- The developed procedure can serve as the performance evaluation protocol for the decentralized BF-MBR systems.
- The possibility of development of the soft sensor for the prediction of COD_{dis} based on the automated MLSS monitoring in MBBR and MBR chambers should be explored.

During the comparative study of the Al- and Fe-based coagulants as membrane flux enhancers for the BF-MBR system, prepolymerized aluminum chloride coagulants provided the greatest extent of fouling mitigation at the dose 1.1–1.9 $\mu\text{molAl/mgSS}$, by affecting the charge, hydrophobicity, and size of flocs, and SMPs content of the system. The observed efficiencies correspond to a tenfold increase in filtration length of the membrane separation cycle and 30.0–56.0% increase in net flux (depending on the operational period) of the BF-MBR pilot system in comparison to this system without the coagulant dosing. The necessity of the pH adjustment for the efficient flux enhancement was substantiated. The optimum pH levels and dosages with regard to flux enhancement efficiency of every coagulant were determined.

Statistical prediction of the mixed liquor fouling propensity and the determination of the principal mechanisms of flux enhancement during the coagulant addition in the BF-MBR system was performed by applying PLS analysis. According to the obtained results, coagulant efficiency was primarily attributed to the dominance of a complex adsorption/charge neutralization mechanism of the removal of floc-bound EPSs in the BF-MBR, giving the best results in the case of prepolymerized aluminum chloride with medium basicity (OH/Al 1.3), characterised by the highest bearing charge.

As a result of the PLS analysis, the fouling prediction model for early warnings and process control for the coagulant-assisted BF-MBR was developed and validated, which was based on the electrostatic double-layer interactions between the floc-bound EPSs and the studied coagulants. The analysis of the model also provided the tools for the investigation of the prevailing mechanisms of coagulant action.

The analysis of the two-level factorial design, which allowed for considerable reduction of the required experiments, provided the models and the levels of the factors for optimization of membrane filtration using the prepolymerized aluminium chloride with medium basicity in BF-MBR. The significance of MLSS, coagulant dose, temperature, pH, and their interaction factors in the filtration processes and the vital tendencies in factorial interactions were revealed. The models will help to minimize the adverse effect of low influent sewage temperatures, caused by climate change, by adjusting sludge retention time, pH, and coagulant dose in the membrane separation chamber of the BF-MBR system.

- Apart from zeta potential measurements, no additional testing is required to evaluate the fouling alleviation propensity of the new inorganic coagulants with regard to the floc-bound EPSs removal in the BF-MBR system, which will help to simplify the testing procedure and bring the technology to the next level.
- The integration of the developed PLS model and the recurrent fuzzy neural network in the supervised intelligent detecting system for the online detection of membrane fouling in BF-MBR should be explored.
- The possibility of coagulant dosing in the MBBR part and the effect of the application of the optimum coagulant in pairs with organic flocculants in BF-MBR should be checked.

Polysaccharides in the structure of SMPs (i.e, SMP_c) were recognized as the major foulants in MBR and BF-MBR systems, whereas the Al₁₃²⁺ complex was identified as the major hydrolysis species of the prepolymerized aluminium chloride with medium basicity at pH 5.5–6. The analysis of the electrostatic potential maps allowed for the determination of the active centers of the monosaccharides, which are the basic building blocks of polysaccharide molecules, and the Al₁₃²⁺ complex. Based on quantum chemical and thermodynamic calculations, the principal mechanisms of the interactions between the selected monosaccharides and the Al₁₃²⁺ complex were determined.

The incorporation of the results of quantum chemical and thermodynamic analysis into the PLS analysis enabled the development of the model for membrane fouling assessment and

prediction based on the thermodynamic properties of the chemical coordination of the SMP_c to the Al_{13}^{2+} complex during chemical flux enhancement in BF-MBR.

Cluster analysis of the raw (statistically unprocessed) thermodynamic parameters of the system was the basis for the development of an unsupervised classification model for the continuous online discrimination of the thermodynamically stable and less stable Al_{13} -monosaccharide complexes formed during coagulation in BF-MBR. Moreover, by combining the PLS model and cluster analysis, a two-stage supervised classifier was developed, designed to keep the above-mentioned (unsupervised) model revised in terms of new incoming data, which will help to achieve a well-timed adaptive process control in the BF-MBR system.

- The quantum chemical and thermodynamic calculations for the prediction of the coagulant efficiency with regard to the SMP_c removal can substantially reduce the number of the required experiments for the coagulant selection.
- The role of the stabilizing factors in the formation of Al_{13} -monosaccharide complexes requires further investigation.
- Efforts should be directed at studying the thermodynamic properties of the interaction of the Al_{13}^{2+} complex with the monosaccharide–amino acid network assemblages.

To sum up, the results of the present thesis will contribute to the advancement of the system operation and performance and reduce the required experiments and unexpected operational costs. In addition, the present research broadened the knowledge on membrane fouling modelling and developed a more progressive mechanistic-statistical approach to process control in BF-MBR. The results of the study are practically significant for the development of the data-driven sensor based on the partial least squares-artificial neural network (PLS-ANN) hybrid model for the process control in the coagulant-assisted BF-MBR.

References

1. Food and Agricultural Organization of the United Nations. Water Scarcity Available online: <http://www.fao.org/land-water/water/water-scarcity/en/> (accessed on Jul 29, 2019).
2. UNESCO *Nature-Based Solutions for Water. WWDR 2018. The United Nations World Water Development Report 2018*; Paris, France, 2018.
3. European Commission *Regulation of the European Parliament and the Council on minimum requirements for water reuse*; Belgium, 2018; Vol. 0169, p. 28.
4. United Nations 2030 Agenda for Sustainable Development. Sustainable Development Goals. Goal 6: Ensure availability and sustainable management of water and sanitation for all Available online: <https://www.un.org/sustainabledevelopment/water-and-sanitation/> (accessed on Jul 29, 2019).
5. United Nations 2030 Agenda for Sustainable Development. Sustainable Development Goals. Goal 6: Ensure availability and sustainable management of water and sanitation for all. Targets Available online: <https://sustainabledevelopment.un.org/sdg6> (accessed on Jul 30, 2019).
6. European Commission Water Reuse. Proposal for a regulation on minimum requirements for water reuse Available online: <https://ec.europa.eu/environment/water/reuse.htm> (accessed on Jul 30, 2019).
7. UNESCO *LEAVING NO ONE BEHIND. WWDR 2019. The United Nations World Water Development Report 2019*; UNESCO: Paris, France, 2019; ISBN 9789231003097.
8. IWA *Wastewater Report 2018. The Reuse Opportunity*; London, UK, 2018.
9. Central Arizona Project (CAP) Arizona: a national leader in water reuse Available online: <https://www.cap-az.com/public/blog/75-arizona-a-national-leader-in-wate-reuse> (accessed on Jul 30, 2018).
10. Desai, S.; Rosenberg, S.; Hermsen, N. Minimal Liquid Discharge: Adopting A “Less is More” Mindset Available online: <https://www.wateronline.com/doc/minimal-liquid-discharge-adopting-a-less-is-more-mindset-0001> (accessed on Aug 17, 2019).
11. Global \$ 8.27 Bn Membrane Bioreactor Market, 2025 Available online: <http://markets.businessinsider.com/news/stocks/global-8-27-bn-membrane-bioreactor-market-2025-1005680257> (accessed on Dec 15, 2017).
12. Meng, F.; Zhang, S.; Oh, Y.; Zhou, Z.; Shin, H. S.; Chae, S. R. Fouling in membrane bioreactors: An updated review. *Water Res.* **2017**, *114*, 151–180, doi:10.1016/j.watres.2017.02.006.
13. Buer, T.; Cumin, J. MBR module design and operation. *Desalination* **2010**, *250*, 1073–1077, doi:10.1016/j.desal.2009.09.111.
14. Bouhadjar, S. I.; Deowan, S. A.; Galiano, F.; Figoli, A.; Hoinkis, J.; Djennad, M. Performance of commercial membranes in a side-stream and submerged membrane bioreactor for model textile wastewater treatment. *Desalin. Water Treat.* **2015**, 1–11, doi:10.1080/19443994.2015.1022005.
15. Judd, S. *The MBR book Principles and Applications of Membrane Bioreactors in Water and Wastewater Treatment*; Judd, C., Ed.; First Edit.; Elsevier Ltd: London, UK, 2006; ISBN 9781856174817.
16. Geilvoet, S. P. *The Delft Filtration Characterisation method: Assessing membrane bioreactor activated sludge filterability*, Delft University of Technology: Delft, Netherlands, 2010.
17. Krzeminski, P.; Leverette, L.; Malamis, S.; Katsou, E. Membrane bioreactors – A review on recent developments in energy reduction, fouling control, novel configurations, LCA and market prospects. *J. Memb. Sci.* **2017**, *527*, 207–227, doi:10.1016/j.memsci.2016.12.010.
18. Hai, F. I.; Riley, T.; Shawkat, S.; Magram, S. F.; Yamamoto, K. Removal of pathogens by membrane

- bioreactors: A review of the mechanisms, influencing factors and reduction in chemical disinfectant dosing. *Water* **2014**, *6*, 3603–3630, doi:10.3390/w6123603.
19. Ivanovic, I.; Leiknes, T. O. The biofilm membrane bioreactor (BF-MBR)—a review. *Desalin. Water Treat.* **2012**, *37*, 288–295, doi:10.1080/19443994.2012.661283.
 20. Jørgensen, M. K.; Nierychlo, M.; Nielsen, A. H.; Larsen, P.; Christensen, M. L.; Nielsen, P. H. Unified understanding of physico-chemical properties of activated sludge and fouling propensity. *Water Res.* **2017**, *120*, 117–132, doi:10.1016/j.watres.2017.04.056.
 21. Drews, A. Membrane fouling in membrane bioreactors—Characterisation, contradictions, cause and cures. *J. Memb. Sci.* **2010**, *363*, 1–28, doi:10.1016/j.memsci.2010.06.046.
 22. Martí-Calatayud, M. C.; Schneider, S.; Yüce, S.; Wessling, M. Interplay between physical cleaning, membrane pore size and fluid rheology during the evolution of fouling in membrane bioreactors. *Water Res.* **2018**, *147*, 393–402, doi:10.1016/j.watres.2018.10.017.
 23. Zhang, W.; Tang, B.; Bin, L. Research Progress in Biofilm-Membrane Bioreactor: A Critical Review. *Ind. Eng. Chem. Res.* **2017**, *56*, 6900–6909, doi:10.1021/acs.iecr.7b00794.
 24. Zheng, Y.; Zhang, W.; Tang, B.; Ding, J.; Zheng, Y.; Zhang, Z. Membrane fouling mechanism of biofilm-membrane bioreactor (BF-MBR): Pore blocking model and membrane cleaning. *Bioresour. Technol.* **2018**, *250*, 398–405, doi:10.1016/j.biortech.2017.11.036.
 25. Ng, K. K.; Lin, C. F.; Lateef, S. K.; Panchangam, S. C.; Hong, P. K. A.; Yang, P. Y. The effect of soluble microbial products on membrane fouling in a fixed carrier biological system. *Sep. Purif. Technol.* **2010**, *72*, 98–104, doi:10.1016/j.seppur.2010.01.011.
 26. Phattaranawik, J.; Leiknes, T. Study of Hybrid Vertical Anaerobic Sludge–Aerobic Biofilm Membrane Bioreactor for Wastewater Treatment. *Water Environ. Res.* **2010**, *82*, 273–280, doi:10.2175/106143009X447948.
 27. Sun, C.; Leiknes, T.; Fredriksen, R. H.; Riviere, E. Comparison of membrane filtration performance between biofilm-MBR and activated sludge-MBR. *Desalin. Water Treat.* **2012**, *48*, 285–293, doi:10.1080/19443994.2012.698824.
 28. Leiknes, T.; Ødegaard, H. The development of a biofilm membrane bioreactor. *Desalination* **2007**, *202*, 135–143, doi:10.1016/j.desal.2005.12.049.
 29. Meng, S.; Fan, W.; Li, X.; Liu, Y.; Liang, D.; Liu, X. Intermolecular interactions of polysaccharides in membrane fouling during microfiltration. *Water Res.* **2018**, *143*, 38–46, doi:10.1016/j.watres.2018.06.027.
 30. Nouri, N.; Mehrnia, M. R.; Sarrafzadeh, M. H.; Nabizadeh, R. Performance of membrane bioreactor in presence of flocculants. *Desalin. Water Treat.* **2013**, *52*, 2933–2938, doi:10.1080/19443994.2013.833880.
 31. Ivanovic, I.; Leiknes, T. O. Improved Performance through Particle Surface Modifications by Coagulation with Inorganic Coagulants in a Biofilm Membrane Bioreactor (BF-MBR). *Sep. Sci. Technol.* **2012**, *48*, 288–294, doi:10.1080/01496395.2012.685822.
 32. Chen, W.; Liu, J. The possibility and applicability of coagulation-MBR hybrid system in reclamation of dairy wastewater. *Desalination* **2012**, *285*, 226–231, doi:10.1016/j.desal.2011.10.007.
 33. Hankins, N. P.; Singh, R. *Emerging Membrane Technology for Sustainable Water Treatment*; Marinakis, K., Ed.; Elsevier: Amsterdam, Netherlands; Oxford, UK; Cambridge, USA, 2016; ISBN 978-0-444-63312-5.
 34. Wu, J.; Chen, F.; Huang, X.; Geng, W.; Wen, X. Using inorganic coagulants to control membrane fouling in a submerged membrane bioreactor. *Desalination* **2006**, *197*, 124–136, doi:10.1016/j.desal.2005.11.026.
 35. Gkotsis, P. K.; Batsari, E. L.; Peleka, E. N.; Tolkou, A. K.; Zouboulis, A. I. Fouling control in a lab-scale MBR system: Comparison of several commercially applied coagulants. *J. Environ. Manage.* **2016**, 1–9,

- doi:10.1016/j.jenvman.2016.03.003.
36. Stumm, W.; Morgan, J. J. Chemical Aspects of Coagulation. *J. Am. Water Works Assoc.* **1962**, *54*, 971–991, doi:<https://doi.org/10.1002/j.1551-8833.1962.tb00922.x>.
 37. Miller, D. J.; Kasemset, S.; Paul, D. R.; Freeman, B. D. Comparison of membrane fouling at constant flux and constant transmembrane pressure conditions. *J. Memb. Sci.* **2014**, *454*, 505–515, doi:10.1016/j.memsci.2013.12.027.
 38. Lee, W.-N.; Chang, I.-S.; Hwang, B.-K.; Park, P.-K.; Lee, C.-H.; Huang, X. Changes in biofilm architecture with addition of membrane fouling reducer in a membrane bioreactor. *Process Biochem.* **2007**, *42*, 655–661, doi:10.1016/j.procbio.2006.12.003.
 39. Rosenberg, M.; Gutnick, D.; Rosenberg, E. Adherence of bacteria to hydrocarbons: A simple method for measuring cell-surface hydrophobicity. *FEMS Microbiol. Lett.* **1980**, *9*, 29–33, doi:10.1111/j.1574-6968.1980.tb05599.x.
 40. Van den Broeck, R.; Krzeminski, P.; Van Dierdonck, J.; Gins, G.; Lousada-Ferreira, M.; Van Impe, J. F. M.; van der Graaf, J. H. J. M.; Smets, I. Y.; van Lier, J. B. Activated sludge characteristics affecting sludge filterability in municipal and industrial MBRs: Unraveling correlations using multi-component regression analysis. *J. Memb. Sci.* **2011**, *378*, 330–338, doi:10.1016/j.memsci.2011.05.010.
 41. Micrometrix Corporation. Particle Charge Analyser. Operating Manual 2012, 19.
 42. Adgar, A.; Cox, C. S.; Jones, C. A. Enhancement of coagulation control using the streaming current detector. *Bioprocess Biosyst. Eng.* **2005**, *27*, 349–357, doi:10.1007/s00449-005-0413-5.
 43. Muzi Sibiya, S. Evaluation of the streaming current detector (SCD) for coagulation control. *Procedia Eng.* **2014**, *70*, 1211–1220, doi:10.1016/j.proeng.2014.02.134.
 44. Walker, C. A.; Kirby, J. T.; Dentel, S. K. The streaming current detector: A quantitative model. *J. Colloid Interface Sci.* **1996**, *182*, 71–81, doi:10.1006/jcis.1996.0438.
 45. Dentel, S. K.; Abu-Orf, M. M. Application of the streaming current detector in sludge conditioner selection and control. *Water Sci. Technol.* **1993**, *28*, 169–179.
 46. Van den Winkel, P.; Mertens, J.; Massart, D. L. Streaming Potentials in Automatic Potentiometric Systems. *Anal. Chem.* **1974**, *46*, 1765–1768, doi:10.1021/ac60348a016.
 47. Hubbe, M. A.; Sundberg, A.; Mocchiutti, P.; Ni, Y.; Pelton, R. Dissolved and colloidal substances (DCS) and the charge demand of papermaking process waters and suspensions: A review. *BioResources* **2012**, *7*, 6109–6193, doi:10.15376/biores.7.4.6109-6193.
 48. Kikuchi, Y.; Kubota, N. Permeability Control of Polyelectrolyte Complex Membrane Including Chitosan Derivative as a Component. *Chem. Soc. Japan* **1988**, *61*, 2943–2947.
 49. Striegel, A. M.; Yau, W. W.; Kirkland, J. J.; Bly, D. D. *MODERN SIZE-EXCLUSION LIQUID CHROMATOGRAPHY. Practice of Gel Permeation and Gel Filtration Chromatography*; 2nd ed.; John Wiley & Sons, Inc.: Hoboken, New Jersey, 2009; ISBN 9780471201724.
 50. Fanali, S.; Haddad, P.; Poole, C.; Schoenmakers, P.; Lloyd, D. *Liquid Chromatography: Fundamentals and Instrumentation*; Elsevier: Waltham, Oxford, Amsterdam, 2013; ISBN 9780124158078.
 51. Sun, T. A Study of the Separation Principle in Size Exclusion Chromatography. *Macromolecules* **2004**, *37*, 4304–4312, doi:10.1021/ma030586k.
 52. Wang, Y.; Teraoka, I.; Hansen, F. Y.; Peters, G. H.; Hassager, O. A theoretical study of the separation principle in size exclusion chromatography. *Macromolecules* **2010**, *43*, 1651–1659, doi:10.1021/ma902377g.
 53. CAMO Analytics AS PCA Basics August 2015 Available online: <https://www.youtube.com/watch?v=OavBOzsc3KM> (accessed on May 31, 2019).

54. CAMO *The Unscrambler Tutorials. CAMO Process AS 2006*; CAMO Software AS: Oslo, Norway, 2006; p. 179.
55. Torgersen, G. Sustainable Planning to Reduce Urban Flooding – an Interdisciplinary Approach. PhD thesis, Norwegian University of Life Sciences, 2017.
56. Olivieri, A. C. *Introduction to Multivariate Calibration: A Practical Approach*; Springer: Cham, Switzerland, 2018; ISBN 9783319970974.
57. *Practical Guide to Chemometrics*; Gemperline, P., Ed.; 2nd ed.; Taylor & Francis Group: Boca Raton, London, New York, 2006; ISBN 9781574447835.
58. Tao, E. P.; Shen, W. H.; Liu, T. L.; Chen, X. Q. Fault diagnosis based on PCA for sensors of laboratorial wastewater treatment process. *Chemom. Intell. Lab. Syst.* **2013**, *128*, 49–55, doi:10.1016/j.chemolab.2013.07.012.
59. Vandeginste, B. G. M.; Massart, D. L.; Buydens, L. M. K.; Jong, S. D.; Lewi, P. J.; Smeyers-Verbeke, J. *Handbook of Chemometrics and Qualimetrics: part B*; Vandeginste, B. G. M., Rutan, S. C., Eds.; Elsevier Science B.V.: Amsterdam, Netherlands, 1998; ISBN 0-444-82853-2.
60. Blanchard, G.; Kramer, N. Kernel Partial Least Squares is Universally Consistent. In *Proceedings of the 13th International Conference on Artificial Intelligence and Statistics (AISTATS)*; Chia Laguna Resort, Sardinia, Italy, 2010; Vol. 9, pp. 57–64.
61. Rosipal, R.; Kramer, N. Overview and Recent Advances in Partial Least Squares. In *Latent Structure and Feature Selection. SLSFS 2005. Lecture Notes in Computer Science, vol. 3940*; Saunders C., Grobelnik M., Gunn S., S.-T. J., Ed.; Springer: Berlin, Heidelberg, 2006; pp. 34–51 ISBN 978-3-540-34138-3.
62. Wold, S.; Sjostrom, M.; Eriksson, L. PLS-regression: a basic tool of chemometrics. *Chemom. Intell. Lab. Syst.* **2001**, *58*, 109–130, doi:10.1016/S0169-7439(01)00155-1.
63. Brereton, R. G. *Chemometrics. Data Analysis for the Laboratory and Chemical Plant*; Wiley: Bristol, UK, 2003; Vol. 8; ISBN 0-471-48977-8.
64. Andersson, M. A comparison of nine PLS1 algorithms. *J. Chemom.* **2009**, *23*, 518–529, doi:10.1002/cem.1248.
65. Björck, Å.; Indahl, U. G. Fast and stable partial least squares modelling: A benchmark study with theoretical comments. *J. Chemom.* **2017**, *31*, 1–15, doi:10.1002/cem.2898.
66. Wang, X. Optimisation of Wastewater Treatment Systems with Data Mining and Process Modelling. Ph.D. Thesis, Norwegian University of Life Sciences, Ås, 2018.
67. Wise, B. M.; Gallagher, N. B.; Bro, R.; Shaver, J. M.; Windig, W.; Koch, R. S. Chemometrics Tutorial for PLS_Toolbox and Solo 2006, 420.
68. King, R. S. *Cluster Analysis and Data Mining: An Introduction*; David Pallai, Mercury Learning and Information: Dulles, USA, 2015; ISBN 978-1-938549-38-0.
69. Hair, J. F.; Black, W. C.; Babin, B. J.; Anderson, R. E. *Multivariate Data Analysis. Pearson New International Edition*; Seventh Ed.; Pearson Education Limited: Harlow, 2014; ISBN 9781292021904.
70. Massart, D. L.; Vandeginste, B. G. M.; Buydens, L. M. K.; Jong, S. D.; Lewi, P. J.; Smeyers-Verbeke, J. *Handbook of Chemometrics and Qualimetrics: part A*; 1st ed.; Elsevier Science Inc.: New York, USA, 1997; ISBN 9780080551906.
71. Collins, L. M.; Dziak, J. J.; Li, R. Design of Experiments with Multiple Independent Variables: A Resource Management Perspective on Complete and Reduced Factorial Designs. *Phiscol Methods* **2009**, *14*, 202–224, doi:10.1037/a0015826.Design.
72. Minitab LLC Orthogonal designs Available online: <https://support.minitab.com/en-us/minitab/18/help->

- and-how-to/modeling-statistics/doi/supporting-topics/basics/orthogonal-designs/ (accessed on Jun 10, 2019).
73. Montgomery, D. C. *Design and Analysis of Experiments*; Ratts, L., Melhorn, A., Eds.; Eighth Edi.; John Wiley & Sons, Inc. All: Hoboken, New Jersey, 2013; ISBN 9781118146927.
 74. Leica Microsystems Objective Classes Available online: <https://www.leica-microsystems.com/products/microscope-objectives/objective-classes/> (accessed on Jul 3, 2019).
 75. ImageJ: Image Processing and Analysis in Java Available online: <https://imagej.nih.gov/ij/> (accessed on Feb 1, 2019).
 76. International Organization for Standardization. *International Standard. ISO 9276-1. Representation of results of particle size analysis — Part 1: Graphical representation*; Switzerland, 1998; p. 9.
 77. Mingard, K.; Morrell, R.; Jackson, P.; Lawson, S.; Patel, S.; Buxton, R. *Good Practice Guide for Improving the Consistency of Particle Size Measurement*; Teddington, Middlesex, London, 2009.
 78. McQuarrie, D. *Statistical Mechanics*; Rice, S. A., Ed.; Harper & Row: New York, Evanston, San Francisco, London, 1976; ISBN 06-044366-9.
 79. Hypercube, I. HyperChem® Release 7 for Windows® Getting Started. *Man. HC70-00-01-00* 2002, 860.
 80. Esposito, G.; Marmo, G.; Sudarshan, G. *From classical to quantum mechanics: an introduction to the formalism, foundations and applications*; Cambridge University Press: New York, USA, 2004; ISBN 978-0-511-18490-1.
 81. Thiel, W. Semiempirical Methods. In *Modern Methods and Algorithms of Quantum Chemistry, Proceedings*; John von Neumann Institute for Computing: Jülich, Germany, 2000; pp. 1–23 ISBN 3000058346.
 82. Hasanein, A. A.; Evans, M. W. *Computational methods in quantum chemistry. Quantum chemistry Vol.2*; World Scientific Publishing Co. Pte. Ltd.: Singapore, New Jersey, London, Hong Kong, 1996; Vol. 2; ISBN 981-02-2611-X.
 83. Young, D. C. 4. Semiempirical Methods. In *COMPUTATIONAL CHEMISTRY. A practical Guide for Applying Techniques to Real-World Problems*; Wiley-Interscience, John Wiley & Sons, Inc.: New York, Chichester, Weinheim, Brisbane, Singapore, Toronto, 2001; p. 408.
 84. Zuthi, M. F. R.; Guo, W.; Ngo, H. H.; Nghiem, D. L.; Hai, F. I.; Xia, S.; Li, J.; Li, J.; Liu, Y. New and practical mathematical model of membrane fouling in an aerobic submerged membrane bioreactor. *Bioresour. Technol.* **2017**, *238*, 86–94, doi:10.1016/j.biortech.2017.04.006.
 85. Shi, Y.; Huang, J.; Zeng, G.; Gu, Y.; Hu, Y.; Tang, B.; Zhou, J.; Yang, Y.; Shi, L. Evaluation of soluble microbial products (SMP) on membrane fouling in membrane bioreactors (MBRs) at the fractional and overall level: a review. *Rev. Environ. Sci. Biotechnol.* **2018**, *17*, 71–85, doi:10.1007/s11157-017-9455-9.
 86. Chellam, S.; Cogan, N. G. Colloidal and bacterial fouling during constant flux microfiltration: Comparison of classical blocking laws with a unified model combining pore blocking and EPS secretion. *J. Memb. Sci.* **2011**, *382*, 148–157, doi:10.1016/j.memsci.2011.08.001.
 87. Wang, F.; Tarabara, V. V. Pore blocking mechanisms during early stages of membrane fouling by colloids. *J. Colloid Interface Sci.* **2008**, *328*, 464–469, doi:10.1016/j.jcis.2008.09.028.
 88. Jelemenský, M.; Sharma, A.; Paulen, R.; Fikar, M. Time-optimal control of diafiltration processes in the presence of membrane fouling. *Comput. Chem. Eng.* **2016**, *91*, 343–351, doi:10.1016/j.compchemeng.2016.04.018.
 89. Bowen, W. R.; Calvo, J. I.; Hernández, A. Steps of membrane blocking in flux decline during protein microfiltration. *J. Memb. Sci.* **1995**, *101*, 153–165, doi:10.1016/0376-7388(94)00295-A.
 90. Park, H.-D.; Chang, I.-S.; Lee, K.-J. *Principles of Membrane Bioreactors for Wastewater Treatment*; 1st ed.; CRC Press. Taylor and Francis Group: Boca Raton, London, New York, 2015; ISBN 9781466590373.

91. Baker, R. W. *Membrane Technology and Applications*; 2nd ed.; John Wiley & Sons, Ltd: Chichester, West Sussex, England, 2004; ISBN 0470854456.
92. Chu, H. P.; Li, X. Y. Membrane fouling in a membrane bioreactor (MBR): Sludge cake formation and fouling characteristics. *Biotechnol. Bioeng.* **2005**, *90*, 323–331, doi:10.1002/bit.20409.
93. Fonseca, A. C.; Summers, R. S.; Greenberg, A. R. Extra-Cellular Polysaccharides, Soluble Microbial Products, and Natural Organic Matter Impact on Nanofiltration Membranes Flux Decline. *Environ. Sci. Technol.* **2007**, *41*, 2491–2497, doi:10.1021/es060792i.
94. Jin, L.; Ong, S. L.; Ng, H. Y. Fouling control mechanism by suspended biofilm carriers addition in submerged ceramic membrane bioreactors. *J. Memb. Sci.* **2013**, *427*, 250–258, doi:10.1016/j.memsci.2012.09.016.
95. Ivanovic, I.; Leiknes, T. Effect of addition of different additives on overall performance of biofilm-MBR (BF-MBR). *Desalin. Water Treat.* **2011**, *34*, 129–135, doi:10.5004/dwt.2011.2861.
96. Ye, Y.; Clech, P. Le; Chen, V.; Fane, A. G. Evolution of fouling during crossflow filtration of model EPS solutions. *J. Memb. Sci.* **2005**, *264*, 190–199, doi:10.1016/j.memsci.2005.04.040.
97. Kola, A.; Ye, Y.; Ho, A.; Le-Clech, P.; Chen, V. Application of low frequency transverse vibration on fouling limitation in submerged hollow fibre membranes. *J. Memb. Sci.* **2012**, *409–410*, 54–65, doi:10.1016/j.memsci.2012.03.017.
98. Neemann, F.; Rosenberger, S.; Jefferson, B.; McAdam, E. J. Non-covalent protein–polysaccharide interactions and their influence on membrane fouling. *J. Memb. Sci.* **2013**, *446*, 310–317, doi:10.1016/J.MEMSCI.2013.06.054.
99. Banti, D. C.; Samaras, P.; Tsiptsias, C.; Zouboulis, A.; Mitrakas, M. Mechanism of SMP aggregation within the pores of hydrophilic and hydrophobic MBR membranes and aggregates detachment. *Sep. Purif. Technol.* **2018**, *202*, 119–129, doi:10.1016/j.seppur.2018.03.045.
100. Choi, J. H.; Ng, H. Y. Effect of membrane type and material on performance of a submerged membrane bioreactor. *Chemosphere* **2008**, *71*, 853–859, doi:10.1016/j.chemosphere.2007.11.029.
101. Zhou, Z.; Meng, F.; He, X.; Chae, S.-R.; An, Y.; Jia, X. Metaproteomic analysis of biocake proteins to understand membrane fouling in a submerged membrane bioreactor. *Environ. Sci. Technol.* **2015**, *49*, 1068–77, doi:10.1021/es504489r.
102. Soler-Cabezas, J. L.; Torà-Grau, M.; Vincent-Vela, M. C.; Mendoza-Roca, J. A.; Martínez-Francisco, F. J. Ultrafiltration of municipal wastewater: study on fouling models and fouling mechanisms. *Desalin. Water Treat.* **2015**, *56*, 3427–3437, doi:10.1080/19443994.2014.969320.
103. Miyoshi, T.; Aizawa, T.; Kimura, K.; Watanabe, Y. Identification of proteins involved in membrane fouling in membrane bioreactors (MBRs) treating municipal wastewater. *Int. Biodeterior. Biodegrad.* **2012**, *75*, 15–22, doi:10.1016/j.ibiod.2012.08.003.
104. Wu, J.; Huang, X. Effect of mixed liquor properties on fouling propensity in membrane bioreactors. *J. Memb. Sci.* **2009**, *342*, 88–96, doi:10.1016/j.memsci.2009.06.024.
105. Kimura, K.; Naruse, T.; Watanabe, Y. Changes in characteristics of soluble microbial products in membrane bioreactors associated with different solid retention times: Relation to membrane fouling. *Water Res.* **2009**, *43*, 1033–1039, doi:10.1016/j.watres.2008.11.024.
106. Zhang, H.; Gao, Z.; Zhang, L.; Song, L. Performance enhancement and fouling mitigation by organic flocculant addition in membrane bioreactor at high salt shock. *Bioresour. Technol.* **2014**, *164*, 34–40, doi:10.1016/j.biortech.2014.04.053.
107. Chuang, S. H.; Chang, W. C.; Chang, M. C.; Sung, M. A. The effects of soluble organic matters on

- membrane fouling index. *Bioresour. Technol.* **2009**, *100*, 1875–1877, doi:10.1016/j.biortech.2008.09.054.
108. Kimura, K.; Ogyu, R.; Miyoshi, T.; Watanabe, Y. Transition of major components in irreversible fouling of MBRs treating municipal wastewater. *Sep. Purif. Technol.* **2015**, *142*, 326–331, doi:10.1016/j.seppur.2014.12.030.
109. Malamis, S.; Andreadakis, A. Fractionation of proteins and carbohydrates of extracellular polymeric substances in a membrane bioreactor system. *Bioresour. Technol.* **2009**, *100*, 3350–3357, doi:10.1016/j.biortech.2009.01.053.
110. Gkotsis, P. K.; Zouboulis, A. I. Biomass Characteristics and Their Effect on Membrane Bioreactor Fouling. *Molecules* **2019**, *24*, 1–19, doi:10.3390/molecules24162867.
111. Rahimi, Y.; Torabian, A.; Mehrdadi, N.; Habibi-Rezaie, M.; Pezeshk, H.; Nabi-Bidhendi, G. R. Optimizing aeration rates for minimizing membrane fouling and its effect on sludge characteristics in a moving bed membrane bioreactor. *J. Hazard. Mater.* **2011**, *186*, 1097–1102, doi:10.1016/j.jhazmat.2010.11.117.
112. Xu, R.; Yu, Z.; Zhang, S.; Meng, F. Bacterial assembly in the bio-cake of membrane bioreactors: Stochastic vs. deterministic processes. *Water Res.* **2019**, *157*, 535–545, doi:10.1016/j.watres.2019.03.093.
113. Di, G.; Di, D.; Freni, G.; Torregrossa, M. Analysis of Biomass Characteristics in MBR and MB-MBR Systems Fed with Synthetic Wastewater: Influence of a Gradual Salinity Increase. **2014**, *38*, 445–450, doi:10.3303/CET1438075.
114. Deng, L.; Guo, W.; Hao Ngo, H.; Zhang, H.; Wang, J.; Li, J.; Xia, S.; Wu, Y. Biofouling and control approaches in membrane bioreactors. *Bioresour. Technol.* **2016**, doi:10.1016/j.biortech.2016.09.105.
115. Gkotsis, P. K.; Mitrakas, M. M.; Tolkou, A. K.; Zouboulis, A. I. Batch and continuous dosing of conventional and composite coagulation agents for fouling control in a pilot-scale MBR. *Chem. Eng. J.* **2017**, *311*, 255–264, doi:10.1016/j.cej.2016.11.099.
116. Janus, T.; Ulanicki, B. A behavioural membrane fouling model for integrated simulation of membrane bioreactors for wastewater treatment. *Procedia Eng.* **2015**, *119*, 1328–1337, doi:10.1016/j.proeng.2015.08.964.
117. Judd, S. The status of membrane bioreactor technology. *Trends Biotechnol.* **2008**, *26*, 109–116, doi:10.1016/j.tibtech.2007.11.005.
118. Wang, Z.; Ma, J.; Tang, C. Y.; Kimura, K.; Wang, Q.; Han, X. Membrane cleaning in membrane bioreactors: A review. *J. Memb. Sci.* **2014**, *468*, 276–307, doi:10.1016/j.memsci.2014.05.060.
119. Field, R. W.; Wu, D.; Howell, J. A.; Gupta, B. B. Critical flux concept for microfiltration fouling. *J. Memb. Sci.* **1995**, *100*, 259–272, doi:10.1016/0376-7388(94)00265-Z.
120. Aslam, M.; Lee, P. H.; Kim, J. Analysis of membrane fouling with porous membrane filters by microbial suspensions for autotrophic nitrogen transformations. *Sep. Purif. Technol.* **2015**, *146*, 284–293, doi:10.1016/j.seppur.2015.03.042.
121. Etemadi, H.; Yegani, R.; Seyfollahi, M. The effect of amino functionalized and polyethylene glycol grafted nanodiamond on anti-biofouling properties of cellulose acetate membrane in membrane bioreactor systems. *Sep. Purif. Technol.* **2017**, *177*, 350–362, doi:10.1016/j.seppur.2017.01.013.
122. El Rayess, Y.; Albasi, C.; Bacchin, P.; Taillandier, P.; Mietton-Peuchot, M.; Devatine, A. Analysis of membrane fouling during cross-flow microfiltration of wine. *Innov. Food Sci. Emerg. Technol.* **2012**, *16*, 398–408, doi:10.1016/j.ifset.2012.09.002.
123. Kumar, R. V.; Goswami, L.; Pakshirajan, K.; Pugazhenthii, G. Dairy wastewater treatment using a novel low cost tubular ceramic membrane and membrane fouling mechanism using pore blocking models. *J. Water Process Eng.* **2016**, *13*, 168–175, doi:10.1016/j.jwpe.2016.08.012.

124. Lee, S. J.; Dilaver, M.; Park, P. K.; Kim, J. H. Comparative analysis of fouling characteristics of ceramic and polymeric microfiltration membranes using filtration models. *J. Memb. Sci.* **2013**, *432*, 97–105, doi:10.1016/j.memsci.2013.01.013.
125. Gkotsis, P. K.; Mitrakas, M. M.; Tolkou, A. K.; Zouboulis, A. I. Batch and continuous dosing of conventional and composite coagulation agents for fouling control in a pilot-scale MBR. *Chem. Eng. J.* **2016**, *311*, 255–264, doi:10.1016/j.cej.2016.11.099.
126. Ratnaweera, H. *Phosphorus recovery from wastewater - should we rebuild our wastewater treatment plants? (Translated)*; Oslo, Norway, 2013.
127. Eliassen, H. *Central treatment plants – new discharge permits «Optimization of Bekkelaget wastewater treatment plant» (Translated)*; Oslo, Norway, 2016.
128. Ødegaard, H.; Fettig, J.; Ratnaweera, H. Coagulation with Prepolymerized Metal Salts. In *Chemical water and wastewater treatment. Proceedings of the 4th Gothenburg Symposium 1990 October 1–3, 1990 Madrid, Spain*; Gothenburg, Sweden, 1990; Vol. 304, pp. 189–220.
129. Koseoglu, H.; Yigit, N. O.; Civelekoglu, G.; Harman, B. I.; Kitis, M. Effects of chemical additives on filtration and rheological characteristics of MBR sludge. *Bioresour. Technol.* **2012**, *117*, 48–54, doi:10.1016/j.biortech.2012.04.067.
130. Song, K. G.; Kim, Y.; Ahn, K. H. Effect of coagulant addition on membrane fouling and nutrient removal in a submerged membrane bioreactor. *Desalination* **2008**, *221*, 467–474, doi:10.1016/j.desal.2007.01.107.
131. Bratby, J. *Coagulation and flocculation in water and wastewater treatment*; 3rd ed.; IWA Publishing: London, UK, 2016; ISBN 9781780407500.
132. Zhang, P.; Shen, Y.; Guo, J.; Li, C.; Wang, H.; Chen, Y.; Yan, P. Extracellular protein analysis of activated sludge and their functions in wastewater treatment plant by shotgun proteomics. *Nat. Publ. Gr.* **2015**, 1–11, doi:10.1038/srep12041.
133. Rijnaarts, H. H. M.; Norde, W.; Lyklema, J.; Zehnder, A. J. B. The isoelectric point of bacteria as an indicator for the presence of cell surface polymers that inhibit adhesion. *Colloids Surfaces B Biointerfaces* **1995**, *4*, 191–197, doi:10.1016/0927-7765(94)01164-Z.
134. She, Q.; Wang, R.; Fane, A. G.; Tang, C. Y. Membrane fouling in osmotically driven membrane processes: A review. *J. Memb. Sci.* **2016**, *499*, 201–233, doi:10.1016/j.memsci.2015.10.040.
135. Liao, B. Q.; Allen, D. G.; Droppo, I. G.; Leppard, G. G.; Liss, S. N. Surface properties of sludge and their role in bioflocculation and settleability. *Water Res.* **2001**, *35*, 339–350, doi:10.1016/S0043-1354(00)00277-3.
136. Guo, W.; Ngo, H. H.; Vigneswaran, S.; Dharmawan, F.; Nguyen, T. T.; Aryal, R. Effect of different flocculants on short-term performance of submerged membrane bioreactor. *Sep. Purif. Technol.* **2010**, *70*, 274–279, doi:10.1016/j.seppur.2009.10.003.
137. Zhang, H. feng; Sun, B. sheng; Zhao, X. hua; Gao, Z. hong. Effect of ferric chloride on fouling in membrane bioreactor. *Sep. Purif. Technol.* **2008**, *63*, 341–347, doi:10.1016/j.seppur.2008.05.024.
138. Zhang, Z.; Wang, Y.; Leslie, G. L.; Waite, T. D. Effect of ferric and ferrous iron addition on phosphorus removal and fouling in submerged membrane bioreactors. *Water Res.* **2015**, *69*, 210–222, doi:10.1016/j.watres.2014.11.011.
139. Ji, J.; Qiu, J.; Wai, N.; Wong, F. S.; Li, Y. Influence of organic and inorganic flocculants on physical-chemical properties of biomass and membrane-fouling rate. *Water Res.* **2010**, *44*, 1627–1635, doi:10.1016/j.watres.2009.11.013.
140. Wu, J.; Huang, X. Effect of dosing polymeric ferric sulfate on fouling characteristics, mixed liquor properties and performance in a long-term running membrane bioreactor. *Sep. Purif. Technol.* **2008**, *63*,

- 45–52, doi:10.1016/j.seppur.2008.03.033.
141. Isma, M. I. A.; Idris, A.; Omar, R.; Razreena, A. R. P. Effects of SRT and HRT on Treatment Performance of MBR and Membrane Fouling. *2014*, *8*, 488–492.
 142. Van den Broeck, R.; Van Dierdonck, J.; Nijskens, P.; Dotremont, C.; Krzeminski, P.; van der Graaf, J. H. J. M.; van Lier, J. B.; Van Impe, J. F. M.; Smets, I. Y. The influence of solids retention time on activated sludge bioflocculation and membrane fouling in a membrane bioreactor (MBR). *J. Memb. Sci.* **2012**, *401–402*, 48–55, doi:10.1016/j.memsci.2012.01.028.
 143. Chen, W.; Liu, J.; Xie, F. Identification of the moderate SRT for reliable operation in MBR. *Desalination* **2012**, *286*, 263–267, doi:10.1016/j.desal.2011.11.033.
 144. American Public Health Association; Water Environment Federation; American Water Works Association *Standard Methods for the Examination of Water and Wastewater. 22nd Edition*; Rice, E. W., Baird, R. B., Eaton, A. D., Clesceri, L. S., Eds.; 22nd Revis.; American Public Health Association: Washington, DC, United Kingdom, 2012; ISBN 9780875530130.
 145. Le-Clech, P.; Chen, V.; Fane, T. A. G. Fouling in membrane bioreactors used in wastewater treatment. *J. Memb. Sci.* **2006**, *284*, 17–53, doi:10.1016/j.memsci.2006.08.019.
 146. Yigit, N. O.; Harman, I.; Civelekoglu, G.; Koseoglu, H.; Cicek, N.; Kitis, M. Membrane fouling in a pilot-scale submerged membrane bioreactor operated under various conditions. *Desalination* **2008**, *231*, 124–132, doi:10.1016/j.desal.2007.11.041.
 147. Ratnaweera, H. C. Influence of the degree of coagulant prepolymerization on wastewater coagulation mechanisms. Ph.D. Thesis, The University of Trondheim. The Norwegian Institute of Technology, 1991.
 148. European Commission *EU-level instruments on water reuse: Final report to support the commission's impact assessment*; European Commission: Brussels, Belgium, 2016.
 149. United States Environmental Protection Agency *EPA ambient water quality criteria for Aluminium*; Office of Water Regulations and Standards Criteria and Standards Division: United States, 1988.
 150. Eignor, D. Draft National 304(a) Aluminum Aquatic Life Criteria Available online: <https://www.epa.gov/sites/production/files/2017-09/documents/aluminum-webinar-9192017.pdf> (accessed on Dec 1, 2018).
 151. Zouboulis, A. I.; Tzoupanos, N. D. Polyaluminium silicate chloride-A systematic study for the preparation and application of an efficient coagulant for water or wastewater treatment. *J. Hazard. Mater.* **2009**, *162*, 1379–1389, doi:10.1016/j.jhazmat.2008.06.019.
 152. Gao, B. Y.; Yue, Q. Y.; Wang, B. J.; Chu, Y. B. Poly-aluminum-silicate-chloride (PASiC) - A new type of composite inorganic polymer coagulant. *Colloids Surfaces A Physicochem. Eng. Asp.* **2003**, *229*, 121–127, doi:10.1016/j.colsurfa.2003.07.005.
 153. Zhang, P.; Hahn, H. H.; Hoffmann, E.; Zeng, G. Influence of some additives to aluminium species distribution in aluminium coagulants. *Chemosphere* **2004**, *57*, 1489–1494, doi:10.1016/j.chemosphere.2004.08.066.
 154. Tzoupanos, N. D.; Zouboulis, A. I.; Tsoleridis, C. A. A systematic study for the characterization of a novel coagulant (polyaluminium silicate chloride). *Colloids Surfaces A Physicochem. Eng. Asp.* **2009**, *342*, 30–39, doi:10.1016/j.colsurfa.2009.03.054.
 155. Stat-Ease Inc. Design-Expert 11.1.0. Documentation. Tutorials. Available online: <https://www.statease.com/docs/v11/index.html> (accessed on Oct 31, 2018).
 156. Maletskiy, Z.; Zigta, D. K.; Kulesha, O.; Ratnaweera, H. *Chemical enhancement for retrofitting Moving Bed Biofilm and Integrated Fixed film Activated Sludge systems into Membrane Bioreactors*; Submitted to

- Membranes journal; Ås, Norway, 2019.
157. Stumm, W.; O'Melia, C. Stoichiometry of coagulation. *Am. Water Work. Assoc.* **1968**, *60*, 514–539.
 158. Haimi, H.; Mulas, M.; Corona, F.; Vahala, R. Data-derived soft-sensors for biological wastewater treatment plants: An overview. *Environ. Model. Softw.* **2013**, *47*, 88–107, doi:10.1016/j.envsoft.2013.05.009.
 159. Wang, X.; Kvaal, K.; Ratnaweera, H. Characterization of influent wastewater with periodic variation and snow melting effect in cold climate area. *Comput. Chem. Eng.* **2017**, *106*, 202–211, doi:10.1016/j.compchemeng.2017.06.009.
 160. Liltved, H.; Ratnaweera, H.; Plo, B. G. Climate change impacts on activated sludge wastewater treatment: a case study from Norway. *Water Sci. Technol. - WST* **2009**, *60*, 533–541, doi:10.2166/wst.2009.386.
 161. Kimura, K.; Kakuda, T.; Iwasaki, H. Membrane fouling caused by lipopolysaccharides: A suggestion for alternative model polysaccharides for MBR fouling research. *Sep. Purif. Technol.* **2019**, *223*, 224–233, doi:10.1016/j.seppur.2019.04.059.
 162. Silva, A. F.; Antunes, S.; Saunders, A.; Freitas, F.; Vieira, A.; Galinha, C. F.; Nielsen, P. H.; Barreto Crespo, M. T.; Carvalho, G. Impact of sludge retention time on MBR fouling: role of extracellular polymeric substances determined through membrane autopsy. *Biofouling* **2017**, *33*, 556–566, doi:10.1080/08927014.2017.1333112.
 163. Silva, A. F.; Antunes, S.; Saunders, A.; Freitas, F.; Vieira, A.; Galinha, C. F.; Nielsen, P. H.; Barreto Crespo, M. T.; Carvalho, G. Impact of sludge retention time on the fine composition of the microbial community and extracellular polymeric substances in a membrane bioreactor. *Appl. Microbiol. Biotechnol.* **2016**, *100*, 8750–8521, doi:10.1007/s00253-016-7617-2.
 164. Feng, L.; Li, X.; Song, P.; Du, G.; Chen, J. Physicochemical properties and membrane biofouling of extracellular polysaccharide produced by a *Micrococcus luteus* strain. *World J. Microbiol. Biotechnol.* **2014**, *30*, 2025–2031, doi:10.1007/s11274-014-1627-y.
 165. Miura, Y.; Okabe, S. Quantification of cell specific uptake activity of microbial products by uncultured chloroflexi by microautoradiography combined with fluorescence in situ hybridization. *Environ. Sci. Technol.* **2008**, *42*, 7380–7386, doi:10.1021/es800566e.
 166. Miyoshi, T.; Naruse, T.; Yamato, N.; Kimura, K.; Watanabe, Y. Influence of operating conditions on chemically reversible fouling in submerged MBRs. In *2nd IWA National Young Water Professionals Conference, Germany "Membrane Technologies for Wastewater Treatment and Reuse"*; Lesjean, B., Ed.; KompetenzZentrum Wasser Berlin gGmbH: Berlin, Germany, 2007; pp. 231–234.
 167. Christensen, B. E. The role of extracellular polysaccharides in biofilms. *J. Biotechnol.* **1989**, *10*, 181–202, doi:10.1016/0168-1656(89)90064-3.
 168. Lastuhin, Y.; Voronov, S. *Organic Chemistry (Translated)*; Ganushchak, M., Ed.; 3rd ed.; Centre of Europe: Lviv, Ukraine, 2006; ISBN 9667022196.
 169. Sarpola, A. The Hydrolysis of Aluminium, A Mass Spectrometric Study. Ph.D. Thesis, University of Oulu, 2007.
 170. Sarpola, A.; Postdoctoral Fellow, Faculty of Technology, Energy and Environmental Engineering Research Unit, University of Oulu, Oulu, Finland; Business Director at Eurofins Lactium Oy, Sodankylä, Finland. Personal communication, 2019.
 171. Pernitsky, D. J.; Edzwald, J. K. Solubility of polyaluminium coagulants. *J. Water Supply Res. Technol. - AQUA* **2003**, *52*, 395–406, doi:10.2166/aqua.2003.0036.
 172. Bi, Z.; Chen, Y.; Wang, S.; Wang, D. Hydrolyzed Al(III)-clusters. II: Speciation transformation and stability of Al13aggregates. *Colloids Surfaces A Physicochem. Eng. Asp.* **2014**, *440*, 59–62,

- doi:10.1016/j.colsurfa.2012.09.055.
173. Bottero, J. Y.; Cases, J. M.; Fiessinger, F.; Polrier, J. E. Studies of hydrolyzed aluminum chloride solutions. 1. Nature of aluminum species and composition of aqueous solutions. *J. Phys. Chem.* **1980**, *84*, 2933–2939, doi:10.1021/j100459a021.
174. Feng, C.; Zhao, S.; Bi, Z.; Wang, D.; Tang, H. Speciation of prehydrolyzed Al salt coagulants with electrospray ionization time-of-flight mass spectrometry and ²⁷Al NMR spectroscopy. *Colloids Surfaces A Physicochem. Eng. Asp.* **2011**, *392*, 95–102, doi:10.1016/j.colsurfa.2011.09.039.
175. Rämö, J. H.; Sarpola, A. T.; Hellman, A. H.; Leiviskä, T. A.; Hietapelto, V. K.; Jokela, J. T.; Laitinen, R. S. Colloidal surfaces and oligomeric species generated by water treatment chemicals. *Chem. Speciat. Bioavailab.* **2008**, *20*, 13–22, doi:10.3184/095422908X297058.
176. Seichter, W.; Mögel, H.-J.; Brand, P.; Salah, D. Crystal Structure and Formation of the Aluminium Hydroxide Chloride [Al₁₃(OH)₂₄(H₂O)₂₄]Cl₁₅·13H₂O. *Eur. J. Inorg. Chem.* **1998**, *13*, 795–797.
177. Atkins, P.; de Paula, J. *Physical Chemistry for the Life Sciences*; 2nd ed.; W.H. Freeman and Company: New York, USA, 2011; ISBN 9781429231145.
178. Oxtoby, D.; Gillis, H. P.; Campion, A. *Principles of modern chemistry*; Lockwood, L., Martin, T., Eds.; 7th ed.; Brooks/Cole, Cengage Learning: Belmont, USA, 2012; ISBN 978-0-8400-4931-5.
179. Google Trends: Machine Learning Available online: [https://trends.google.com/trends/explore?date=today-5-y&q=machine learning](https://trends.google.com/trends/explore?date=today-5-y&q=machine%20learning) (accessed on Jun 28, 2019).
180. Rubini, P.; Lakatos, A.; Champmartin, D.; Kiss, T. Speciation and structural aspects of interactions of Al(III) with small biomolecules. *Coord. Chem. Rev.* **2002**, *228*, 137–152, doi:10.1016/S0010-8545(01)00467-2.
181. Fernandez de Canete, J.; Del Saz-Orozco, P.; Baratti, R.; Mulas, M.; Ruano, A.; Garcia-Cerezo, A. Soft-sensing estimation of plant effluent concentrations in a biological wastewater treatment plant using an optimal neural network. *Expert Syst. Appl.* **2016**, *63*, 8–19, doi:10.1016/j.eswa.2016.06.028.
182. Choi, D. J.; Park, H. A hybrid artificial neural network as a software sensor for optimal control of a wastewater treatment process. *Water Res.* **2001**, *35*, 3959–3967, doi:10.1016/S0043-1354(01)00134-8.

Appendix A

Synopsis of the appended papers

The following is a brief summary of each paper.

Paper I: State of the art on membrane fouling, its prevention, and control in membrane bioreactor

Membrane fouling is the key bottleneck towards further expansion of MBR technology. It is a complex phenomenon, whose nature and mitigation still require intensive investigations. Polysaccharides are the primary membrane foulants in MBR and BF-MBR. Proteins and humic substances contribute to membrane fouling mainly via the interaction with the polysaccharides. All together they make up a large group of foulants defined as the soluble microbial products (SMPs). SMPs, together with extracellular polymeric substances (EPSs) (the latter are of bound/particulate nature), are considered the main foulants. The foulants cause reversible, irreversible, and irrecoverable membrane fouling, which helps to distinguish a suitable cleaning approach (if applicable). The modification of the mixed liquor characteristics by applying coagulants, flocculants, bio-flocculants, adsorbents, and ozonation, are the promising directions of membrane fouling mitigation in MBR and BF-MBR. Many bacterial solid surfaces have readily ionizable or active functional groups, which facilitates their interaction with coagulants, flocculants, and bio-flocculants. The application of Al- and Fe- based coagulants as flux enhancers is among the most promising approaches to the reduction of the mixed liquor fouling propensity. Al- and Fe-based coagulants exhibited a significant improvement of filtration performance in MBR systems by acting according to the following mechanisms of fouling mitigation: enhancement of adsorption/charge neutralization, increase of relative hydrophobicity and mean size of the flocs, reduction of SMPs level in mixed liquor, and increase of cake porosity/inhibition of gel layer formation. Bridging the gap in process control of the MBR and BF-MBR, including flux enhancement part is as an important and perspective direction of future research.

Paper II: Statistical approach to the assessment of membrane fouling patterns and fouling control in biofilm ceramic membrane bioreactor

Biofilm membrane bioreactor (BF-MBR) is the advancement of the existing MBR with regard to the reduced predisposition to membrane fouling. BF-MBR employs the incorporation of the biofilm inoculated on the suspended carriers prior to the membrane filtration. Despite the advantages, BF-MBR is still affected by membrane fouling. The following knowledge gaps in the development of BF-MBR systems could be singled out:

there was no complete statistical investigation of the interrelation between operating parameters, fouling development, and mixed liquor characteristics; whereas a controversy over the influence of the selected mixed liquor parameters on the fouling intensity was apparent. Besides, there was a lack of research data on the application of the partial least squares (PLS) analysis to characterization of the processes in the biofilm membrane bioreactor. **Paper II** provides the development of the chemometric approach to the assessment of membrane fouling, its monitoring, and control in the BF-MBR with the ceramic membranes, which encapsulated the relationship between the significant mixed liquor characteristics (COD_{dis}, MLSS, and SVI), membrane fouling indicators (the average normalized permeability), and the operation conditions (sludge retention time (SRT), intensity of sludge recirculation, and net and gross permeate fluxes). The developed validated models were used to adjust operational parameters of the BF-MBR pilot system during 114 days of operation according to the characteristics of mixed liquor, keeping fouling development below the critical limits.

Paper III: Strategy for Flux Enhancement in Biofilm Ceramic Membrane Bioreactor Applying Prepolymerized and Non-prepolymerized Inorganic Coagulants based on the mechanisms of EPSs removal

An overview of the cutting-edge research works reveals limited studies and controversial results on chemical flux enhancement and its mechanisms applying the inorganic coagulants in the biofilm membrane bioreactor. No studies were reported on the use of multivariate statistics to assess fouling mitigation potential of the coagulants and mechanisms of their action; or filtration optimization in the BF-MBR systems. **Paper III** introduced the concept of chemical flux enhancement in the BF-MBR based on complex adsorption/charge neutralization mechanism of the floc-bound EPSs removal. The analysis was based on the comparative study of prepolymerized and non-prepolymerized inorganic coagulants as flux enhancers, applying the PLS analysis for the investigation of the membrane fouling control and its mechanisms. In addition, a two-level factorial design of the experiment for optimization of membrane filtration in BF-MBR system was developed. Research results substantiated the necessity for pH-controlled coagulation of mixed liquor in BF-MBR depending on coagulant type, which influences charge, hydrophobicity, and size of flocs; and organic content of the system. The results indicated that, in contrast to the non-prepolymerized coagulants, prepolymerized aluminium coagulants were much more efficient with respect to

flux enhancement. The prepolymerized aluminium chloride with medium basicity demonstrated the greatest extent of fouling alleviation among the tested coagulants.

Paper IV: Monitoring and prediction of the chemical coordination of the SMP_c to the coagulant active species during chemical flux enhancement in BF-MBR

The processes taking place in the MBR and BF-MBR system after adding the coagulants as flux enhancers still partly remain a black box due to their complexity and rapidness. The electro-surface phenomena, described by the theories of double layer and electrostatic interactions, are not applicable to the explanation of the interactions between the SMPs in the form of solutes/macromolecular sols and the soluble hydrolyzed coagulant species. SMPs, particularly SMP_c (carbohydrate fraction of soluble microbial products), exhibit a higher contribution to membrane fouling than the colloidal matter. The polysaccharides (designated as SMP_c) are the dominant species in SMPs, being responsible for the reversible, irreversible, and irrecoverable membrane fouling. The concept, presented in **Paper IV**, provides physicochemical and statistical verification of the reasons for the observations on the SMP_c removal, which were obtained during the filtration tests in coagulant-assisted BF-MBR, conducted in the previous study. According to the results, the investigation of the chemical coordination processes is among the key approaches to the comprehension of the SMP_c removal mechanisms in BF-MBR. **Paper IV** introduces the relationship — fouling as a function of the standard Gibbs energy change, which is able to provide the optimum solution for the selection of the chemical flux enhancer in MBR and BF-MBR at the lowest cost. The mechanisms of the most thermodynamically favourable interactions between the Al₁₃²⁺ complex and the monosaccharides were defined based on the results of the quantum chemical and thermodynamic analyses. They were followed by the PLS and cluster analyses, which are the basis for developing a classifier that enables continuous discrimination of the thermodynamically stable and less stable Al₁₃-monosaccharide complexes depending on the coagulant type and content of the monosaccharide species in mixed liquor. The acquired results are the basis for the automated process control with regard to SMP_c removal during chemical flux enhancement with the aid of coagulants in the BF-MBR systems.

Appendix B

Paper I

Kulesha, O.; Maletskyi, Z.; Ratnaweera, H. State-of-the-art of membrane flux enhancement in membrane bioreactor. *Cogent Eng.* **2018**, *5*, 1–30; DOI:10.1080/23311916.2018.1489700.



CIVIL & ENVIRONMENTAL ENGINEERING | REVIEW ARTICLE

State-of-the-art of membrane flux enhancement in membrane bioreactor

O. Kulesha^{1,2*}, Z. Maletskyi¹ and H. Ratnaweera¹

Received: 23 March 2018
Accepted: 13 June 2018
First Published: 22 June 2018

*Corresponding author: O. Kulesha, Norwegian University of Life Sciences, PO Box 5003, 1432 Aas, Norway; Department of General and Inorganic Chemistry, Kyiv Polytechnic Institute, Kyiv, Ukraine.
E-mail: olga.kulesha@nmbu.no

Reviewing editor: Mutiu Kolade Amosa, University of the Witwatersrand, South Africa

Additional information is available at the end of the article

Abstract: Membrane bioreactor (MBR) is a progressive alternative to conventional waste-water treatment. However, membrane fouling is one of the most significant barriers to further development of the MBR technology since it has a detrimental effect on system performance and stability. Therefore, a number of studies have been developed to comprehend the fouling nature and distinguish the effective flux enhancers, so as to develop a highly effective fouling control strategy. Key findings of these studies are summarized in the current review. Polysaccharides, proteins and humic substances tend to play the prime role in inducing fouling. The main factors affecting fouling behaviour in MBRs are membrane characteristics, membrane operation conditions and activated sludge properties, and recent evidence points out that the modification of the biomass characteristics with the use of chemical agents and adsorbents is among the most efficient fouling-hindering techniques. The current review not only aims to provide a comprehensive overview of the up-to-date methods of fouling alleviation using membrane flux enhancers in MBR but also intends to shed light on the mechanisms of their action, which, together with the experience of previous findings, can be the basis for developing a new advanced fouling mitigation strategy.

Subjects: Civil, Environmental and Geotechnical Engineering; Waste & Recycling; Water Science; Pollution

ABOUT THE AUTHORS

The authors belong to the Water, Environment, Sanitation and Health (WESH) research group at the Norwegian University of Life Sciences, Faculty of Science and Technology. The group focuses on new engineering solutions and concepts in waste-water treatment, combining membrane separation processes and chemical treatment methods. This paper opens a series of publications related to the research on chemical enhancement and fouling prevention in membrane biological reactors.

PUBLIC INTEREST STATEMENT

Water crisis and hunger are among the most urgent global problems of the current century. Therefore, clean water and sanitation and zero hunger are among the prime goals of the 2030 Agenda for Sustainable Development adopted by the United Nations. This brings a strong need for resource recovery and water reuse. The MBR process is among the most sophisticated methods for future water reuse due to its exceptional capabilities. However, membrane fouling is the main barrier towards the increase of its economic efficiency. Based on a number of research works, this review intends to provide a holistic overview of the cutting-edge technologies of fouling mitigation, and, hence, an increase of system efficiency. The provided results can serve as a basis for developing a new advanced fouling mitigation strategy, which has the potential to make MBR systems a dominating technology in the cost-sensitive water-reuse markets.



Keywords: MBR; flux enhancers; fouling

1. Introduction

Excellent nutrient removal efficiency, compactness, complete biomass retention without a secondary clarifier, together with low carbon footprint increase the competitiveness of membrane bioreactor (MBR) technology in municipal and industrial waste-water treatments. In addition, stringent environmental regulations and shift of the waste-water management paradigm towards the circular economy, resulting in high-quality effluent requirements, will drive the expansion of the global MBR market to 8.27 USD billion by 2025 (Research and Markets, 2014).

Risk of high operating costs, primarily attributed to membrane fouling, and the need for skilled technical support, able to deal with fouling events, are the main restraints to the further penetration of MBR into cost-sensitive markets, including small communities and developing countries. Straightforward decrease of membrane flux in order to alleviate fouling will increase the capital investments due to the rising demand in the membrane area and therefore is not a market-wise solution.

Membrane fouling in MBR has been a subject of numerous academic studies, focused on fouling mechanisms and prevention and control strategies, which also represents the practical interest of the waste-water treatment industry (Gkotsis, Banti, Peleka, Zouboulis, & Samaras, 2014). According to the Web of Science, the number of publications related to “MBR” and “fouling” is over 1700, with average citation rating 14.8, including major contributions from China—601 papers, USA—154 papers and Australia—157 papers. All these studies pursue one goal—to improve the understanding of fouling mechanisms: current challenges, research needs and to provide practical inputs on fouling mitigation for the industry.

Several comprehensive analytical reviews, published since early 2000s, have summarized studies on membrane fouling in MBR (Table 1). According to the Scopus, the works of Drews (2010), Judd (2008), Le-Clech, Chen, and Fane (2006), Meng et al. (2009) and Porcelli and Judd (2010) are the most comprehensive and highly cited. These reviews perfectly cover the identification, investigation and characterization of membrane fouling as well as the optimization of MBR operating conditions for fouling mitigation. The latest one has been published by Meng et al. (2017). It updates the progress in the fundamental understanding of MBR fouling and fouling control strategies, summarizes recent findings on the composition and characteristics of foulants and microbial ecology in bio-cake layers as well as novel fouling control strategies in lab-, pilot- and full-scale MBRs.

It appears from the available reviews that the chemical cleaning of membranes, including chemically enhanced backwash (CEB) and cleaning in place (CIP), is generally considered as the essential practical process of membrane permeability recovery while dealing with fouling (Meng et al., 2017). At the same time, all the above-mentioned authors associate chemical cleaning with numerous adverse effects to membrane integrity and sludge activity due to the frequent exposure of membranes and biomass to aggressive chemicals (D. Zhao & Yu, 2015). The remaining fouling mitigation strategies either are based on the mechanical scouring effects of limited efficiency and applicability (Hoffmann & Krause, 2013) or have not matured to the level of validation in operational or sometimes even in a relevant environment.

Notably, the existing reviews identify the prospective concept of membrane flux enhancement in MBR but provide very limited analysis of publications related to this research. Membrane flux enhancement in MBR is the concept of dosing various additives to the MBR mixed liquor to improve filterability. In this case, additives can act by various mechanisms: adsorption, coagulation, flocculation, oxidation, etc. Limited studies are also available on a combination of additives (Drews, 2010; Ji, Li, Qiu, & Li, 2014; J. C. Lee et al., 2001; Nguyen, Guo, Ngo, & Vigneswaran, 2010; Zarei, Moslemi, &

Table 1. Prior art reviews on membrane fouling in MBR			
Direction of fouling studies	Research area	Research focus	Cutting-edge reviews and studies
Identification and investigation	Fouling characterization	Fouling mechanisms and characterization of the fouling layers	(J. Chen et al., 2016; Hong, Zhang, He, Chen, & Lin, 2014; Le-Clech et al., 2006; Poorasgari, Bugge, Christensen, & Jørgensen, 2015; Rosenberger, Evenblij, Te Poele, Wintgens, & Laabs, 2005; Z. Wang & Wu, 2009)
Modelling	Fouling characterization, prediction and prevention	Physicochemical aspects, mechanisms, the main contributors, influence of hydrodynamic forces and intensity at different conditions	(Böhm, Drews, Prieske, Bérubé, & Kraume, 2012; Cao, Van De Staey, & Smets, 2015; Dalmau, Atanasova, Gabarrón, Rodríguez-Roda, & Comas, 2015; Hong et al., 2016; Mannina & Di Bella, 2012; Zarragoitia-González, Schetrite, Alliet, Jauregui-Haza, & Albasi, 2008; Zuthi et al., 2017)
Prevention and control	Mixed liquor pretreatment	Screening	(Frechen, Schier, & Linden, 2008)
		Pre-sedimentation	(Hameed, 2017; Moustafa, 2011)
	Membrane cleaning	Physical: back-flushing, air injection, relaxation, addition of carriers	(Amirafzabi, Mostaufi, Hosseinzadeh, & Mehrnia, 2014; Jiang, Kennedy, Guinzbourg, Vanrolleghem, & Schippers, 2005; Lin, Lee, & Huang, 2010; Psoch & Schiewer, 2006; Viero, Sant'Anna, & Nobrega, 2007; Yonekawa, Tomita, & Watanabe, 2004; F. Chen, Bi, & Ng, 2016; Christensen et al., 2016; Jin, Ong, & Ng, 2013; Yigit, Civelekoglu, Harman, Köseoğlu, & Kitis, 2011; Yin, Tarabara, & Xagorarakí, 2016)
		Chemical	(Evenblij, Verrecht, Van Der Graaf, & Van Der Bruggen, 2005; Gabarrón et al., 2014; Joss, Böhler, Wedi, & Siegrist, 2009; M. J. Kim, Sankararao, & Yoo, 2011; Sun, Fang, Liang, & Huang, 2016; Z. Wang et al., 2014)
	Optimal operating conditions	Permeate flux	(Brookes, Jefferson, Guglielmi, & Judd, 2006; Jiang et al., 2005; Le Clech, Jefferson, Chang, & Judd, 2003)
		Aeration	(Chang & Judd, 2002; Kraume, Wedi, Schaller, Iversen, & Drews, 2009; Sofia, Ng, & Ong, 2004; Xia, Law, & Fane, 2013)
		Feedback control	(Drews, 2010; Evenblij et al., 2005; González, Diaz, Vera, Rodríguez-Gómez, & Rodríguez-Sevilla, 2018; Joss et al., 2009; Miller, Kasemset, Paul, & Freeman, 2014; Yusuf, Wahab, & Abusam, 2017)
	Membrane modification	Coating	(C. Wang et al., 2010; W. Song et al., 2018)
		Grafting	(Etemadi, Yegani, & Seyfollahi, 2017; Yu, Xu, Lei, Hu, & Yang, 2007; Zhou et al., 2013)
		Patterned membranes	(I. Kim et al., 2015; Marbelia, Bilad, Bertels, Laine, & Vankelecom, 2016; Won et al., 2012)

(Continued)

Table1. (Continued)			
Direction of fouling studies	Research area	Research focus	Cutting-edge reviews and studies
		Plasma treatment	(Yu, Hu, Xu, Wang, & Wang, 2005; Zhao et al., 2015)
		Nanoparticles	(Deowan et al., 2016; Jhaveri & Murthy, 2016; Mehrnia & Homayoonfal, 2016; C. Zhao, Xu, Chen, Wang, & Yang, 2014; Rahimi, Zinatizadeh, & Zinadini, 2015)
	Mixed liquor treatment	Quorum sensing and quorum quenching	(Ergön-Can, Köse-Mutlu, Koyuncu, & Lee, 2017; S. Lee et al., 2016; Waheed, Xiao, Hashmi, Stuckey, & Zhou, 2017; Weerasekara, Choo, & Lee, 2014; Xiao, Waheed, Xiao, Hashmi, & Zhou, 2018; Yavuztürk Gül & Koyuncu, 2017; W. Jiang, Xia, Liang, Zhang, & Hermanowicz, 2013; Maqbool et al., 2015)
		Enzymatic and bacterial degradation of biopolymers	(Berg, Kalfas, Malmsten, & Arnebrant, 2001; Hocaoglu & Orhon, 2010; Miura & Okabe, 2008; Molobela, Cloete, & Beukes, 2010)
		Ozone	(Huang & Wu, 2008; K. R. Lee & Yeom, 2007; J. Wu & Huang, 2010; Yeom et al., 2005)
		Coagulants	(P. K. Gkotsis, Mitrakas, Tolkou, & Zouboulis, 2016; Iversen, 2011; Ji, Qiu, Wai, Wong, & Li, 2010; J. Wu, Chen, Huang, Geng, & Wen, 2006)
		Ultrasound and vibration	(Ábel, Szabó, Poser, László, & Hodúr, 2013; Kola, Ye, Ho, Le-Clech, & Chen, 2012; M. Xu, Wen, Huang, Yu, & Zhu, 2013)
		Electric field	(Hua, Huang, Su, Nguyen, & Chen, 2015; J. Huang et al., 2015; Ibeid, Elektorowicz, & Oleszkiewicz, 2015; Y. K. Wang, Li, Sheng, Shi, & Yu, 2013; J. Zhang et al., 2015)

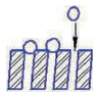

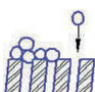
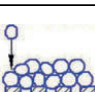
Mirzaei, 2016). Therefore, membrane flux enhancement is, by nature, a combination of MBR and various physicochemical waste-water treatment processes at the membrane separation stage, developed to the level of successful commercial operation that provides a good opportunity for practical fouling mitigation solutions.

This paper focuses on MBR membrane fouling characterization, prevention and mitigation in relation to and by means of membrane flux enhancement, highlighting the types of research on adsorption, coagulation, flocculation, bio-flocculation and oxidation mechanisms.

2. Membrane foulants and flux enhancers

Application of various additives for membrane flux enhancement in MBR is a response to the current understanding of fouling mechanisms that can be influenced by such additives. Therefore, it is reasonable to mention that currently, membrane fouling is classified based on several criteria: nature and phase of foulants, stage and nature of fouling process and the ability to recover membrane permeability after the fouling occurred (Table 2).

Table 2. Types of membrane pore blocking in terms of Hermia's pore-blocking models

Pore-blocking model	Schematic illustration	Relation to pore size	Physical concept	References
Complete pore blocking		$d_{\text{foulant}} > d_{\text{pore}}$	Sealing of the membrane pores, no superimposing with other particles	(Field, Wu, Howell, & Gupta, 1995; Aslam, Lee, & Kim, 2015; Drews, 2010; Zheng et al., 2018; Bowen et al., 1995; F. Wang & Tarabara, 2008; Etemadi et al., 2017; El Rayess et al., 2012, Kumar, Goswami, Pakshirajan, & Pugazhenthii, 2016)
Standard (internal) pore blocking or pore constriction		$d_{\text{foulant}} < d_{\text{pore}}$	Deposition onto the internal pore walls, the pore volume decreases proportionally to the volume of the deposited particles	
Intermediate pore blocking		$d_{\text{foulant}} \approx d_{\text{pore}}$	Pore sealing + deposition on other particles accumulated on the surface (formation of multilayers)	
Cake formation		$d_{\text{foulant}} > d_{\text{pore}}$	Accumulation of the foulant on the surface/sealed pores with subsequent stacking	

Membrane pore clogging occurs because of suspended solids agglomeration and should be distinguished from membrane surface fouling, even though both lead to the same result—a decrease of membrane permeability. The deposition of foulants in the membrane pores and on their surface follows a number of blocking filtration mechanisms. Hermia's pore-blocking models (Table 2) are the fundamental unified analytical description of the blocking mechanisms formulated in the common frame of power-law non-Newtonian (further extended to Newtonian) fluids (Chellam & Cogan, 2011; F. Wang & Tarabara, 2008; Jelemenský, Sharma, Paulen, & Fikar, 2016; Bowen, Calvo, & Hernández, 1995).

Although clogging is the most frequent problem of MBR plants, it is not of the prime interest to the authors of the current review.

The main practical interest, from the point of view of membrane flux enhancement, is the investigation of the interactions of additives with biopolymers and biofilms that can be present as particles, colloids or solutes and incorporate or promote inorganic binding, precipitation, adhesion, etc. (Table 3).

2.1. Biopolymers

According to Hu, Wang, Tian, Ngo, and Chen (2016), Juang, Lee, and Lai (2010), Kunacheva and Stuckey (2014) and Zhang, Yu, Zhang, and Song (2015), **polysaccharides** and **proteins** are the major components of biopolymers causing membrane fouling in low-pressure membrane filtration processes. **Polysaccharides** are the primary membrane foulants in MBRs (Chu & Li, 2005; Fonseca, Summers, & Greenberg, 2007; Jin et al., 2013; Lesjean et al., 2005; Meng et al., 2017; Satyawali & Balakrishnan, 2009; Sweity et al., 2011; Tarnacki, Lyko, Wintgens, Melin, & Natau,

Table 3. Membrane fouling classifications in MBR

Criteria					
Nature of foulants	Particles	Organic	Inorganic	Biological	
Foulants phase	Solids	Colloids	Solutes		
Nature of fouling process	Adsorption	Gel formation	Precipitation	Adhesion	Chemical reaction
Stage of development	Conditioning fouling	Steady fouling	TMP jump		
Membrane permeability recovery	Reversible	Irreversible	Irrecoverable		

2005; Tu, Zhang, Xu, Zhang, & Zhu, 2010; J. Zhang, Chua, Zhou, & Fane, 2006). This is primarily attributed to the gelling properties of polysaccharides that can be enhanced in the presence of multivalent cations acting as bridges for the carboxyl groups (Xin, Bligh, Kinsela, Wang, & David Waite, 2015). Owing to the reversibility of gels, several studies have reasonably referred to a polysaccharide-caused fouling as reversible (Merle, Dramas, Gutierrez, Garcia-Molina, & Croué, 2016). On the one hand, the formation of a gel layer on the membrane surface decreases membrane flux, but on the other hand, it serves as a substrate for bacteria attachment and further biofilm development.

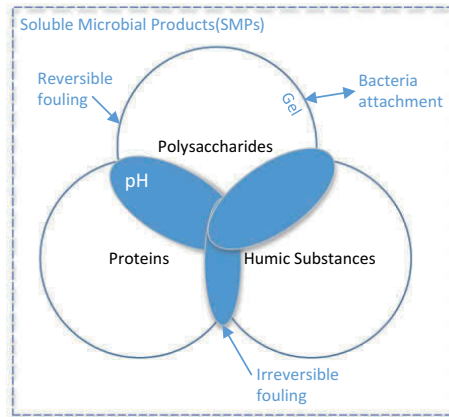
It is generally well accepted that **proteins** are the key organic constituents that contribute to the foulant layer, interacting with polysaccharides (Neemann, Rosenberger, Jefferson, & McAdam, 2013; X.-M. Wang & Waite, 2009). The protein-polysaccharide interaction is non-covalent and can be classified by electrostatics, steric exclusion, hydrophobic interactions and hydrogen bonding. It is well known that pH and ionic strength influence the physical state of proteins and polysaccharides when present in the mixture. For pH conditions close to but still above the pH of isoelectric point, positively charged micro-regions on proteins can bridge over to discrete regions of the long-chain polysaccharide molecules, increasing the solute size and subsequently the probability of non-covalent network formation that imparts high fouling rates, thus explaining the apparent role of protein in the irreversible fouling fraction previously reported in the literature (McClements, 2006). It is also clear that proteins provide an easy food for bacteria in further biofilm development.

Humic substance is another massive organic component of MBR mixed liquor (Aryal et al., 2009). They are introduced into the sewer network presumably through rainwater and storm-water runoff, along with other constituents of domestic sewage, due to insufficient drinking water preparation (Bratby, 2016) and through cell decay (S. C. Wu & Lee, 2011). In addition, 40–50% of soluble microbial products (SMPs) were observed to be humic, fulvic and humathomelanolic acids (W. Chen, Westerhoff, Leenheer, & Booksh, 2003). In the study by Chuang, Chang, Chang, and Sung (2009), humic substances in the effluent were singled out as those having significant fouling potential. Being small but strongly hydrophobic, molecules of humic substances adsorb to membranes and bind with polysaccharides and proteins via hydrophobic and electrostatic interactions (Z. Wang, Cao, & Meng, 2015), forming large molecular assemblies on the membrane surface and inside pores, facilitating further deposition of hydrophobic fragments (Kimura, Ogyu, Miyoshi, & Watanabe, 2015). Such complex interaction makes humic substances responsible for the development of irreversible fouling.

All together, polysaccharides, proteins and humic substances constitute the large group of foulants determined in the literature as SMPs (Figure 1).

SMPs are thought to form biomolecular assemblies, adsorb onto the membrane surface, block membrane pores and/or form a gel structure on the membrane surface where they provide not

Figure 1. Organic fouling development by biopolymers.



only hydraulic resistance to permeate flow resulting in membrane flux decrease, but also a substrate for biofilm formation and possible nutrient source for biofilm development.

2.2. Biofilms and bio-cakes

In the MBR systems, biomolecular assemblies tend to attach to the membrane surface or to the gel layer of other biopolymers, accumulating at the solid-liquid interface or being suspended in the bulk solution in the form of biofilms. Biofilms represent a stable highly competitive agglomeration, which causes severe fouling problems (Saeki, Karkhanechi, Matsuura, & Matsuyama, 2016; Flemming & Wingender, 2010).

Biofilms develop bacteria cohesion and the further production of extracellular polymeric substances (EPSs) that are determined as autochthonous macromolecules found at or outside the cell surface and in the intercellular space of microbial aggregates (Flemming & Wingender, 2001). In further steps, biofilm maturation and bacterial detachment take place (Vanysacker, Boerjan, Declerck, & Vankelecom, 2014), escalating biofouling development.

A complex system of biofilm and EPSs forms a bio-cake on the membrane surface, causing a steep decrease of membrane flux. SMPs play an important role in the initial fouling, whereas EPSs produced by the deposited microbial cells become a major foulant after the TMP increase (Z. Zhou et al., 2015). Meanwhile, the presence of SMPs and colloids in the cake layer highly increases cake resistance.

One of the most complex subjects involved is the influence of activated sludge constituents and floc characteristics on sludge fouling propensity, as several parameters interact and influence sludge filterability simultaneously (Jørgensen et al., 2017). The size of activated sludge flocs affects the membrane biofouling rate at all stages of initial biofilm formation and bio-cake development. Small flocs have high specific contact interaction energy and easily adhere to the membrane surface (Shen et al., 2015). In the complex process of biofilm formation and development, the surface hydrophobicity of sludge flocs is another important factor affecting the membrane fouling rate through the promotion of bacteria adhesion (Gutman, Walker, Freger, & Herzberg, 2013). In general, for all major foulants, higher MLSS concentration increases the membrane fouling rates and flux declines due to a higher probability of biopolymerization, fostering of biofilm growth and particle aggregation.

As is often observed in real-life chemical and biological processes, in real MBR systems, all types of fouling discussed above take place continuously, changing from one form to another. In fact, each

fouling process occurs temporarily and results not only in a membrane flux decline, but also in a release of products that initiate another fouling stage: dead cells release SMPs to the mixed liquor and SMPs form the depositions on the membrane surface and in the pores, feeding living microorganisms that produce further SMPs and EPSs. Because of the accumulation of dead cells and biopolymers in the bottom fouling layers, the system becomes clearly different from biofilms applied in waste-water treatment processes (Meng et al., 2017). The system of bio-cake is characterized by concentration gradients of oxygen and substrates from the surface to bottom layers, close to the membrane. In addition to the biological processes occurring in the bio-cake, hydrolysis and humification take place, converting polysaccharides and proteins into hardly degradable and heavily removable assemblies.

A number of studies have pointed out that the major foulants act according to the particular pore-blocking models, which helps distinguish the fouling nature and a suitable cleaning approach (Table 4).

Concerning the fouling types, in terms of membrane permeability recovery, they can be categorized as reversible, irreversible and irrecoverable fouling (Table 5). Reversible fouling is caused by deposition of the foulants on the membrane surface, leading to the formation of the cake layer. It can be removed by means of physical cleaning. However, irreversible and irrecoverable fouling are associated with internal pore blocking and pore constriction, caused by adsorption/deposition of the dissolved/colloidal matter inside the membrane pores and near their openings. Irreversible biofouling can be removed by a more aggressive cleaning approach—chemical cleaning: 1) CEB, applying NaOCl, NaOH, H₂O₂ and biocides (SBS) and 2) CIP or

Table 4. Analysis of the characteristic pore-blocking patterns for the typical foulants

Foulant	Pore-blocking nature			
	Complete pore blocking	Standard (internal) pore blocking or pore constriction	Intermediate pore blocking	Cake formation
Proteins	Molecular aggregates/particles (Bowen et al., 1995)	Molecular aggregates/particles (Bowen et al., 1995) Molecules (Soler-Cabezas, Torà-Grau, Vincent-Vela, Mendoza-Roca, & Martínez-Francisco, 2015)	Bacterial EPS, molecular aggregates/particles (Xu & Chellam, 2005; Bowen et al., 1995) Aggregates (Soler-Cabezas et al., 2015; Jelemenský et al., 2016)	Molecular aggregates/particles (Bowen et al., 1995) Slurry particles (Kumar et al., 2016)
Polysaccharides	Gel-forming particles (Sarkar, 2013)		Bacterial EPS (Xu & Chellam, 2005) Particles (Soler-Cabezas et al., 2015) Gel layer formed by macro-solutes (Jelemenský et al., 2016)	Gel-forming particles (Sarkar, 2013); Particles (Kumar et al., 2016)
Humic substances	Particles (Lee, Dilaver, Park, & Kim, 2013)	Gel-forming particles (Ruohomaki & Nyström, 2000) Large molecular aggregates (Yuan, Kocic, & Zydny, 2002)		Large molecular aggregates (Yuan et al., 2002) Particles (Lee et al., 2013)

Table 5. Characteristic fouling types for the blocking mechanisms and the best suitable cleaning methods

Pore-blocking nature	Fouling type	Cleaning
Complete pore blocking	Irreversible (Lee et al., 2013)	
Standard (internal) pore blocking or pore constriction	Irrecoverable (Soler-Cabezas et al., 2015) Irreversible (Lee et al., 2013)	Not applicable (irrecoverable fouling)
Intermediate pore blocking	Irreversible (F. Wang & Tarabara, 2008)	Chemical (NaOCl, NaOH, H ₂ O ₂ , etc.)
Cake formation	Reversible (Kumar et al., 2016; Gkotsis et al., 2017) Reversible and irreversible (Lee et al., 2013)	Physical (back-flushing, air injection, relaxation, addition of carriers) Physical + chemical

“cleaning in air” (CIA) via soaking the membranes in NaOCl and NaOH solutions. On the contrary, irrecoverable fouling, being the result of the gradual long-term accumulation of the foulants in membrane pores, is robust to all the cleaning strategies and cannot be removed by the existing means of cleaning (Geilvoet, 2010; Gkotsis, Mitrakas, Tolkou, & Zouboulis, 2017; Janus & Ulanicki, 2015; Judd, 2008; Wang et al., 2014).

However, as admitted by Lee et al. (2013), in some cases, the definition of each fouling type might not directly correspond to the fouling mechanisms defined in the filtration models.

2.3. Highlighted flux enhancers

Membrane flux enhancement is an emerging strategy, tested to a certain degree in the lab with promising first results, but with very limited experience from the field.

A range of chemicals have been evaluated as membrane flux enhancers in various studies (Table 6). Their flux enhancement activity is strongly associated with the membrane fouling nature that they are able to affect. The most well-studied ones are adsorbents, coagulants and flocculants. Further studies have shown that membrane flux enhancers are additives that not only help with fouling but also solve other important tasks—a reduction of the carbon footprint of the MBR plant, improvement of related sludge properties, costs of sludge processing, etc.

This work reviews laboratory research and piloting experience with major flux enhancers, with specific regard to adsorption, coagulation, flocculation, bio-flocculation and oxidation mechanisms.

3. Mechanisms of membrane flux enhancement in MBR

Review of the recent studies shows five main points of focus in membrane fouling enhancement in terms of the mechanisms of action and types of applied chemicals: adsorption, coagulation, flocculation, bio-flocculation and oxidation.

3.1. Adsorption

According to Iorhemen, Hamza and Tay (2016), the adsorbents in biological treatment systems adsorb dissolved organic matter, especially SMP and, consequently, mitigate membrane fouling. Different adsorbents can be used for this purpose, but the most studied ones are granular and powdered activated carbons.

Granular activated carbon (GAC) was successfully applied in several MBR fouling studies due to its well-predictable ability not only to adsorb organic constituents of mixed liquor but also to provide additional scouring on the membrane surface. Owing to the relatively low specific gravity,

Table 6. Membrane flux enhancement in MBR			
Fouling nature & mechanism	Foulants	Membrane flux enhancers	References
Colloidal pore blocking	EPS	Addition of coagulants, adsorbents	Alum (J. C. Lee et al., 2001; Nouri, Mehrnia, Sarrafzadeh, & Nabizadeh, 2013; K. G. Song, Kim, & Ahn, 2008; J. Wu et al., 2006) PACI (Kimura, Tanaka, & Watanabe, 2014; Nouri et al., 2013; J. Wu et al., 2006) FeCl₃ (J. Wu et al., 2006; Z. Zhang, Wang, Leslie, & Waite, 2015) PFS¹ (Ji et al., 2010; J. Wu et al., 2006; J. Wu & Huang, 2008) PAC² (J. S. Kim & Lee, 2003)
	Synthetic organics (grease, oil, surfactants)	Addition of coagulants Rhamnolipids	FeCl₃, Chitosan (Pendashteh et al., 2011; Qin et al., 2012)
	SMP/EPS	Coagulants Flocculants Adsorbents	Alum (Holbrook et al., 2003), FeCl₃ (W. Guo et al., 2010; Ivanovic & Leiknes, 2011; H. F. Zhang, Sun, Zhao, & Gao, 2008) PACI (W. Guo et al., 2010; Huyskens et al., 2012) PolyDADMAC (Collins et al., 2006; Huyskens et al., 2012; Koseoglu et al., 2008; H. Zhang, Gao, Zhang, & Song, 2014) PAC (Huyskens et al., 2012)
	Humic substances		PolyDADMAC, PAC (V. Iversen, Mehrez, et al., 2009) PACI + PolyDADMAC (Tzoupanos & Zouboulis, 2010)

GAC is easy to fluidize and therefore it can be a perspective and energy-efficient flux enhancer (Kim et al., 2011). Being bifunctional, GAC mostly acts as a mechanical flux enhancer, rapidly increasing the membrane flux after dosing due to bio-cake detachment, but not affecting irreversible fouling at all (Wu et al., 2017). Various studies have reported 20–60% of flux enhancement with GAC (Johir, Aryal, Vigneswaran, Kandasamy, & Grasmick, 2011, Johir, Shanmuganathan, Vigneswaran, & Kandasamy, 2013).

At the same time, those studies took into account only a part of the GAC properties that can affect flux enhancement in MBR:

- granule size strongly affects the mechanical scouring effectiveness of GAC (Johir, 2013; Wang et al., 2016);
- a low mechanical strength of GAC granules negatively affects the overall flux enhancement due to membrane pore blocking with small particles; and
- GAC porous type (related to carbon source and production technology) and adsorption activity were not studied at a proper level.

One of the most common additives is powdered activated carbon (PAC). When PAC is mixed with activated sludge, biologically activated carbon is formed, which improves the removal efficiency and mitigates membrane fouling (Aun Ng, Sun, & Fane, 2006; Seo, Suzuki, & Ohgaki, 1996). According to Kim and Lee (2003), lower fouling propensity was detected in the MBR process when the PAC was directly inserted into the bulk solution and mixed with biomass.

A much lower fouling rate (TMP rise) for the MBR with PAC addition, compared to the system without this agent, was observed in the study by Aun Ng et al. (2006). In the work by Ying and Ping (2006), reduction of the EPS deposition on the membrane surface was noticed, which occurred

after the addition of PAC to the sewage. On the contrary, at much higher PAC dosages, the effect of this additive was significantly weakened.

PAC is effective for treating highly toxic effluents, as shown by Lesage, Sperandio, and Cabassud (2005). Additionally, according to Satyawali and Balakrishnan (2009), it exhibited significant efficiency while treating high-strength waste water from the alcohol distillery, especially in terms of improving sludge de-waterability and affecting the SMP composition (protein/carbohydrate ratio). It is noteworthy that PAC dosing enhances system stability and promotes the maintenance of consistent permeate flux in terms of TOC removal, as shown by Guo, Vigneswaran, Ngo, Van Nguyen, and Ben Aim (2006), Iversen, Koseoglu, et al. (2009) and Munz, Gori, Mori, and Lubello (2007).

Except for PAC, other adsorbents can be used to mitigate fouling in the MBR system. This was illustrated by J. C. Lee et al. (2001), where **natural zeolites** in combination with alum were employed for such a purpose. Zeolite-added sludge possessed buffer capacity towards ammonium ion. Furthermore, the nitrification rate, as well as the organic removal efficiency, was also remarkably improved.

Nevertheless, weaknesses of applying the adsorbents, such as their high cost and the issue of exhausted material disposal, still remain the main limiting factors for their application as membrane flux enhancers in MBR.

3.2. Coagulation

One of the promising strategies to reduce fouling in MBR is to modify sludge filtration characteristics by the addition of coagulants. At the same time, practitioners should be careful with the use of some flux enhancers, such as ferric ions, which can potentially enhance the gelation of polysaccharides on the membranes.

While studying the effect of inorganic salts, such as ferric chloride, aluminium sulphate, polyaluminium chloride (PACl) and polymeric ferric sulphate (PFS), on fouling reduction in MBR, a significant improvement of filtration performance was observed. According to Wu et al. (2006), PACl, PFS and their mixture had a better influence on mixed liquor filterability enhancement than monomeric additives. Polymeric coagulants exhibited a reduction of the initial TMP and TMP increase rates; in other words, membrane fouling was successfully alleviated, and among all of the additives, PFS was the most effective. Several further studies (Ji et al., 2010; Ji, Qiu, Wong, & Li, 2008; J. Wu & Huang, 2008) also demonstrated the high effectiveness of PFS use as a fouling mitigation agent. In the work by Wu and Huang (2008), PFS was the focus of interest as a fouling retardation agent during long-term runs of MBR. According to the findings, PFS removed organic compounds of high molecular weight from supernatants via coagulation, entailing the mitigation of gel-layer formation on the membrane surface and suspended flocs enlarging by supplying positive charges to organic particles and enhancing charge neutralization. The positive influence of PACl on filtration performance was indicated by Guo et al. (2010), Koseoglu, Yigit, Civelekoglu, Harman, and Kitis (2012) and Nouri et al. (2013).

However, according to other studies, monomeric metal salts also exhibited high efficiency in sewage treatment. Short-term experiments conducted by Guo et al. (2010) revealed that FeCl_3 along with PACl considerably reduced SMP concentration in the effluent stream, improved sludge settleability together with oxygen transfer and gained superior efficiency in terms of fouling control compared to their organic analogues, like starch. As specified by Song et al. (2008), FeCl_3 was efficient in the reduction of specific resistance, whereas the addition of alum, which was also examined, assured high phosphorus removal and the decrease in membrane filtration resistance without any deterioration in the nitrogen removal efficiency. Enhancement of the filterability in

MBR applying either FeCl₃ or aluminium sulphate was also discussed by Huyskens et al. (2012), Iversen, Koseoglu, et al. (2009), Koseoglu et al. (2008), Ji et al. (2008) and Nouri et al. (2013).

Eventually, based on all the aforementioned studies and according to the recent findings, prime foulants such as effluent organic matter, whose elimination via coagulation and flocculation is of high priority, generally comprise two main forms: proteins in conjunction with polysaccharides and humic substances (Fang, Shi, & Zhang, 2006; Flemming & Wingender, 2001; V. Iversen, Mehrez, et al., 2009; Miyoshi, Tsuyuhara, Ogyu, Kimura, & Watanabe, 2009).

According to Geng and Hall (2007), bound EPSs in activated sludge flocs are not directly associated with membrane fouling; however, EPSs are responsible for the release of SMPs into the effluent stream, and, as demonstrated before, SMPs in the mixed liquor cause the deterioration of filtration performance. This necessitates the defying of the mechanism by which chemical additives remove SMPs from the water. In the study by Bratby (2016), the authors elucidated the origin of the surface charge of bacteria, which, as assumed, arises from chemical reactions at the surface. Many bacterial solid surfaces contain functional groups that are readily ionizable, such as -OH, -COOH and -OPO₃H₂ (Bratby, 2016):



Thus, the charge of such particles becomes dependent on the degree of ionization (proton transfer) and, hence, on the pH of the surrounding liquid. At low pH values, a positively charged surface prevails, whereas under alkaline conditions, the surface becomes mainly negatively charged.

Ipso facto, since typically investigations on the performance of filter aids are conducted at higher pH values, the surfaces of SMP carry net negative charges due to the broken edges of the hydroxyl groups (Ibeid, Elektorowicz, & Oleszkiewicz, 2017).

When Al/Fe-based coagulants are added to the water, the salts dissociate and metal ions react with water molecules, by breaking the bonds of the lowest energy between the protons and the hydroxyl groups and, subsequently, interacting with the latter ones. As a result, metal hydrolysis occurs (Gregory & Duan, 2001; Hem & Roberson, 1967), followed by the formation of colloidal particles, the so-called “micelles”, depicted below.

Positively charged granules of the micelles attract negatively charged SMPs by means of electrostatic forces, van der Waals attraction and, presumably, electric or magnetic forces, resulting in the formation of organic/inorganic solid complexes and the ruining of aggregative stability of the disperse system (Figure 2).

In addition, the newly formed particulate matter of the metal hydroxides possesses very high adsorption ability, thus accumulating SMP on its surface. Consequently, the aggregated flocs agglomerate with each other via adhesion forces, increase in size, being held together by weak physical interactions, and, finally, precipitate (Inan, Dimoglo, Şimşek, & Karpuzcu, 2004).

Concerning humic substances, as stated by Bolto (1995), at pH 5–6, various aluminium humates may be formed through the polynuclear aluminium species, produced during the following stoichiometric reaction:



The more explicit mechanism for aluminium salt coagulation of humic substances is depicted in Figure 3.

Figure 2. The formation of organic/inorganic solid complexes with the aid of a) ferric (III) and b) aluminium coagulants.

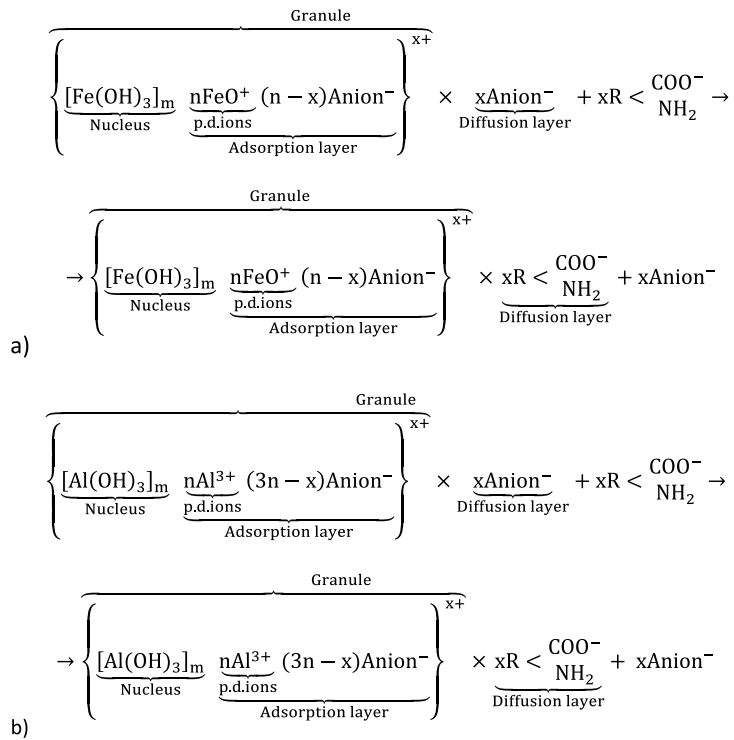
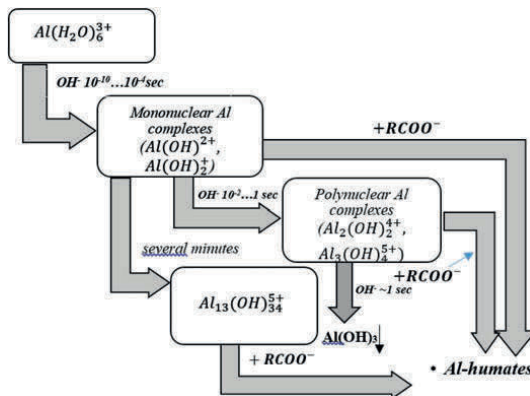


Figure 3. Pathways for the coagulation of humic substances by aluminium ions at higher pH levels (Bolto, 1995; Bratby, 2016).



These and higher pH levels foster the adsorption of organic materials onto the flocs of aluminium hydroxide, occurring by the ligand-exchange reaction (Bolto, 1995):



Almost identical mechanisms of hydrolysis with the subsequent coagulation are involved when applying ferric salts (Gregory & Duan, 2001; Ødegaard, Fettig, & Ratnaweera, 1990).

The interaction of ferric salts with such a form of humic substances as fulvic acids has been described by Van Breemen, Nieuwstad, and Van Der Meent-Olieman (1979), where the interaction between iron ions and organic groups depends on the content of fulvic acids. As assumed, in diluted solutions, the complex-like ions $\text{RCOO} - \text{Fe}(\text{OH})_n^{(2-n)+}$ are formed, due to the combination of one Fe^{3+} ion with the COO^- group. Such complexes may attract each other, resulting in the formation of polymeric iron hydroxides. The excess of ferric (III) coagulant promotes the yielding of hydroxide flocs and a subsequent co-precipitation of colloidal particles with their aid. Moreover, in the case of a high concentration of fulvic acids, they precipitate in the form of iron fulvinate, as three Fe^{3+} ions combine with the corresponding amount of COO^- groups.

It is suggested that further investigations should be conducted to gain a better insight into the key mechanism controlling the removal of the high MW biopolymer molecules, with a view to further optimizing the coagulation process.

3.3. Flocculation

Another commonly used flocculant is homopolymer 2-propen-1-aminium, N,N-dimethyl-N-2-propenyl-chloride (PolyDADMAC or MPE50—the product of Nalco®), whose high effectiveness as a membrane fouling reducer was proven by various research teams (Huyskens et al., 2012; V. Iversen, Mehrez, et al., 2009; Jamal Khan, Visvanathan, & Jegatheesan, 2012; Koseoglu et al., 2008). In the study by Hwang, Lee, Park, Lee, and Chang (2007), attempts to elucidate the mechanism of such significant flux enhancement through analysing the images acquired under a confocal laser scanning microscope (CLSM) were made. According to the attained results, the inhibited fouling rate could be attributed to an increase in cake porosity and uniform distributions of the boundary-layer components along its depth after adding PolyDADMAC to the bulk phase. The positive influence of this additive on MBR filtration performance was also confirmed by W. S. Guo, Vigneswaran, Ngo, Kandasamy, and Yoon (2008). High levels of dissolved organic carbon (DOC) and chemical oxygen demand (COD) removal efficiency (over 95%) were attained with the aid of this chemical when running over a 7-day period. Besides $\text{NH}_4\text{-N}$ elimination being over 95–98%, $\text{PO}_4\text{-P}$ removal increased with time to over 99% after 7 days of operation. However, in terms of phosphorus elimination, the MBR with PolyDADMAC exhibited worse results than the sponge system. PolyDADMAC also enhanced the microbial activity of the biomass in the MBR. In the study by Yoon and Collins (2006), the extent of short-term and long-term flux improvements by PolyDADMAC was tested at low temperatures (10–13°C) in order to overcome low permeate production under such conditions and, consequently, to reduce capital costs. As a result, at 10°C, the long-term flux increased from 17 LMH to 25 LMH with the extension of filtration ability from 22 days to more than 30 days. Additionally, a small municipal MBR plant succeeded in increasing the daily flux by 150% via dosing PolyDADMAC during the long-term run.

In the work by Nguyen et al. (2010), the combination of PolyDADMAC and FeCl_3 was applied with the evaluation of its impact on the treatment performance in a long-term submerged MBR. According to the results, this combined flocculant demonstrated that almost 100% of the total phosphates and DOC removal and 90% of the ammonia ($\text{NH}_4\text{-N}$) compounds were eliminated during the 80-day operation. In addition, a good microbial activity with a stable specific oxygen uptake rate (SOUR), stable values of SVI and soluble carbohydrate concentration and a low rate of TMP rise were observed.

In the study by Ji et al. (2010), among the various compounds, polyacrylamide (PAM) was investigated, and, as noticed, it significantly alleviated membrane fouling by affecting the zeta potential and viscosity. Additionally, according to the results obtained in the work by Ji et al. (2014), where the fouling mitigation ability of PAM in combination with other modified starches was examined, the composites exhibited a strong positive effect on SMP, the fractal dimension of sludge flocs and floc size in sustainable filtration.

Meanwhile, it is quite difficult to figure out the exact mechanism for system destabilization, governed by the polyelectrolyte additives. The type of predominant phenomenon depends on whether the polymer is used as a primary coagulant or as a flocculant aid and the polymer characteristics (charge density and molecular weight). Three main pathways of their action have been distinguished (Bolto, 1995; Bratby, 2016; Ji et al., 2008): charge neutralization, bridging and the electrostatic charge patch mechanism.

According to McEwen (1998) and Amjad (2010), the charge neutralization model deals with the use of relatively low MW cationic polymers with a high charge density, such as PolyDADMAC, which causes the destabilization of negatively charged colloids through charge neutralization, accomplished by the adsorption of the polymer on the particle surface. The cationic nature of PolyDADMAC and PAM is caused by the presence of quaternary ammonium functional groups in the polymer skeleton. Relevant interactions are shown in Figures 4 and 5.

The superior role of the neutralization mechanism in flocculation employing PolyDADMAC was discussed in the studies by Hahn, Hoffmann, and Ødegaard (1996) and Zahrim and Dexter (2016). Meanwhile, as discussed in the latter work, flocculation occurs through the bridging mechanism as well.

The importance of the charge neutralization phenomenon, while applying PAM-based cationic polyelectrolytes for sludge conditioning, was noticed by Tiravanti, Lore, and Sonnante (1985). However, this governing the flocculation of negatively charged organic matter since cationic polyelectrolytes possessing high charge densities also act through the electrostatic charge patch mechanism (Bratby, 2016; Tiravanti et al., 1985). It is based on the complete adsorption of polyelectrolyte segments onto the surface of the impurity, followed by the generation of charge mosaics with positively and negatively charged regions and the final destabilization of the system, resulting from the alignment of the charge mosaics of adjacent particles, which provides strong electrostatic attraction (Figure 6) (Bolto, 1995; Bratby, 2016).

Figure 4. The interaction between PolyDADMAC and functional groups of the bacterium surface.

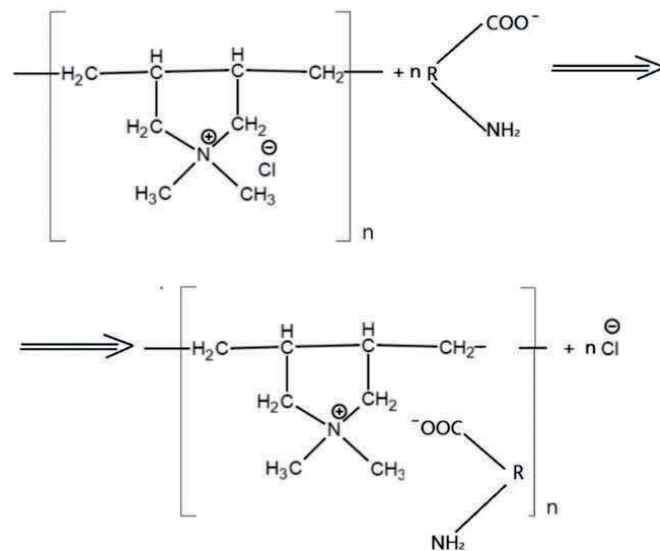


Figure 5. The elimination of bacterium with the aid of cationic PAM via the charge neutralization mechanism.

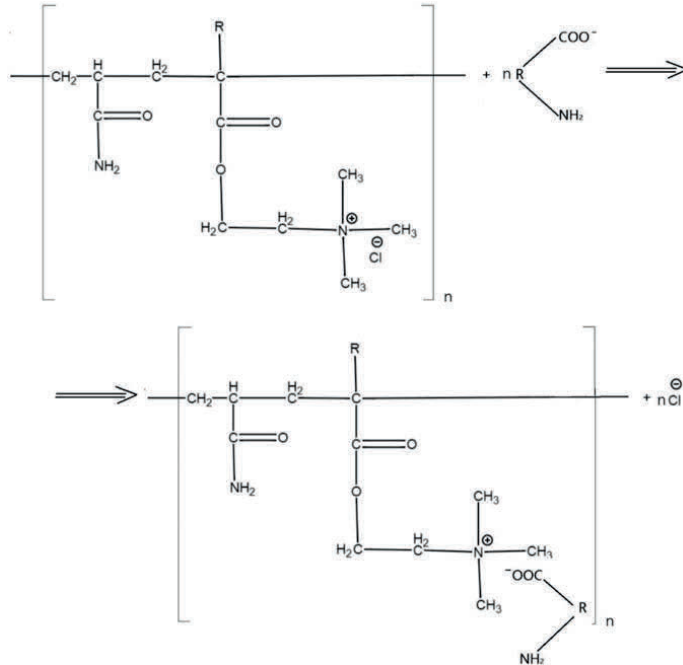
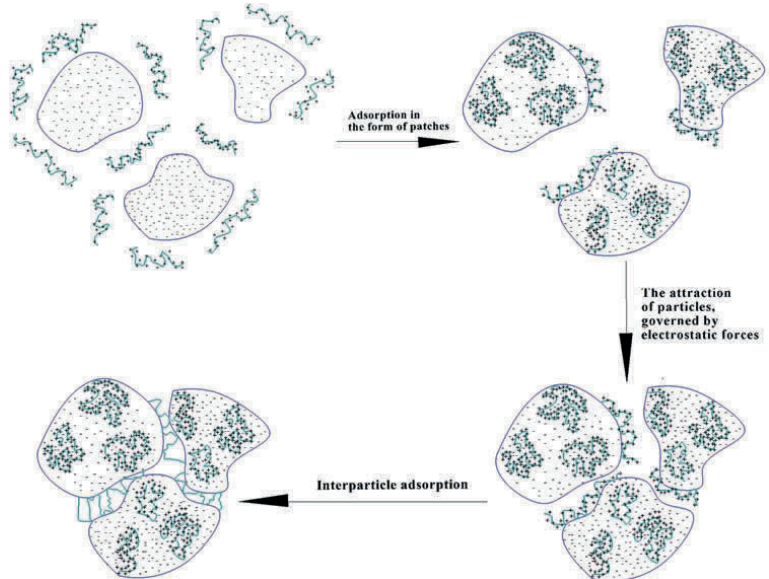


Figure 6. Possible arrangement of the cations on the surface of the suspended solid and the charge patch agglomeration mechanism (Bolto, 1995).



Thus, this mechanism is assumed to be predominant when applying PolyDADMAC (high MW) and low MW cationic PAM of high charge densities at relatively low particle concentrations (less than 10^{14} particles/L).

When discussing the flocculation mechanism of cationic polymers at high particle concentration, significant bridging effects are detected in the interim between the initial adsorption stages and the reaching of the equilibrium state, since higher particle concentrations intensify the collision frequency of suspended solids at the same time as the pendant polyelectrolyte loops are greatly extended into the solution (Bratby, 2016). Hence, presumably, the bridging mechanism plays an essential role in the case of applying PolyDADMAC and high MW cationic PAM of low charge density at high concentrations of suspended solids in the mixed liquor.

3.4. Bio-flocculation

Modified starches solely (in the form of starch-based cationic flocculants) were investigated by Deng et al. (2015), W. Guo et al. (2010), Huyskens et al. (2012) and Koseoglu et al. (2008, 2012), since they are inexpensive, offering inherent advantages over inorganic and synthetic polymers such as being derived from a renewable source of raw materials with simpler degradability after the use. However, the controversial effect of starches on membrane performance was discussed in the study by Drews (2010). Presumably, this is caused by the fact that biopolymers like starch and chitosan do not tolerate wide dosing ranges, since over- or under-dosing might cause further fouling on the membrane (Vera Iversen, 2011). On this account, in the study by Koseoglu et al. (2008), starch along with chitosan was reported to trigger the flocculation mechanism apparently better than the metal salts, whereas, according to Huyskens et al. (2012), both polymers caused a considerable increase in irreversible fouling observed in the MBR. In a number of studies (Iversen, Mehrez, et al., 2009; Iversen, Mohaupt, Drews, Lesjean, & Kraume, 2008; Koseoglu et al., 2012), starch also had a detrimental effect on the system due to strong fouling phenomena. Additionally, in the work by Iversen, Koseoglu, et al. (2009), a negative impact of starch-based flocculant on the oxygen uptake rate (OUR) was indicated, stressing that this polymer might therefore not be appropriate for application in MBR.

Concerning chitosan, Ji et al. (2008) indicated the significant positive influence of this additive on the flocculation of sludge particles with the subsequent reduction of the fouling rates for both short- and long-term operations, which were about seven times lower than in the control MBR. In further research (Ji et al., 2010), chitosan was revealed to have a crucial effect on biomass morphological properties and successfully alleviated membrane fouling. Fouling mitigation ability of this agent was noticed by Shuyan (2015) as well. Additionally, in the study by Iversen et al. (2008), chitosan considerably reduced SMP levels in the supernatant. Furthermore, enhanced OURs were observed when using chitosan, according to Iversen et al. (2008), Nouri et al. (2013).

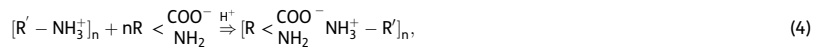
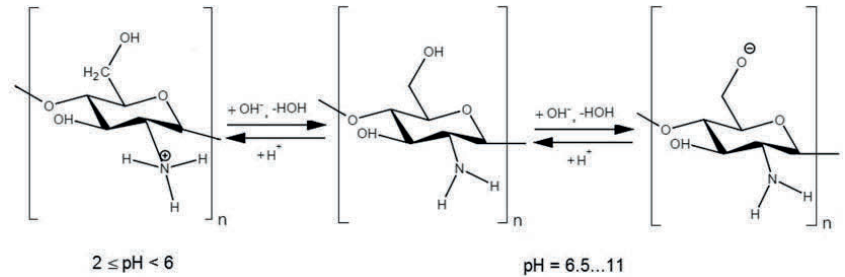
In marked contrast to all these findings, according to Guo et al. (2010) and Koseoglu et al. (2012), chitosan exhibited either the highest fouling rates among the tested additives or the lowest SMP removal because of the significant sludge viscosity increase.

In the study by Ngo and Guo (2009), a modified green bio-flocculant (GBF) was introduced, which served as a membrane fouling reducer and an agent for improving microbial activity. The positive impact of this additive on treatment performance and fouling mitigation was also discussed in the work by Guo, Ngo, Wu, Hu, and Listowski (2011).

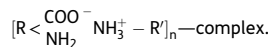
Regarding effective natural bio-flocculants, particularly chitosan, its structure highly depends on pH (Figure 7).

The mechanism for the removal of microbial substances using chitosan at acidic pH is as follows:

Figure 7. Structure of chitosan depending on pH conditions (Kumirska, Weinhold, Thöming, & Stepnowski, 2011; Sakkayawong, Thiravetyan, & Nakbanpote, 2005).



where $[\text{R}' - \text{NH}_3^+]_n$ is chitosan and $\text{R} < \begin{matrix} \text{COO}^- \\ \text{NH}_2 \end{matrix}$ is the ionized carboxyl group of the bacterial surface;



According to the findings, at acidic pH by its protonated amino groups, chitosan interacts electrostatically with negatively charged organic matter, resulting in their chemisorption. Therefore, in acidic solutions, chitosan exhibits strong antibacterial activity, as shown in the study by Kumirska et al. (2011). Nevertheless, according to Guibal and Roussy (2007), sometimes the amount of protonated amino groups is insignificant, far below the number of charges required for neutralization of the anions carried by suspended solids. In such cases, as assumed, the removal is assured by the combination of electrostatic patch and bridging mechanisms. At higher pH values between 6.0 and 6.5, amino groups of chitosan become less protonated and turn out to be fully deprotonated at pH 6.5. However, as shown in the work by Sakkayawong et al. (2005), even in this case chitosan doesn't lose its treatment efficiency, which is presumably entailed by the hydrophobic interactions of chitosan molecules with sludge aggregates of the same nature. Besides, since chitosan possesses a high molecular weight, the elimination of organic matter is expected to happen through the bridging mechanism. In the alkaline media, chitosan can adsorb organic contaminants through covalent bonding.

Starch grafts cationic moieties during carboxylation with the aid of the quaternary ammonium compound. According to Ji et al. (2014), cationic starches act through the charge neutralization mechanism since they get attracted to the surface of negatively charged organic particles and result in the decrease of the absolute electrokinetic potential value, resulting in system destabilization and subsequent agglomeration of the particles. The starches are characterized by the ability to generate larger flocs, although their binding to colloid particles is incomplete (Koseoglu et al., 2012). On the contrary, according to Pal, Mal, and Singh (2005), the main mechanism of action for cationic starches is the bridging phenomenon; moreover, longer chains of the polymer backbone are preferable since they foster the extension of the tail from one particle surface to another, thus assuring high flocculation efficiency.

3.5. Oxidation

Ozonation can be applied as an alternative method to modify the mixed liquor properties in order to alleviate membrane fouling. The positive effect of ozone on long-term MBR performance was confirmed by X. Huang and Wu (2008) and J. Wu and Huang (2010), who determined the optimum ozone concentration, which could assure slow formation of the gel layer on the membrane surface as well as the enhancement of suspended particles' flocculation ability in the ozone-MBR system.

Table 7. Intrinsic mechanisms of chemical action in the reduction of a system's fouling propensity under membrane flux enhancement in MBR

Mechanisms of membrane flux enhancement in MBR	Monomeric inorganic coagulants		Polymerized inorganic coagulants		Organic flocculants			Bio-flocculants	
	FeCl ₃	Al ₂ (SO ₄) ₃ · xH ₂ O	Polymeric ferric sulphate (PFS)	Poly-aluminium chloride (PACl)	Poly(diallyl-dimethyl-ammonium chloride) (PolyDADMAC)	Cationic polyacrylamide	Chitosan	Modified Starch	
Reduction of SMP level in the mixed liquor	(W. Guo et al., 2010; Ivanovic & Leiknes, 2011; Zhang, Sun, Zhao, & Gao, 2008; Zhang, Wang et al., 2015)	(Ji et al., 2010)	(Ji et al., 2010)	(W. Guo et al., 2010)	(Collins et al., 2006; Huyskens et al., 2012; V. Iversen, Mehrez, et al., 2009; Koseoglu et al., 2008; W.-N. Lee et al., 2007; Haifeng Zhang et al., 2014)	(Dizge, Koseoglu-Imer, Karagunduz, & Keskinler, 2011; P. Gkotsis, Peleka, et al., 2016)	(W. Guo et al., 2010; Koseoglu et al., 2008)	(Koseoglu et al., 2008)	
Biopolymer elimination					(V. Iversen, Mehrez, et al., 2009; Yoon & Collins, 2006)			(V. Iversen, Mehrez, et al., 2009)	
Increasing mean sludge floc size, drop fractal dimension	(Zhang, Sun, et al., 2008)	(Nouri et al., 2013; K. G.Song et al., 2008; J. Wu et al., 2006)	(Ji et al., 2010; J. Wu et al., 2006; J. Wu & Huang, 2008)	(Nouri et al., 2013; J. Wu et al., 2006)	(Collins et al., 2006; Huyskens et al., 2012; V. Iversen, Mehrez, et al., 2009; W.-N. Lee et al., 2007; Haifeng Zhang et al., 2014)	(Dizge et al., 2011; P. Gkotsis, Peleka, et al., 2016; Ji et al., 2010)	(W. Guo et al., 2010; Ji et al., 2010; Ji et al., 2008)	(V. Iversen, Mehrez, et al., 2009; Koseoglu et al., 2012)	

(Continued)

Table 7. (Continued)

Mechanisms of membrane flux enhancement in MBR	Monomeric inorganic coagulants		Polymerized inorganic coagulants		Organic flocculants		Bio-flocculants	
	FeCl ₃	Al ₂ (SO ₄) ₃ · xH ₂ O	Polymeric ferric sulphate (PFS)	Poly-aluminium chloride (PACl)	Poly(diallyl-dimethyl-ammonium chloride) (PolyDADMAC)	Cationic polyacrylamide	Chitosan	Modified Starch
Enhancing charge neutralization	(Zhang, Sun, et al., 2008)		(Ji et al., 2010; J. Wu et al., 2006; J. Wu & Huang, 2008)	(Ji et al., 2010; J. Wu et al., 2006)	(Huyskens et al., 2012)	(P. Gkotsis, Peleka, et al., 2016)		
Increasing sludge relative hydrophobicity	(Ji et al., 2010)	(Ji et al., 2010)	(Ji et al., 2010)	(Ji et al., 2010)		(Dizge et al., 2011)		
Lowering gel-layer formation, cake porosity increase and specific cake-resistance reduction	(K. G. Song et al., 2008)	(Nouri et al., 2013; K. G. Song et al., 2008)	(Ji et al., 2008)	(Nouri et al., 2013)	(W.-N. Lee et al., 2007)		(Ji et al., 2008)	

According to the investigation carried out by K. R. Lee and Yeom (2007), ozone played a crucial role in membrane fouling control since it promoted keeping the dynamic viscosity of the activated sludge at a relatively low level, thus permitting stable membrane filtration for more than 150 days without chemical cleaning of the membrane. In the study by Yeom et al. (2005), ozone was applied in combination with alkaline for biomass pretreatment in a pilot-scale MBR-type aerobic digestion process. As discussed, the experiment ran smoothly without significant membrane fouling, even at the relatively high levels of MLSS concentration (11,000–25,000 mg/L).

4. Research needs

The current literature review provides background and identifies the most prospective additives as membrane fouling enhancers in MBR (Table 7). However, the use of additives is not usually practised in full-scale MBRs since it is uncertain whether the cost of chemical use is justified by membrane fouling decrease (Krzeminski, Leverette, Malamis, & Katsou, 2017). Furthermore, the long-term implications of using or stopping to use the additives have not been researched in detail, and there is a gap in process control approaches for the application of flux enhancers in MBR.

Since adsorption was proven to be an efficient fouling alleviation tool, it is worth mentioning that its application in the MBR process still has a high potential. However, in order to make it more feasible, cost-effective adsorbents should be used. A number of cheap non-conventional materials can serve this purpose. For example, nano-magnetic polymers, cyclodextrin and covalent organic polymers were found to have great binding/degrading capacities for organic compounds (Alaba et al., 2018). In addition, agricultural and industrial waste materials like wood char, rice husk, fruit peels, fly/zeolite incinerator ash and polymer resins are gaining more interest as potential adsorbents (Mallampati, Xuanjun, Adin, & Valiyaveetil, 2015; Mateen et al., 2016; Rene & Lewis, 2017). However, these materials need to be thoroughly tested for their effectiveness to mitigate fouling in the MBR system.

Concerning ozonation, additional trials are needed to make its application more economical when dealing with the mixed liquor, characterized by high levels of suspended solids. Moreover, the possibility of the generation of highly toxic non-biodegradable/inseparable ozonation by-products should be checked.

5. Conclusions

In conclusion, membrane flux enhancement applying coagulants, flocculants and bio-flocculants is a prospective direction of membrane fouling mitigation in MBR that has the potential to facilitate further penetration of MBR into cost-sensitive markets, including small communities and developing countries.

Further lab research in this direction should be focused on combining various agents as membrane flux enhancers, considering the identified mechanisms of their action: retention of SMP, reduction of specific cake resistance, an increase of sludge floc size and hydrophobicity as well as the neutralization of their charge. The possibility of applying them all together with non-conventional cost-effective adsorbents or oxidizing agents should also be taken into consideration.

In general, applied future research should be focused on developing pilot case studies with various membrane flux enhancers as well as bridging the gap in MBR process control, including the flux enhancement part.

Funding

The authors received no direct funding for this research.

Competing Interests

The authors declare no competing interests of a personal, professional or financial nature.

Author details

O. Kulesha^{1,2}
E-mail: olga.kulesha@nmbu.no

Z. Maletskyi¹

E-mail: zakhar.maletskyi@nmbu.no

ORCID ID: <http://orcid.org/0000-0002-1356-3588>

H. Ratnaweera¹

E-mail: harsha.ratnaweera@nmbu.no

ORCID ID: <http://orcid.org/0000-0003-1456-2541>

¹ Department of Mathematical Sciences and Technology, Norwegian University of Life Sciences, Aas, Norway.

² Department of General and Inorganic Chemistry, Kyiv Polytechnic Institute, Kyiv, Ukraine.

Citation information

Cite this article as: State-of-the-art of membrane flux enhancement in membrane bioreactor, O. Kulesha, Z. Maletskiy & H. Ratnaweera, *Cogent Engineering* (2018), 5: 1489700.

Notes

1. PFS, polymeric ferric sulphate.
2. PAC, powdered activated carbon.

References

- Ábel, M., Szabó, G., Poser, O., László, Z., & Hodúr, C. (2013). Enzyme recovery and fouling mitigation by ultrasound-enhanced ultrafiltration. *Desalination and Water Treatment*, 51(25–27), 4921–4926. doi:10.1080/19443994.2013.795325
- Alaba, P. A., Oladoja, N. A., Sani, Y. M., Ayodele, O. B., Mohammed, I. Y., Olupina, S. F., & Daud, W. M. W. (2018). Insight into wastewater decontamination using polymeric adsorbents. *Journal of Environmental Chemical Engineering*, 6(2), 1651–1672. doi:10.1016/j.jece.2018.02.019
- Amirafzabi, M. S., Mostoufi, N., Hosseinzadeh, M., & Mehrnia, M. R. (2014). Reduction of membrane fouling by innovative method (injection of air jet). *Journal of Environmental Health Science and Engineering*, 12(1), 1–8. doi:10.1186/s40201-014-0128-0
- Amjad, Z. (2010). *The science and technology of industrial water treatment*. London, New York: IWA Publishing.
- Aryal, R. K., Lebeque, J., Shon, H. K., Vigneswaran, S., Kandasamy, J., & Grasmick, A. (2009). Temporal variation of foulant characteristics in membrane bioreactor. *Desalination and Water Treatment*, 6(1–3), 69–73. doi:10.5004/dwt.2009.647
- Aslam, M., Lee, P. H., & Kim, J. (2015). Analysis of membrane fouling with porous membrane filters by microbial suspensions for autotrophic nitrogen transformations. *Separation and Purification Technology*, 146, 284–293. doi:10.1016/j.seppur.2015.03.042
- Aun Ng, C., Sun, D., & Fane, A. G. (2006). Operation of membrane bioreactor with powdered activated carbon addition. *Separation Science and Technology*, 41(7), 1447–1466. doi:10.1080/01496390600634632
- Berg, C. H., Kalfas, S., Malmsten, M., & Arnebrant, T. (2001). Proteolytic degradation of oral biofilms in vitro and in vivo: Potential of proteases originating from *Euphausia superba* for plaque control. *European Journal of Oral Sciences*, 109(5), 316–324. doi:10.1034/j.1600-0722.2001.00099.x
- Böhm, L., Drews, A., Prieske, H., Bérubé, P. R., & Kraume, M. (2012). The importance of fluid dynamics for MBR fouling mitigation. *Bioresource Technology*, 122, 50–61. doi:10.1016/j.biortech.2012.05.069
- Bolto, B. A. (1995). Soluble polymers in water purification. *Progress in Polymer Science*, 20(6), 987–1041. doi:10.1016/0079-6700(95)00010-D
- Bowen, W. R., Calvo, J. I., & Hernández, A. (1995). Steps of membrane blocking in flux decline during protein microfiltration. *Journal of Membrane Science*, 101(1–2), 153–165. doi:10.1016/0376-7388(94)00295-A
- Bratby, J. (2016). *Coagulation and flocculation in water and wastewater treatment* (3d ed.). London: IWA Publishing. doi:10.2166/9781780407500
- Brookes, A., Jefferson, B., Guglielmi, G., & Judd, S. J. (2006). Sustainable flux fouling in a membrane bioreactor: Impact of flux and MLSS. *Separation Science and Technology*, 41(7), 1279–1291. doi:10.1080/01496390600634509
- Cao, T. A., Van De Staey, G., & Smets, I. Y. (2015). Integrating activated sludge floc size information in MBR fouling modeling. *Water Science and Technology*, 71(7), 1073–1080. doi:10.2166/wst.2015.070
- Chang, I. S., & Judd, S. J. (2002). Air sparging of a submerged MBR for municipal wastewater treatment. *Process Biochemistry*, 37(8), 915–920. doi:10.1016/S0032-9592(01)00291-6
- Chellam, S., & Cogan, N. G. (2011). Colloidal and bacterial fouling during constant flux microfiltration: Comparison of classical blocking laws with a unified model combining pore blocking and EPS secretion. *Journal of Membrane Science*, 382(1–2), 148–157. doi:10.1016/j.memsci.2011.08.001
- Chen, F., Bi, X., & Ng, H. Y. (2016). Effects of bio-carriers on membrane fouling mitigation in moving bed membrane bioreactor. *Journal of Membrane Science*, 499, 134–142. Retrieved from <http://www.sciencedirect.com/science/article/pii/S0376738815302829>
- Chen, J., Zhang, M., Li, F., Qian, L., Lin, H., Yang, L., ... Liao, B. Q. (2016). Membrane fouling in a membrane bioreactor: High filtration resistance of gel layer and its underlying mechanism. *Water Research*, 102, 82–89. doi:10.1016/j.watres.2016.06.028
- Chen, W., Westerhoff, P., Leenheer, J. A., & Booksh, K. (2003). Fluorescence excitation-emission matrix regional integration to quantify spectra for dissolved organic matter. *Environmental Science and Technology*, 37(24), 5701–5710. doi:10.1021/es034354c
- Christensen, M. L., Bugge, T. V., Hede, B. H., Nierychlo, M., Larsen, P., & Jørgensen, M. K. (2016). Effects of relaxation time on fouling propensity in membrane bioreactors. *Journal of Membrane Science*. doi:10.1016/j.memsci.2016.01.006
- Chu, H. P., & Li, X. Y. (2005). Membrane fouling in a membrane bioreactor (MBR): Sludge cake formation and fouling characteristics. *Biotechnology and Bioengineering*, 90(3), 323–331. doi:10.1002/bit.20409
- Chuang, S. H., Chang, W. C., Chang, M. C., & Sung, M. A. (2009). The effects of soluble organic matters on membrane fouling index. *Bioresource Technology*, 100(5), 1875–1877. doi:10.1016/j.biortech.2008.09.054
- Collins, J. H., Yoon, S. H., Musale, D., Kong, J. F., Koppes, J., Sundararajan, S., ... Kronover, K. (2006). Membrane performance enhancer evaluations on pilot- and full-scale membrane bioreactors. *Water and Environment Journal*, 20(1), 43–47. doi:10.1111/j.1747-6593.2006.00030.x
- Dalmou, M., Atanasova, N., Gabarrón, S., Rodriguez-Roda, I., & Comas, J. (2015). Comparison of a deterministic and a data driven model to describe MBR fouling. *Chemical Engineering Journal*, 260, 300–308. doi:10.1016/j.cej.2014.09.003
- Deng, L., Guo, W., Hao, H., Farzana, M., Zuthi, R., Zhang, J., ... Zhang, X. (2015). Membrane fouling reduction and improvement of sludge characteristics by biofloculant addition in submerged membrane bioreactor. *Separation and Purification Technology*, 156, 450–458. doi:10.1016/j.seppur.2015.10.034
- Deowan, S. A., Galiano, F., Hoinkis, J., Johnson, D., Altinkaya, S. A., Gabriele, B., ... Figoli, A. (2016). Novel low-fouling membrane bioreactor (MBR) for industrial wastewater treatment. *Journal of Membrane Science*, 510, 524–532. doi:10.1016/j.memsci.2016.03.002
- Dizge, N., Koseoglu-Imer, D. Y., Karagunduz, A., & Keskinler, B. (2011). Effects of cationic polyelectrolyte on filterability and fouling reduction of submerged membrane bioreactor (MBR). *Journal of Membrane Science*, 377(1–2), 175–181. doi:10.1016/j.memsci.2011.04.048

- Drews, A. (2010). Membrane fouling in membrane bioreactors-Characterisation, contradictions, cause and cures. *Journal of Membrane Science*, 363(1-2), 1-28. doi:10.1016/j.memsci.2010.06.046
- El Rayess, Y., Albasi, C., Bacchin, P., Taillandier, P., Mietton-Peuchot, M., & Devatine, A. (2012). Analysis of membrane fouling during cross-flow microfiltration of wine. *Innovative Food Science & Emerging Technologies*, 16, 398-408. doi:10.1016/j.ifset.2012.09.002
- Ergön-Can, T., Köse-Mutlu, B., Koyuncu, İ., & Lee, C. H. (2017). Biofouling control based on bacterial quorum quenching with a new application: Rotary microbial carrier frame. *Journal of Membrane Science*, 525 (December 2015), 116-124. doi:10.1016/j.memsci.2016.10.036
- Etemadi, H., Yegani, R., & Seyfollahi, M. (2017). The effect of amino functionalized and polyethylene glycol grafted nanodiamond on anti-biofouling properties of cellulose acetate membrane in membrane bioreactor systems. *Separation and Purification Technology*, 177, 350-362. doi:10.1016/j.seppur.2017.01.013
- Evenblij, H., Verrecht, B., Van Der Graaf, J. H. J. M., & Van Der Bruggen, B. (2005). Manipulating filterability of MBR activated sludge by pulsed substrate addition. *Desalination*, 178(1-3 SPEC. ISS.), 193-201. doi:10.1016/j.desal.2005.02.006
- Fang, H. H. P., Shi, X., & Zhang, T. (2006). Effect of activated carbon on fouling of activated sludge filtration. *Desalination*, 189(1-3 SPEC. ISS.), 193-199. doi:10.1016/j.desal.2005.02.087
- Field, R. W., Wu, D., Howell, J. A., & Gupta, B. B. (1995). Critical flux concept for microfiltration fouling. *Journal of Membrane Science*, 100(3), 259-272. doi:10.1016/0376-7388(94)00265-Z
- Flemming, H., & Wingender, J. (2010). Nature reviews, *The Biofilm Matrix*, 8(9), 623-33. doi:10.1038/nrmicro2415
- Flemming, H.-C.-C., & Wingender, J. (2001). Relevance of microbial extracellular polymeric substances (EPSs) - Part I: Structural and ecological aspects. *Water Science and Technology: A Journal of the International Association on Water Pollution Research*, 43(6), 9-16. Retrieved from <http://www.ncbi.nlm.nih.gov/pubmed/11381977> %5Cnhttp://www.ncbi.nlm.nih.gov/pubmed/11381954
- Fonseca, A. C., Summers, R. S., & Greenberg, A. R. (2007). Extra-cellular polysaccharides, soluble microbial products, and natural organic matter impact on nanofiltration membranes flux decline. *Environmental Science & Technology*, 41(7), 2491-2497. doi:10.1021/es060792i
- Frechen, F. B., Schier, W., & Linden, C. (2008). Pre-treatment of municipal MBR applications. *Desalination*, 231(1-3), 108-114. doi:10.1016/j.desal.2007.10.025
- Gabarrón, S., Gómez, M., Dvořák, L., Růžicková, I., Rodríguez-Roda, I., & Comas, J. (2014). Ragging in MBR: Effects of operational conditions, chemical cleaning, and pre-treatment improvements. *Separation Science and Technology (Philadelphia)*, 49(14), 2115-2123. doi:10.1080/01496395.2014.927489
- Geilvoet. (2010). *The Delft Filtration Characterisation method. Assessing membrane bioreactor activated sludge filterability (Doctoral Dissertation)*. Delft University of Technology, The Netherlands. Retrieved from: [uuiid:5fb0f3b-146b-4a67-9239-333482ad62bd](https://www.researchgate.net/publication/333482ad62bd).
- Geng, Z., & Hall, E. R. (2007). A comparative study of fouling-related properties of sludge from conventional and membrane enhanced biological phosphorus removal processes. *Water Research*, 41 (19), 4329-4338. doi:10.1016/j.watres.2007.07.007
- Gkotsis, P., Banti, D., Peleka, E., Zouboulis, A., & Samaras, P. (2014). Fouling issues in Membrane Bioreactors (MBRs) for wastewater treatment: Major mechanisms, prevention and control strategies. *Processes*, 2(4), 795-866. doi:10.3390/pr2040795
- Gkotsis, P., Peleka, E., Zamboulis, D., Mitrakas, M., Tolkou, A., & Zouboulis, A. (2016). Wastewater treatment in membrane bioreactors: The use of polyelectrolytes to control membrane fouling. *Environmental Processes*. doi:10.1007/s40710-016-0168-9
- Gkotsis, P. K., Mitrakas, M. M., Tolkou, A. K., & Zouboulis, A. I. (2016). Batch and continuous dosing of conventional and composite coagulation agents for fouling control in a pilot-scale MBR. *Chemical Engineering Journal*, 311, 255-264. doi:10.1016/j.ccej.2016.11.099
- Gkotsis, P. K., Mitrakas, M. M., Tolkou, A. K., & Zouboulis, A. I. (2017). Batch and continuous dosing of conventional and composite coagulation agents for fouling control in a pilot-scale MBR. *Chemical Engineering Journal*, 311, 255-264. doi:10.1016/j.ccej.2016.11.099
- González, E., Díaz, O., Vera, L., Rodríguez-Gómez, L. E., & Rodríguez-Sevilla, J. (2018). Feedback control system for filtration optimisation based on a simple fouling model dynamically applied to membrane bioreactors. *Journal of Membrane Science*, 552(December 2017), 243-252. doi:10.1016/j.memsci.2018.02.007
- Gregory, J., & Duan, J. (2001). Hydrolyzing metal salts as coagulants. *Pure and Applied Chemistry*, 73(12), 2017-2026. doi:10.1351/pac200173122017
- Guibal, E., & Roussy, J. (2007). Coagulation and flocculation of dye-containing solutions using a biopolymer (Chitosan). *Reactive and Functional Polymers*, 67(1), 33-42. doi:10.1016/j.reactfunctpolym.2006.08.008
- Guo, W., Ngo, H., Wu, Z., Hu, A. Y., & Listowski, A. (2011). Application of biofloculant and nonwoven supporting media for better biological nutrient removal and fouling control in a submerged MBR. *Sustainable Environment Research*, 21(1), 53-58.
- Guo, W., Ngo, H. H., Vigneswaran, S., Dharmawan, F., Nguyen, T. T., & Aryal, R. (2010). Effect of different flocculants on short-term performance of submerged membrane bioreactor. *Separation and Purification Technology*, 70(3), 274-279. doi:10.1016/j.seppur.2009.10.003
- Guo, W. S., Vigneswaran, S., Ngo, H. H., Kandasamy, J., & Yoon, S. (2008). The role of a membrane performance enhancer in a membrane bioreactor: A comparison with other submerged membrane hybrid systems. *Desalination*, 231, 305-313. doi:10.1016/j.desal.2007.10.034
- Guo, W. S., Vigneswaran, S., Ngo, H. H., Van Nguyen, T. B., & Ben Aim, R. (2006). Influence of bioreaction on a long-term operation of a submerged membrane adsorption hybrid system. *Desalination*, 191(1-3), 92-99. doi:10.1016/j.desal.2005.06.034
- Gutman, J., Walker, S. L., Freger, V., & Herzberg, M. (2013). Bacterial attachment and viscoelasticity: Physicochemical and motility effects analyzed using quartz crystal microbalance with dissipation (QCM-D). *Environmental Science and Technology*, 47(1), 398-404. doi:10.1021/es303394w
- Hahn H.H., Hoffmann E., Døgaard H. (Eds.). (1996, September). *Chemical water and wastewater treatment IV. Proceedings of the 7th Gothenburg Symposium 1996*. Berlin: Springer.
- Hameed, S. (2017). Effect of the pre-treatment on the performance of MBR, Al-Kut WWTP, wasit governorate. *Journal of Chemical Engineering & Process*

- Technology, 8(1), 1–6. doi:10.4172/2157-7048.1000320
- Hem, J. D., & Roberson, C. E. (1967). Form and stability of aluminum hydroxide complexes in dilute solution. *USGS Water Supply Paper*, 1827–A, 55.
- Hocaoglu, S. M., & Orhon, D. (2010). Fate of proteins and carbohydrates in membrane bioreactor operated at high sludge age. *Journal of Environmental Science and Health - Part A Toxic/Hazardous Substances and Environmental Engineering*, 45(9), 1101–1108. doi:10.1080/10934529.2010.486342
- Hoffmann, C., & Krause, S. (2013). An innovative approach to improve energy efficiency of Membrane Bioreactors (MBR). *Filtrieren und Separieren*, 13, 49–52.
- Holbrook, R. D., Higgins, M. J., Murthy, S. N., Fonseca, A. D., Fleischer, E. J., Daigger, G. T., ... Novak, J. T. (2003). Effect of alum addition on the performance of submerged membranes for wastewater treatment. *Water Environment Research: A Research Publication of the Water Environment Federation*, 76(7), 2699–2702. Retrieved from <http://www.ncbi.nlm.nih.gov/pubmed/16042118>
- Hong, H., Lin, H., Mei, R., Zhou, X., Liao, B. Q., & Zhao, L. (2016). Membrane fouling in a membrane bioreactor: A novel method for membrane surface morphology construction and its application in interaction energy assessment. *Journal of Membrane Science*, 516, 135–143. doi:10.1016/j.memsci.2016.06.006
- Hong, H., Zhang, M., He, Y., Chen, J., & Lin, H. (2014). Fouling mechanisms of gel layer in a submerged membrane bioreactor. *Bioresource Technology*, 166, 295–302. doi:10.1016/j.biortech.2014.05.063
- Hu, Y., Wang, X. C., Tian, W., Ngo, H. H., & Chen, R. (2016). Towards stable operation of a dynamic membrane bioreactor (DMBR): Operational process, behavior and retention effect of dynamic membrane. *Journal of Membrane Science*, 498, 20–29. doi:10.1016/j.memsci.2015.10.009
- Hua, L.-C., Huang, C., Su, Y.-C., Nguyen, T.-N.-P., & Chen, P.-C. (2015). Effects of electro-coagulation on fouling mitigation and sludge characteristics in a coagulation-assisted membrane bioreactor. *Journal of Membrane Science*. 495, 29–36. Retrieved from <http://www.sciencedirect.com/science/article/pii/S0376738815300909>
- Huang, J., Wang, Z., Zhang, J., Zhang, X., Ma, J., & Wu, Z. (2015). A novel composite conductive microfiltration membrane and its anti-fouling performance with an external electric field in membrane bioreactors. *Scientific Reports*, 5, 1–8. doi:10.1038/srep09268
- Huang, X., & Wu, J. (2008). Improvement of membrane filterability of the mixed liquor in a membrane bioreactor by ozonation. *Journal of Membrane Science*, 318(1–2), 210–216. doi:10.1016/j.memsci.2008.02.031
- Huyskens, C., De Wever, H., Fovet, Y., Wegmann, U., Diels, L., & Lenaerts, S. (2012). Screening of novel MBR fouling reducers: Benchmarking with known fouling reducers and evaluation of their mechanism of action. *Separation and Purification Technology*, 95, 49–57. doi:10.1016/j.seppur.2012.04.024
- Hwang, B.-K., Lee, W.-N., Park, P.-K., Lee, C.-H., & Chang, I.-S. (2007). Effect of membrane fouling reducer on cake structure and membrane permeability in membrane bioreactor. *Journal of Membrane Science*, 288(1–2), 149–156. doi:10.1016/j.memsci.2006.11.032
- Ibeid, S., Elektorowicz, M., & Oleszkiewicz, J. A. (2015). Electro-conditioning of activated sludge in a membrane electro-bioreactor for improved dewatering and reduced membrane fouling. *Journal of Membrane Science*, 494, 136–142. doi:10.1016/j.memsci.2015.07.051
- Ibeid, S., Elektorowicz, M., & Oleszkiewicz, J. A. (2017). Impact of electrocoagulation of soluble microbial products on membrane fouling at different volatile suspended solids' concentrations. *Environmental Technology (United Kingdom)*, 38(4), 385–393. doi:10.1080/09593330.2016.1195879
- Inan, H., Dimoglo, A., Şimşek, H., & Karpuzcu, M. (2004). Olive oil mill wastewater treatment by means of electro-coagulation. *Separation and Purification Technology*, 36(1), 23–31. doi:10.1016/S1383-5866(03)00148-5
- Iorhemen, O. T., Hamza, R. A., & Tay, J. H. (2016). Membrane bioreactor (MBR) technology for wastewater treatment and reclamation: Membrane fouling. *Membranes*, 6(2), 13–16. Retrieved from <http://doi.org/10.3390/membranes6020033>
- Ivanovic, I., & Leiknes, T. (2011). Effect of addition of different additives on overall performance of biofilm-MBR (BF-MBR). *Desalination and Water Treatment*, 34, 129–135.
- Iversen, V. (2010). *Comprehensive assessment of flux enhancers in membrane bioreactors for wastewater treatment* (Doctoral Dissertation). Technical University of Berlin, Germany.
- Iversen, V., Koseoglu, H., Yigit, N. O., Drews, A., Kitis, M., Lesjean, B., & Kraume, M. (2009). Impacts of membrane flux enhancers on activated sludge respiration and nutrient removal in MBRs. *Water Research*, 43(3), 822–830. doi:10.1016/j.watres.2008.11.022
- Iversen, V., Mehrez, R., Horng, R. Y., Chen, C. H., Meng, F., Drews, A., ... Kraume, M. (2009). Fouling mitigation through flocculants and adsorbents addition in membrane bioreactors: Comparing lab and pilot studies. *Journal of Membrane Science*. doi:10.1016/j.memsci.2009.08.014
- Iversen, V., Mohaupt, J., Drews, A., Lesjean, B., & Kraume, M. (2008). Side effects of flux enhancing chemicals in membrane bioreactors (MBRs): Study on their biological toxicity and their residual fouling propensity. *Water Science and Technology*, 57(1), 117–123. doi:10.2166/wst.2008.660
- Jamal Khan, S., Visvanathan, C., & Jegatheesan, V. (2012). Effect of powdered activated carbon (PAC) and cationic polymer on biofouling mitigation in hybrid MBRs. *Bioresource Technology*, 113, 165–168. doi:10.1016/j.biortech.2011.12.107
- Janus, T., & Ulanicki, B. (2015). A behavioural membrane fouling model for integrated simulation of membrane bioreactors for wastewater treatment. *Procedia Engineering*, 119(1), 1328–1337. doi:10.1016/j.proeng.2015.08.964
- Jelemenský, M., Sharma, A., Paulen, R., & Fikar, M. (2016). Time-optimal control of diafiltration processes in the presence of membrane fouling. *Computers and Chemical Engineering*, 91, 343–351. doi:10.1016/j.compchemeng.2016.04.018
- Jhaveri, J. H., & Murthy, Z. V. P. (2016). A comprehensive review on anti-fouling nanocomposite membranes for pressure driven membrane separation processes. *Desalination*. 379, 137–154. Retrieved from <http://www.sciencedirect.com/science/article/pii/S0011916415301119>
- Ji, J., Li, J., Qiu, J., & Li, X. (2014). Polyacrylamide-starch composite flocculant as a membrane fouling reducer: Key factors of fouling reduction. *Separation and Purification Technology*, 131, 1–7. doi:10.1016/j.seppur.2014.04.013
- Ji, J., Qiu, J., Wai, N., Wong, F. S., & Li, Y. (2010). Influence of organic and inorganic flocculants on physical-

- chemical properties of biomass and membrane-fouling rate. *Water Research*, 44(5), 1627–1635. doi:10.1016/j.watres.2009.11.013
- Ji, J., Qiu, J., Wong, F., sin, & Li, Y. (2008). Enhancement of filterability in MBR achieved by improvement of supernatant and floc characteristics via filter aids addition. *Water Research*, 42(14), 3611–3622. doi:10.1016/j.watres.2008.05.022
- Jiang, T., Kennedy, M. D., Guinzbourg, B. F., Vanrolleghem, P. A., & Schippers, J. C. (2005). Optimising the operation of a MBR pilot plant by quantitative analysis of the membrane fouling mechanism. *Water Science and Technology*, 51(6–7), 19–25.
- Jiang, W., Xia, S., Liang, J., Zhang, Z., & Hermanowicz, S. W. (2013). Effect of quorum quenching on the reactor performance, biofouling and biomass characteristics in membrane bioreactors. *Water Research*, 47(1), 187–196. doi:10.1016/j.watres.2012.09.050
- Jin, L., Ong, S. L., & Ng, H. Y. (2013). Fouling control mechanism by suspended biofilm carriers addition in submerged ceramic membrane bioreactors. *Journal of Membrane Science*, 427, 250–258. doi:10.1016/j.memsci.2012.09.016
- Johir, M. A., Shanmuganathan, S., Vigneswaran, S., & Kandasamy, J. (2013). Performance of submerged membrane bioreactor (smbr) with and without the addition of the different particle sizes of gac as suspended medium. *Bioresour. Technology*, 141, 13–18. doi:10.1016/j.biortech.2013.03.032
- Johir, M. A. H., Aryal, R., Vigneswaran, S., Kandasamy, J., & Grasmick, A. (2011). Influence of supporting media in suspension on membrane fouling reduction in submerged membrane bioreactor (smbr). *Journal of Membrane Science*, 374(1–2), 121–128. Retrieved from doi:10.1016/j.memsci.2011.03.023
- Jørgensen, M. K., Nierychlo, M., Nielsen, A. H., Larsen, P., Christensen, M. L., & Nielsen, P. H. (2017). Unified understanding of physico-chemical properties of activated sludge and fouling propensity. *Water Research*, 120, 117–132. doi:10.1016/j.watres.2017.04.056
- Joss, A., Böhler, M., Wedi, D., & Siegrist, H. (2009). Proposing a method for online permeability monitoring in membrane bioreactors. *Water Science and Technology*, 60(2), 497–506. doi:10.2166/wst.2009.370
- Juang, Y.-C., Lee, D.-J., & Lai, J.-Y. (2010). Visualizing fouling layer in membrane bioreactor. *Separation Science and Technology*, 45(7), 962–966. doi:10.1080/01496391003666882
- Judd, S. (2008). The status of membrane bioreactor technology. *Trends in Biotechnology*, 26(2), 109–116. doi:10.1016/j.tibtech.2007.11.005
- Kim, I., Choi, D. C., Lee, J., Chae, H. R., Hee Jang, J., Lee, C. H., ... Won, Y. J. (2015). Preparation and application of patterned hollow-fiber membranes to membrane bioreactor for wastewater treatment. *Journal of Membrane Science*, 490, 190–196. doi:10.1016/j.memsci.2015.04.026
- Kim, J., Kim, K., Ye, H., Lee, E., Shin, C., McCarty, P. L., & Bae, J. (2011). Anaerobic fluidized bed membrane bioreactor for wastewater treatment. *Environmental Science & Technology*, 45(2), 576–581. doi:10.1021/es1027103
- Kim, J. S., & Lee, C. H. (2003). Effect of powdered activated carbon on the performance of an aerobic membrane bioreactor: Comparison between cross-flow and submerged membrane systems. *Water Environment Research*, 75(4), 300–307. doi:10.2175/106143003X141105
- Kim, M. J., Sankararao, B., & Yoo, C. K. (2011). Determination of MBR fouling and chemical cleaning interval using statistical methods applied on dynamic index data. *Journal of Membrane Science*, 375(1–2), 345–353. doi:10.1016/j.memsci.2011.04.001
- Kimura, K., Ogyu, R., Miyoshi, T., & Watanabe, Y. (2015). Transition of major components in irreversible fouling of MBRs treating municipal wastewater. *Separation and Purification Technology*, 142, 326–331. doi:10.1016/j.seppur.2014.12.030
- Kimura, K., Tanaka, K., & Watanabe, Y. (2014). Microfiltration of different surface waters with/without coagulation: Clear correlations between membrane fouling and hydrophilic biopolymers. *Water Research*, 49, 434–443. doi:10.1016/j.watres.2013.10.030
- Kola, A., Ye, Y., Ho, A., Le-Clech, P., & Chen, V. (2012). Application of low frequency transverse vibration on fouling limitation in submerged hollow fibre membranes. *Journal of Membrane Science*, 409–410, 54–65. doi:10.1016/j.memsci.2012.03.017
- Koseoglu, H., Yigit, N. O., Civelekoglu, G., Harman, B. I., & Kitis, M. (2012). Effects of chemical additives on filtration and rheological characteristics of MBR sludge. *Bioresour. Technology*, 117, 48–54. doi:10.1016/j.biortech.2012.04.067
- Koseoglu, H., Yigit, N. O., Iversen, V., Drews, A., Kitis, M., Lesjean, B., & Kraume, M. (2008). Effects of several different flux enhancing chemicals on filterability and fouling reduction of membrane bioreactor (MBR) mixed liquors. *Journal of Membrane Science*, 320(1–2), 57–64. doi:10.1016/j.memsci.2008.03.053
- Kraume, M., Wedi, D., Schaller, J., Iversen, V., & Drews, A. (2009). Fouling in MBR: What use are lab investigations for full scale operation? *Desalination*, 236(1–3), 94–103. doi:10.1016/j.desal.2007.10.055
- Krzeminski, P., Leverette, L., Malamis, S., & Katsou, E. (2017). Membrane bioreactors – A review on recent developments in energy reduction, fouling control, novel configurations, LCA and market prospects. *Journal of Membrane Science*, 527(December 2016), 207–227. doi:10.1016/j.memsci.2016.12.010
- Kumar, R. V., Gaswami, L., Pakshiraj, K., & Pugazhenth, G. (2016). Dairy wastewater treatment using a novel low cost tubular ceramic membrane and membrane fouling mechanism using pore blocking models. *Journal of Water Process Engineering*, 13, 168–175. doi:10.1016/j.jwpe.2016.08.012
- Kumirska, J., Weinhold, M. X., Thöming, J., & Stepnowski, P. (2011). Biomedical activity of chitin/chitosan based materials- influence of physicochemical properties apart from molecular weight and degree of N-Acetylation. *Polymers*, 3(4), 1875–1901. doi:10.3390/polym3041875
- Kunacheva, C., & Stuckey, D. C. (2014). Analytical methods for soluble microbial products (SMP) and extracellular polymers (ECP) in wastewater treatment systems: A review. *Water Research*, 61(September 2016), 1–18. doi:10.1016/j.watres.2014.04.044
- Le Clech, P., Jefferson, B., Chang, I. S., & Judd, S. J. (2003). Critical flux determination by the flux-step method in a submerged membrane bioreactor. *Journal of Membrane Science*, 227(1–2), 81–93. doi:10.1016/j.memsci.2003.07.021
- Le-Clech, P., Chen, V., & Fane, T. A. G. (2006). Fouling in membrane bioreactors used in wastewater treatment. *Journal of Membrane Science*, 284(1–2), 17–53. doi:10.1016/j.memsci.2006.08.019
- Lee, J. C., Kim, J. S., Kang, I. J., Cho, M. H., Park, P. K., & Lee, C. H. (2001). Potential and limitations of alum or zeolite addition to improve the performance of a submerged membrane bioreactor. *Water Science and Technology*, 43(11), 59–66.

- Lee, K. R., & Yeom, I. T. (2007). Evaluation of a membrane bioreactor system coupled with sludge pretreatment for aerobic sludge digestion. *Environmental Technology*, 28(7), 723–730. doi:10.1080/09593332808618837
- Lee, S., Park, S.-K., Kwon, H., Lee, S. H., Lee, K., Nam, C. H., ... Yi, T. (2016). Crossing the border between laboratory and field: Bacterial quorum quenching for anti-biofouling strategy in an MBR. *Environmental Science & Technology*. doi:10.1021/acs.est.5b04795
- Lee, S. J., Dilaver, M., Park, P. K., & Kim, J. H. (2013). Comparative analysis of fouling characteristics of ceramic and polymeric microfiltration membranes using filtration models. *Journal of Membrane Science*, 432, 97–105. doi:10.1016/j.memsci.2013.01.013
- Lee, W.-N., Chang, I.-S., Hwang, B.-K., Park, P.-K., Lee, C.-H., & Huang, X. (2007). Changes in biofilm architecture with addition of membrane fouling reducer in a membrane bioreactor. *Process Biochemistry*, 42(4), 655–661. doi:10.1016/j.procbio.2006.12.003
- Lesage, N., Sperandio, M., & Cabassud, C. (2005). Performances of hybrid adsorption/submerged membrane biological process for toxic waste removal. *Water Science & Technology*, 51(6-7), 173–180.
- Lesjean, B., Rosenberger, S., Laabs, C., Jekel, M., Gnirss, R., & Amy, G. (2005). Correlation between membrane fouling and soluble/colloidal organic substances in membrane bioreactors for municipal wastewater treatment. *Water Science and Technology*, 51(6-7), 1–8.
- Lin, J. C. T., Lee, D. J., & Huang, C. (2010). Membrane fouling mitigation: Membrane cleaning. *Separation Science and Technology*, 45(7), 858–872. doi:10.1080/01496391003666940
- Mallampati, R., Xuanjun, L., Adin, A., & Valiyaveetil, S. (2015). Fruit peels as efficient renewable adsorbents for removal of dissolved heavy metals and dyes from water. *ACS Sustainable Chemistry and Engineering*, 3(6), 1117–1124. doi:10.1021/acssuschemeng.5b00207
- Mannina, G., & Di Bella, G. (2012). Comparing two start-up strategies for MBRs: Experimental study and mathematical modelling. *Biochemical Engineering Journal*, 68, 91–103. doi:10.1016/j.bej.2012.07.011
- Maqbool, T., Khan, S. J., Waheed, H., Lee, C. H., Hashmi, I., & Iqbal, H. (2015). Membrane biofouling retardation and improved sludge characteristics using quorum quenching bacteria in submerged membrane bioreactor. *Journal of Membrane Science*, 483, 75–83. doi:10.1016/j.memsci.2015.02.011
- Marbella, L., Bilad, M. R., Bertels, N., Laine, C., & Vankelecom, I. F. J. (2016). Ribbed PVC-silica mixed matrix membranes for membrane bioreactors. *Journal of Membrane Science*, 498, 315–323. doi:10.1016/j.memsci.2015.10.017
- Mateen, F., Javed, I., Rafique, U., Tabassum, N., Sarfraz, M., Safi, S. Z., ... Ashraf, M. A. (2016). New method for the adsorption of organic pollutants using natural zeolite incinerator ash (ZIA) and its application as an environmentally friendly and cost-effective adsorbent. *Desalination and Water Treatment*, 57(14), 6230–6238. doi:10.1080/19443994.2015.1005146
- McClements, D. J. (2006). Non-covalent interactions between proteins and polysaccharides. *Biotechnology Advances*, 24(6), 621–625. doi:10.1016/j.biotechadv.2006.07.003
- McEwen, J. B. (Ed.). (1998). *Treatment process selection for particle removal*. Denver: American Water Works Association.
- Mehrnia, M. R., & Homayoonfal, M. (2016). Fouling mitigation behavior of magnetic responsive nanocomposite membranes in a magnetic membrane bioreactor. *Journal of Membrane Science*, 520, 881–894. doi:10.1016/j.memsci.2016.08.046
- Meng, F., Chae, S. R., Drews, A., Kraume, M., Shin, H. S., & Yang, F. (2009). Recent advances in membrane bioreactors (MBRs): Membrane fouling and membrane material. *Water Research*, 43(6), 1489–1512. doi:10.1016/j.watres.2008.12.044
- Meng, F., Zhang, S., Oh, Y., Zhou, Z., Shin, H. S., & Chae, S. R. (2017). Fouling in membrane bioreactors: An updated review. *Water Research*, 114, 151–180. doi:10.1016/j.watres.2017.02.006
- Merle, T., Dramas, L., Gutierrez, L., Garcia-Molina, V., & Croué, J.-P. (2016). Investigation of severe UF membrane fouling induced by three marine algal species. *Water Research*, 93, 10–19. doi:10.1016/j.watres.2016.02.001
- Miller, D. J., Kasemset, S., Paul, D. R., & Freeman, B. D. (2014). Comparison of membrane fouling at constant flux and constant transmembrane pressure conditions. *Journal of Membrane Science*, 454, 505–515. doi:10.1016/j.memsci.2013.12.027
- Miura, Y., & Okabe, S. (2008). Quantification of cell specific uptake activity of microbial products by uncultured chloroflexi by microautoradiography combined with fluorescence in situ hybridization quantification of cell specific uptake activity of microbial products by uncultured Ch. *Environmental Science & Technology*, 42(19), 7380–7386. doi:10.1021/es800566e
- Miyoshi, T., Tsuyuhara, T., Ogyu, R., Kimura, K., & Watanabe, Y. (2009). Seasonal variation in membrane fouling in membrane bioreactors (MBRs) treating municipal wastewater. *Water Research*, 43. doi:10.1016/j.watres.2009.08.035
- Molobela, I. P., Cloete, T. E., & Beukes, M. (2010). Protease and amylase enzymes for biofilm removal and degradation of extracellular polymeric substances (EPS) produced by *Pseudomonas fluorescens* bacteria. *African Journal of Microbiology Research*, 4(14), 1515–1524. Retrieved from <http://www.academicjournals.org/ajmr>
- Moustafa, M. A. E. (2011). Effect of the pre-treatment on the performance of MBR, Berghausen WWTP. Germany. *Alexandria Engineering Journal*, 50(2), 197–202. doi:10.1016/j.aej.2011.01.019
- Munz, G., Gori, R., Mori, G., & Lubello, C. (2007). Powdered activated carbon and membrane bioreactors (MBRPAC) for tannery wastewater treatment: Long term effect on biological and filtration process performances. *Desalination*, 207(1-3), 349–360. doi:10.1016/j.desal.2006.08.010
- Neemann, F., Rosenberger, S., Jefferson, B., & McAdam, E. J. (2013). Non-covalent protein-polysaccharide interactions and their influence on membrane fouling. *Journal of Membrane Science*, 446, 310–317. doi:10.1016/j.memsci.2013.06.054
- Ngo, H. H., & Guo, W. (2009). Membrane fouling control and enhanced phosphorus removal in an aerated submerged membrane bioreactor using modified green bioflocculant. *Bioresour Technol*, 100(18), 4289–4291. doi:10.1016/j.biortech.2009.03.057
- Nguyen, T. T., Guo, W., Ngo, H. H., & Vigneswaran, S. (2010). A new combined inorganic-organic flocculant (CIOF) as a performance enhancer for aerated submerged membrane bioreactor. *Separation and Purification Technology*, 75(2), 204–209. doi:10.1016/j.seppur.2010.07.010
- Nouri, N., Mehria, M. R., Sarrafzadeh, M. H., & Nabizadeh, R. (2013). Performance of membrane bioreactor in presence of flocculants. *Desalination and Water Treatment*, 52(16-18), 2933–2938. doi:10.1080/19443994.2013.833880

- Ødegaard, H., Fettig, J., & Ratnaweera, H. (1990). Coagulation with prepolymerized metal salts. *Chemical Water and Wastewater Treatment. Proceedings of the 4th Gothenburg Symposium 1990 October 1–3, 1990 Madrid, Spain*, 304, 189–220. Retrieved from http://link.springer.com/chapter/10.1007%252F978-3-642-76093-8_14
- Pal, S., Mal, D., & Singh, R. P. (2005). Cationic starch: An effective flocculating agent. *Carbohydrate Polymers*, 59(4), 417–423. doi:10.1016/j.carbpol.2004.06.047
- Pendashteh, A. R., Fakhru'l-Razi, A., Madaeni, S. S., Abdullah, L. C., Abidin, Z. Z., & Bialk, D. R. A. (2011). Membrane foulants characterization in a membrane bioreactor (MBR) treating hypersaline oily wastewater. *Chemical Engineering Journal*, 168(1), 140–150. doi:10.1016/j.cej.2010.12.053
- Poorasgari, E., Bugge, T. V., Christensen, M. L., & Jørgensen, M. K. (2015). Compressibility of fouling layers in membrane bioreactors. *Journal of Membrane Science*, 475, 65–70. doi:10.1016/j.memsci.2014.09.056
- Porcelli, N., & Judd, S. (2010). Chemical cleaning of potable water membranes: A review. *Separation and Purification Technology*, 71(2), 137–143. doi:10.1016/j.seppur.2009.12.007
- Psoch, C., & Schiewer, S. (2006). Anti-fouling application of air sparging and backflushing for MBR. *Journal of Membrane Science*. doi:10.1016/j.memsci.2006.06.042
- Qin, L., Zhang, G., Meng, Q., Zhang, H., Xu, L., & Lv, B. (2012). Enhanced submerged membrane bioreactor combined with biosurfactant rhamnolipids: Performance for frying oil degradation and membrane fouling reduction. *Bioresource Technology*, 126, 314–320. doi:10.1016/j.biortech.2012.08.103
- Rahimi, Z., Zinatizadeh, A. A. L., & Zinadini, S. (2015). Preparation of high antibiofouling amino functionalized MWCNTs/PES nanocomposite ultrafiltration membrane for application in membrane bioreactor. *Journal of Industrial and Engineering Chemistry*, 29, 366–374. doi:10.1016/j.jiec.2015.04.017
- Rene, E. R., & Lewis, A. (2017). *Sustainable heavy metal remediation* (Vol. 2). Switzerland: Springer.
- Research and Markets. (2014). *Membrane Bioreactor (MBR) Market Analysis by Product (Hollow Fiber, Flat Sheet, Multi-Tubular), by Configuration (Submerged, Side stream), by Application and Segment*, 120.
- Rosenberger, S., Evenblij, H., Te Poele, S., Wintgens, T., & Laabs, C. (2005). The importance of liquid phase analyses to understand fouling in membrane assisted activated sludge processes - Six case studies of different European research groups. *Journal of Membrane Science*, 263(1–2), 113–126. doi:10.1016/j.memsci.2005.04.010
- Ruohomäki, K., & Nyström, M. (2000). Fouling of ceramic capillary filters in vacuum filtration of humic acid. *Filtration and Separation*, 37(1), 51–57. doi:10.1016/S0015-1882(00)87633-8
- Saeki, D., Karkhanечи, H., Matsuura, H., & Matsuyama, H. (2016). Effect of operating conditions on biofouling in reverse osmosis membrane processes: Bacterial adhesion, biofilm formation, and permeate flux decrease. *Desalination*, 378, 74–79. doi:10.1016/j.desal.2015.09.020
- Sakkayawong, N., Thiravetyan, P., & Nakbanpote, W. (2005). Adsorption mechanism of synthetic reactive dye wastewater by chitosan. *Journal of Colloid and Interface Science*, 286(1), 36–42. doi:10.1016/j.jcis.2005.01.020
- Sarkar, B. (2013). A combined complete pore blocking and cake filtration model during ultrafiltration of polysaccharide in a batch cell. *Journal of Food Engineering*, 116(2), 333–343. doi:10.1016/j.jfoodeng.2012.12.013
- Satyawali, Y., & Balakrishnan, M. (2009). Effect of PAC addition on sludge properties in an MBR treating high strength wastewater. *Water Research*, 43(6), 1577–1588. doi:10.1016/j.watres.2009.01.003
- Seo, G. T., Suzuki, Y., & Ohgaki, S. (1996). Biological powdered activated carbon (BPAC) microfiltration for wastewater reclamation and reuse. *Desalination*, 106(1–3), 39–45. doi:10.1016/0011-9164(96)00090-2
- Shen, L. G., Lei, Q., Chen, J. R., Hong, H. C., He, Y. M., & Lin, H. J. (2015). Membrane fouling in a submerged membrane bioreactor: Impacts of floc size. *Chemical Engineering Journal*, 269, 328–334. doi:10.1016/j.cej.2015.02.002
- Shuyan, Q. (2015). Nanofiber as Flocculant or modifier in membrane bioreactors. *PhD Proposal*, 1. doi:10.1017/CBO9781107415324.004
- Sofia, A., Ng, W. J., & Ong, S. L. (2004). Engineering design approaches for minimum fouling in submerged MBR. *Desalination*, 160(1), 67–74. doi:10.1016/S0011-9164(04)90018-5
- Soler-Cabezas, J. L., Torà-Grau, M., Vincent-Vela, M. C., Mendoza-Roca, J. A., & Martínez-Francisco, F. J. (2015). Ultrafiltration of municipal wastewater: Study on fouling models and fouling mechanisms. *Desalination and Water Treatment*, 56(13), 3427–3437. doi:10.1080/19443994.2014.969320
- Song, K. G., Kim, Y., & Ahn, K. H. (2008). Effect of coagulant addition on membrane fouling and nutrient removal in a submerged membrane bioreactor. *Desalination*, 221(1–3), 467–474. doi:10.1016/j.desal.2007.01.107
- Song, W., Li, Z., Li, Y., You, H., Qi, P., Liu, F., & Loy, D. A. (2018). Facile sol-gel coating process for anti-biofouling modification of poly(vinylidene fluoride) microfiltration membrane based on novel zwitterionic organosilica. *Journal of Membrane Science*, 550 (December 2017), 266–277. doi:10.1016/j.memsci.2017.12.076
- Sun, Y., Fang, Y., Liang, P., & Huang, X. (2016). Effects of online chemical cleaning on removing biofouling and resilient microbes in a pilot membrane bioreactor. *International Biodeterioration and Biodegradation*, 112, 119–127. doi:10.1016/j.ibiod.2016.05.010
- Sweity, A., Ying, W., Ali-Shtayeh, M. S., Yang, F., Bick, A., Oron, G., & Herzberg, M. (2011). Relation between EPS adherence, viscoelastic properties, and MBR operation: Biofouling study with QCM-D. *Water Research*, 45(19), 6430–6440. doi:10.1016/j.watres.2011.09.038
- Tarnacki, K., Lyko, S., Wintgens, T., Melin, T., & Nataf, F. (2005). Impact of extra-cellular polymeric substances on the filterability of activated sludge in membrane bioreactors for landfill leachate treatment. *Desalination*, 179(1–3 SPEC. ISS.), 181–190. doi:10.1016/j.desal.2004.11.066
- Tiravanti, G., Lore, F., & Sonnante, G. (1985). Influence of the charge density of cationic polyelectrolytes on sludge conditioning. *Water Research*, 19(1), 93–97. doi:10.1016/0043-1354(85)90329-X
- Tu, X., Zhang, S., Xu, L., Zhang, M., & Zhu, J. (2010). Performance and fouling characteristics in a membrane sequence batch reactor (MSBR) system coupled with aerobic granular sludge. *Desalination*, 261(1–2), 191–196. doi:10.1016/j.desal.2010.03.034
- Tzoupanos, N. D., & Zouboulis, A. I. (2010). Novel inorganic-organic composite coagulants based on aluminium. *Desalination and Water Treatment*, 13(1–3), 340–347. doi:10.5004/dwt.2010.1042

- Van Breemen, A. N., Nieuwstad, T. J., & Van Der Meent-Olieman, G. C. (1979). The fate of fulvic acids during water treatment. *Water Research*, 13(8), 771–779. doi:10.1016/0043-1354(79)90241-0
- Vansacker, L., Boerjan, B., Declerck, P., & Vankelecom, I. F. J. (2014). Biofouling ecology as a means to better understand membrane biofouling. *Applied Microbiology and Biotechnology*, 98(19), 8047–8072. doi:10.1007/s00253-014-5921-2
- Viera, A. F., Sant'Anna, G. L., & Nobrega, R. (2007). The use of polyetherimide hollow fibres in a submerged membrane bioreactor operating with air backwashing. *Journal of Membrane Science*, 302(1–2), 127–135. doi:10.1016/j.memsci.2007.06.036
- Waheed, H., Xiao, Y., Hashmi, I., Stuckey, D., & Zhou, Y. (2017). Insights into quorum quenching mechanisms to control membrane biofouling under changing organic loading rates. *Chemosphere*, 182, 40–47. doi:10.1016/j.chemosphere.2017.04.151
- Wang, C., Yang, F., Meng, F., Zhang, H., Xue, Y., & Fu, G. (2010). High flux and antifouling filtration membrane based on non-woven fabric with chitosan coating for membrane bioreactors. *Bioresour Technol*, 101(14), 5469–5474. doi:10.1016/j.biortech.2010.01.126
- Wang, F., & Tarabara, V. V. (2008). Pore blocking mechanisms during early stages of membrane fouling by colloids. *Journal of Colloid and Interface Science*, 328(2), 464–469. doi:10.1016/j.jcis.2008.09.028
- Wang, J., Wu, B., Yang, S., Liu, Y., Fane, A. G., & Chew, J. W. (2016). Characterizing the scouring efficiency of granular activated carbon (gac) particles in membrane fouling mitigation via wavelet decomposition of accelerometer signals. *Journal of Membrane Science*, 498, 105–115. doi:10.1016/j.memsci.2015.09.061
- Wang, X.-M., & Waite, T. D. (2009). Role of gelling soluble and colloidal microbial products in membrane fouling. *Environmental Science & Technology*, 43(24), 9341–9347. doi:10.1021/es9013129
- Wang, Y. K., Li, W. W., Sheng, G. P., Shi, B. J., & Yu, H. Q. (2013). In-situ utilization of generated electricity in an electrochemical membrane bioreactor to mitigate membrane fouling. *Water Research*, 47(15), 5794–5800. doi:10.1016/j.watres.2013.06.058
- Wang, Z., Cao, J., & Meng, F. (2015). Interactions between protein-like and humic-like components in dissolved organic matter revealed by fluorescence quenching. *Water Research*, 68, 404–413. doi:10.1016/j.watres.2014.10.024
- Wang, Z., Ma, J., Tang, C. Y., Kimura, K., Wang, Q., & Han, X. (2014). Membrane cleaning in membrane bioreactors: A review. *Journal of Membrane Science*, 468, 276–307. doi:10.1016/j.memsci.2014.05.060
- Wang, Z., & Wu, Z. (2009). A review of membrane fouling in MBRs: Characteristics and role of sludge cake formed on membrane surfaces. *Separation Science and Technology*, 44(15), 3571–3596. doi:10.1080/01496390903182578
- Weerasekara, N. A., Choo, K. H., & Lee, C. H. (2014). Hybridization of physical cleaning and quorum quenching to minimize membrane biofouling and energy consumption in a membrane bioreactor. *Water Research*, 67, 1–10. doi:10.1016/j.watres.2014.08.049
- Won, Y. J., Lee, J., Choi, D. C., Chae, H. R., Kim, I., Lee, C. H., & Kim, I. C. (2012). Preparation and application of patterned membranes for wastewater treatment. *Environmental Science and Technology*, 46(20), 11021–11027. doi:10.1021/es3020309
- Wu, B., Zamani, F., Lim, W., Liao, D., Wang, Y., Liu, Y., Chew, J. W., & Fane, A. G. (2017). Effect of Mechanical Scouring by Granular Activated Carbon (Gac) on Membrane Fouling Mitigation. *Desalination*, 403, 80–87. doi:10.1016/j.desal.2015.12.003
- Wu, J., Chen, F., Huang, X., Geng, W., & Wen, X. (2006). Using inorganic coagulants to control membrane fouling in a submerged membrane bioreactor. *Desalination*, 197(1–3), 124–136. doi:10.1016/j.desal.2005.11.026
- Wu, J., & Huang, X. (2008). Effect of dosing polymeric ferric sulfate on fouling characteristics, mixed liquor properties and performance in a long-term running membrane bioreactor. *Separation and Purification Technology*, 63(1), 45–52. doi:10.1016/j.seppur.2008.03.033
- Wu, J., & Huang, X. (2010). Use of ozonation to mitigate fouling in a long-term membrane bioreactor. *Bioresour Technol*, 101(15), 6019–6027. doi:10.1016/j.biortech.2010.02.081
- Wu, S. C., & Lee, C. M. (2011). Correlation between fouling propensity of soluble extracellular polymeric substances and sludge metabolic activity altered by different starvation conditions. *Bioresour Technol*, 102(9), 5375–5380. doi:10.1016/j.biortech.2010.11.093
- Xia, L., Law, A. W. K., & Fane, A. G. (2013). Hydrodynamic effects of air sparging on hollow fiber membranes in a bubble column reactor. *Water Research*, 47(11), 3762–3772. doi:10.1016/j.watres.2013.04.042
- Xiao, Y., Waheed, H., Xiao, K., Hashmi, I., & Zhou, Y. (2018). In tandem effects of activated carbon and quorum quenching on fouling control and simultaneous removal of pharmaceutical compounds in membrane bioreactors. *Chemical Engineering Journal*. doi:10.1016/j.cej.2018.02.073
- Xin, Y., Bligh, M. W., Kinsela, A. S., Wang, Y., & David Waite, T. (2015). Calcium-mediated polysaccharide gel formation and breakage: Impact on membrane fouling hydraulic properties. *Journal of Membrane Science*, 475, 395–405. doi:10.1016/j.memsci.2014.10.033
- Xu, M., Wen, X., Huang, X., Yu, Z., & Zhu, M. (2013). Mechanisms of membrane fouling controlled by online ultrasound in an anaerobic membrane bioreactor for digestion of waste activated sludge. *Journal of Membrane Science*, 445, 119–126. doi:10.1016/j.memsci.2013.06.006
- Xu, W., & Chellam, S. (2005). Initial stages of bacterial fouling during dead-end microfiltration. *Environmental Science and Technology*, 39(17), 6470–6476. doi:10.1021/es0500862
- Yavuztürk Gül, B., & Koynucu, I. (2017). Assessment of new environmental quorum quenching bacteria as a solution for membrane biofouling. *Process Biochemistry*, 61(December 2016), 137–146. doi:10.1016/j.procbio.2017.05.030
- Yeom, I. T., Lee, K. R., Choi, Y. G., Kim, H. S., Kwon, J. H., Lee, U. J., & Lee, Y. H. (2005). A pilot study on accelerated sludge degradation by a high-concentration membrane bioreactor coupled with sludge pretreatment. *Water Science and Technology*, 52(10–11), 201–210.
- Yigit, N., Civelekoglu, G., Harman, I., Köseoğlu, H., & Kitis, M. (2011). Effects of various backwash scenarios on membrane fouling in a membrane bioreactor. *Environmental Earth Sciences*, 237(1–3), 917–929. doi:10.1007/978-3-540-95991-5-87
- Yin, Z., Tarabara, V. V., & Xagorarakis, I. (2016). Effect of pressure relaxation and membrane backwash on adenovirus removal in a membrane bioreactor.

- Water Research*, 88, 750–757. doi:10.1016/j.watres.2015.10.066
- Ying, Z., & Ping, G. (2006). Effect of powdered activated carbon dosage on retarding membrane fouling in MBR. *Separation and Purification Technology*, 52(1), 154–160. doi:10.1016/j.seppur.2006.04.010
- Yonekawa, H., Tomita, Y., & Watanabe, Y. (2004). Behavior of micro-particles in monolith ceramic membrane filtration with pre-coagulation. *Water Science and Technology*, 50(12), 317–325.
- Yoon, S.-H.-H., & Collins, J. H. (2006). A novel flux enhancing method for membrane bioreactor (MBR) process using polymer. *Desalination*, 191(1–3), 52–61. doi:10.1016/j.desal.2005.04.124
- Yu, H. Y., Hu, M. X., Xu, Z. K., Wang, J. L., & Wang, S. Y. (2005). Surface modification of polypropylene microporous membrane to improve its antifouling property in MBR: CO₂ plasma treatment. *Separation and Purification Technology*, 45(1), 8–15. doi:10.1016/j.seppur.2005.01.012
- Yu, H. Y., Xu, Z. K., Lei, H., Hu, M. X., & Yang, Q. (2007). Photoinduced graft polymerization of acrylamide on polypropylene microporous membranes for the improvement of antifouling characteristics in a submerged membrane-bioreactor. *Separation and Purification Technology*, 53(1), 119–125. doi:10.1016/j.seppur.2006.07.002
- Yuan, W., Kocic, A., & Zydney, A. L. (2002). Analysis of humic acid fouling during microfiltration using a pore blockage-cake filtration model. *Journal of Membrane Science*, 198(1), 51–62. doi:10.1016/S0376-7388(01)00622-6
- Yusuf, Z., Wahab, N. A., & Abusam, A. (2017). Neural network-based model predictive control with CPSOGSA for SMBR filtration. *International Journal of Electrical and Computer Engineering (IJECE)*, 7(3), 1538. doi:10.11591/ijece.v7i3.pp1538-1545
- Zahrim, A. Y., & Dexter, Z. D. (2016). Decolourisation of palm oil mill biogas plant wastewater using Poly-Diallyldimethyl Ammonium Chloride (polyDADMAC) and other chemical coagulants. *IOP Conference Series: Earth and Environmental Science*, 36, 1. doi:10.1088/1755-1315/36/1/012025
- Zarei, A., Moslemi, M., & Mirzaei, H. (2016). The combination of KMnO₄ oxidation and polymeric flocculation for the mitigation of membrane fouling in a membrane bioreactor. *Separation and Purification Technology*, 159, 124–134. doi:10.1016/j.seppur.2016.01.003
- Zarragoitia-González, A., Schetrite, S., Alliet, M., Jáuregui-Haza, U., & Albasi, C. (2008). Modelling of submerged membrane bioreactor: Conceptual study about link between activated sludge biokinetics, aeration and fouling process. *Journal of Membrane Science*, 325(2), 612–624. doi:10.1016/j.memsci.2008.08.037
- Zhang, H., Gao, Z., Zhang, L., & Song, L. (2014). Performance enhancement and fouling mitigation by organic flocculant addition in membrane bioreactor at high salt shock. *Bioresource Technology*, 164, 34–40. doi:10.1016/j.biortech.2014.04.053
- Zhang, H., Sun, B., Zhao, X., & Gao, Z. (2008). Effect of ferric chloride on fouling in membrane bioreactor. *Separation and Purification Technology*, 63(2), 341–347. doi:10.1016/j.seppur.2008.05.024
- Zhang, H., Yu, H., Zhang, L., & Song, L. (2015). Bioreactor technology stratification structure of polysaccharides and proteins in activated sludge with different aeration in membrane bioreactor. *Bioresource Technology*, 192, 361–366. doi:10.1016/j.biortech.2015.05.025
- Zhang, J., Chua, H. C., Zhou, J., & Fane, A. G. (2006). Factors affecting the membrane performance in submerged membrane bioreactors. *Journal of Membrane Science*, 284(1–2), 54–66. doi:10.1016/j.memsci.2006.06.022
- Zhang, J., Satti, A., Chen, X., Xiao, K., Sun, J., Yan, X., ... Huang, X. (2015). Low-voltage electric field applied into MBR for fouling suppression: Performance and mechanisms. *Chemical Engineering Journal*, 273, 223–230. doi:10.1016/j.cej.2015.03.044
- Zhang, Z., Wang, Y., Leslie, G. L., & Waite, T. D. (2015). Effect of ferric and ferrous iron addition on phosphorus removal and fouling in submerged membrane bioreactors. *Water Research*, 69, 210–222. doi:10.1016/j.watres.2014.11.011
- Zhao, C., Xu, X., Chen, J., Wang, G., & Yang, F. (2014). Highly effective antifouling performance of PVDF/graphene oxide composite membrane in membrane bioreactor (MBR) system. *Desalination*, 340(1), 59–66. doi:10.1016/j.desal.2014.02.022
- Zhao, D., & Yu, S. (2015). A review of recent advance in fouling mitigation of NF/RO membranes in water treatment: Pretreatment, membrane modification, and chemical cleaning. *Desalination and Water Treatment*, 55(4), 870–891. doi:10.1080/19443994.2014.928804
- Zhao, R. J., Wang, W. S., Zhu, F. F., Liu, T., Li, Y. H., & Bian, Y. L. (2015). Surface modification of PVDF membrane by simultaneously using low temperature plasma and ammonium carbonate solution. *Desalination and Water Treatment*, 56(9), 2276–2283. doi:10.1080/19443994.2014.961172
- Zheng, Y., Zhang, W., Tang, B., Ding, J., Zheng, Y., & Zhang, Z. (2018). Membrane fouling mechanism of biofilm-membrane bioreactor (BF-MBR): Pore blocking model and membrane cleaning. *Bioresource Technology*, 250(August 2017), 398–405. doi:10.1016/j.biortech.2017.11.036
- Zhou, S., Xue, A., Zhao, Y., Li, M., Wang, H., & Xing, W. (2013). Grafting polyacrylic acid brushes onto zirconia membranes: Fouling reduction and easy-cleaning properties. *Separation and Purification Technology*, 114, 53–63. doi:10.1016/j.seppur.2013.04.023
- Zhou, Z., Meng, F., He, X., Chae, S.-R., An, Y., & Jia, X. (2015). Metaproteomic analysis of biocake proteins to understand membrane fouling in a submerged membrane bioreactor. *Environmental Science & Technology*, 49(2), 1068–1077. doi:10.1021/es504489r
- Zuthi, M. F. R., Guo, W., Ngo, H. H., Nghiem, D. L., Hai, F. I., Xia, S., ... Liu, Y. (2017). New and practical mathematical model of membrane fouling in an aerobic submerged membrane bioreactor. *Bioresource Technology*, 238, 86–94. doi:10.1016/j.biortech.2017.04.006



© 2018 The Author(s). This open access article is distributed under a Creative Commons Attribution (CC-BY) 4.0 license.



You are free to:

Share — copy and redistribute the material in any medium or format.

Adapt — remix, transform, and build upon the material for any purpose, even commercially.

The licensor cannot revoke these freedoms as long as you follow the license terms.

Under the following terms:

Attribution — You must give appropriate credit, provide a link to the license, and indicate if changes were made.

You may do so in any reasonable manner, but not in any way that suggests the licensor endorses you or your use.

No additional restrictions

You may not apply legal terms or technological measures that legally restrict others from doing anything the license permits.

Cogent Engineering (ISSN: 2331-1916) is published by Cogent OA, part of Taylor & Francis Group.

Publishing with Cogent OA ensures:

- Immediate, universal access to your article on publication
- High visibility and discoverability via the Cogent OA website as well as Taylor & Francis Online
- Download and citation statistics for your article
- Rapid online publication
- Input from, and dialog with, expert editors and editorial boards
- Retention of full copyright of your article
- Guaranteed legacy preservation of your article
- Discounts and waivers for authors in developing regions

Submit your manuscript to a Cogent OA journal at www.CogentOA.com



Paper II

Kulesha, O.; Maletskyi, Z.; Ratnaweera, H. Multivariate Chemometric Analysis of Membrane Fouling Patterns in Biofilm Ceramic Membrane Bioreactor. *Water* **2018**, *10*, 982, 1–23; DOI:10.3390/w10080982.

Article

Multivariate Chemometric Analysis of Membrane Fouling Patterns in Biofilm Ceramic Membrane Bioreactor

Olga Kulesha ^{1,2,*}, Zakhar Maletskyi ¹  and Harsha Ratnaweera ¹

¹ Faculty of Science and Technology (REALTEK), Norwegian University of Life Sciences, P.O. Box 5003, 1432 Aas, Norway; zakhar.maletskyi@nmbu.no (Z.M.); harsha.ratnaweera@nmbu.no (H.R.)

² Department of General and Inorganic Chemistry, Faculty of Chemical Technology, National Technical University of Ukraine “Igor Sikorsky Kyiv Polytechnic Institute”, Peremohy 37, 03056 Kyiv, Ukraine

* Correspondence: olga.kulesha@nmbu.no; Tel.: +47-406-755-92

Received: 27 June 2018; Accepted: 22 July 2018; Published: 26 July 2018



Abstract: Membrane fouling highly limits the development of Membrane bioreactor technology (MBR), which is among the key solutions to water scarcity. The current study deals with the determination of the fouling propensity of filtered biomass in a pilot-scale biofilm membrane bioreactor to enable the prediction of fouling intensity. The system was designed to treat domestic wastewater with the application of ceramic microfiltration membranes. Partial least squares regression analysis of the data obtained during the long-term operation of the biofilm-MBR (BF-MBR) system demonstrated that Mixed liquor suspended solids (MLSS), diluted sludge volume index (DSVI), chemical oxygen demand (COD), and their slopes are the most significant for the estimation and prediction of fouling intensity, while normalized permeability and its slope were found to be the most reliable fouling indicators. Three models were derived depending on the applied operating conditions, which enabled an accurate prediction of the fouling intensities in the system. The results will help to prevent severe membrane fouling via the change of operating conditions to prolong the effective lifetime of the membrane modules and to save energy and resources for the maintenance of the system.

Keywords: water crisis; biofilm membrane bioreactor; membrane fouling; operation; ceramic membranes; multivariate statistics

1. Introduction

The World Economic Forum (WEF) includes water crises in the group of risks with the highest likelihood and impact, which are strongly interconnected with the trends in climate change that can degrade the environment and cause food crises [1]. According to the WEF, the main reason for a water crisis is a significant decline in the available quality and quantity of fresh water, thus resulting in harmful effects to human health and economic activity. Competition for water between agriculture, industry and municipal supply is being complicated by political tension around water in stressed regions, thus leading to the future shock of so-called “grim reaping” [2].

Water reuse is gaining momentum as a reliable alternative source of freshwater in the face of growing water demand, which is shifting the paradigm of wastewater management from “disposal” to “reuse and resource recovery” [3]. Growing globally [4], water reuse plays a key role in bringing significant environmental, social and economic benefits [5]. Advanced tertiary treatment is a rule of thumb in water reuse and is an important factor of system resilience in the case of wastewater reuse as a part of a decentralized water supply [6]. However, of all the wastewater produced worldwide, only a very small fraction actually undergoes tertiary treatment [3]. Efficient, reliable, sustainable and

economically feasible technologies are highly demanded when it comes to potential cost recovery by treating wastewater to a water quality standard acceptable to users.

Membrane bioreactor technology (MBR) is a highly competitive technology when applied in water reuse schemes. It provides excellent nutrient removal efficiency, compactness, complete biomass retention with no use of a secondary clarifier, and produces a low carbon footprint [7–9]. Additionally, strengthening requirements for reclaimed water quality is expected to drive the MBR market to USD 8.27 billion by 2025 [10].

However, membrane fouling is the main restraint to further penetration of MBR into cost-sensitive markets, including the water reuse market in small communities and developing countries, which is primarily due to the occurrence of unplanned high operating costs [11–14]. Several approaches to detect, control and prevent membrane fouling in MBR have been developed during the last decades, focusing on pre-treatment or modification of mixed liquor, membrane properties, operating conditions, etc. [15–19]. Considering the pros and cons of the aforementioned, there is no unified approach to dealing with membrane fouling.

Several types of research demonstrated that a combination of two or more fouling prevention factors gives the best practical results through the synergy of anti-fouling mechanisms [20–22]. Therefore, the current research considers the use of a combination of biofilm-MBR (BF-MBR) process configuration with the application of ceramic flat-sheet membranes.

BF-MBR combines membrane separation, biological contact oxidation and fluidized bed wastewater treatment (as in the moving-bed-biofilm reactor (MBBR) process). This results in better effluent quality due to reliable degradation of organics and nutrients, a lower sludge production rate and a smaller footprint, together with stable and reliable operation, strong resistance to shock loading, and adaptability due to high biomass concentration and diversity in bacterial population [23]. The BF-MBR process has demonstrated lower membrane fouling rates and better settling ability of suspended biomass than in conventional MBR and MBBR processes separately [12,24].

In another study [25], porous suspended biofilm carriers were introduced to a submerged ceramic membrane bioreactor to explore their effectiveness in membrane flux enhancement. Alleviation of membrane fouling, in this case, is anticipated via mechanical scouring of the cake layer on the membrane surface and modification of mixed liquor characteristics. It has been shown that a combination of biofilm carriers with the ceramic membrane in MBR leads to 2.7 times lower cake resistance and 1.5 times lower total resistance.

Mixed liquor suspended solids (MLSS), chemical oxygen demand (COD) and sludge relative hydrophobicity (RH) are among the main characteristic parameters of activated sludge suspension that are traditionally monitored in an MBR system [22,26–31].

MLSS provides information about mixed liquor fouling propensity, apart from indicating a biomass potential to decompose wastewater impurities, determining an aeration tank volume, and affecting the aeration demand and sludge production [28,32]. Several researchers acknowledged there was a complex relationship between MLSS and membrane fouling [9,29,33].

The COD parameter accounts for the organic load and the biological treatment efficiency in terms of the degradation of organic contaminants [34]. In addition, as specified by Le-Clech et al. [29], Ji and Zhou [35], Meng et al. [36], in MBR systems, soluble COD is an indicator of the soluble microbial product (SMP) level. SMP is generally considered to be one of the major foulants in MBR [37–39].

Biomass RH is one of the key parameters used to estimate the resistance caused by microbial aggregates. RH determines flocculation ability of the sludge flocs based on their hydrophobic interactions with each other, which in turn controls their dewaterability [32,40,41]. RH of the activated sludge influences initial biomass attachment to the membrane and, therefore, membrane permeability (i.e., determines whether a membrane can be more or less sensitive to different foulants).

The sludge volume index (SVI)/diluted sludge volume index (DSVI) is another characteristic that is monitored in MBR systems. Although this parameter primarily characterizes the activated sludge settling properties, it is also widely applied in MBRs, since it indicates the flocculation characteristics of

the activated sludge and is associated with filamentous bacteria. The latter induces membrane fouling through the release of SMPs from the sludge flocs, thus increasing their concentration via viscosity increase and by fixing the foulants on the membrane surface, thus forming practically a non-porous cake layer [9,33,42–44].

In general, a number of studies indicated that the above-mentioned biomass characteristics exhibit specific tendencies in influencing fouling in MBR (Table 1).

Table 1. The influence of activated sludge parameters on the biomass fouling propensity.

Parameter	Correlation with the Fouling	Possible Fouling Mechanism	References
MLSS ¹	Positive	Intense cake layer formation on the membrane surface. Increase in the suspension viscosity. Excessive growth of filamentous bacteria. Increase in microbial metabolic products such as SMP ² and EPS ³ , which are the major foulants.	[34,45–51]
MLSS ¹	Negative (irreversible fouling)	MLSS ¹ 12–18 g/L: The formed cake layer causes the prevention of the pore blocking development and induces an increased porosity of the cake layer.	[15,45]
COD ⁴	Positive	COD ⁴ in the form of colloids proteins (adsorption mechanism) and other soluble organic fractions, causing irreversible fouling; higher organic load causes an increase in the production of specific EPS ³ and macromolecules in the SMP ² /EPS ³ fractions, deflocculation of the mixed liquor, and a fast formation of cake layers.	[9,29,35,52–56]
RH ⁶ (mostly hydrophilic membranes)	Negative	RH ⁶ increase: Enhanced AS ⁵ flocculation due to more intense hydrophobic interactions between sludge flocs, resulting in the formation of larger aggregates with less water content, and decreased interaction between the flocs and membrane surface. RH ⁶ decrease: Floc deterioration.	[57–62]
	Positive	RH ⁶ increase: A formation of a thin cake layer, promoting the adhesion of proteins and carbohydrates in the form of SMP ² on the membrane surface and its pores, resulting in irreversible and irrecoverable fouling.	[26,63]
SVI (DSVI) ⁷	Positive	High DSVI ⁷ : Evolution of the flocs to the more irregular rougher shapes which more likely adhere to the surface of the membrane, intertwisting with the fibers. This forms a dense, non-porous cake with large thickness. The possible decrease of the bound protein and release of SMP ² triggers deflocculation and the increase in fouling intensity.	[64–69]

Notes: ¹ Mixed liquor suspended solids; ² Soluble microbial products; ³ Extracellular polymeric substances; ⁴ Chemical oxygen demand; ⁵ Activated sludge; ⁶ Relative hydrophobicity; ⁷ Sludge volume index (diluted sludge volume index).

It is worth noting that application of ceramic membranes in MBR started from a niche where polymer membranes either failed or provided insufficient results: The cases when high effluent quality is required or the process depends on ceramic membrane robustness [70]. Compared to their polymeric counterparts, ceramic membranes have the following advantages:

1. Higher mechanical strength and chemical resistance to oxidants and solvents. The modules are backwashable with the possible application of high backwash pressure/flux [71,72] and can withstand much more aggressive operation and chemical cleaning conditions (i.e., can be used in combination with ultrasonic irradiation and undergo a soaking in more concentrated NaClO, NaOH, and acidic solutions). In addition, they can undergo the influence of higher temperatures and pH without damaging the active layer [73–77].
2. Higher hydrophilicity, thus no affinity to organic foulants which are mostly of a hydrophobic nature [70,78,79].

The outcomes are: High permeability recovery [80]; a longer period of operation between the chemical cleanings due to more efficient removal of reversible and irreversible fouling [29,79]; enhanced concentration polarization control; and, higher applicable net permeate fluxes and permeabilities are sustained [81–83], consequently leading to a long lifespan.

Ceramic membranes proved to be an effective and reliable MBR component, leading to higher treatment efficiencies of COD, ammonium, and phosphorus elimination [84,85]. In addition, higher

treatment performance in terms of COD and MLSS removal, more stable operation and less transmembrane pressure (TMP) increase was exhibited by the MBR with ceramic modules, compared to the system with the polymeric units [86]. Lower TMP increase, higher removal of non-purgeable organic compounds and lower UV absorbance of the permeate was demonstrated by Hofs et al. [87] in relation to the surface water samples being treated by ceramic modules.

From an economic point of view, the tremendously higher cost of the application of the MBR systems with the ceramic membranes in comparison to the use of the systems with the polymeric modules is rather a stereotype than a reality at present. According to a study by Park et al. [83], the incorporation of membrane modules into the water treatment plant (WTP) makes up 13% and 24% of the total capital cost for polymeric and ceramic WTP, respectively. The comparative analysis demonstrated that the polymeric WTP (with capacity 30,000 m³/day) are indeed cheaper in terms of the capital costs than their ceramic counterparts, but the difference is not significant: USD 28,019 vs. USD 32,634, respectively. Moreover, the annual operating expenses of the filtration process are more than twice as high for the polymeric modules (USD 562,717) as for the ceramic modules (USD 217,725). This is mainly due to the membrane replacement costs for polymeric WTP, which constitute 61% of the operational expenses. Low operation costs of the systems with ceramic membranes were also acknowledged by Jin et al. [74]. As specified by Park et al. [83], the assessed life cycle costs (LCC) of water from the ceramic and polymeric membrane WTPs are, USD 0.28/m³ and USD 0.274/m³, respectively (at the flux of 41.7 LMH). If fluxes of 63 LMH and higher are applied, the LCC of the produced water decreases for the ceramic membranes, thus increasing their feasibility.

In addition, since the manufacturing of the ceramic membranes is an energy-consuming process, a number of recent studies have successfully developed and evaluated the performance of low-cost ceramic membranes [88–93].

Despite many studies on membrane fouling in general, and on BF-MBR or the application of ceramic membranes in particular, only a few findings that are relevant to detection and control of membrane fouling in submerged ceramic BF-MBR come from a pilot or full-scale product. Nevertheless, understanding, detection, and control of membrane fouling via applying advanced statistics and mathematical modelling represents a significant potential for improvement of the cost-efficiency of the process and provides the instruments for dynamic and real-time process control.

Chemometrics serves as a bridge between the state of a chemical system and its measured characteristics, which enhances the efficiency of automatic control systems. Chemometric analysis is based on the application of mathematical and statistical techniques to improve comprehension of the system properties and to link them to analytical measurements. The modelling of the patterns in the dataset results in model derivation. This model can be further used to predict identical parameters as in the initial model but in application to new data [94]. The following multivariate statistical data analysis methods are commonly used as chemometric tools for the interpretation of the acquired data: Cluster analysis (CA), discriminant analysis (DA), principal component analysis (PCA), partial least squares analysis (PLS), multiple linear regression (MLR), principal component regression (PCR), and partial least squares discriminant analysis (PLS-DA) [94–96].

It is worth mentioning that PLS is an advanced statistical technique due to the applied validation tools, noise elimination, and the ability to determine the independent influence of each input variable, even if there is a collinearity between them [59].

A number of recent studies were devoted to the application of modelling using multivariate data analysis for fouling control in MBR. In the study by Philippe et al. [97], the authors performed a PCA to distinguish a correlation between the operational parameters and the characteristics of filtered biomass in a full-scale municipal MBR. Among all the variables, solids retention time (SRT), MLSS, the food to microorganism ratio (F:M), pH and temperature (T) were found to be representative for describing the fouling behaviour. According to the plot of weighted variables, SRT, MLSS and pH positively contributed to the principal components (PCs) one and two, while the F:M ratio exhibited a negative influence. Temperature has a controversial contribution to the PCs in the model. However, the attained

models managed to predict the development of permeability merely in one membrane tank and failed while applying them at different operation stages for all four membrane tanks in the system.

In the work by Kaneko and Funatsu [98], wastewater temperature, the duration of filtration, water temperature, and the inverse of flux and TMP were inputted into the model. PCA was applied as a visualization tool for the discriminant model. As concluded, the accuracy and the predictive ability of the derived model can be increased if the additional parameters related to the water quality and operating conditions are used.

A similar choice of variables was made in the study by De Temmerman et al. [99], where PCA was based on temperature, flux, TMP slope, and pressure peaks during the filtration and chemically enhanced backwash (CEB) for the full-scale MBR. The detection of the fouling types (reversible/irreversible and irrecoverable) was among the prime research goals. The TMP slope and pressure peak during the filtration were found to have a positive relationship. Meanwhile, they were negatively linked to the temperature and the CEB pressure peak along the PC-1 axis. Along the PC-3 axis, flux exhibited a negative correlation with water temperature and the backwash pressure peak. The variance of the CEB pressure peak was attributed to irrecoverable fouling, while pressure peaks during the filtration were attributed to reversible and irreversible fouling types. However, the scores plot indicated no clear trends.

Partial least squares regression analysis applying leave-one-out cross-validation was performed in the work by Van den Broeck [59] to find the influence of the activated sludge parameters on filterability in industrial and municipal MBRs. A relatively deep analysis of the biomass characteristics was conducted. The content of proteins and polysaccharides, sludge relative hydrophobicity, sludge dissociation constant, mean particle size, and the surface fraction of activated sludge particles equal to 1 pixel were used to predict any change of filtration resistance. An accurate estimation of the filtration resistance was observed, which was characterized by the sum of square errors equal to 0.076 (R -squared = 0.99). However, a number of factors (latent variables) exceeded 9, indicating a complexity of the derived model. As concluded, a combination of chosen activated sludge parameters succeeded in predicting sludge filterability, while, when taken individually, they were poor indicators of the biomass fouling propensity.

Consequently, the following knowledge gaps can be identified: The studies which are focused on the modelling of the relationship between operating parameters and filterability do not typically take into consideration biomass characteristics as potential fouling indicators, despite the fact that these are among the main factors affecting the fouling process [9,100,101]. Meanwhile, those studying the statistical evaluation of the relationship between mixed liquor parameters and biomass fouling propensity do not provide the information on the influence of the operating parameters on the fouling intensity. Most importantly, there is also still a need to study the application of the PLS regression to the processes in the biofilm membrane bioreactor due to the lack of research data. In addition, there is a controversy over the influence of the selected biomass parameters on the fouling intensity (Table 1), whereas the development of a reliable BF-MBR system requires concrete patterns.

Applying PLS analysis, the current work encapsulates the relationship between the mixed liquor characteristics, fouling indicators and the operation conditions in BF-MBR with ceramic modules, and thus provides a comprehensive analysis of the system performance and the mechanisms for influencing it.

The purpose of this research was to develop and validate a PLS regression model based on the mixed liquor characteristics and the indicators of fouling intensity, considering the influence of the operation parameters on the filtration performance in the BF-MBR with ceramic membranes, in order to detect membrane fouling patterns and to develop process control and a fouling mitigation approach.

2. Materials and Methods

In general, this study consists of the acquisition of operational data from a BF-MBR pilot plant at various sets of operating conditions followed by statistical analysis.

The BF-MBR pilot plant had a four-stage design (Figure 1) comprising equalization (I) and treated water (IV) compartments, and a MBBR chamber (II) and a separation chamber (III) with the submerged membranes being in contact with suspended biofilm carriers. Compartments I, II and III were interconnected through overflow, while the separation process from chamber III to chamber IV was driven by a reversible peristaltic pump (Verderflex, Castleford, UK), controlled from the programmable logic controller (PLC) (MoreControl, Aas, Norway). A return activated sludge (RAS) line was incorporated into the system between chambers III and II, and was controlled by RAS pumping intervals: With lower RAS intervals, more sludge is returned.

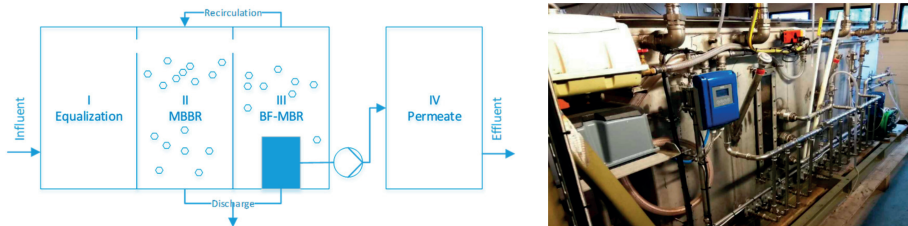


Figure 1. The BF-MBR pilot plant: Schematic diagram (left) and the photo of installation (right).

Wastewater was supplied at $0.3 \text{ m}^3/\text{day}$ through the screens to the equalization tank (I) from the source-separated sewer network, keeping the ratio of black to grey water at 1:9. Black water was collected from the toilets and grey water from all other discharge points of the households around the pilot site [102]. This allowed maintenance of the influent quality at $1\text{--}1.3 \text{ g/L}$ by suspended solids and $100\text{--}350 \text{ mg-O}_2/\text{L}$ by COD.

Flat sheet SiC microfiltration membranes with $0.1 \text{ }\mu\text{m}$ pore size (Cembrane, Lyngø, Denmark) were used in the separation chamber (III), providing total filtering area of 0.828 m^2 . Aeration was organized in chambers II and III by a MEDO LA-60E air compressor at 60 L/min .

Initial biological activity in the system was provided by inoculation with sludge from the municipal MBBR wastewater treatment plant (BEVAS, Oslo, Norway).

The BF-MBR pilot plant was operated in automatic mode under constant flux conditions, controlled through the PLC. The initial filtration settings were: 300 s of filtration at net-flux 8.2 LMH , 60 s relaxation, 15 s backwash with permeate at net-flux 180 LMH , 120 s relaxation. Further changes were introduced into the plant operation settings in order to reach different operation states (Table 2), which divided full operation time of 114 days into 8 relevant periods.

Plant operation data was continuously recorded every 3 s to the data-logger, in-built in the PLC. Values of system inflow, level in the separation chamber, TMP and permeate flow were stored and recalculated further to analytical values.

Filtration settings were programmed as $t_{\text{filtr}/\text{relax}/\text{BW}}$, filtration/relaxation/backwash time, and $\text{RAS}_{\text{pulse interval}} = \text{RAS}_{\text{PI}}$, the pulse interval of the return activated sludge. For every period of operation, normalized net membrane flux was calculated ($J_{\text{n(net)}}$). The normalized permeability, P_{n} , and permeability slope, dP_{n}/dt , were determined.

Permeate flow was used to calculate membrane flux J (LMH; Equation (1)), normalized to $20 \text{ }^\circ\text{C}$ as J_{n} (Equation (2)), and used to calculate normalized permeability, P_{n} (Equation (3)), and the fouling rate in terms of membrane permeability decrease, dP_{n}/dt (Equation (4)):

$$J = \frac{F}{S_f} \quad (1)$$

$$J_n = J \cdot e^{(-0.032 \cdot (t-20))} \quad (2)$$

$$P_n = \frac{J_n}{TMP} \quad (3)$$

$$\frac{dP_n}{dt} = \frac{P_{ni} - P_{ni-1}}{t_i - t_{i-1}} \quad (4)$$

where F is permeate flow, L/h, and S_f is the active filtration surface (m²).

Table 2. BF-MBR pilot plant operation settings.

Period	Days	Adjustments in Settings	Processes and Changes in the System
I	1–20	J _{n(net)} ¹ = 8.2 LMH, J _{n(gross)} ² = 37.6 LMH Filtration cycle settings: t _{filtr} = 300 s, t _{relaxI} = 60 s, t _{relaxII} = 120 s, t _{BW} = 15 s RAS _{pulse interval} ³ = 1620 s, SRT _{av} ⁴ = 20 days	Conditions for sludge adaptation and conditional fouling of fresh membranes.
II	21–34	J _{n(net)} ¹ = 5.3 LMH, J _{n(gross)} ² = 32.6 LMH, RAS _{pulse interval} ³ = 740 s, SRT _{av} ⁴ = 20 days	System stabilization and an increase of sludge recirculation between separation and MBBR ⁵ chambers through the decrease of RAS ⁶ interval.
III	35–36	J _{n(net)} ¹ = 12.2 LMH, J _{n(gross)} ² = 44.0 LMH	Increase of net-flux in order to get close to TMP ⁷ jump.
IV	37–44	J _{n(net)} ¹ = 10.0 LMH, J _{n(gross)} ² = 43.7 LMH, t _{BW} = 19.5, t _{relaxI} = 30	Prolongation of backwash in order to stabilize the system and TMP ⁷ jump.
V	45–47	CIP ⁸ I, 1% NaOCl, 2% Citric acid	TMP ⁷ ↓; P _n ↑ (58%), dP _n /dt ↑ (88%)—removal of reversible and irreversible fouling.
VI	48–77	Same as in period IV, SRT = 31 days	Reproduction of last stable operation.
VII	78–85	CIP ⁸ II	TMP ⁷ ↓ (82%), P _n ↑ (82%), dP _n /dt ↑.
VIII	86–114	J _{n(net)} ¹ = 4.5 LMH, J _{n(gross)} ² = 30.4 LMH, Infinite SRT (no wastage/sludge discharge)	Lower hydraulic loading.

Notes: ¹ Normalized net flux; ² Normalized gross flux; ³ The pulse interval of the return activated sludge; ⁴ Average solids retention time; ⁵ Moving-bed-biofilm reactor; ⁶ Return activated sludge; ⁷ Transmembrane pressure; ⁸ Cleaning-in-place.

The data array of hydraulic parameters was statistically treated and expressed in the form of 8 representative filtration cycles for every day. For a single cycle, a set of average initial (TMP_i, J_{Ni}, P_{ni}) and final parameters (TMP_{i-1}, J_{Ni-1}, P_{ni-1}) was calculated, excluding ramp and relaxation periods of the peristaltic pump.

Recovery of membrane permeability was expressed as the ratio of permeability after chemical cleaning and before chemical cleaning [103]:

$$\text{Recovery}_{P_n} = \frac{P_{\text{CIP}/\text{BW}_{\text{fin}}} - P_{\text{CIP}/\text{BW}_{\text{in}}}}{P_{\text{in}} - P_{\text{fin}}} \quad (5)$$

where: P_{CIP/BW_{fin}} is a permeability of the new filtration cycle after the backwash/Chemical cleaning (CIP); P_{CIP/BW_{in}} is the initial permeability before the cleaning, which is equal to P_{fin}, the permeability at the end of previous filtration cycle; and, P_{in} is the initial permeability at the beginning of the previous filtration cycle.

In other words, recovery of permeability expresses the extent to which membrane permeability is restored after the application of different types of cleaning to remove the foulants [104].

A sampling of mixed liquor, and raw and treated wastewater was organized on a daily basis. Samples of raw wastewater (chamber I), MBBR mixed liquor (chamber II), BF-MBR mixed liquor (chamber III) and permeate (chamber IV) were analyzed accordingly for suspended solids (SS, MLSS), COD of the filtrates, DSVI, and RH. COD was measured by COD-cuvette test (HACH, Manchester, UK)

applying the dichromate method, DSVI was measured by a settleability test. RH was determined by the MATH (microbial adherence to hydrocarbons) method. The analyses were conducted in accordance with SMWW (Standard Methods for the Examination of Water and Wastewater) (22nd edition) and the MATH test [59,105]. Flow in permeate line and TMP were measured through flow and pressure sensors (Krohne, Dilling, Norway) and logged every second to the PLC together with filtration cycle settings.

PLS regression was used to distinguish the relationship between the parameters of the mixed liquor and the fouling indicators and to predict the fouling intensity. The statistical software, The Unscrambler® X10.3 (CAMO Software AS, Oslo, Norway), was used to perform the analysis of the monitored data.

3. Results and Discussion

3.1. Pilot Plant Operation Results

During 114 days of operation of the BF-MBR pilot plant, notable trends in TMP, permeability, permeability slope, MLSS in the membrane separation chamber (MLSS-III) and COD removal were observed (Figure 2), allowing the development of the qualitative description of the biological activity and its influence on membrane separation process.

The first period (1–20 days) can be described as the period of biological adaptation and biomass development. It is characterized by moderate growth of biomass up to MLSS-III 5–6 g/L and increasing biodegradation of organics in the range of 67–81%, together with a steep TMP growth and a respective decrease of permeability at a relatively high rate of 0.35–0.47 LMH/bar/s. This state can be identified as conditioning fouling.

After reaching the conditionally critical value of 1.7 times permeability decrease, the return of suspended solids from separation chamber (III) to MBBR chamber (II) was doubled, leading to stabilization of permeability and MLSS-III in the next period (21–34 days) and decreasing the membrane fouling rate to 0.25–0.27 LMH/bar/s by permeability, which is considered steady fouling.

In order to increase the system productivity in terms of permeate, membrane flux was increased, entailing the TMP jump during the third period (35–36 days), which indicates a severe fouling. Following that, backwash and relaxation times were adjusted in order to stabilize rapid fouling development during 37–44 days.

Chemical cleaning (CIP), applied in the fifth period, exhibited relatively high values of the recovered membrane permeability. While recovery of the permeability between the backwashes performed at the end of every filtration cycle was in the range 88–126%, recovery of the permeability after CIP was in the range of 158–182%.

The sixth period (48–77 days) was another steady fouling state. It reproduced the same trends from the second period (21–34 days), except for a more stable COD degradation due to well-developed biofilms in MBBR part and on carriers in the separation chamber (III). After reaching 400 mbar of TMP, a second chemical cleaning was provided, applying higher backwash pressure with the subsequent soaking of the membrane elements in the cleaning solutions, which caused the permeability to recover to the initial value.

The last, eighth period of system operation is a control period which is characterized by both conditional and steady fouling in the permeability pattern.

In general, in the way described above, the operation of the BF-MBR pilot plant was observed during all the states, which is important for the determination of membrane fouling patterns: Conditional fouling, steady fouling, and TMP jump at different fluxes. Two chemical cleaning procedures were conducted to estimate the recovery of permeability. Data, which were recorded during these states, were taken as the basis for further statistical analysis.

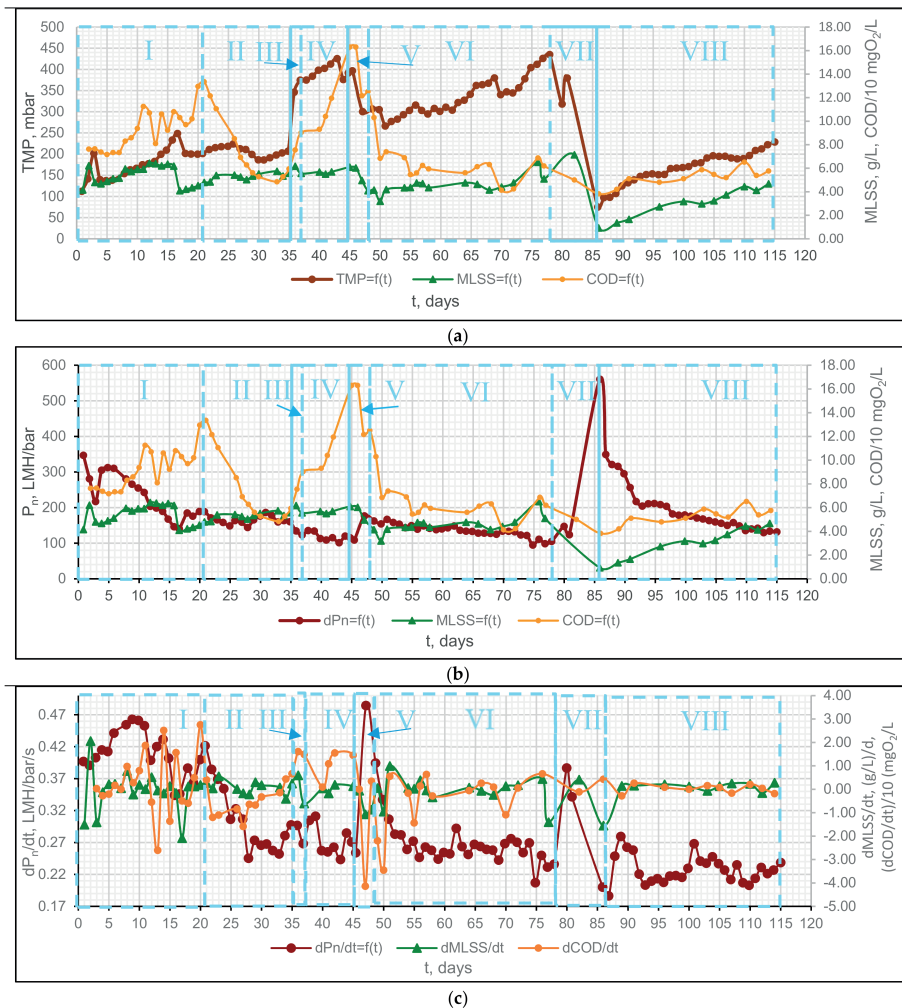


Figure 2. BF-MBR pilot plant operation profile: (a) TMP, MLSS-III, COD-III change within operation time; (b) normalized permeability (P_n), MLSS-III, COD-III change within operation time; (c) first derivative of normalized permeability (dP_n/dt), MLSS-III ($dMLSS/dt$), COD-III ($dCOD/dt$) within operation time.

3.2. Statistical Determination of Membrane Fouling Patterns

According to the literature, the influence of the mixed liquor parameters (i.e., MLSS, SVI (DSVI), COD, and RH) on the filtration performance and fouling intensity is controversial. Indeed, a positive impact of higher MLSS concentration on MBR hydraulic performance has been indicated [15,106]. On the contrary, Chang et al. [46] observed a positive link between the MLSS increase and the flux decline, which is the opposite of its effect on the specific cake resistance, while Brookes et al. [107] and Jefferson et al. [108] showed that MLSS concentration is not a governing factor influencing the overall membrane fouling, and no consistent correlation was observed between MLSS and fouling intensity.

The influence of the relative hydrophobicity on system performance is also not fully comprehended. According to the findings by Deng et al. [40] and Huang et al. [109], high RH fosters the mitigation of fouling due to the weaker interactions of hydrophobic flocs with a hydrophilic membrane. In addition, lower RH values entail floc deterioration and the consequent increase of cake layer resistance [29], whereas higher RH values are associated with better flocculation [60]. Meanwhile, as specified by Meng et al. [36] and Tian et al. [64], higher RH of sludge causes the formation of a more dense cake layer on the membrane surface, resulting in a greater TMP rise.

There is a lack of data on the correlation between SVI and membrane fouling intensity. Chae et al. [110] stated that high SVI values corresponded to severe membrane fouling in an MBR system. Ng et al. [111] linked the increased SVI values to the higher ratio of non-flocculating components of the activated sludge but did not mention if this affected the fouling intensity. In contrast, according to Fan et al. [112] and Wu and Huang [113], this parameter is not a reliable indicator to predict the membrane fouling potential for MBR systems and has no effect on membrane filterability.

As found, COD is indirectly related to the fouling intensity. COD is linked to the concentration of soluble foulants which have a negative effect on membrane filterability [114]. In addition, COD in the effluent from aerobic and anaerobic biological systems is encountered in the form of soluble microbial products which are among the foulants in MBRs [115]. Meanwhile, Lesjean et al. [116] found no clear correlation between COD and the fouling intensity.

Hence, to gain a deeper understanding of the role of the mixed liquor characteristics in the filtration performance of the investigated system, it was decided to monitor these parameters and their variation over time in the separation chamber (Table 3) and to process the collected data statistically.

Table 3. Parameters of the mixed liquor in the separation chamber.

Parameter	Value
MLSS, g/L	5–6.5
dMLSS/dt, (g/L)/day	−0.61–2.06
DSVI, mL/g	118–272
dDSVI/dt, (mL/g)/day	−91–57
RH, %	20.5–61.5
dRH/dt, %/day	−27–35
COD _{dis} , mgO ₂ /L	38–134
dCOD/dt, mgO ₂ /L/day	−35–27.5

Since the operating conditions varied significantly throughout the whole filtration period (Table 2), which influenced both the activated sludge parameters and the fouling indicators, it was decided to split the whole data range into its characteristic phases and statistically analyze them separately from each other, excluding the data which covered the chemical cleanings. Hence, three basic periods were established: period A (days 3–34), period B (days 49–77) and period C (days 86–114).

PLS regression (also known as a projection of latent structures) was used as an advanced mathematical and statistical tool to model the relations between the X variables and the Y responses within every single period (Table 4).

Table 4. Model inputs.

Period	Predictors	Responses
A	MLSS, dMLSS/dt, DSVI dDSVI/dt, RH, dRH/dt, COD _{dis} , dCOD/dt	TMP, P _n , dP _n /dt
B	MLSS, dMLSS/dt, DSVI dDSVI/dt, COD _{dis} , dCOD/dt	TMP, P _n , dP _n /dt
C	MLSS, dMLSS/dt, DSVI dDSVI/dt, COD _{dis} , dCOD/dt	TMP, P _n , dP _n /dt

The X- and Y-matrices were modelled simultaneously to find the latent variables in input X parameters that best predicted the latent variables in the corresponding Y responses (i.e., PCAs on the

X- and Y-data were performed with the subsequent acquisition of the relative scores). Then, the plotting of two sets of the scores (those related to X and Y) against each other was conducted, maximizing the covariance between X and Y [117].

The obtained model was validated by applying a random cross-validation in PLS. The number of PLS components (factors), was chosen according to the explained variance.

The results of the performed analyses of the data from the initial period of the system performance (Period A) are shown below (Figure 3).

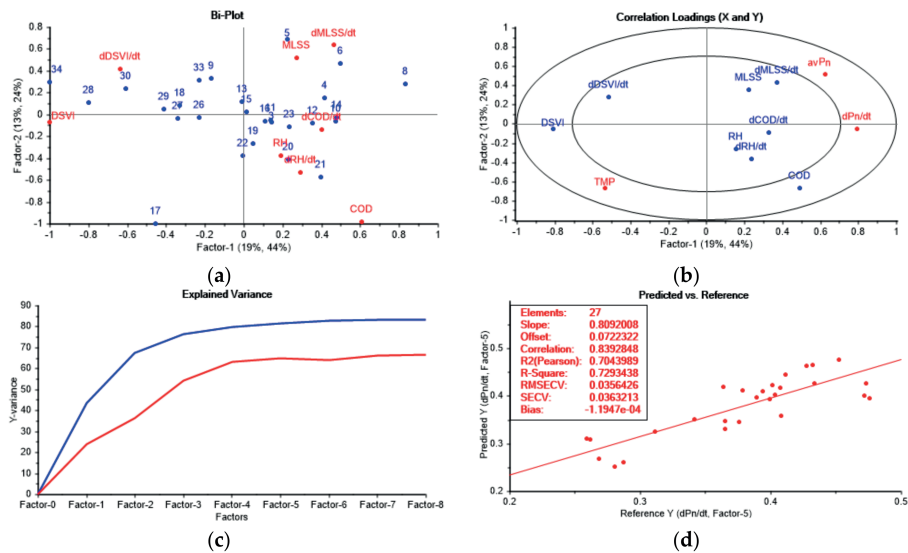


Figure 3. Results of PLS of the data from the period A of the filtration performance monitoring: (a) Bi-plot; (b) loadings plot; (c) explained variance plot; (d) fouling intensity prediction model.

The correlation loadings plot is computed by accounting for each variable for the displayed latent variables (factors). From the loadings plot, Factor-1 clearly describes DSVI, dDSVI/dt, TMP, COD, dMLSS/dt, permeability, P_n , and its slope, dP_n/dt , since the first three variables are located at the far left, and the rest at the far right along the Factor-1 axis. Factor-1 also accounts for dCOD/dt, while MLSS and dRH/dt mainly contribute to Factor-2. According to the PLS loadings plot, COD and DSVI explain more than 50% of the variance and are probably the most important variables. DSVI has a negative correlation with both permeability and permeability slope, but is positively linked to TMP. Particularly in this case, COD has a negative correlation with the variables DSVI, dDSVI/dt, MLSS and dMLSS/dt, and is negatively linked to the average normalized permeability (nP). Although the rest of the variables are located in the inner ellipse, which indicates up to 50% of the explained variance and thus does not contain enough structured variation to discriminate between the mixed liquor samples, it was decided to keep them to make the model more reliable.

The analysis of the scores and loadings plot and the bi-plot demonstrates that the samples from days 1–20 are mostly characterized by higher RH, dRH/dt, MLSS, dMLSS/dt, COD, and dCOD/dt, while the samples taken during the period 22–34 day have higher DSVI and dDSVI/dt values.

As demonstrated by the graph of explained variance (Figure 3c), it is preferable to use five components, since this number gives a lower residual variance.

According to the Figure 3d (the validation graph), the developed model is linear (R -squared = 0.73) and with a reasonable fit to the majority of data: Slope = 0.81, offset 0.07 and the dispersion of the validation samples around the regression line (Root Mean Square Error of Cross Validation–RMSEV)

and the standard error of cross-validation (SECV) are approximately 0.036. Consequently, the model is reliable and can be used for future predictions for the defined number of factors under the operational conditions applied during the period A.

Relative hydrophobicity and its change required much more effort and time to be experimentally determined than other variables. In addition, RH and dRH/dt are characterized by relatively low-weighted regression coefficients: 0.02 and -0.086 , respectively (Factor-2); and, 0.07 and 0.04, respectively (Factor-1) (i.e., these variables are not well explained by the components). Considering the above-mentioned aspects, it was decided to exclude RH and dRH/dt from further monitoring and analysis.

The second period, B, covers the filtration performance data collected between the first and the second chemical cleanings of the system. Obtained results of the PLS analysis are represented below (Figure 4).

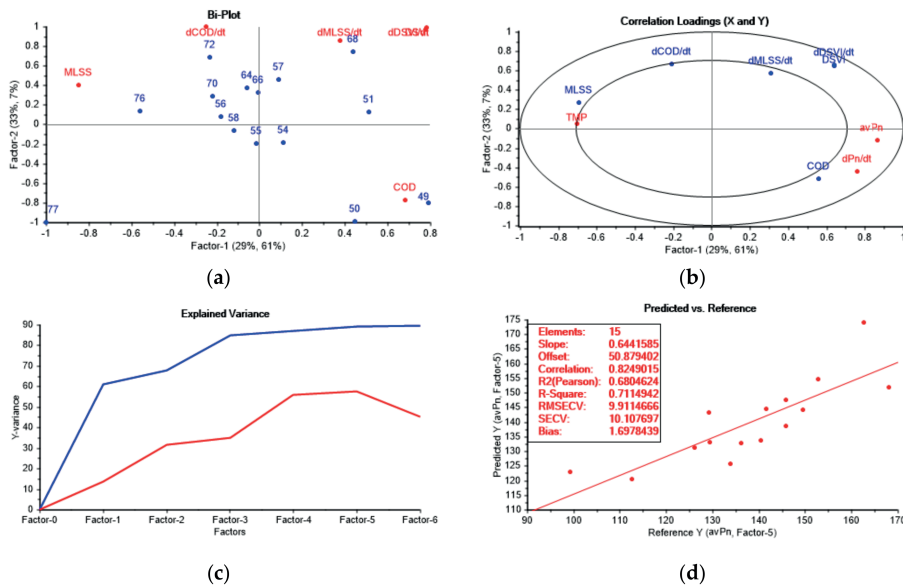


Figure 4. Results of PLS of the data from the period B of the filtration performance monitoring: (a) Bi-plot; (b) loadings plot; (c) explained variance plot; (d) fouling intensity prediction model.

According to the bi-plot (Figure 4b), the majority of the samples within period B are characterized by higher dCOD/dt values. Meanwhile, the samples taken on days 49–50 are characterized by higher COD values; on days 51, 57 and 68 by relatively high dMLSS/dt, DSVI, and dDSVI/dt values; on day 72 by comparatively high dCOD/dt values; and on days 76 and 77 by more significant MLSS values.

According to the correlation loadings plot, Factor-1 apparently describes TMP, MLSS, COD, average permeability (avP_n), dP_n/dt , DSVI and dDSVI/dt. Factor-2 is related to dCOD/dt and dMLSS/dt. All the variables were marked as significant according to the plot of correlation loadings, even though the MLSS variable gives slightly less than 50% of the explained variance. MLSS and dCOD/dt are positively linked to the TMP response, in contrast to dMLSS/dt, DSVI, dDSVI/dt, which have a negative correlation with TMP and the permeability slope (dP_n/dt). The COD variable has a high positive correlation with dP_n/dt and is positively linked to the average permeability (avP_n).

Figure 4 demonstrates that the optimum number of factors is five, which provides more than 57% of the explained Y-variance.

An analysis of the validation plot shows that the developed model is linear, having R-squared = 0.71 and with a good fit to the majority of data (i.e., slope = 0.64). RMSEV and SECV are approximately 10, but it is essential to acknowledge that the mentioned errors have the same units as the reference Y (in this case, average normalized permeability, avP_n). R-squared (Pearson) is close to R-squared correlation (0.68 vs. 0.82), which indicates the reliability of the model. Consequently, a good prediction is attained with the developed model, which proves that the model is reliable and can be used during further stages when the operating conditions applied in the period B are replicated.

The output from the PLS modelling of the data acquired after the second CIP (the period C) is demonstrated below (Figure 5).

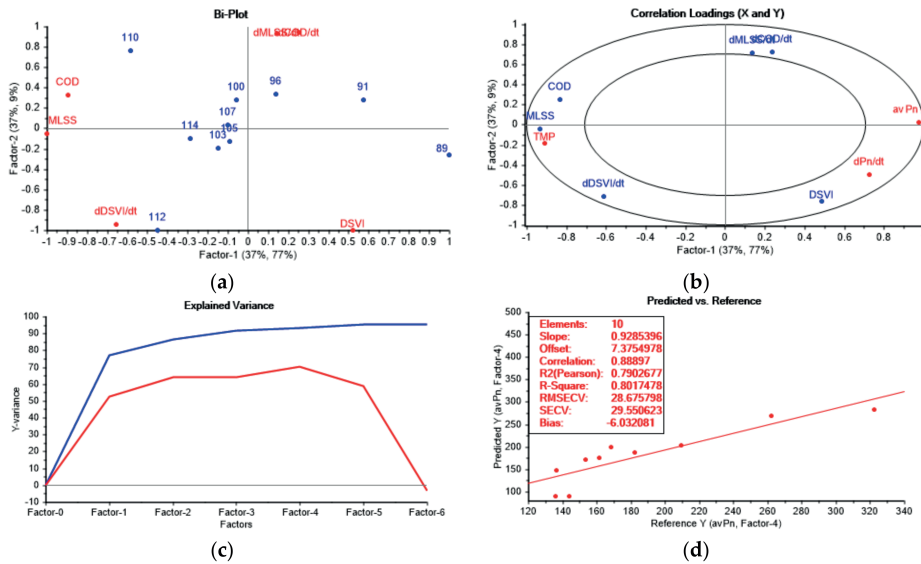


Figure 5. Results of PLS of the data from the period C of the filtration performance monitoring: (a) Bi-plot; (b) loadings plot; (c) explained variance plot; (d) fouling intensity prediction model.

The bi-plot shows that the samples from day 89 have a higher DSVI value, while dMLSS/dt and dCOD/dt are the most distinctive parameters for days 91 and 96. Days 100, 107 and 110 are characterized by higher COD content, whereas days 103, 105 and 114 have higher MLSS values. Day 112 is characterized by a higher dDSVI/dt.

From the correlation loadings plot (Figure 5b), COD, MLSS, TMP, dDSVI/dt, DSVI, avP_n and dP_n/dt contribute to Factor-1, while Factor-2 describes dMLSS/dt and dCOD/dt. All the specified variables explain more than 50% of the variance and thus have high importance in relation to Factor-1 and Factor-2. MLSS and dDSVI/dt are positively linked to TMP and have a negative correlation with the permeability indicators, avP_n and dP_n/dt . DSVI is positively correlated to dP_n/dt , while dMLSS/dt and dCOD/dt have a negative correlation with the permeability slope.

The explained variance plot indicates that the optimum number of factors is four, which provides more than 70% of explained Y-variance.

The points of the validation graph in Figure 5d have a linear trend (R-squared = 0.8), having a good fit to the majority of data (slope = 0.93). R-squared (Pearson) is close to R-squared correlation (0.79 vs. 0.89), which indicates the reliability of the model. Only the errors RMSEV and SECV are higher than in previous cases, but this can be explained by the higher values of the response function (average permeability) in this particular case.

Since the higher amount of data was available to be collected during the last period C (Table 5) in comparison to the previous modes, it was decided to apply the predict function to new data.

Table 5. Mixed liquor characteristics and fouling indicators during period VIII (new data).

	TMP _{av} ¹ , Bar	av dP _n /dt ²	avP _n ³ , LMH/Bar	DSVI ⁴ , mL/g	dDSVI/dt ⁵	MLSS ⁶ , g/L	dMLSS/dt ⁷	COD _f ⁸ , mgO ₂ /L	dCOD/dt ⁹
max.	266.16	0.26	125.45	185.41	5.52	5.74	0.35	69.80	5.00
min.	232.30	0.23	112.98	142.60	-7.79	5.32	-0.17	45.40	-3.83
average	249.26	0.24	120.66	166.56	-1.96	5.48	0.02	55.52	-0.44

Notes: ¹ Average transmembrane pressure; ² Average normalized permeability slope; ³ Average normalized permeability; ⁴ Diluted sludge volume index; ⁵ Diluted sludge volume index slope; ⁶ Mixed liquor suspended solids; ⁷ Mixed liquor suspended solids slope; ⁸ Chemical oxygen demand (filtered); ⁹ Chemical oxygen demand slope.

Full prediction with the identification of outliers was used. The following results were obtained (Figure 6).

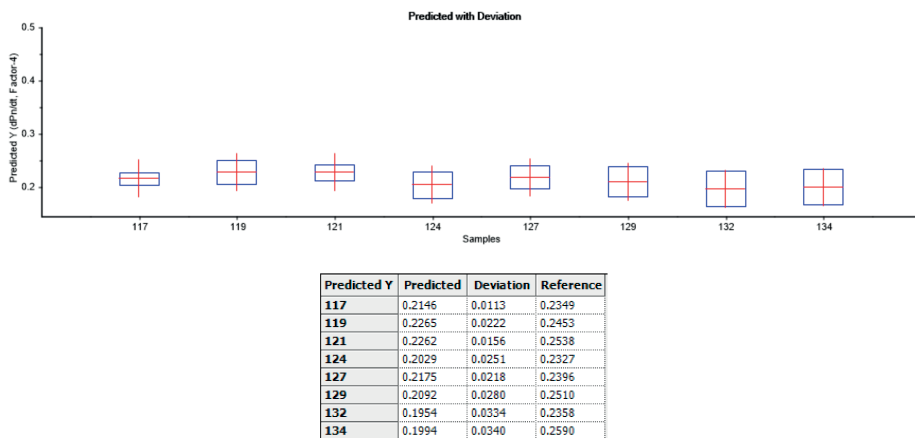


Figure 6. Prediction results for the new data from Period C for four factors using the derived PLS model for the relevant period.

The deviation between the predicted and the reference values is in the range 0.01–0.034, which demonstrates the reliability of the applied model.

Consequently, a good prediction is attained by applying the developed model, which proves that the model is reliable and can be used during further stages under the operating conditions that were applied during period C.

In addition, MLR was performed using leverage correction. However, obtained results are unreliable since the same data was validated and used for the prediction, which provided overly optimistic results. The application of the test matrix in MLR would merely copy the PLS strategy but do so in a more difficult way. MLR is a simpler way of doing the calculations, but PLS is much more advanced due to the applied validation techniques.

SRT and permeate flux are among the key operating parameters controlling fouling intensity in MBR.

In order to estimate the influence of SRT on the performance of the current system, this parameter was included in the models as an additional variable. The acquired results are represented in Figure 7.

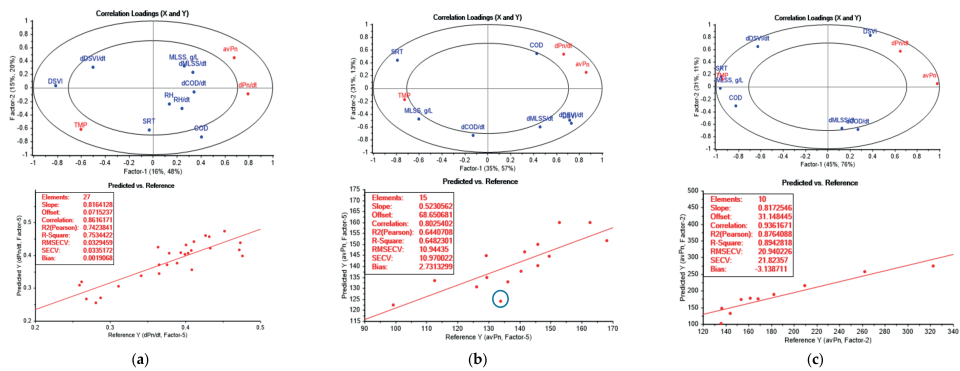


Figure 7. Results of PLSs of the data from all the periods of the filtration performance monitoring, including SRT: (a) period A; (b) period B; (c) period C.

According to the correlation loadings plot related to period A, SRT explains less than 50% of the variance and thus has relatively little influence. In this particular case, SRT exhibits an independent variation in relation to other variables, except for COD, which has a weak positive link with SRT. Meanwhile, SRT exhibits a slightly negative correlation with the normalized permeability and permeability slope for period A. Concerning the model enhancement, the introduction of the new variable did not entail any significant improvement: RMSECV was just 0.002 less than its value in the initial model, while the bias, on the contrary, showed an order of magnitude increase in absolute value.

The results related to period B demonstrate that SRT is an important variable which explains more than 50% of the variance in the dataset. It has a strong negative correlation with COD and the normalized permeability. In addition, SRT is positively correlated with MLSS along Factor-1. The negative correlation between SRT and COD during this period can be attributed to the higher treatment performance of the biomass, which becomes well-developed at SRT up to 40 days and thus is capable of a more efficient biodegradation of organic contaminants, particularly SMPs, causing the decrease of COD values [118,119]. Meanwhile, the increase in SRT promotes the development of higher MLSS concentrations [120], thus inducing membrane fouling.

The introduction of the new variable into the existing model decreased its linearity R -squared = 0.65 vs. R -squared = 0.71 (values in the new model vs. values characteristic for the basic model related to period B), with a slightly worse fit to the majority of data (slope = 0.52 vs. slope = 0.64), RMSEV 10.9 vs. 9.9, SECV 10.97 vs. 10.1, bias 2.73 vs. 1.7. In addition, the new model underestimated a sample from day 72 (marked with the blue circle).

The modelling of the dataset from period C demonstrates the importance of the SRT variable. SRT is highly positively correlated with MLSS and TMP, and is negatively linked to normalized permeability and its slope, hence indicating the fouling enhancement through the increase of MLSS at higher SRTs, which agrees with the previous findings by Le-Clech et al. [29], Van den Broeck et al. [120], Yigit et al. [121]. The positive link between SRT and COD along Factor-1 during this period can be attributed to the accumulation of small microbial by-products (SMP with the molecular weight (MW) < 1 kDa), which contribute to fouling through deflocculation at high SRTs (>31 days) [118,121,122]. However, further studies are required to confirm the presence of different groups of microorganisms at various SRTs in this system (for example, tightly and loosely bound EPS, small SMP, etc.), since the deep investigation of the biomass content was not in the scope of the current research.

The new model exhibits higher linearity (R -squared = 0.89 vs. R -squared = 0.80) and a slightly higher accuracy (RMSEV = 20.9 vs. RMSEV = 28.7; SECV = 21.8 vs. SECV = 29.6; and, bias = -3.4 vs. bias = -6.0) than the initial model.

It is noteworthy that the purpose of including SRT in modelling was not to improve the models for the relevant periods developed earlier in this work, since the inclusion of a new variable is undesirable as it could complicate the model (i.e., it is preferable to use as low a number of variables as possible) [123]. Besides, the introduction of the SRT variable to the model covering period C barely decreased the deviation in the prediction of the new dataset (Table 4; 0.016–0.0261 vs. 0.011–0.034), making the extension of the model size unreasonable for its further use in the system controller. The scope was to show the influence of SRT on the operational parameters and fouling intensity in the current system to achieve the highest possible fouling inhibition.

As discovered, SRT should be less than 31 days to avoid a severe membrane fouling. This can be called the critical SRT. The SRT that can be applied without a sharp decrease in permeability is 20 days for the current BF-MBR system. In the studied pilot plant, SRT was adjusted by changing the frequency of sludge removal and the volume of the removed sludge per batch.

Concerning the permeate flux, it can be decreased in order to minimize the filtration resistance if the biomass exhibits high fouling propensity. The current system worked at a constant permeate flux, which varied depending on the monitoring period (Table 2). In general, all the applied fluxes were below the critical flux value to avoid a severe membrane fouling [124–126]. The critical net flux was determined by the flux-step method, described by Miller et al. [127], and was in a range of 12–15 LMH.

In addition to the desludging option, the concentration of the mixed liquor in the separation and biological chambers was regulated by adjusting the RAS pumping intensity (i.e., pulse length and frequency). The introduction of the RAS line made it possible to build up the desired level of biomass in biological and separation chambers, and to adjust the endogenous decay of the biomass, thus providing sufficient COD and NH_4^+ removal.

To summarize, the monitored mixed liquor characteristics allowed the controlling of the fouling intensity by adjusting the operating conditions which helped to maintain the stability of the system performance and, hence, the permeate quality: BF-MBR installation assured 100% MLSS elimination and 67–90% treatment efficiency in terms of COD removal, keeping the TMP below 500 mbar.

4. Conclusions

The developed chemometric approach to the assessment of membrane fouling in membrane bioreactor advances the field of fouling monitoring and provides a statistical tool for its control in submerged membrane bioreactors.

The approach was based on PLS regression analysis and was used to detect membrane fouling patterns in the biofilm ceramic membrane bioreactor pilot system during 114 days of operation, varying membrane flux and solid retention time, and covering the periods of steady fouling and TMP jumps, followed by two chemical cleanings in the system.

The mixed liquor parameters MLSS, dMLSS/dt , DSVI, dDSVI/dt , COD, and dCOD/dt were found to be significant for estimation and prediction of fouling intensity, while relative hydrophobicity of mixed liquor and its slope seemed to play a secondary role. Normalized permeability and its slope were identified as the most reliable fouling indicators, while critical solid retention time was introduced as another quantitative parameter, influencing the intensity of membrane fouling.

The cross-validation of every model and the complete validation of the model, covering the last phase of the filtration, demonstrated low uncertainty of the predictions, and hence high reliability of the models, allowing further implementation of the developed fouling control strategies.

The models were used to adjust operational parameters of the pilot system according to the characteristics of biomass, keeping the system running below critical transmembrane pressure (500 mbar), with 67–90% removal of chemical oxygen demand and 100% retention of suspended solids, resulting in good recovery of membrane permeability after chemical cleanings, thus removing irreversible fouling.

Further work is foreseen in the validation of the developed approach in an operational environment of decentralized membrane bioreactors, where the sustainable operation is frequently a critical issue due to the lack of qualified supervision, and which raises the barrier to penetration of membrane bioreactors into cost-sensitive markets.

Author Contributions: O.K. and Z.M. conceived and designed the experiments; O.K. performed the experiments under supervision of Z.M. and analyzed the data; H.R. contributed reagents, materials and analysis tools, and contributed to the discussion of the article; O.K. wrote the paper with advice from Z.M.

Funding: This research was co-funded by the Erasmus+ Program of the European Union (project number: 561755-EPP-1-2015-1-NOEPPKA2-CBHE-JP).

Acknowledgments: Authors express their gratitude to Daniel Todt from Ecomotive AS for facilitating pilot plant studies; Yuliia Dzhiora and Stella Saliu for their inputs as Erasmus+ exchange students; Knut Kvaal for his guidance on mathematical modelling using the Unscrambler software.

Conflicts of Interest: The authors declare no conflict of interest. The founding sponsors had no role in the design of the study; in the collection, analyses, or interpretation of data; in the writing of the manuscript, and in the decision to publish the results.

References

1. World Economic Forum. The Global Risks Report 2018. Available online: <https://www.weforum.org/reports/the-global-risks-report-2018> (accessed on 9 December 2017).

2. World Economic Forum. Grim Reaping. Available online: <http://reports.weforum.org/global-risks-2018/grim-reaping/> (accessed on 10 December 2017).
3. United Nations World Water Assessment Programme (WWAP). *The United Nations World Water Development Report 2017, Wastewater: The Untapped Resource*; UNESCO: Paris, France, 2017.
4. Lautze, J.; Stander, E.; Drechsel, P.; da Silva, A.K.; Keraita, B. *Global Experiences in Water Reuse*; International Water Management Institute (IWMI): Colombo, Sri Lanka; CGIAR Research Program on Water, Land and Ecosystems (WLE): Montpellier, France, 2014; 31p.
5. European Commission. Water is too Precious to Waste. Available online: http://ec.europa.eu/environment/water/pdf/water_reuse_factsheet_en.pdf (accessed on 13 January 2018).
6. Hwang, H.; Forrester, A.; Lansley, K. Decentralized water reuse: Regional water supply system resilience benefits. *Procedia Eng.* **2014**, *70*, 853–856. [[CrossRef](#)]
7. Lesjean, B.; Leiknes, T.; Hochstrat, R.; Schories, R.; Gonzalez, G.; Gonzalez, A. MBR: Technology gets timely EU cash boost. *Filtr. Sep.* **2006**, *43*, 20–23. [[CrossRef](#)]
8. Hai, F.I.; Yamamoto, K.; Lee, C.-H. *Membrane Biological Reactors: Theory, Modeling, Design, Management and Applications to Wastewater Reuse*; IWA Publishing: London, UK, 2014; 504p, ISBN 9781780400655.
9. Geilvoet, S.P. The Delft Filtration Characterisation Method: Assessing Membrane Bioreactor Activated Sludge Filterability. Ph.D. Thesis, Delft University of Technology, Delft, The Netherlands, 12 February 2010.
10. Global \$8.27 Bn Membrane Bioreactor Market, 2025. Available online: <http://markets.businessinsider.com/news/stocks/global-8-27-bn-membrane-bioreactor-market-2025-1005680257> (accessed on 15 December 2017).
11. Böhm, L.; Drews, A.; Prieske, H.; Bérubé, P.R.; Kraume, M. The importance of fluid dynamics for MBR fouling mitigation. *Bioresour. Technol.* **2012**, *122*, 50–61. [[CrossRef](#)] [[PubMed](#)]
12. Ivanovic, I.; Leiknes, T.O. The biofilm membrane bioreactor (BF-MBR)—A review. *Desalination Water Treat.* **2012**, *37*, 288–295. [[CrossRef](#)]
13. Ivanovic, I.; Leiknes, T.O.; Ødegaard, H. Fouling control by reduction of submicron particles in a BF-MBR with an integrated flocculation zone in the membrane reactor. *Sep. Sci. Technol.* **2008**, *43*, 1871–1883. [[CrossRef](#)]
14. Yu, H.Y.; Xu, Z.K.; Lei, H.; Hu, M.X.; Yang, Q. Photoinduced graft polymerization of acrylamide on polypropylene microporous membranes for the improvement of antifouling characteristics in a submerged membrane-bioreactor. *Sep. Purif. Technol.* **2007**, *53*, 119–125. [[CrossRef](#)]
15. Brookes, A.; Jefferson, B.; Guglielmi, G.; Judd, S.J. Sustainable Flux Fouling in a Membrane Bioreactor: Impact of Flux and MLSS. *Sep. Sci. Technol.* **2006**, *41*, 1279–1291. [[CrossRef](#)]
16. Kraume, M.; Wedi, D.; Schaller, J.; Iversen, V.; Drews, A. Fouling in MBR: What use are lab investigations for full scale operation? *Desalination* **2009**, *236*, 94–103. [[CrossRef](#)]
17. Yusuf, Z.; Wahab, N.A.; Abusam, A. Neural Network-based Model Predictive Control with CPSOGSA for SMBR Filtration. *Int. J. Electr. Comput. Eng.* **2017**, *7*, 1538–1545. [[CrossRef](#)]
18. Song, W.; Li, Z.; Li, Y.; You, H.; Qi, P.; Liu, F.; Loy, D.A. Facile sol-gel coating process for anti-biofouling modification of poly (vinylidene fluoride) microfiltration membrane based on novel zwitterionic organosilica. *J. Membr. Sci.* **2018**, *550*, 266–277. [[CrossRef](#)]
19. Gkotsis, P.K.; Mitrakas, M.M.; Tolkou, A.K.; Zouboulis, A.I. Batch and continuous dosing of conventional and composite coagulation agents for fouling control in a pilot-scale MBR. *Chem. Eng. J.* **2016**, *311*, 255–264. [[CrossRef](#)]
20. Lee, J.C.; Kim, J.S.; Kang, I.J.; Cho, M.H.; Park, P.K.; Lee, C.H. Potential and limitations of alum or zeolite addition to improve the performance of a submerged membrane bioreactor. *Water Sci. Technol.* **2001**, *43*, 59–66. [[CrossRef](#)] [[PubMed](#)]
21. Zarei, A.; Moslemi, M.; Mirzaei, H. The Combination of KMnO₄ Oxidation and Polymeric Flocculation for the Mitigation of Membrane Fouling in a Membrane Bioreactor. *Sep. Purif. Technol.* **2016**, *159*, 124–134. [[CrossRef](#)]
22. Drews, A. Membrane fouling in membrane bioreactors—Characterisation, contradictions, cause and cures. *J. Membr. Sci.* **2010**, *363*, 1–28. [[CrossRef](#)]
23. Zheng, Y.; Zhang, W.; Tang, B.; Ding, J.; Zheng, Y.; Zhang, Z. Membrane fouling mechanism of biofilm-membrane bioreactor (BF-MBR): Pore blocking model and membrane cleaning. *Bioresour. Technol.* **2018**, *250*, 398–405. [[CrossRef](#)] [[PubMed](#)]

24. Leiknes, T.; Ødegaard, H. The development of a biofilm membrane bioreactor. *Desalination* **2007**, *202*, 135–143. [[CrossRef](#)]
25. Jin, L.; Ong, S.L.; Ng, H.Y. Fouling control mechanism by suspended biofilm carriers addition in submerged ceramic membrane bioreactors. *J. Membr. Sci.* **2013**, *427*, 250–258. [[CrossRef](#)]
26. Arabi, S.; Nakhla, G. Impact of cation concentrations on fouling in membrane bioreactors. *J. Membr. Sci.* **2009**, *343*, 110–118. [[CrossRef](#)]
27. Chang, I.S.; Judd, S.J. Domestic wastewater treatment by a submerged MBR (membrane bio-reactor) with enhanced air sparging. *Water Sci. Technol.* **2003**, *47*, 149–154. [[CrossRef](#)] [[PubMed](#)]
28. Judd, S. *The MBR Book Principles and Applications of Membrane Bioreactors in Water and Wastewater Treatment*, 1st ed.; Elsevier Ltd.: London, UK, 2006; p. 325, ISBN-13 978-1-85-617481-7.
29. Le-Clech, P.; Chen, V.; Fane, T.A.G. Fouling in membrane bioreactors used in wastewater treatment. *J. Membr. Sci.* **2006**, *284*, 17–53. [[CrossRef](#)]
30. Mafirad, S.; Mehrnia, M.R.; Azami, H.; Sarrafzadeh, M.H. Effects of biofilm formation on membrane performance in submerged membrane bioreactors. *Biofouling* **2011**, *27*, 477–485. [[CrossRef](#)] [[PubMed](#)]
31. Meng, F.; Zhang, S.; Oh, Y.; Zhou, Z.; Shin, H.-S.; Chae, S.-R. Fouling in membrane bioreactors: An updated review. *Water Res.* **2017**, *114*, 151–180. [[CrossRef](#)] [[PubMed](#)]
32. Fallis, A. Experimental Methods in Wastewater Treatment. *J. Chem. Inf. Model.* **2013**, *53*. [[CrossRef](#)]
33. Ferreira, M.L. Filterability and Sludge Concentration in Membrane Bioreactors. Ph.D. Thesis, Delft University of Technology, Delft, The Netherlands, 15 September 2011.
34. Meng, F.; Shi, B.; Yang, F.; Zhang, H. Effect of hydraulic retention time on membrane fouling and biomass characteristics in submerged membrane bioreactors. *Bioprocess Biosyst. Eng.* **2007**, *30*, 359–367. [[CrossRef](#)] [[PubMed](#)]
35. Ji, L.; Zhou, J. Influence of aeration on microbial polymers and membrane fouling in submerged membrane bioreactors. *J. Membr. Sci.* **2006**, *276*, 168–177. [[CrossRef](#)]
36. Meng, F.; Zhang, H.; Yang, F.; Zhang, S.; Li, Y.; Zhang, X. Identification of activated sludge properties affecting membrane fouling in submerged membrane bioreactors. *Sep. Purif. Technol.* **2006**, *51*, 95–103. [[CrossRef](#)]
37. Vanysacker, L.; Boerjan, B.; Declerck, P.; Vankelecom, I.F.J. Biofouling ecology as a means to better understand membrane biofouling. *Appl. Microbiol. Biotechnol.* **2014**, *98*, 8047–8072. [[CrossRef](#)] [[PubMed](#)]
38. Wu, B.; Fane, A.G. Microbial relevant fouling in membrane bioreactors: Influencing factors, characterization, and fouling control. *Membranes* **2012**, *2*, 565–584. [[CrossRef](#)] [[PubMed](#)]
39. Zhou, Z.; Meng, F.; He, X.; Chae, S.-R.; An, Y.; Jia, X. Metaproteomic analysis of biocake proteins to understand membrane fouling in a submerged membrane bioreactor. *Environ. Sci. Technol.* **2015**, *49*, 1068–1077. [[CrossRef](#)] [[PubMed](#)]
40. Deng, L.; Guo, W.; Hao, H.; Farzana, M.; Zuthi, R.; Zhang, J.; Liang, S.; Li, J.; Wang, J.; Zhang, X. Membrane fouling reduction and improvement of sludge characteristics by biofloculant addition in submerged membrane bioreactor. *Sep. Purif. Technol.* **2015**, *156*, 450–458. [[CrossRef](#)]
41. Lee, W.; Kang, S.; Shin, H. Sludge characteristics and their contribution to microfiltration in submerged membrane bioreactors. *J. Membr. Sci.* **2003**, *216*, 217–227. [[CrossRef](#)]
42. Meng, F.; Chae, S.R.; Drews, A.; Kraume, M.; Shin, H.S.; Yang, F. Recent advances in membrane bioreactors (MBRs): Membrane fouling and membrane material. *Water Res.* **2009**, *43*, 1489–1512. [[CrossRef](#)] [[PubMed](#)]
43. Meng, F.; Zhang, H.; Yang, F.; Li, Y.; Xiao, J.; Zhang, X. Effect of filamentous bacteria on membrane fouling in submerged membrane bioreactor. *J. Membr. Sci.* **2006**, *272*, 161–168. [[CrossRef](#)]
44. Krzeminski, P. Activated Sludge Filterability and Full-Scale Membrane Bioreactor Operation. Ph.D. Thesis, Delft University of Technology, Delft, The Netherlands, 22 January 2013.
45. Azami, H.; Sarrafzadeh, M.H.; Mehrnia, M.R. Influence of sludge rheological properties on the membrane fouling in submerged membrane bioreactor. *Desalin. Water Treat.* **2011**, *34*, 117–122. [[CrossRef](#)]
46. Chang, I.S.; Kim, S.N. Wastewater treatment using membrane filtration—Effect of biosolids concentration on cake resistance. *Process Biochem.* **2005**, *40*, 1307–1314. [[CrossRef](#)]
47. Wang, Z.; Chu, J.; Song, Y.; Cui, Y.; Zhang, H.; Zhao, X.; Li, Z.; Yao, J. Influence of operating conditions on the efficiency of domestic wastewater treatment in membrane bioreactors. *Desalination* **2009**, *245*, 73–81. [[CrossRef](#)]

48. Radjenović, J.; Matošić, M.; Mijatović, I. Membrane bioreactor (MBR) as an advanced wastewater treatment technology. In *Handbook of Environmental Chemistry*; Springer: Berlin/Heidelberg, Germany, 2008; Volume 5, pp. 37–101.
49. Iorhemen, O.T.; Hamza, R.A.; Tay, J.H. Membrane bioreactor (MBR) technology for wastewater treatment and reclamation: Membrane fouling. *Membranes* **2016**, *6*, 33. [[CrossRef](#)] [[PubMed](#)]
50. Reid, E.; Liu, X.; Judd, S.J. Sludge characteristics and membrane fouling in full-scale submerged membrane bioreactors. *Desalination* **2008**, *219*, 240–249. [[CrossRef](#)]
51. Fan, F.; Zhou, H. Interrelated Effects of Aeration and Mixed Liquor Fractions on Membrane Fouling for Submerged Membrane Bioreactor Processes in Wastewater Treatment. *Environ. Sci. Technol.* **2007**, *41*, 2523–2528. [[CrossRef](#)] [[PubMed](#)]
52. Hernandez Rojas, M.E.; Van Kaam, R.; Schetrite, S.; Albasi, C. Role and variations of supernatant compounds in submerged membrane bioreactor fouling. *Desalination* **2005**, *17*, 95–107. [[CrossRef](#)]
53. Salazar-Peláez, M.L.; Morgan-Sagastume, J.M.; Noyola, A. Influence of hydraulic retention time on UASB post-treatment with UF membranes. *Water Sci. Technol.* **2011**, *64*, 2299–2305. [[CrossRef](#)] [[PubMed](#)]
54. Chen, R.; Nie, Y.; Hu, Y.; Miao, R.; Utashiro, T.; Li, Q.; Xu, M.; Li, Y.Y. Fouling behaviour of soluble microbial products and extracellular polymeric substances in a submerged anaerobic membrane bioreactor treating low-strength wastewater at room temperature. *J. Membr. Sci.* **2017**, *531*, 1–9. [[CrossRef](#)]
55. Jiang, T. Characterization and Modelling of Soluble Microbial Products in Membrane Bioreactors. Ph.D. Thesis, Ghent University, Gent, Belgium, 2007.
56. Xie, W.M.; Ni, B.J.; Sheng, G.P.; Seviour, T.; Yu, H.Q. Quantification and kinetic characterization of soluble microbial products from municipal wastewater treatment plants. *Water Res.* **2016**, *88*, 703–710. [[CrossRef](#)] [[PubMed](#)]
57. Deng, L.; Guo, W.; Ngo, H.H.; Zhang, J.; Liang, S.; Xia, S.; Zhang, Z.; Li, J. A comparison study on membrane fouling in a sponge-submerged membrane bioreactor and a conventional membrane bioreactor. *Bioresour. Technol.* **2014**, *165*, 69–74. [[CrossRef](#)] [[PubMed](#)]
58. Jørgensen, M.K.; Nierychlo, M.; Nielsen, A.H.; Larsen, P.; Christensen, M.L.; Nielsen, P.H. Unified understanding of physico-chemical properties of activated sludge and fouling propensity. *Water Res.* **2017**, *120*, 117–132. [[CrossRef](#)] [[PubMed](#)]
59. Van den Broeck, R.; Krzeminski, P.; Van Dierdonck, J.; Gins, G.; Lousada-Ferreira, M.; Van Impe, J.F.M.; van der Graaf, J.H.J.M.; Smets, I.Y.; van Lier, J.B. Activated sludge characteristics affecting sludge filterability in municipal and industrial MBRs: Unraveling correlations using multi-component regression analysis. *J. Membr. Sci.* **2011**, *378*, 330–338. [[CrossRef](#)]
60. Liu, Y.; Fang, H.H.P. Influences of extracellular polymeric substances (EPS) on flocculation, settling, and dewatering of activated sludge. *Crit. Rev. Environ. Sci. Technol.* **2003**, *33*, 237–273. [[CrossRef](#)]
61. Tu, X.; Zhang, S.; Xu, L.; Zhang, M.; Zhu, J. Performance and fouling characteristics in a membrane sequence batch reactor (MSBR) system coupled with aerobic granular sludge. *Desalination* **2010**, *261*, 191–196. [[CrossRef](#)]
62. Jang, N.; Ren, X.; Choi, K.; Kim, I.S. Comparison of membrane biofouling in nitrification and denitrification for the membrane bioreactor (MBR). *Water Sci. Technol.* **2006**, *53*, 43–49. [[CrossRef](#)] [[PubMed](#)]
63. Nittami, T.; Tokunaga, H.; Satoh, A.; Takeda, M.; Matsumoto, K. Influence of surface hydrophilicity on polytetrafluoroethylene flat sheet membrane fouling in a submerged membrane bioreactor using two activated sludges with different characteristics. *J. Membr. Sci.* **2014**, *463*, 183–189. [[CrossRef](#)]
64. Tian, Y.; Chen, L.; Zhang, S.; Cao, C.; Zhang, S. Correlating membrane fouling with sludge characteristics in membrane bioreactors: An especial interest in EPS and sludge morphology analysis. *Bioresour. Technol.* **2011**, *102*, 8820–8827. [[CrossRef](#)] [[PubMed](#)]
65. Rahimi, Y.; Torabian, A.; Mehrdadi, N.; Habibi-Rezaie, M.; Pezeshk, H.; Nabi-Bidhendi, G.R. Optimizing aeration rates for minimizing membrane fouling and its effect on sludge characteristics in a moving bed membrane bioreactor. *J. Hazard. Mater.* **2011**, *186*, 1097–1102. [[CrossRef](#)] [[PubMed](#)]
66. Delrue, F.; Stricker, A.E.; Mietton-Peuchot, M.; Racault, Y. Relationships between mixed liquor properties, operating conditions and fouling on two full-scale MBR plants. *Desalination* **2011**, *272*, 9–19. [[CrossRef](#)]
67. Wang, Z.; Wu, Z.; Tang, S. Impact of temperature seasonal change on sludge characteristics and membrane fouling in a submerged membrane bioreactor. *Sep. Sci. Technol.* **2010**, *45*, 920–927. [[CrossRef](#)]

68. Li, X.F.; Zhang, L.N.; Du, G.C. Influence of sludge discharge on sludge settleability and membrane flux in a membrane bioreactor. *Environ. Technol.* **2010**, *31*, 1289–1294. [[CrossRef](#)] [[PubMed](#)]
69. Kim, D.S.; Kang, J.S.; Lee, Y.M. The Influence of Membrane Surface Properties on Fouling in a Membrane Bioreactor for Wastewater Treatment. *Sep. Sci. Technol.* **2005**, *39*, 833–854. [[CrossRef](#)]
70. Gitis, V.; Rothenberg, G. *Ceramic Membranes: New Opportunities and Practical Applications*; Wiley-VCH Verlag GmbH & Co. KGaA: Weinheim, Germany, 2016; p. 394, ISBN 978-3-527-33493-3.
71. Iversen, V. Comprehensive Assessment of Flux Enhancers in Membrane Bioreactors for Wastewater Treatment. Ph.D. Thesis, Technical University of Berlin, Berlin, Germany, 4 October 2010.
72. Yonekawa, H.; Tomita, Y.; Watanabe, Y. Behavior of micro-particles in monolith ceramic membrane filtration with pre-coagulation. *Water Sci. Technol.* **2004**, *50*, 317–325. [[CrossRef](#)] [[PubMed](#)]
73. Dickhout, J.M.; Moreno, J.; Biesheuvel, P.M.; Boels, L.; Lammertink, R.G.H.; de Vos, W.M. Produced water treatment by membranes: A review from a colloidal perspective. *J. Colloid Interface Sci.* **2017**, *487*, 523–534. [[CrossRef](#)] [[PubMed](#)]
74. Jin, L.; Ong, S.L.; Ng, H.Y. Comparison of fouling characteristics in different pore-sized submerged ceramic membrane bioreactors. *Water Res.* **2010**, *44*, 5907–5918. [[CrossRef](#)] [[PubMed](#)]
75. Meabe, E.; Lopetegui, J.; Olló, J.; Lardies, S. Ceramic Membrane Bioreactor: Potential applications and challenges for the future. In Proceedings of the MBR Asia International Conference, Kuala Lumpur, Malaysia, 25–26 April 2011.
76. Shi, X.; Tal, G.; Hankins, N.P.; Gitis, V. Fouling and cleaning of ultrafiltration membranes: A review. *J. Water Process Eng.* **2014**, *1*, 121–138. [[CrossRef](#)]
77. Wang, Z.; Ma, J.; Tang, C.Y.; Kimura, K.; Wang, Q.; Han, X. Membrane cleaning in membrane bioreactors: A review. *J. Membr. Sci.* **2014**, *468*, 276–307. [[CrossRef](#)]
78. Chen, F.; Bi, X.; Ng, H.Y. Effects of bio-carriers on membrane fouling mitigation in moving bed membrane bioreactor. *J. Membr. Sci.* **2016**, *499*, 134–142. [[CrossRef](#)]
79. Lee, S.J.; Dilaver, M.; Park, P.K.; Kim, J.H. Comparative analysis of fouling characteristics of ceramic and polymeric microfiltration membranes using filtration models. *J. Membr. Sci.* **2013**, *432*, 97–105. [[CrossRef](#)]
80. Larrea, A.; Rambor, A.; Fabiyi, M. Ten years of industrial and municipal membrane bioreactor (MBR) systems—Lessons from the field. *Water Sci. Technol.* **2014**, *70*, 279–288. [[CrossRef](#)] [[PubMed](#)]
81. Bérubé, P.R.; Hall, E.R.; Sutton, P.M. Parameters Governing Permeate Flux in an Anaerobic Membrane Bioreactor Treating Low-Strength Municipal Wastewaters: A Literature Review. *Water Environ. Res.* **2006**, *78*, 887–896. [[CrossRef](#)] [[PubMed](#)]
82. Lin, H.; Gao, W.; Meng, F.; Liao, B.-Q.; Leung, K.-T.; Zhao, L.; Chen, J.; Hong, H. Membrane Bioreactors for Industrial Wastewater Treatment: A Critical Review. *Crit. Rev. Environ. Sci. Technol.* **2012**, *42*, 677–740. [[CrossRef](#)]
83. Park, S.H.; Park, Y.G.; Lim, J.-L.; Kim, S. Evaluation of ceramic membrane applications for water treatment plants with a life cycle cost analysis. *Desalin. Water Treat.* **2015**, *54*, 973–979. [[CrossRef](#)]
84. Çiçek, N.; Franco, H.P.; Suidan, M.T.; Urbain, V.; Manem, J. Characterization and Comparison of a Membrane Bioreactor and a Conventional Activated-Sludge System in the Treatment of Wastewater Containing High-Molecular-Weight Compounds. *Water Environ. Res.* **1999**, *71*, 64–70. [[CrossRef](#)]
85. Shang, R.; Verliède, A.R.D.; Hu, J.; Heijman, S.G.J.; Rietveld, L.C. The impact of EfOM, NOM and cations on phosphate rejection by tight ceramic ultrafiltration. *Sep. Purif. Technol.* **2014**, *132*, 289–294. [[CrossRef](#)]
86. Jeong, Y.; Kim, Y.; Jin, Y.; Hong, S.; Park, C. Comparison of filtration and treatment performance between polymeric and ceramic membranes in anaerobic membrane bioreactor treatment of domestic wastewater. *Sep. Purif. Technol.* **2018**, *199*, 182–188. [[CrossRef](#)]
87. Hofs, B.; Ogier, J.; Vries, D.; Beerendonk, E.F.; Cornelissen, E.R. Comparison of ceramic and polymeric membrane permeability and fouling using surface water. *Sep. Purif. Technol.* **2011**, *79*, 365–374. [[CrossRef](#)]
88. Jeong, Y.; Cho, K.; Kwon, E.E.; Tsang, Y.F.; Rinklebe, J.; Park, C. Evaluating the feasibility of pyrophyllite-based ceramic membranes for treating domestic wastewater in anaerobic ceramic membrane bioreactors. *Chem. Eng. J.* **2017**, *328*, 567–573. [[CrossRef](#)]
89. Jeong, Y.; Lee, S.; Hong, S.; Park, C. Preparation, characterization and application of low-cost pyrophyllite-alumina composite ceramic membranes for treating low-strength domestic wastewater. *J. Membr. Sci.* **2017**, *536*, 108–115. [[CrossRef](#)]

90. Kaniganti, C.M.; Emani, S.; Thorat, P.; Uppaluri, R. Microfiltration of Synthetic Bacteria Solution Using Low Cost Ceramic Membranes. *Sep. Sci. Technol.* **2015**, *50*, 121–135. [CrossRef]
91. Li, L.; Chen, M.; Dong, Y.; Dong, X.; Cerneaux, S.; Hampshire, S.; Caoa, J.; Zhua, L.; Zhua, Z.; Liu, J. A low-cost alumina-mullite composite hollow fiber ceramic membrane fabricated via phase-inversion and sintering method. *J. Eur. Ceram. Soc.* **2016**, *36*, 2057–2066. [CrossRef]
92. Lorente-ayza, M.; Pérez-fernández, O.; Alcalá, R.; Sánchez, E.; Mestre, S.; Coronas, J.; Menéndez, M. Comparison of porosity assessment techniques for low-cost ceramic membranes. *Boletín de La Sociedad Española de Cerámica Y Vidrio* **2017**, *56*, 29–38. [CrossRef]
93. Tewari, P.K.; Singh, R.K.; Batra, V.S.; Balakrishnan, M. Membrane bioreactor (MBR) for wastewater treatment: Filtration performance evaluation of low cost polymeric and ceramic membranes. *Sep. Purif. Technol.* **2010**, *71*, 200–204. [CrossRef]
94. Chemometric Analysis for Spectroscopy. Available online: http://www.camo.com/downloads/resources/application_notes/Chemometric%20Analysis%20for%20Spectroscopy.pdf (accessed on 19 July 2018).
95. Singh, K.P.; Malik, A.; Mohan, D.; Sinha, S.; Singh, V.K. Chemometric data analysis of pollutants in wastewater—A case study. *Anal. Chim. Acta* **2005**, *532*, 15–25. [CrossRef]
96. Torgersen, G.; Rød, J.K.; Kvaal, K.; Bjerkholt, J.T.; Lindholm, O.G. Evaluating flood exposure for properties in Urban areas using a multivariate modelling technique. *Water* **2017**, *9*, 318. [CrossRef]
97. Philippe, N.; Racault, Y.; Stricker, A.E.; Spérandio, M.; Vanrolleghem, P.A. Modelling the long-term evolution of permeability in full-scale municipal MBRs: A multivariate statistical modelling approach. *Procedia Eng.* **2012**, *44*, 574–580. [CrossRef]
98. Kaneko, H.; Funatsu, K. Visualization of Models Predicting Transmembrane Pressure Jump for Membrane Bioreactor. *Ind. Eng. Chem. Res.* **2012**, *51*, 9679–9686. [CrossRef]
99. De Temmerman, L.; Naessens, W.; Maere, T.; Marsili-Libelli, S.; Villez, K.; Nopens, I.; Temmink, H.; Nopens, I. Detecting membrane fouling occurrences in a full-scale membrane bioreactor with principal component analysis. In Proceedings of the 11th IWA Conference on Instrumentation Control and Automation (ICA), Narbonne, France, 18–20 September 2013.
100. Ji, J.; Qiu, J.; Wong, F.; Li, Y. Enhancement of filterability in MBR achieved by improvement of supernatant and floc characteristics via filter aids addition. *Water Res.* **2008**, *42*, 3611–3622. [CrossRef] [PubMed]
101. Wu, J.; Huang, X. Use of ozonation to mitigate fouling in a long-term membrane bioreactor. *Bioresour. Technol.* **2010**, *101*, 6019–6027. [CrossRef] [PubMed]
102. Todt, D.; Heistad, A.; Jenssen, P.D. Load and distribution of organic matter and nutrients in a separated household wastewater stream. *Environ. Technol.* **2015**, *36*, 1584–1593. [CrossRef] [PubMed]
103. Ying, Z.; Ping, G. Effect of powdered activated carbon dosage on retarding membrane fouling in MBR. *Sep. Purif. Technol.* **2006**, *52*, 154–160. [CrossRef]
104. Judd, S. The status of membrane bioreactor technology. *Trends Biotechnol.* **2008**, *26*, 109–116. [CrossRef] [PubMed]
105. Rosenberg, M.; Gutnick, D.; Rosenberg, E. Adherence of bacteria to hydrocarbons: A simple method for measuring cell-surface hydrophobicity. *FEMS Microbiol. Lett.* **1980**, *9*, 29–33. [CrossRef]
106. Effect of MLSS on Flux—MLSS Paradox. Available online: <http://onlinemembr.info/membrane-process/effect-of-mlss-on-flux-mlss-paradox/> (accessed on 22 January 2018).
107. Brookes, A.; Judd, S.; Reid, E.; Germain, E.; Smith, S.; Alvarez-Vazquez, H.; Le-Clech, P.; Stephenson, T.; Turra, E.; Jefferson, B. Biomass characterisation in membrane bioreactors. In Proceedings of the International Membrane Science and Technology Conference (IMSTEC), Sydney, Australia, 10–14 November 2003.
108. Jefferson, B.; Brookes, A.; Le-Clech, P.; Judd, S.J. Methods for understanding organic fouling in MBRs. *Water Sci. Technol.* **2004**, *49*, 237–244. [CrossRef] [PubMed]
109. Huang, X.; Wu, J. Improvement of membrane filterability of the mixed liquor in a membrane bioreactor by ozonation. *J. Membr. Sci.* **2008**, *318*, 210–216. [CrossRef]
110. Chae, S.R.; Ahn, Y.T.; Kang, S.T.; Shin, H.S. Mitigated membrane fouling in a vertical submerged membrane bioreactor (VSMBR). *J. Membr. Sci.* **2006**, *280*, 572–581. [CrossRef]
111. Ng, H.Y.; Hermanowicz, S.W. Membrane bioreactor operation at short solids retention times: Performance and biomass characteristics. *Water Res.* **2005**, *39*, 981–992. [CrossRef] [PubMed]
112. Fan, F.; Zhou, H.; Husain, H. Identification of wastewater sludge characteristics to predict critical flux for membrane bioreactor processes. *Water Res.* **2006**, *40*, 205–212. [CrossRef] [PubMed]

113. Wu, J.; Huang, X. Effect of mixed liquor properties on fouling propensity in membrane bioreactors. *J. Membr. Sci.* **2009**, *342*, 88–96. [[CrossRef](#)]
114. Lee, W.-N.; Chang, I.-S.; Hwang, B.-K.; Park, P.-K.; Lee, C.-H.; Huang, X. Changes in biofilm architecture with addition of membrane fouling reducer in a membrane bioreactor. *Process Biochem.* **2007**, *42*, 655–661. [[CrossRef](#)]
115. Kunacheva, C.; Stuckey, D. Analytical methods for soluble microbial products (SMP) and extracellular polymers (ECP) in wastewater treatment systems: A review. *Water Res.* **2014**, *61*, 1–18. [[CrossRef](#)] [[PubMed](#)]
116. Lesjean, B.; Rosenberger, S.; Laabs, C.; Jekel, M.; Gnirss, R.; Amy, G. Correlation between membrane fouling and soluble/colloidal organic substances in membrane bioreactors for municipal wastewater treatment. *Water Sci. Technol.* **2005**, *51*, 1–8. [[CrossRef](#)] [[PubMed](#)]
117. CAMO. *The Unscrambler, Tutorials CAMO Process AS 2006*; CAMO Software AS: Oslo, Norway, 2006.
118. Deng, L.; Guo, W.; Hao Ngo, H.; Zhang, H.; Wang, J.; Li, J.; Xia, S.; Wu, Y. Biofouling and control approaches in membrane bioreactors. *Bioresour. Technol.* **2016**, *221*, 656–665. [[CrossRef](#)] [[PubMed](#)]
119. Isma Aida, M.I.; Idris, A.; Omar, R.; Razreena Putri, A.R. Effects of SRT and HRT on Treatment Performance of MBR and Membrane Fouling. *Int. J. Chem. Mol. Nucl. Mater. Metall. Eng.* **2014**, *8*, 488–492.
120. Van den Broeck, R.; Van Dierdonck, J.; Nijskens, P.; Dotremont, C.; Krzeminski, P.; van der Graaf, J.H.J.M.; van Lier, J.B.; Van Impe, J.F.M.; Smets, I.Y. The influence of solids retention time on activated sludge biofloculation and membrane fouling in a membrane bioreactor (MBR). *J. Membr. Sci.* **2012**, *401–402*, 48–55. [[CrossRef](#)]
121. Yigit, N.O.; Harman, I.; Civelekoglu, G.; Koseoglu, H.; Cicek, N.; Kitis, M. Membrane fouling in a pilot-scale submerged membrane bioreactor operated under various conditions. *Desalination* **2008**, *231*, 124–132. [[CrossRef](#)]
122. Malamis, S.; Andreadakis, A. Fractionation of proteins and carbohydrates of extracellular polymeric substances in a membrane bioreactor system. *Bioresour. Technol.* **2009**, *100*, 3350–3357. [[CrossRef](#)] [[PubMed](#)]
123. Sivchenko, N.; Kvaal, K.; Ratnaweera, H. Evaluation of image texture recognition techniques in application to wastewater coagulation. *Cogent Eng.* **2016**, *3*. [[CrossRef](#)]
124. Jiang, T.; Kennedy, M.D.; Guinzbourg, B.F.; Vanrolleghem, P.A.; Schippers, J.C. Optimising the operation of a MBR pilot plant by quantitative analysis of the membrane fouling mechanism. *Water Sci. Technol.* **2005**, *51*, 19–25. [[CrossRef](#)] [[PubMed](#)]
125. Le Clech, P.; Jefferson, B.; Chang, I.S.; Judd, S.J. Critical flux determination by the flux-step method in a submerged membrane bioreactor. *J. Membr. Sci.* **2003**, *227*, 81–93. [[CrossRef](#)]
126. Ognier, S.; Wisniewski, C.; Grasmick, A. Membrane bioreactor fouling in sub-critical filtration conditions: A local critical flux concept. *J. Membr. Sci.* **2004**, *229*, 171–177. [[CrossRef](#)]
127. Miller, D.J.; Kasemset, S.; Paul, D.R.; Freeman, B.D. Comparison of membrane fouling at constant flux and constant transmembrane pressure conditions. *J. Membr. Sci.* **2014**, *454*, 505–515. [[CrossRef](#)]



Paper III

Kulesha, O.; Maletskyi, Z.; Kvaal, K.; Ratnaweera, H. Strategy for Flux Enhancement in Biofilm Ceramic Membrane Bioreactor Applying Prepolymerized and Non - Prepolymerized Inorganic Coagulants. *Water* **2019**, *11*, 446, 1–42; DOI:10.3390/w11030446.

Article

Strategy for Flux Enhancement in Biofilm Ceramic Membrane Bioreactor Applying Prepolymerized and Non-Prepolymerized Inorganic Coagulants

Olga Kulesha ^{1,2,*} , Zakhar Maletskyi ¹ , Knut Kvaal ¹ and Harsha Ratnaweera ¹

¹ Faculty of Science and Technology (REALTEK), Norwegian University of Life Sciences, PO Box 5003, 1432 Aas, Norway; zakhar.maletskyi@nmbu.no (Z.M.); knut.kvaal@nmbu.no (K.K.); harsha.ratnaweera@nmbu.no (H.R.)

² Department of General and Inorganic Chemistry, Faculty of Chemical Technology, National Technical University of Ukraine "Igor Sikorsky Kyiv Polytechnic Institute", Peremohy 37, 03056 Kyiv, Ukraine

* Correspondence: olga.kulesha@nmbu.no; Tel.: +47-406-755-92

Received: 11 February 2019; Accepted: 22 February 2019; Published: 2 March 2019



Abstract: Considering new legislative and economic restrictions caused by the water crisis, this work focuses on a more efficient wastewater treatment process, which combines biological treatment in a moving bed biofilm system with a membrane bioreactor (BF-MBR) and coagulation, particularly addressing fouling alleviation in the separation stage. The study justifies the positive impact of coagulant dosing in BF-MBR regarding membrane flux and fouling rate. Statistical techniques connect the results of coagulation and membrane separation experiments with properties of mixed liquor, obtained after biotreatment in the representative pilot plant and characteristics of prepolymerized and non-prepolymerized inorganic coagulants. Research results substantiate the need for a pH-controlled coagulation of mixed liquor in BF-MBR depending on coagulant type, which influences charge, hydrophobicity and size of flocs and organic content of the system. It is suggested, that the adsorption/charge neutralization mechanism dominates in flux enhancement in BF-MBR, giving the best results in the case of prepolymerized aluminium coagulants. Together with high quality of permeate, the application of prepolymerized aluminium chloride of medium basicity entails a tenfold increase in filtration time of the membrane separation cycle and increases net membrane flux by 30–56%. The results of the study are practically significant for the development of an automated control system for BF-MBR, optimizing treatment rates together with membrane separation efficiency.

Keywords: biofilm membrane bioreactor; membrane fouling; coagulants; membrane flux enhancement; multivariate statistics; factorial experimental design

1. Introduction

Climate change, which is thought to be the reason for more frequent and intense droughts, results in dramatic environmental and economic consequences, entailing the losses of billions of euros [1]. As expected, this trend will continue to worsen, which, along with the gradually increasing population, will naturally deepen water stress in the European region [1]. According to estimations, by 2030, water stress and scarcity will potentially affect 50% of the river basins in Europe [2], which emphasizes the need for water reuse and the reduction of environmental impacts of wastewater treatment facilities.

Membrane bioreactor technology (MBR) is an advanced solution for water scarcity, which is gaining momentum worldwide. This tendency is mainly caused by drivers of the global MBR market such as stringent environmental legislation on wastewater discharge and reuse, water reuse advantages (resource and financial savings), beneficial application of decentralized wastewater management,

low footprint, easiness of automation, flexibility of the modular design, minimal requirements for daily supervision by the qualified staff, energy-cost efficiency and the decrease of membrane price [3–6].

However, membrane fouling deteriorates the membrane system's operation and remains a major bottleneck for MBR expansion. It is attributed to the deposition of biopolymers such as soluble microbial products (SMPs) and extracellular polymeric substances (EPSs) on the membrane surface and its pores [7–10].

Biofilm membrane bioreactor (BF-MBR) is an advanced innovation in the evolution of MBR technology, which allows reduction of membrane fouling to a certain extent and application of higher operational fluxes via the combination of a moving bed biofilm reactor (MBBR) and membrane bioreactor [11]. The MBBR part is based on the utilization of biofilm carriers at a high volumetric filling fraction (around 2/3 of the reactor volume), which are continuously suspended in the reactor by aeration [12]. Their introduction into the system minimizes the possibility of the occurrence of dead zones and creates a large contact area between the wastewater impurities and the active biomass.

According to the findings by Ivanovic and Leiknes [12], Ødegaard [13] and Phattaranawik and Leiknes [14], the biodegradation in BF-MBR is profoundly shifted towards the attached growth mechanism, which requires much lower concentrations of mixed liquor in the membrane separation part, entails lower fouling potential of mixed liquor, reduces the amount of the produced excess activated sludge and provides a resilient biological treatment.

Membrane fouling caused by the solids, colloidal matter and solutes remains a critical issue for BF-MBR, as is the case in MBR systems. The above-mentioned team indicated a higher content of the submicron particle size fraction in mixed liquor of the BF-MBR system [15], which was particularly apparent at high loading rates (high chemical oxygen demand (COD), short hydraulic retention time (HRT)) [16]. This effect is caused by a higher tendency of BF-MBR for floc breakage (deflocculation), induced by the biofilm carriers and intense aeration. It results in the production of the soluble microbial products and the particles of a diameter proportional to the membrane pore size, which tend to cause irreversible and irrecoverable membrane fouling [12,17–20].

The studies by Kulesha et al. [7] and Nouri et al. [21], reported high efficiency of chemical flux enhancement when applying inorganic coagulants in MBR, especially with regard to their flocculating ability. Therefore, application of inorganic coagulants is expected to be beneficial for the performance of the BF-MBR system, since they can aggregate fine particles generated in BF-MBR and hence, reduce permeability losses, thus contributing to steady membrane separation.

Since the attached growth part is decoupled from the MBR chamber and there is a minimum or zero demand on biomass recirculation in the BF-MBR system [3,22], the application of BF-MBR allows for using the chemical enhancement of the membrane filtration process with no concern about reducing biomass treatment potential.

Five primary mechanisms of fouling mitigation via coagulant/flocculant addition in MBR systems have been identified [7,23–25]: (1) enhancement of adsorption/charge neutralization, (2) the increase of relative hydrophobicity of the flocules, (3) the increase of the mean flocule size, (4) the reduction of the SMPs level in mixed liquor/decrease of supernatant organic concentration and (5) inhibition of gel layer formation and the reduction of specific cake layer resistance. However, the principal mechanisms and effects of coagulant action with respect to membrane fouling alleviation in the biofilm membrane bioreactor (BF-MBR) system are still unclear.

The following parameters of mixed liquor were found to be fundamental for the characterization of its fouling propensity and the mechanisms of fouling mitigation during chemical flux enhancement in MBR/BF-MBR: electrokinetic potential (ζ -potential), relative hydrophobicity (RH) of the flocs, the mean particle size or particle size distribution, chemical oxygen demand (COD) and mixed liquor suspended solids (MLSS) [15,16,26–28].

A successful application of Me-based coagulants for membrane fouling mitigation in MBR systems was admitted by different research groups [21,29–34]. Meanwhile, a limited number of studies can be found on chemical flux enhancement via coagulant addition in BF-MBR [22,35].

The prepolymerized aluminium coagulants have several advantages over non-prepolymerized Al- and Fe-based coagulants in the coagulation process; and likewise in membrane filtration systems—enhanced adsorption/charge neutralization potential, less alkalinity consumption (pH drop) for a given Me-dose, lower sensitivity to low temperatures and broader operational pH range [36,37]. Better performance of the prepolymerized aluminium chloride (PACl) in the MBR system was observed by Wu et al. [38] and Chen and Liu [39]. On the other hand, some research works reported a superior flux enhancement potential of non-prepolymerized Me-based coagulants in comparison to their prepolymerized counterparts [22,40]. The mechanisms behind the observed differences in coagulant performance are not well understood. There is a variety of PACl commercial products, with the variation in composition, depending on the supplier. It would be necessary to underline the governing mechanisms of membrane fouling mitigation by Me-based coagulants to select the optimum flux enhancer or compound basicity (in case PACl shows the highest fouling mitigation propensity).

The purpose of the current research is to present a viable concept of membrane fouling alleviation and optimization of membrane filtration based on a systematic comparative study of prepolymerized and non-prepolymerized inorganic coagulants, delving into the mechanisms of flux enhancement by applying chemometric analysis of the resulting membrane fouling mitigation patterns in the BF-MBR.

2. Materials and Methods

Prepolymerized aluminium coagulants have a highly specific nature and the characteristics of the commercial products vary with the supplier. On the other hand, the treated mixed liquor quality can vary depending on the feeding wastewater, system design and location of the facilities. Thus the optimum coagulation conditions for a particular mixed liquor system are case specific and need to be determined via the jar tests [41].

The following sequential strategy was developed to conduct a holistic assessment of the Al- and Fe-based coagulants as membrane flux enhancers for the BF-MBR system:

- (1) the selection of the optimum pH at constant coagulant dosage for every tested coagulant during the jar tests;
- (2) the jar tests, conducted at previously determined optimum pH for every coagulant, with the variation of the coagulant dose, to determine the relevant optimum dosage ranges;
- (3) the total recycle test (TRT), with the pH correction and the application of the tested dosage ranges (depending on the coagulant), which exhibited promising results during the jar tests, to determine the optimum fouling mitigation conditions and the most efficient compound;
- (4) the TRT without the pH correction, to assess the coagulant performance regarding fouling mitigation under the conditions, unfavourable for coagulation;
- (5) partial least squares analysis using the data from the TRT, with and without pH correction, to study the effect of the selected mixed liquor characteristics on the fouling intensity after the chemical dosing and determine the principal mechanisms of coagulant action;
- (6) the determination of the intrinsic coagulant charges and the qualitative analysis of the investigated prepolymerized aluminium coagulants regarding their molecular weight (MW) distribution;
- (7) two-level factorial design of the experiment, applying the selected coagulant of the highest performance, to determine the optimum levels of factors for the maximum permeability/filtration time increase, discover the vital factors for the membrane flux enhancement and the tendencies in their interactions.

2.1. Study Object

Mixed Liquor (ML) for laboratory experiments was supplied by the aerobic BF-MBR pilot system, described in previous work by this team [42]. This decision was made to ensure high reproducibility and accuracy of results, which were intended to be further implemented at the mentioned pilot plant

facility and to have a source of representative mixed liquor, since the experimental laboratory setup, based on TRT, does not reproduce the biodegradation stage (MBBR) of the BF-MBR system.

The pilot system worked at solids retention time (SRT) 20 days, treating daily 0.3 m³ of wastewater from the source-separated sewer network. The feeding inlet was the mixture of black to grey wastewater at the ratio 1:9 (MLSS 0.4–1.31 g/L, COD 142–262 mg-O₂/L, PO₄-P 6.08–10.28 ppm). Air was continuously supplied at the rate 60 L/min by the air compressor MEDO LA-60E (Nitto Kohki®, Nitto Kohki Co., Ltd, Tokyo, Japan). Initial biological activity in the system was provided by inoculation with sludge from the municipal MBBR wastewater treatment plant (BEVAS, Oslo, Norway).

Four chemically different Al- and Fe-based membrane flux enhancers (MFEs) were selected for this study: non-prepolymerized aluminium and iron (III) sulphate and two prepolymerized aluminium coagulants with different basicity (Table 1). The applied coagulants are available from commercial suppliers by active compound name and metal content. Products of Kemira Chemicals AS (Helsinki, Finland) were used in this study.

Table 1. Properties of Membrane Flux Enhancers.

Designation	Active Compound	Metal Content, %	Basicity (OH/Me)	Density (20 °C), g/cm ³	pH
PAX18	[AlCl(OH)] _n	9.0 ± 0.2%	42.0 ± 2% (1.3)	1.37 ± 0.03	0.6
PAXXL61	Al(OH) _x Cl _(3-x-2y) (SiO ₂) _y	5.4 ± 0.3%	68.0 ± 5 % (1.9)	1.26 ± 0.03	2.7
ALS	Al ₂ (SO ₄) ₃	4.3 ± 0.1%	- (0)	1.33 ± 0.01	1.8
PIX313	Fe ₂ (SO ₄) ₃	11.6 ± 0.4%	- (0)	1.52 ± 0.06	<0.5

The correction of the pH values in mixed liquor before and during coagulation was performed with the aid of 0.01N NaOH in the case of aluminium coagulants and 0.1 N NaOH when applying iron (III) sulphate due to the higher tendency of the system for pH decrease in the latter case.

2.2. Jar Tests

After the selection of the proper chemicals, the adapted jar tests were used to simulate their application for the coagulation-flocculation in the separation chamber of the BF-MBR. The use of jar tests helped to accelerate and simplify the determination of the optimum conditions: pH and dosages. For this purpose, the Flocculator 2000 from Kemira Chemicals AS and 1 L beakers were used.

The following mixing conditions were applied during coagulation: 1 min rapid mixing (400 RPM), 10 min slow mixing (30 RPM), followed by 20 min of sedimentation with no mixing.

2.3. Total Recycle Test

The testing of a batch-type MBR in the total recycle mode for membrane fouling mitigation has been recently practiced in several studies [43–45]. It implies a continuous recycling of the whole permeate volume back to the membrane reactor during the experiment. The total recycle test (TRT) allows the experiment to maintain a stable content and volume of the coagulated mixed liquor during the filtration cycle, preventing the introduction of raw, untreated portions of mixed liquor into the system with already added flux enhancers, which could potentially cause high bias in the experiments. In the studies on the use of quorum sensing and quorum quenching to mitigate membrane fouling, TRT is also beneficial due to the maintaining of the effective concentration of the active enzyme throughout the system operation.

Prior to the filtration experiments, the integrity of the membrane sheets was evaluated through the bubble point test and the vacuum decay test via method F 316-03 (Reapproved 2011) and method D 6908-03, respectively, according to the American Society for Testing and Materials. Both tests are based on the determination of the diameter of the pore or defect calculated from its bubble point.

Total recycle tests (TRTs) were conducted in a plastic transparent 2.8 L MBR reactor, where the flat-sheet ceramic membrane was submerged with a provided cross-flow aeration (Figure 1).

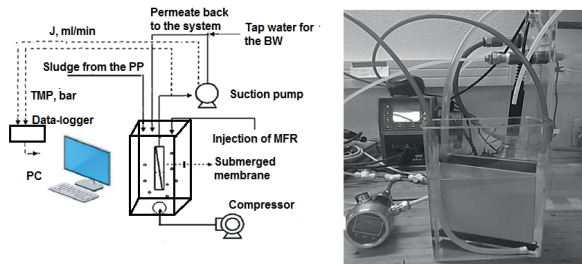


Figure 1. The total recycle test system, adapted from [43].

SiC microfiltration membrane sheets with 0.1 μm nominal pore size and surface areas of 0.0374 and 0.0355 m² were used for these studies (Cembrane, Lyngø, Denmark). The vacuum was applied to the submerged membrane using a Qdos30 peristaltic metering pump. The separation process was carried out under constant flux conditions (80 LMH) with the recycling of all the filtrate to the source container. The pressure in the vacuum line was measured with an electronic pressure transducer (Klay 8000 series) and recorded into the laboratory data-logger. Recycling continued until the TMP reached a critical level of 1.2 times from TMP_{in} (initial transmembrane pressure) but not less than 1010 s. Filtration Time (F) was chosen as one of the fouling indicators during the membrane filtration experiments. Filtration time is the time required for reaching 1.2 × TMP_{in}. Coagulants were added to ML before membrane filtration and intensively mixed, applying aeration during 30 s. After this time, the aeration was turned off and the membrane system remained in the relaxation mode for 90 s more. Then, the aeration was turned on and the filtration started (Figure 2).

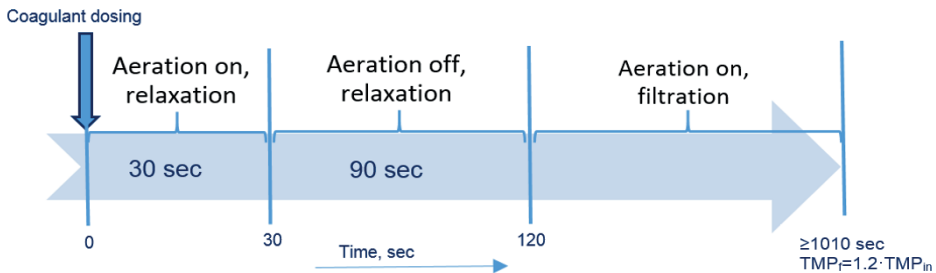


Figure 2. Experimental conditions of the total recycle test.

Ten minutes after the chemical dosing, the first sampling was performed in a quantity of 200 mL to keep the membrane fully submerged in the ML solution. 60 mL of this sample were used to measure MLSS, residual aluminium, PO₄-P and the particle size parameters. The rest of the ML was used for the measurement of electrokinetic potential and turbidity.

When TMP increased to the level of 1.2 × TMP_{in} and more than 1010 sec elapsed after the chemical dosing, the filtration was stopped and the specimens were taken.

Permeability was the other targeted fouling indicator, which was determined using the flux, normalized to 20 °C (Equation (1)).

$$P_N = \frac{J \cdot e^{(-0.032 \cdot (t-20))}}{TMP} \tag{1}$$

where J is a membrane flux, LMH; TMP is a transmembrane pressure, bar; t is an actual temperature of the experiment, °C.

The current research uses capillary suction time (CST) to express relative hydrophobicity. The negative correlation between them is demonstrated in the discussion section of this work.

At the end of filtration, mixed liquor was used for the measurement of capillary suction time (CST) and Time-to-Filter (TTF).

2.4. Applied Analytical Techniques

2.4.1. Mixed Liquor Analysis

Mixed liquor suspended solids (MLSS), capillary suction time (CST) and Time-to-Filter (TTF) were determined via the dry residue test 2540 D, CST test 2710 G and Time-to-Filter test 2710 H, respectively, according to SMWW (Standard Methods for the Examination of Water and Wastewater, 22nd edition).

Prior to the measurement of turbidity and zeta potential, the supernatant of the mixed liquor samples was filtered through the quantitative cellulose filter paper with the pore size 8–12 μm (Grade MN 640 md, Macherey-Nagel™, MACHEREY-NAGEL GmbH & Co. KG, Düren, Germany).

Electrokinetic potential (ζ -potential) was determined through the measurement of electrophoretic mobility and the automatic derivation of ζ -potential, according to Henry's equation under Zetasizer Nano-Z (Malvern™, Malvern Panalytical Ltd, Malvern, UK).

Turbidity was measured under HACH 2100 N IS Turbidimeter, according to ISO method 7027.

COD_{dis} was measured by the COD-cuvette test (HACH, Manchester, UK), applying the dichromate method, according to ISO 15705:2002 [46].

Orthophosphates (PO₄-P) and residual aluminium were measured using the EasyChem Plus colorimetric analyser (Systea™, Systea S.p.A., Anagni, Italy), in accordance with the automated colorimetric method, USEPA Method 365.1 and automated colorimetric Eriochrome Cyanine R method, respectively.

Determination of the particle size distribution was conducted in several steps. First, the acquisition of the images under a light microscope (Leica DM 6B) was performed with the camera Leica DMC4500 (90 \times magnification), which transmitted the images to the computer. For every image, the 2544 \times 1816 pixel area was cropped by manual investigation of the area, followed by further image processing using ImageJ software [47] (Figure 3).

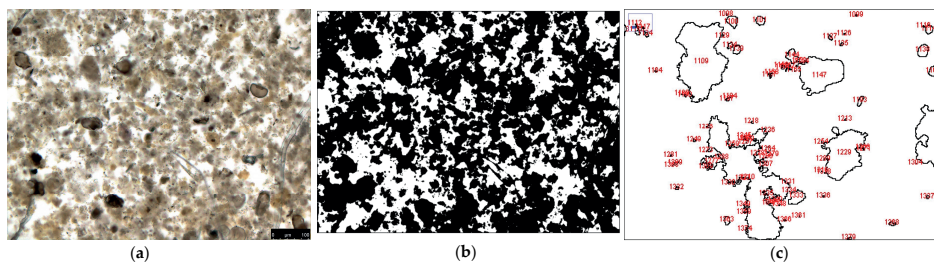


Figure 3. Determination of the particle size by image processing and analysis: (a) the original sample image, acquired under the light microscope; (b) the sample image after the adjusted threshold; (c) 200% magnified area in the image after particle analysis.

Then, the acquired particle areas were recalculated to the diameters, which were used as the basis for the cumulative distribution plot.

The determination of the particle size distribution (PSD) parameters, specified in Table S1 [48–52], helped to quantify and interpret the image analysis data.

2.4.2. Intrinsic Characteristics of the Coagulants

Potentiometric Titration

A streaming current detector (Micrometrix®, Micrometrix Corporation, Atlanta, Georgia, USA), connected to the automatic titrator (EasyPlus™, Mettler Toledo, Columbus, Ohio, USA), was used

for determination of the charges of the tested coagulants as well as for potentiometric titration of the mixed liquor samples.

For the coagulant charge determination, Potassium Polyvinyl Sulphate (PVSK) was used as a standard anionic polymer, while Methyl Glycol Chitosan (MGC)—as a standard cationic polymer. Both standard polymers were accurately prepared to the concentration 0.0005 N from the commercial colloidal titration solutions using 0.0025N PVSK and 0.005N MGC supplied by Wako® (FUJIFILM Wako Chemicals Europe GmbH, Neuss, Germany). PVSK was chosen to be a reference standard and MGC concentration was adjusted to equate to PVSK at pH 7. The ratio factor of polymers was determined at pH 7 and the working pH 1.86, 2.12, 2.3 and 2.7, which were selected according to the intrinsic pH values of the subsequently tested coagulants (Table 1).

Charges of the tested coagulants (1 mmol Me/L) were determined through the potentiometric back titration. At least two parallel measurements were conducted for every coagulant sample. The cationic charge concentration of every coagulant was calculated according to the following formula [53]:

$$\text{Charge concentration} = \frac{\left(\frac{V_{\text{PVSK}} \cdot F - \overline{V}_{\text{MGC}}}{V_{\text{aliquot}}} \cdot 0.0005 \frac{\text{equiv}}{\text{L}} \cdot 10^6 \right)}{m_{\text{salt}} / \text{L}}, \quad (2)$$

where *Charge concentration* is the determined concentration of the positively charged ions in the coagulant sample, $\mu\text{equiv}/\text{mg}_{\text{salt}}$; m_{salt} is mass of the coagulant salt in 1 L, V_{PVSK} is the known added volume of PVSK, mL; F is correction factor; $\overline{V}_{\text{MGC}}$ is the average volume of MGC, mL; 0.0005 is normality of the titrant standard equal to the gram equivalent weight of a solute per litre of solution equiv/L; V_{aliquot} is the aliquot value of the titrated sample, mL.

Potentiometric direct titration of mixed liquor, applying investigated coagulants as titrants, was performed using the specimens, sampled on the same day for all the coagulants. The coagulants were applied as titrants with no dilution. A minimum of two parallel measurements were conducted for every coagulant.

Size Exclusion Chromatography

A total of 25 g of Bio-Gel P-100 Gel (Bio-Rad Laboratories™, Bio-Rad Laboratories, Hercules, California, USA) (medium polyacrylamide beads with wet bead size 90–180 μm , fractionation range 5000–100,000 MW) were suspended in 800 mL of distilled water and allowed to swell overnight. The swollen beads were put into a glass preparative chromatography column (Omnifit®, Diba Industries Inc., Danbury, CT, USA) (1.5 cm in diameter, 48 cm in length, working volume 78.6 mL), equipped with a PTFE/polyethylene frits, allowed to settle and washed with five bed volumes of the eluent–NaCl solution (0.5 mol/L, pH 2–2.7) until a constant height (44.5 cm) was obtained. 1 mL of the prepolymerized aluminium coagulant (PAXXL61 (2.52 mol Al/L) or PAX18 (4.57 mol Al/L)) were injected in the gel column and eluted at 0.7 mL/min, using an LC pump Perkin-Elmer Series 410 to control the elution rate. The fractions were further collected in the disposable sample cuvettes and assayed for total aluminium according to Eriochrome Cyanine R method [54] at appropriate points, using EasyChem Plus colorimetric analyser (Systea™, Systea S.p.A., Anagni, Italy).

For all separations, the same column was used. Before each experiment, gel was conditioned by at least 500 mL of the NaCl solution to wash out residual monomeric aluminium.

2.5. Statistical Mining of the Relationships in the System

In the current investigation, multivariate chemometric approach based on partial least squares analysis (PLS), that is, PLS-regression (PLSR), was applied to distinguish the relationships between the dose of the coagulant, the mixed liquor parameters and the fouling indicators during the Total Recycle Test.

PLS analysis is a multiple linear regression technique, which simultaneously models the matrices of the predictor variables and responses to find the hidden variables in X that will predict the

latent variables in Y. The creation of new predictor variables and responses, which are the weighted combinations of the raw variables, is accomplished through the following steps: (1) extraction of x-scores (t), that are the most correlated to Y; (2) generation of Y-loadings (q) from (t); (3) calculation of Y-scores (u) from (q); (4) plotting (t) and (u) together with the maximized covariance [55].

Due to the creation of the orthonormal weight loadings and the loadings, which are neither orthogonal nor normalized, PLS explains the maximum variance in the original data matrix X and meanwhile provides the maximum correlation between X and the vector of output variables y_n [56]. PLS analysis makes it possible to determine the independent influence of each input variable even if the analysed data is strongly collinear and noisy. Besides, PLS gives an opportunity to model a big number of X-variables with the simultaneous modelling of several response variables, Y [57,58].

The Unscrambler[®] X10.3 (CAMO Software AS, Oslo, Norway) was used to analyse the monitored data. Design-Expert[®] 10 software (Stat-Ease, Inc., Minneapolis, MN, USA) was used to build and analyse factorial experimental design.

3. Results

3.1. Jar Tests

Coagulant efficiency highly depends on the pH of the solution. It is the most critical parameter since it determines the charge of the colloidal impurities and the dominance of certain competitive hydrolysis reactions and hence, the nature of polymeric hydrolysis species [59–61]. According to Ratnaweera [60], the hydrolysis reaction is much faster than the pH correction procedure, using the typical laboratory equipment, which results in the discrepancy between the measured pH after coagulation and the actual pH of the hydrolysis. Hence, it was decided to adjust the pH of the mixed liquor solution mainly before the coagulant dosing. However, the pH adjustment during the coagulation process was also included when the pH decreases during coagulation exceeded 0.5 units.

It was decided to test a different down limit of pH values for PIX313 in comparison to that of the aluminium coagulants, taking into consideration the following findings by Stumm and Morgan [61], further developed by Bratby [59]:

- (1) The ligands, which are representative of ionogenic functional groups and characteristic of the hydrophilic colloids (proteins, polysaccharides and humic substances), such as phosphate, pyrophosphate, oxalate, salicylate (with a carboxyl and an aromatic hydroxyl group), show the tendency to displace the H_2O groups in aquo-metal ions of the coagulant, which satisfies the coordinative requirements of Fe(III) and Al(III), which results in the formation of the Me-ligand complexes;
- (2) OH^- ions have a stronger affinity for the Fe^{3+} and Al^{3+} than other ligands, including the representative of functional groups of colloids; however, the latter may compete with OH^- for the coordinative sites;
- (3) When the ratio ligand/ OH^- increases, which can be reached by pH decrease in the system, ligands, which originate from the functional groups, may partially or entirely substitute for OH^- in the charge neutralization of the metal cations;
- (4) Fe^{3+} has a higher affinity for OH^- than Al^{3+} ; thus, lower pH is required for the formation of ionized function group-Me complexes to limit the statistical opportunity of the complexation of OH^- .

The application of lower pH values for the iron (III) coagulant can also be justified by the diagrams with equilibrium-solubility domains concerning $Fe(OH)_3$ and $Al(OH)_3$ in water as a result of hydrolysis of $Fe(H_2O)_6^{3+}$ and $Al(H_2O)_6^{3+}$, which were introduced by Stumm and O'Melia [62]. According to the diagrams, the iron (III) hydroxo- and polyhydroxy complexes form at lower pH values and wider pH range compared to their aluminium-based counterparts. As specified by Meyn et al. [63], iron (III) complexes, formed at a lower pH, provide higher removal of organic matter, than those which occur at a higher pH.

It is worth noting that, according to Liang et al. [64], the presence of sulphate ion in the skeleton of coagulants shifts their applicable coagulation pH towards the acidic regions, which enables efficient coagulation-flocculation at lower pH than for the species with chloride or nitrate ions in the coordination sphere.

The determination of the optimum pH for the applied coagulants, using the mixed liquor samples, was further conducted (Figure 4). The coagulant dosage is expressed by mixed liquor concentration as $\mu\text{mol Me per mg}$ of suspended solids (SS). It was decided to apply lower dosages: $0.4 \mu\text{mol Al/mg SS}$ of aluminium-based coagulants and $0.9 \mu\text{mol Fe/mg SS}$ of iron (III) sulphate, which would not sharply reduce pH of the solution, consequently, to avoid adding excessive amounts of NaOH and to simplify the maintenance of the desired pH values.

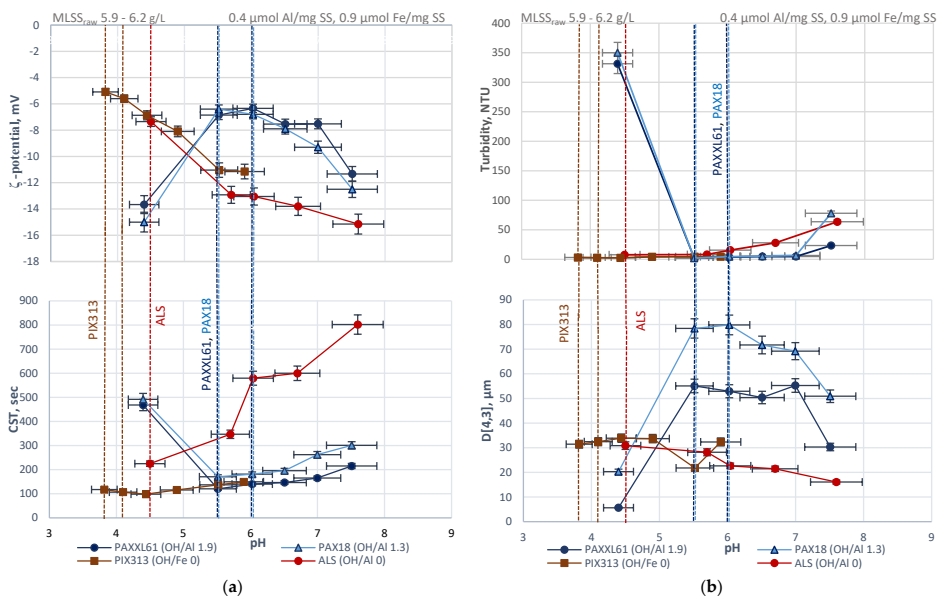


Figure 4. Determination of the optimum pH at fixed coagulant dose during the jar tests according to: (a) zeta potential, capillary suction time (CST); (b) turbidity, the volume moment mean.

Zeta potential profiles demonstrate the nature and intensity of electrostatic interactions between the flux enhancing additives and the negatively charged foulants in the system [65].

Zeta potential (ζ -potential) is the electrokinetic potential at the slip plane between the Stern Layer and the diffuse layer, which is related to the electrophoretic mobility of the particle, according to the Henry equation and is one of the main double layer characteristics in the charged colloid. Zeta potential characterizes the resistance of the colloidal system to aggregation and provides a quantification of the double layer capacity.

If $|\zeta| \geq 30.0 \text{ mV}$, the disperse system is sufficiently stable and no coagulation is observed. According to the classification, introduced by American Water College [66], the average zeta potential equal to -20.0 – $(-11.0) \text{ mV}$ refers to poor coagulation degree, -10.0 – $(-5.0) \text{ mV}$ to fair coagulation degree, -4.0 – $(-1.0) \text{ mV}$ to excellent coagulation degree and 0.0 – 3.0 mV refers to maximum coagulation degree.

According to the represented profiles (Figure 4), the maintenance of pH at 5.5–6.0 during the application of the prepolymerized aluminium coagulants, characterized by high and medium basicity, provided the maximum degree of destabilization of the mixed liquor suspension at the selected dosage. At pH 5.5–6, zeta potential values for PAXXL61 and PAX18 were in the range: -6.9 – $(-6.3) \text{ mV}$ and

−6.8(−6.4) mV, respectively, resulting in the lowest residual turbidity among the tested pH values: 2.5–3.9 NTU and 2.0 and 4.6 NTU, respectively, which indicates the highest coagulation efficiency under the applied conditions. According to the CST plots, pH values 5.5–6.0 also favoured the highest mixed liquor dewaterability and, hence, the highest relative hydrophobicity of the flocs in this set of experiments. The results on the volume moment mean particle size showed that the defined pH range for the prepolymerized aluminium coagulants provided the maximum sizes of the flocules: 53.0–55.0 μm and 78.0–79.8 μm for PAXXL61 and PAX18, respectively.

Meanwhile, the optimum pH values for non-prepolymerized aluminium and iron (III) coagulants were found to be lower than for the prepolymerized aluminium coagulants; they were equal to 4.5 and 3.8–4.1, respectively. The defined pH values for ALS and PIX313 provided the maximum absolute zeta potential levels: −7.4 mV and −5.6(−5.1) mV, respectively; high extent of dewaterability—225.0 s and 107.0–117.5 s, respectively; and relatively large volume moment mean particle size—30.9 μm and 31.4–32.5 μm , respectively, in comparison to the other tested pH values under the maintained conditions.

More detailed data is provided in Table S2.

The required pH around 3.8–4.1 for iron (III) sulphate coagulant, which is more acidic than for the aluminium coagulant, is consistent with the findings by other studies [63,67].

To sum up, the determined optimum pH values foster the enhancement of adsorption/charge neutralization, the increase of relative hydrophobicity of the flocs and the increase of the particle size, which are assumed to be representative indicators of the fouling potential of mixed liquor, whose characteristics are modified with the coagulants.

The next stage was the determination of the optimum coagulant dose, maintaining the established levels of the optimum pH in the system. The obtained results of the relevant jar tests are represented in Figure 5.

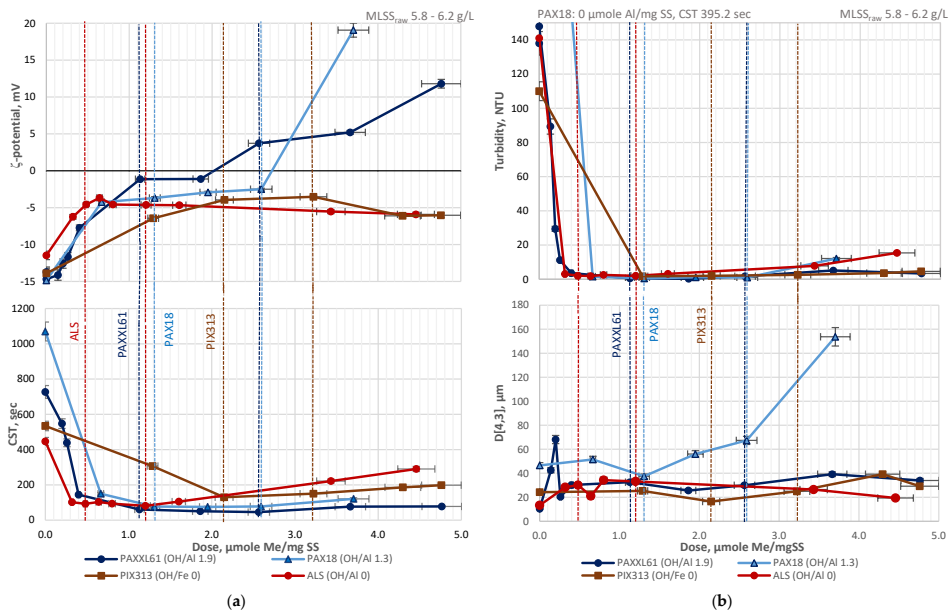


Figure 5. Influence of the coagulant dose on the monitored parameters at fixed pH during the jar tests: (a) zeta potential, capillary suction time (CST); (b) turbidity, the volume moment mean.

Jar tests allowed the team to determine the dosage conditions that promoted the maximum increase of relative hydrophobicity of the flocs, the reduction of the absolute zeta potential value, the

decrease of turbidity and the increase of the mean particle size (expressed through the volume moment mean), which is summarized in Table S3.

The acquired zeta potential profiles (Figure 5a) demonstrate that merely prepolymerized aluminium coagulants provided complete neutralization of mixed liquor, which indicates their higher charges in comparison to their non-prepolymerized counterparts. Both PAXXL61 and PAX18 assured the maximum coagulation degree (0.0–3.0 mV). It is worth noting that high neutralization potential of prepolymerized aluminium coagulants can result in their tendency to overcompensate the particle charges with the subsequent recharging of the system (ζ -potential = 5.0 mV or higher) and its restabilisation, which is observed at the dosages higher than 4.8 $\mu\text{molAl}/\text{mgSS}$ for PAXXL61 and 3.7 $\mu\text{molAl}/\text{mgSS}$ for PAX18. System restabilisation is undesirable since it worsens flocculation of the particles, deteriorates the treatment efficiency, entails additional costs of reagents and can have a detrimental effect on the aquatic fauna after wastewater discharge due to the risk of high residual aluminium concentrations [68,69].

Therefore, a defined range of optimum dosages should be further applied.

According to the results (Figure 5a) for non-prepolymerized aluminium and iron (III) sulphate coagulants, zeta potential remains negative over the whole dosage range. Neither of the non-prepolymerized coagulants was able to reach the maximum degree of coagulation (0.0–3.0 mV) but attained rather fair (−10.0–(−5.0) mV) and in single cases—excellent (−4.0–(−1.0) mV) degree, which is an indicator of weaker charge neutralization capacity possessed by these coagulants. As assumed by Gregory and Duan [37], the coagulation in this region of zeta potential values occurs entirely via the adsorption of suspended matter on the precipitated $\text{Al}(\text{OH})_3$.

Meanwhile, the obtained plots demonstrate, that the overdosing of ALS and PIX313 can still cause the deterioration of the mixed liquor system, which is observed by the elevated levels of turbidity, CST and the decrease of the volume moment mean particle size, which is clearly observed at 3.4–4.5 $\mu\text{molAl}/\text{mgSS}$ and 4.8 $\mu\text{molFe}/\text{mgSS}$.

All of the investigated coagulants are highly efficient with respect to colloidal matter removal, which is indicated by low values of the final turbidity—0.5–2.6 NTU (Figure 5b). Hence, good coagulation performance is achieved for every coagulant in the defined optimum dosage regions.

The character of the CST graphs points out that the studied coagulants highly reduce the affinity of the mixed liquor particles for water, thus increasing their hydrophobicity, the ability to aggregate and settle [70,71] and decreasing their potential to attach to the hydrophilic membrane surface.

Particle size analysis (Figure 5b) demonstrates that the prepolymerized aluminium chloride with medium basicity PAX18 exhibited the greatest flocculation ability among all studied coagulants, which was particularly apparent in the range of dosages 2.0–3.7 $\mu\text{molAl}/\text{mgSS}$, when the volume moment mean, $D[4,3]$, reached 56.0–153.7 μm . The second-highest particle size 42.0–68.0 μm was attained, applying prepolymerized aluminium chloride with high basicity PAXXL61. However, its increase with the dosage was not as continuous as in the case of its counterpart with lower basicity and is characteristic merely for the narrow range of dosages 0.1–0.2 $\mu\text{molAl}/\text{mgSS}$. Concerning non-prepolymerized inorganic coagulants, their flocculating efficiency was not so pronounced, since the particle sizes underwent merely minor changes. Better performance of prepolymerized aluminium coagulants can be explained by their higher charge, which results in enhanced adsorption-charge neutralization of the mixed liquor particles [36,38] and higher sensitivity of the Al hydrolysis species, which originated from the non-prepolymerized coagulants, to mixing conditions [72].

According to Figure 5, prepolymerized aluminium coagulants exhibit fairly broad ranges of optimum dosages in comparison to the non-prepolymerized coagulants, which agrees with the previous findings [36].

As a result, optimum pH values and the optimum coagulant dosages were determined and established as the point of reference for the subsequently conducted total recycle test.

3.2. Total Recycle Test

According to the assessment of the integrity of the membrane sheets, the minimum diameter of the defects on the membrane surfaces ranged from 10.2 to 17.0 μm . Those sheets, characterized by a significant difference between the openings in the membranes ($\Delta_{\text{max}} = 5.5 \mu\text{m}$), were excluded from further experiments in order to eliminate the membrane factor from the potential influences affecting the difference in fouling intensity during the experiments.

The TRT was used to estimate the coagulant performance in the BF-MBR system and to validate the selected fouling indicators as regards their ability to demonstrate the fouling propensity of mixed liquor.

For every sample, the average normalized permeability values were calculated as follows:

$$\text{av}P_N = \overline{P_{N_n}^{\text{in}}}; \overline{P_{N_m}^{\text{fin}}} \quad (3)$$

where N is the number of values taken into consideration, $N = 10$; $\overline{P_{N_n}^{\text{in}}}$ is the mean of the first ten values ($n \approx 210\text{--}400$ s from the beginning of the filtration) of the normalized permeability, excluding the ramp of the peristaltic pump; $\overline{P_{N_m}^{\text{fin}}}$ is the mean of the ten final values ($m \approx 790\text{--}1010$ s from the beginning of the filtration) of the normalized permeability at the end of the filtration cycle.

For this purpose, a steep phase of the normalized permeability (P_N) development over time was chosen, followed by the calculation of the average normalized permeability ($\text{av}P_N$) within the range, that covered the initial rapid flux decline stage—seconds no. 210–1010 (Figure 6a). The selected array of values is related to conditioning fouling, which is characterized by pore blocking and adsorption of the SMPs on the membrane [73].

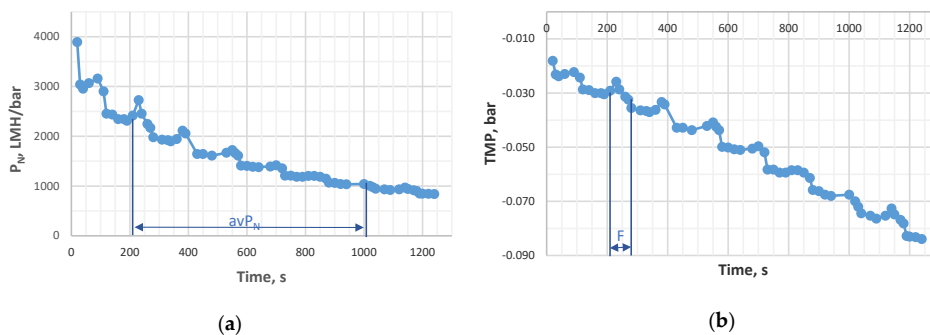


Figure 6. Average normalized permeability (a) and filtration time (b), determined from the total recycle test.

Filtration Time (FT) was calculated from the logged $\text{TMP} = f(\text{time})$ (Figure 6b).

The steep development of the trend $\text{TMP} = f(\text{time})$ in Figure 6b can be explained by the fact, that the graph represents the data of the raw sludge filtration, characterized by a rapid TMP increase. It is worth noting that the constant flux of the filtration during all the experiments equal to 80 LMH lies in the critical flux region, which was intentionally selected after the critical flux experiments, using raw mixed liquor, based on the flux-step method [74], to estimate the coagulant performance in subsequent experiments under conditions unfavourable for membrane filtration.

Optimum pH values and dosage ranges, determined during the jar tests (Tables S2 and S3), were applied during the total recycle tests. The obtained results, related to the monitoring of the traditional parameters of wastewater treatment quality, are demonstrated in Figure 7.

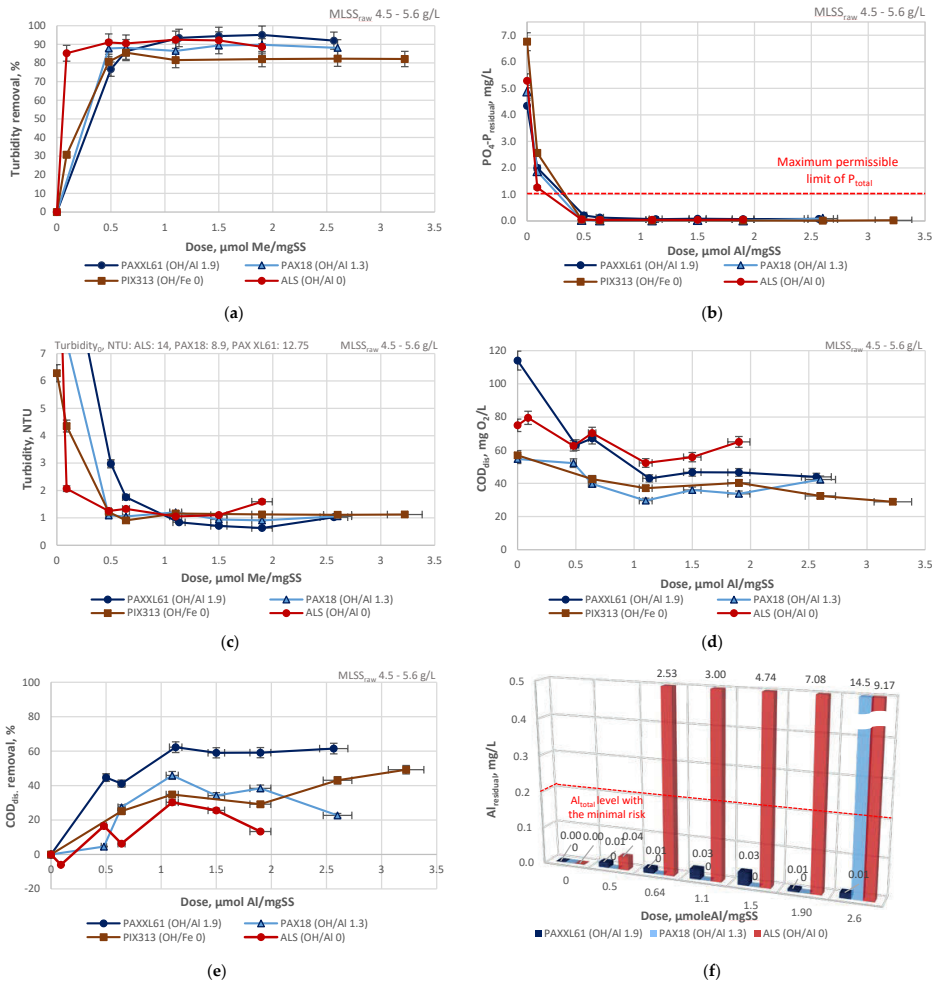


Figure 7. Influence of the coagulant dose on the parameters of treatment efficiency at fixed pH during the total recycle test (TRT): (a) turbidity removal; (b) residual orthophosphates; (c) turbidity, (d) dissolved COD (COD_{dis}); (e) COD_{dis} removal; (f) residual aluminium.

As shown in the graphs (Figure 7a,b), at 0.6 µmole Me/mgSS all the coagulants provide high effluent quality with respect to turbidity removal and residual orthophosphate concentration: 85.5–90.5% and 0.01–0.13 mg P-PO₄/L, respectively. The maximum permissible limit for total Phosphorus in the effluent of WWTP is 1.0 mg P_{total}/L [75]. Hence, all the coagulants provide the effluent quality in compliance with the regulations. The high potential for orthophosphate removal, exhibited by both prepolymerized and non-prepolymerized coagulants at the selected dosage ranges, agrees with the results acquired by Ødegaard et al. [36] and Ratnaweera et al. [76].

According to the turbidity removal plot (Figure 7a), the coagulant with high basicity PAXXL61 provides the highest performance, which agrees with previous works [76].

The comparison of turbidity and COD_{dis} profiles (Figure 7c,d) shows that the restabilisation in the samples applying PAX18 and ALS, which occurs at the dosage 2.6 and 1.9 µmolAl/mgSS, respectively, is equally pronounced in the COD_{dis} and turbidity analysis. This observation indicates that the colloidal particles ≤ 0.45 µm were not transferred to the higher size fraction ≥ 1 µm at

overdosing. In contrast, in the case of PAXXL61, lower residual COD concentration is observed at the overdosing (2.6 $\mu\text{mol Al/mgSS}$), even though the turbidity profile shows the tendency to increase, which apparently is an indicator that PAXXL61 (the coagulant with the highest tested basicity) is responsible for the enlargement of the fine colloidal particles to the size $\geq 1 \mu\text{m}$ at high dosages.

The increase of residual COD_{dis} in the overdosing region for PAX18 could be the result of floc breakage or the formation of some Al-organic complexes and for ALS, probably the Al-organic complex formation, which corresponds to the findings by Zhang et al. [77].

PIX 313 demonstrated, similar to PAXXL61, behaviour in the overdosing region but with a lower treatment efficiency with regard to the removal of COD_{dis} and turbidity. At 5.2 $\mu\text{mol Fe/mgSS}$ (not shown on the graphs) the COD_{dis} removal ($\delta\text{COD}_{\text{dis}}$) increased to 51%, while the residual turbidity increased by 23% in comparison to the relevant values at the dosage 3.2 $\mu\text{mol Fe/mgSS}$, which suggests an improved flocculation of the fine colloids ($\leq 0.45 \mu\text{m}$).

The maximum COD_{dis} removal in the dosage range 0.6–1.9 $\mu\text{mol Me/mgSS}$, was observed for both prepolymerized aluminium coagulants, PAXXL61 and PAX18, being in the range 41–62% and 27–46%, respectively (Figure 7e).

The data-driven sample grouping was manually performed for the dosage range 0.5–3.2 $\mu\text{mol Me/mgSS}$ by dividing the band of the $\delta\text{COD}_{\text{dis}}$ values (Figure 7e) in the whole range between the upper and lower limits into three groups. As a result, the following ranges were generated: –51.0–17.0%; 17.0–27.0% and 27.0–62.3%. The range with the highest level of COD_{dis} removal (27.0–62.3%) was chosen as the target level. This selection agreed with the following mechanism of fouling control: the reduction of the SMPs level in mixed liquor. Consequently, the ranking trend among the studied coagulants in decreasing order of dominance of SMP removal mechanism, can be classified as: PAXXL61 (100% of all PAXXL61 samples) > PAX18 (67.0%) = PIX313 (67.0%) > ALS (20.0%), which corresponds to the findings in the previous works [30,36,60].

In the BF-MBR pilot system, COD removal due to biodegradation was in the range 67.0–92.0%.

According to the residual aluminium plot (Figure 7f), the application of prepolymerized aluminium coagulants is the most preferable, since in the range 0.5–1.9 $\mu\text{mol Al/mgSS}$ they provided the concentrations of soluble Al at the level 0–0.03 mg Al/L, which is well below the regulatory limits [54,78–80]. Meanwhile, in the case of overdosing of PAX18, its residual aluminium concentration drastically increased up to 14.5 mg Al/L, which was almost 15 times higher than its content in the optimum coagulation region. On the contrary, ALS is characterized by incredibly high residual aluminium levels (starting from the dosage 0.64 $\mu\text{mol Al/L}$), which are in the range 2.5–9.2 mg Al/L. Consequently, the use of PAX18 in the overdosing region, as well as ALS at the dosages, higher than 0.5 $\mu\text{mol Al/mgSS}$, is undesirable from the environmental point of view.

The other monitored characteristics of mixed liquor, obtained during the TRT with the pH maintenance, are represented in Figure 8.

The zeta potential plot (Figure 8a) demonstrates that in the range 0.6–1.9 $\mu\text{mol Me/mgSS}$ all of the coagulants provided an “excellent/maximum” coagulation degree, which indicates the achievement of their full charge neutralization potential under the applied conditions. As in the case of jar tests (Figure 5a), the prepolymerized aluminium chloride with medium basicity showed a tendency toward overdosing at a lower dosage than its counterpart with a high OH/Al ratio. Apparently, this is the result of the higher adsorption/charge neutralization potential of PAX18 in comparison to PAXXL61, which should be a subject of further investigation. The overdosing of PAX18 is characterized by severe system recharge, which is demonstrated by the zeta potential plot (Figure 8a), when zeta potential exceeds +18 mV, indicating system restabilisation.

TTF change profiles (Figure 8b) demonstrated a strong advantageous effect of PAXXL61 and ALS on the mixed liquor filterability, since they provided the maximum decrease of the filtering time (time to obtain 100 mL of the filtrate by TTF) by 79.5% and 85.0%, respectively. Meanwhile, PAX18 and PIX313 exhibited a less pronounced performance in affecting the mixed liquor filterability—the maximum TTF reductions were 59.5% and 63.0%, respectively. The acquired profiles (Figure 8b) also

show an increasing tendency of time-to-filter in the overdosing region for every one of the coagulants, which, in practice, can result in the decrease of mixed liquor quality and the deterioration of the membrane filtration process.

CST change graphs (Figure 8c) indicate the highest efficiency of PAXXL61 among the tested coagulants in terms of CST decrease and hence, the increase of relative hydrophobicity of the flocs. PAXXL61 provided a CST reduction equal to 61.0%, while the samples treated with PIX 313, PAX18 and ALS, were characterized by less significant CST alterations—34.0%, 25.0% and 24.6% CST reductions, respectively. Thus, it can be concluded that the coagulant with the highest tested basicity, PAXXL61, exhibited the highest performance with regard to the increase of relative hydrophobicity of the microbial flocules.

According to the plot of volume moment mean change (Figure 8d), the average particle size of the coagulated samples decreases in the following order of applied chemicals: PAX18 > PAXXL61 > PIX313 > ALS. This observation, together with the results of the prior jar tests (Figure 5b), suggests the dominance of the flocculating ability of the prepolymerized aluminium chloride with medium basicity over the other tested coagulants.

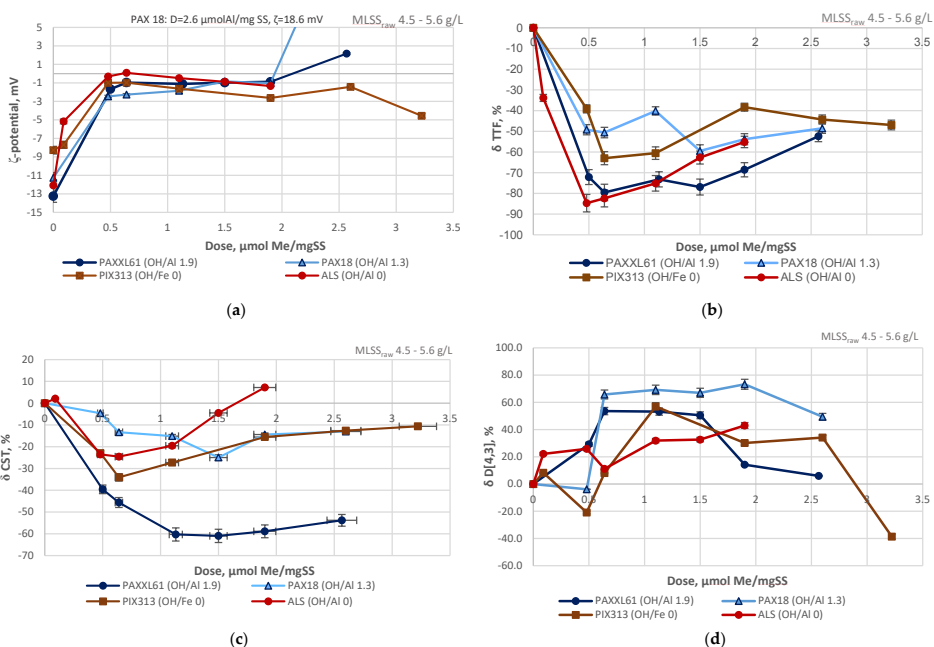


Figure 8. Influence of the coagulant dose on the monitored parameters at fixed pH during the total recycle test (TRT): (a) zeta potential; (b) TRT change; (c) CST change; (d) volume moment mean change.

The filtration time, required for reaching $1.2 \times \text{TMP}_{in}$ and the average normalized permeability were chosen as the indicators of membrane fouling intensity. The acquired tendencies depending on the coagulant type and dosage, which were observed during the TRT at the fixed pH, are demonstrated in Figure 9.

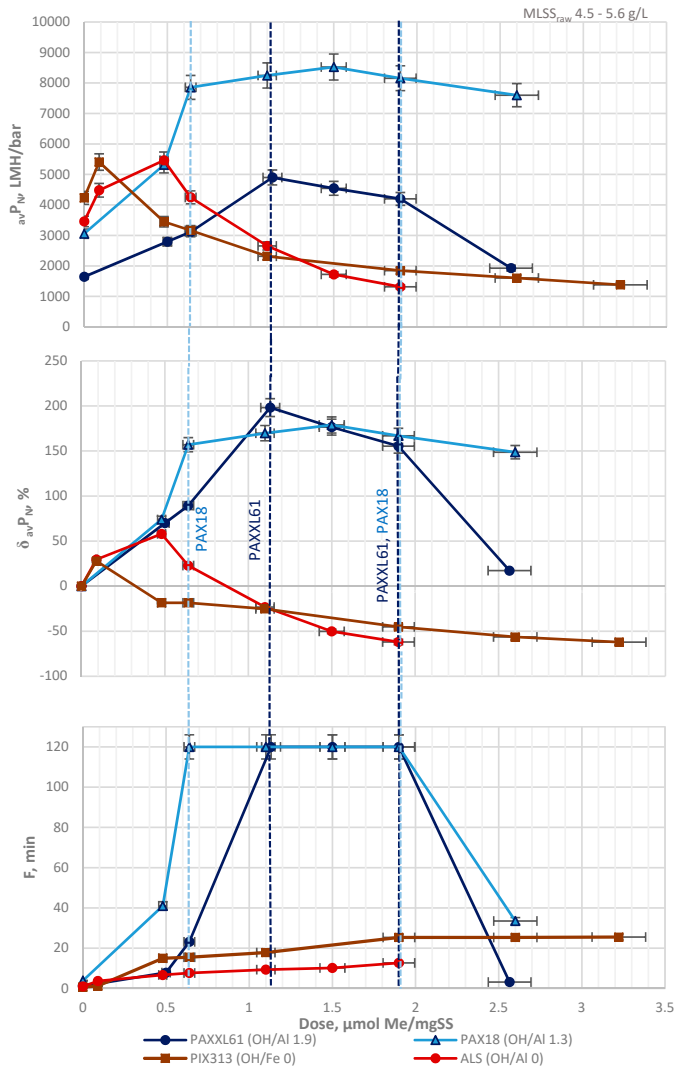


Figure 9. Relationship between the coagulant dose and the filtration performance according to normalized permeability, normalized permeability change and filtration time at fixed pH during the TRI.

According to Figure 9, the prepolymerized aluminium coagulants provided the greatest extent of fouling inhibition among the studied compounds: the maximum filtration time (F) equal to 120 min and the maximum increase of average normalized permeability (δ_{avP_N}) by 155.0–198.0%.

According to the calculations for the BF-MBR pilot system, the obtained prolongation of the filtration times in the dosage range 0.6–1.9 $\mu\text{mol Al/mgSS}$ for PAX18 or 1.1–1.9 $\mu\text{mol Al/mgSS}$ for PAXXL61 (Figure 9) results in a tenfold increase in filtration time of the membrane separation cycle and 30.0–56.0% higher net flux (depending on the operational period), in comparison to the net flux in this system without the PACl dosing. Inhibited fouling intensity requires lower frequencies of the physical cleaning procedures (backwash and relaxation). Consequently, the addition of the studied

prepolymerized aluminium coagulants will highly improve the filtration efficiency of the BF-MBR pilot system.

Nevertheless, the coagulant with medium basicity, PAX18, demonstrated a superior fouling mitigation behaviour to PAXXL61, the prepolymerized aluminium chloride with high OH/Al ratio, since PAX18 has a higher flux enhancing efficiency at lower dosages and a wider range of maximum performance than PAXXL61 (Figure 9). The highest efficiencies of PAX18 during the filtration experiments is predominantly attributed to a greater adsorption/charge neutralization potential of PAX18 over PAXXL61, with subsequent flocculation enhancement, which was indicated by the relevant zeta potential and the mean particle size profiles.

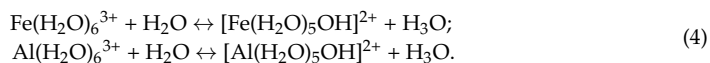
The results of the total recycle test, conducted at the selected pH values, are summarized in Table S4.

Since PAX18 has a broader range of optimum dosages and a lower dose is required to reach the region with maximum values of the response functions, it was decided to apply this coagulant in the further stages of the research.

3.3. TRT with pH Control vs. TRT with Non-Corrected pH

The examination of fouling mitigation efficiencies of the selected coagulants during the total recycle tests without the pH adjustment was performed to estimate if it was reasonable to omit the pH adjustment stage. Such a decision was taken due to the fact that most conventional chemical wastewater treatment plants operate with no pH maintenance. In this case, the pH of the hydrolysis in mixed liquor depends on the characteristics of applied coagulants (acidic properties and the dosage) and the buffering capacity of mixed liquor [36]. The results are demonstrated in Table S5.

The results in Table S5 indicate that the pH of coagulation without the pH correction was the lowest for non-prepolymerized coagulants. Along with the intensive hydrolysis processes, the reason for the drastic pH decrease in the system could be the acidic properties of hydrated iron and aluminium ions, since they belong to Lewis acids, that is, proton donors, which transfer a proton to a solvent water molecule (Equation (4)).



Moreover, the base-10 logarithm of a first acid dissociation constant (pK_a) for $[\text{Al}(\text{H}_2\text{O})_6]^{3+}$ is higher than for $[\text{Fe}(\text{H}_2\text{O})_6]^{3+}$, indicating lower acidity of hexa-aquo-aluminium complexes than hexa-aquo-iron complexes [61]. Hexa-aquo-aluminium complexes tend to decrease the pH of solution less dramatically, than their iron-based counterparts.

According to the obtained results (Table S5), PAXXL61, PAX18 and ALS provide much higher fouling mitigation efficiencies during the TRT, with the controlled pH, than without its maintenance. PIX313 also demonstrates positive tendencies with regard to improvement of membrane filtration. However, for PIX313 during the TRT at fixed pH, the normalized permeability started to decline at the dose $0.5 \mu\text{mol Fe}/\text{mgSS}$, while the fouling rate continued to decrease. The potential reason could be the tendency of iron (III) coagulant at certain concentrations to trigger the formation of the Fe-rich gel matrix of polysaccharides on the membrane surface, thus increasing reversible fouling, which was reported by several studies [8,81,82].

In addition to high improvement of membrane filtration with the pH adjustment, the optimum filtration parameters are reached at lower dosages in comparison to those obtained during TRT with no pH correction. Lower coagulant dosages result in lower excess sludge production. Consequently, pH adjustment is a valuable tool in the optimization of the fouling mitigation based on coagulant dosing.

3.4. Investigation of the Characteristics of the Coagulants

The investigation of the coagulant characteristics was performed in order to describe the mechanism of charge neutralization and the extent of its prevalence depending on the coagulant nature. The results could potentially shed some light on the reason the coagulant with medium basicity, PAX18, performs more efficiently in respect of fouling mitigation than PAXXL61, of high basicity, whose potential to adsorption/charge neutralization was expected to be higher.

3.4.1. Coagulant Charges

The results of potentiometric back titration of the investigated coagulants are represented in Figure 10.

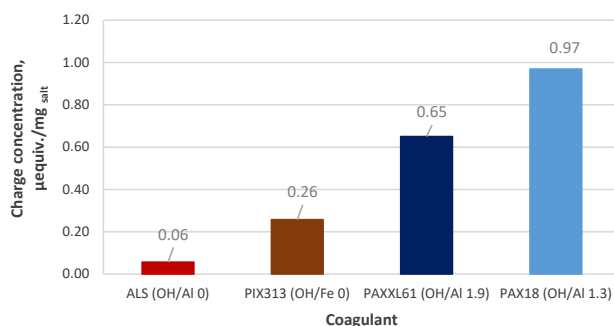


Figure 10. Charge concentrations of the studied coagulants.

According to the acquired charts (Figure 10), PAX18 and PAXXL61 have the highest charge concentrations, which correspond to their high efficiency regarding the increase in average normalized permeability and filtration time (Figure 9). Nevertheless, the charge concentration of PAX18 is still higher ($0.97 \mu\text{equiv./mg}_{\text{salt}}$) than the charge concentration of PAXXL61 ($0.65 \mu\text{equiv./mg}_{\text{salt}}$), which could be caused by the fact that, except for high basicity, PAXXL61 is characterized by the incorporation of SiO_2 group in its skeleton. As calculated by the authors of the current paper, based on the patents for similar commercial products [83,84], PAXXL61 has the approximate ratio of Al/Si of 15–20. The introduction of SiO_2 into the prepolymerized aluminium structure increases the molecular weight (MW) of the coagulant, and, due to the neutrality of silica group, decrements the coagulant charge concentration, which corresponds to the discoveries by Zouboulis et al. [85] and Gao et al. [86]. Besides, the interaction of Al with the polysilicic acid during the formation of polyaluminium silicate chloride species results in the creation of chelate-like bonding between the aluminium atoms and the polysilicic acid, which entails the hindering of the active polymeric $\text{Al}_3\text{O}_4(\text{OH})^{7+}_{24}$ component formation during the subsequent prepolymerization phase. As a result, the content of monomeric octahedral Al_1 species in the final product increases, which reduces its adsorption/charge neutralization potential [87,88].

The charge concentrations of the non-prepolymerized coagulants, PIX313 and ALS were found to be much lower and were equal to 0.26 and $0.06 \mu\text{equiv./mg}_{\text{salt}}$, respectively. Thus, non-prepolymerized coagulants tend to have lower charge concentration and less potential to enhance adsorption/charge neutralization than their prepolymerized counterparts, which confirms the findings of the previous studies [36].

In order to confirm the strength of investigated coagulants with respect to adsorption/charge neutralization, a series of experiments, based on direct potentiometric titration of the mixed liquor samples, was conducted (Figure 11).

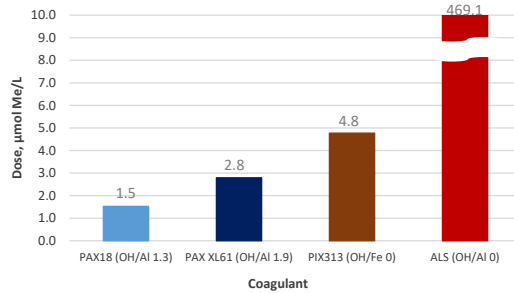


Figure 11. Coagulant dose required for reaching the endpoint during the potentiometric titration of mixed liquor.

According to the obtained results (Figure 11), the application of PAX18 produces the effect of reaching the titration endpoint at the lowest dose of 1.5 $\mu\text{mol Al/L}$. This, together with the acquired zeta potential profiles (Figures 5a and 8a) and the determined coagulant charges, is strong evidence for the highest potential to adsorption/charge neutralization of the coagulant with medium basicity, PAX18, among all the coagulants, studied in this research.

In addition to the determination of coagulant properties, the implementation of the potentiometric titration of mixed liquor with investigated coagulants, based on the streaming current detection, demonstrates that this system can be readily scaled up to perform the coagulant dosing and its online control at industrial BF-MBR. This conclusion refers to the fact that streaming current detectors are commercially available and appear to be among the key solutions to online control of coagulant dosing at wastewater treatment plants [89,90].

3.4.2. Chromatographic Separation of Prepolymerized Aluminium Coagulants

The comparative qualitative analysis of the investigated prepolymerized aluminium coagulants as regards their molecular weight (MW) distribution was performed using size exclusion chromatography. Figure 12 shows the MW distributions of the aluminium species in the samples of the prepolymerized aluminium coagulants of medium and high basicity.

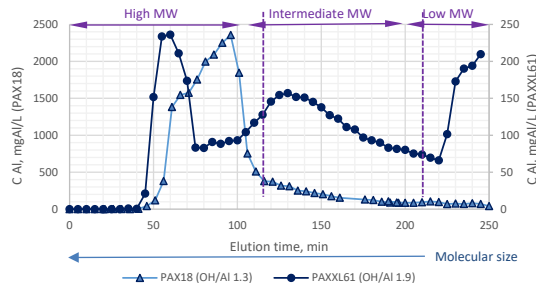


Figure 12. Size exclusion chromatograms of collected prepolymerized aluminium chloride (PACl) fractions.

According to the obtained chromatograms (Figure 12), the PAXXL61 sample was characterized by three different peaks, eluted by size exclusion mechanisms. The peaks were observed at elution times 60 min, 130 min and 245 min, which refer to high, intermediate and low molecular weight bands, respectively. According to Brookes et al. [91] and Striegel [92], the retention time of the molecules in the chromatography column is inversely proportional to their molecular weights. Hence, the largest molecules are eluted at the lowest elution times, which is called an “inverse-sieving” mechanism. For PAXXL61, high MW fraction accounts for 39.1% of the total Al, intermediate MW

fraction exhibited 26.0% of the total Al and low MW isolate made up 34.9% of the total Al of the investigated prepolymerized aluminium coagulant with high basicity.

On the contrary, PAX18 was merely characterized by one broad peak eluted in 96 min. The obtained chromatography profile (Figure 12) suggests that high MW fraction accounts for about 85% of the total Al of the studied prepolymerized aluminium chloride with medium basicity.

High MW isolate of PAXXL61 was obtained 36 min earlier than for PAX18, pointing out that the tested prepolymerized aluminium chloride with high basicity and the incorporated SiO₂ had higher MW fractions in comparison to its counterpart with medium basicity. However, high MW isolates constitute less than half of the total Al in PAXXL61, which suggests they might not be the predominant contributor to the overall MW of the relevant compound.

3.5. Statistical Analysis

3.5.1. Partial Least Squares Regression Analysis

PLS regression analysis was performed for the ML samples from TRT with and without pH correction according to the following variables and response functions (Table 2).

Table 2. Model inputs.

Predictors (X)	Response (Y)
MLSS _{in} ¹ , CST ² , turbidity, pH, D[4,3], D[3,2], span, uniformity, zeta potential, coagulant dosage (Dose)	Average normalized permeability (avP _N), Filtration time (F)

Notes: ¹ Initial mixed liquor suspended solids (MLSS of the raw sample); ² Capillary suction time.

The obtained model was validated by applying random cross-validation in PLS. During the cross-validation, the dataset was divided into 20 segments. Some elements were taken out of analysis since they were indicated as potential outliers. The number of PLS components (factors), was chosen according to the explained variance.

Eventually, the following results were obtained (Figure 13).

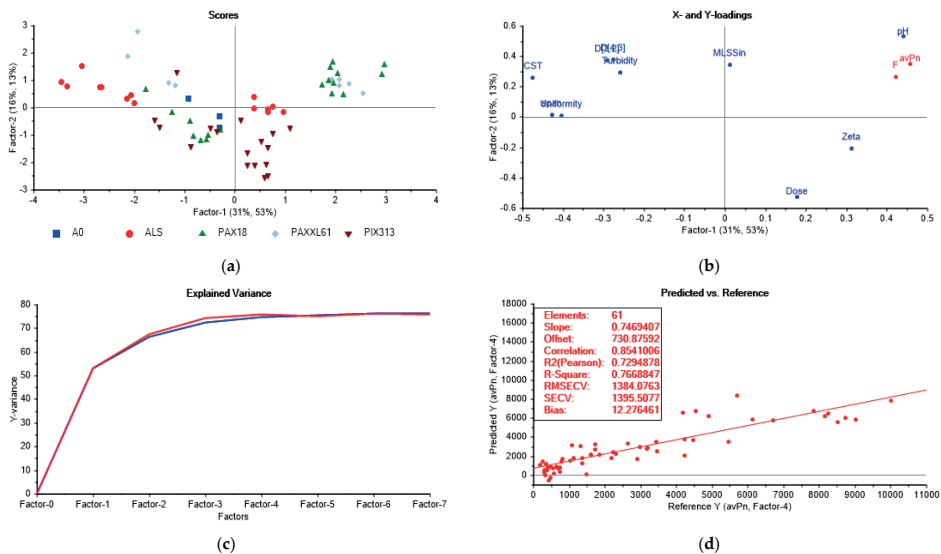


Figure 13. Results of partial least squares (PLS) of the data from the TRT-regression overview: (a) scores plot; (b) loadings plot; (c) total residual variance plot; (d) fouling intensity prediction model.

According to the acquired results (Figure 13), the first two factors describe 47.0% and 66.0% of the variance in the dataset for x and y, respectively.

The scores plot demonstrates the case with four distinctive clusters: the activated sludge samples treated with PAX18, PAXXL61, ALS and PIX313. Samples within a cluster contain similar samples. The difference between the clusters is explained by Factor-1 and Factor-2.

According to the PLS loadings plot, Factor-1 clearly describes span, uniformity, CST, zeta potential, pH, filtration time and the average normalized permeability. Factor-2 apparently accounts for D[4,3], D[3,2], turbidity, MLSS_{in} and coagulant dose. From the loadings plot, all the variables appeared to be significant and provided stability and reliability to the model. Span and uniformity are highly positively correlated with each other and exhibit a positive link to CST, turbidity, D[4,3] and D[3,2]. Such PSD parameters as D[4,3] and D[3,2], have a positive correlation with each other. However, they show a negative correlation to coagulant dose and zeta potential. CST and turbidity are negatively linked to zeta potential and coagulation dose. Meanwhile, the coagulant dose is positively correlated with zeta potential. CST has a high negative correlation with the response variables and pH along Factor-1.

The total residual variance plot indicates how much of the variation in the data is described by the different numbers of factors [55,56]. According to the total residual variance plot (Figure 13), the highest explained Y-variance (76%) is attained while applying four factors and then reaches a plateau.

An analysis of the validation plot shows that the developed model is linear, has a R-squared value of 0.77 and has a good fit for the majority of data (i.e., slope = 0.75). The Root Mean Square Error of Cross Validation (RMSEV) and the standard error of cross-validation (SECV) are equal to 1384 and 1395, respectively. However, it is essential to acknowledge that the mentioned errors have the same units as the reference Y (in this case, the average normalized permeability, *av*P_N). R-squared (Pearson) is close to R-squared correlation (0.73 vs. 0.85), which indicates the reliability of the model. The developed model has a relatively low bias equal to 12.3, indicating that it has a low tendency to over- or underestimate the validation values. Hence, the developed model demonstrates a good prediction capability, which proves its reliability and high potential to be used during further stages when the operating conditions applied in this work are replicated.

In order to determine a predominant mechanism, which governs the behaviour of every coagulant, the data-driven sample grouping was automatically performed by equally dividing the band of the target parameter values in the whole range between the upper and lower limits into five groups. As a result, the relevant ranges were generated (Figure 14).

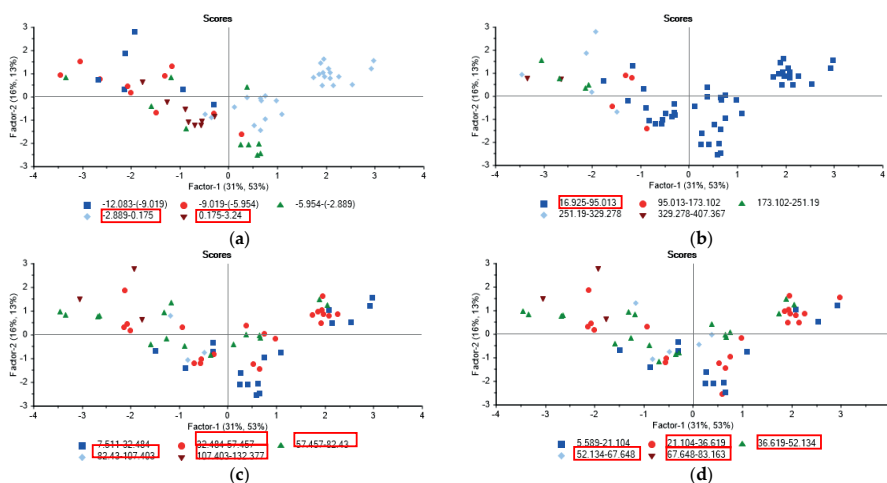


Figure 14. Results of partial least squares analysis (PLS) for the tested membrane flux enhancers—scores plot with the sample grouping according to: (a) zeta potential; (b) CST; (c) D[4,3]; (d) D[3,2].

The target levels of interest (marked with the red rectangles in the legends in Figure 14) were chosen in accordance with the variables: for zeta potential, the upper limit of values (group -2.9 – 3.2 mV); for CST, the lower boundary (group 17.0 – 95.0 s); and for the volume/mass moment mean, the range of higher values, including the upper boundary (group 32.5 – 132.0 μm / 21.0 – 83.0 μm). This selection was congruent with the main mechanisms of fouling control: adsorption/charge neutralization (preferential decrease of zeta potential absolute value), the increase of relative hydrophobicity of the flocs (the decrease of dewaterability) and the increase of the mean particle size. According to the obtained PLS scores plot (Figure 14), the ranking trend among the studied coagulants, in decreasing order of dominance of each particular fouling mitigation mechanism, can be classified as:

- enhanced adsorption/charge neutralization (zeta potential -2.9 – 3.2 mV): PAX18 (100% of all PAX18 samples) > PAXXL61 (55.6%) > PIX313 (41.0%) > ALS (36.0%);
- the increase of relative hydrophobicity of the flocs (CST 17 – 95 s): PAX18 (100%) > PIX313 (82.0 %) > PAXXL61 (56.0%) > ALS (43.0%);
- the increase in particle size (D[4,3] 32.5 – 132 μm /D[3,2] 21 – 83 μm): ALS (100/100%) > PAX18 (78.0/94.0%) > PAXXL61 (78.0/78.0%) > PIX313 (41.0%/53.0%).

It was decided to denominate the mechanism of fouling inhibition as dominant if 55.0% or more of a total number of the samples of every coagulant is characterized by the above-mentioned ranges of the monitored parameters. As determined earlier (during the analysis of the TRT with pH correction), based on Figure 7e, the highest level of COD_{dis} removal (i.e., the reduction of the SMPs content) was observed for the majority of samples of prepolymerized aluminium coagulants PAXXL61 and PAX18 (100% and 67.0%) and iron (III) sulphate PIX313 (67.0%) for a total number of the samples in the selected dosage range, respectively. Consequently, the principal mechanism differs depending on the coagulant nature (Table 3).

Table 3. Prevailing mechanisms of action for the tested coagulants.

Mechanism of Action Coagulant	Enhanced Adsorption/Charge Neutralization	The Increase in Relative Hydrophobicity of the Flocs	The Increase in Particle Size	The Reduction of the SMPs Level
PAX18 (OH/Al 1.3)	+	+	+	+
PAXXL61 (OH/Al 1.9)	+	+	+	+
PIX313 (OH/Fe 0)		+		+
ALS (OH/Al 0)			+	

3.5.2. Two-Level Factorial Design of the Experiment

A factorial design was built in order to characterize how the selected factors interact and individually affect the fouling mitigation process and to determine the optimum combination of factor levels, that simultaneously satisfy the criteria of the maximum permeability/filtration time for the chosen coagulant.

The Average Permeability

To study the possible options of permeability maximization systematically, a two-level alternative factorial design was set up on the key factors: pH, temperature, MLSS and coagulant dose with two replicates (Tables 4 and 5).

Table 4. Factors and levels for two-level alternative factorial design.

Factor	Units	Low Level	High Level
pH	-	5.5	6.5
Temperature	°C	20	25
MLSS	g/L	4.0	6.0
D ¹	μmoleAl/mgSS	1.1	1.9

Notes: ¹ Coagulant dose.

Table 5. Layout for a designed experiment.

	Factor 1	Factor 2	Factor 3	Factor 4	Response 1
Run	A:pH	B:Temperature, C	C:MLSS, g/L	D:D, μmolAl/mgSS	Permeability, LMH/bar
1	5.5	20	4.0	1.1	8725.6
2	6.5	25	6.0	1.9	6614.1
3	6.5	20	6.0	1.1	2055.5
4	5.5	20	4.0	1.1	8698.6
5	5.5	25	4.0	1.9	12,204.9
6	5.5	25	6.0	1.1	7146.1
7	6.5	20	4.0	1.9	10,020.4
8	6.5	25	6.0	1.9	6578.7
9	6.5	20	4.0	1.9	10,046.9
10	6.5	25	4.0	1.1	11,168.8
11	6.5	20	6.0	1.1	2024.6
12	6.5	25	4.0	1.1	11,196.9
13	5.5	20	6.0	1.9	6827.6
14	5.5	25	6.0	1.1	7169.4
15	5.5	20	6.0	1.9	6859.4
16	5.5	25	4.0	1.9	12,233.0

A preliminary analysis was conducted to understand the general relationships between the factors and the response function before carrying out an in-depth analysis. The relevant graphs (Figure S1) represent the impact of every factor on the permeability.

According to the obtained plots (Figure S1), coagulant dose and temperature are positively linked to the average permeability, while the increase in pH and MLSS cause the permeability to drop.

This analysis was followed by the use of more sophisticated tools.

The values of the response function ranged from 2024.6 to 12,233.0, which results in a ratio of its maximum to a minimum value of 6.04, which is greater than 3, indicating a high potential for the model improvement [93,94]. In the current work, a power family of transformations $y^* = y^\lambda$ (λ , the transformation parameter; y , the observed response function; y^* , the transformed response function) was selected. The transformation of the response function was performed in order to increase the fit of the model to the data. An empirical graphical technique in the form of a Box-Cox plot (the graph is not presented) was applied to determine the optimum transformation parameter λ of the response function. As the present study discovered, the value of λ equal to 1.61 resulted in the minimum residual sum of squares. Therefore, power transformation was chosen at the beginning of the analysis, applying $\lambda = 1.61$.

In order to detect the important effects among the variables and their interactions, the analyses of a half-normal plot and Pareto chart (Figure 15) were carried out.

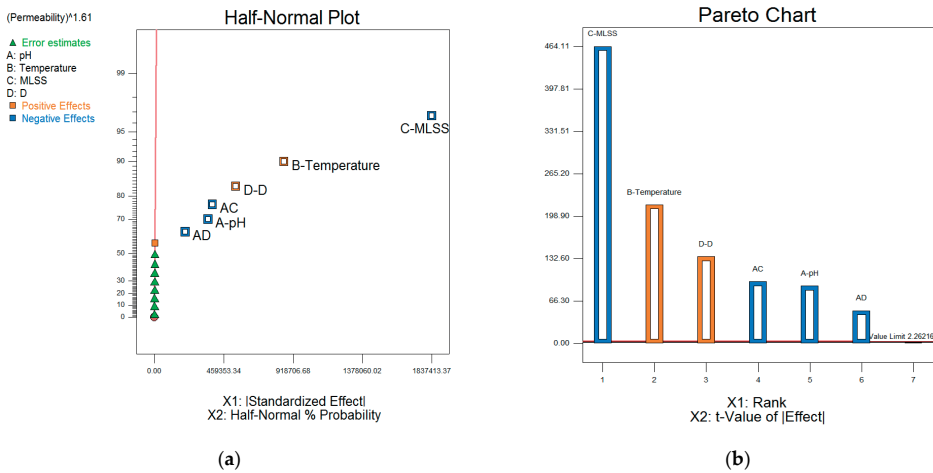


Figure 15. The selection of the effects to be modelled: (a) half-normal plot of effects; (b) Pareto chart.

The half-normal plot of effects demonstrates the absolute values of the squares of effects plotted against their cumulative normal probabilities [93,94]. The terms, which were selected as significant, that is, included in the model, were C (MLSS), B (temperature), D (coagulant dose), AC (the interaction effect of pH-MLSS), A (pH) and AD (the interaction effect of pH-coagulant dose). The negligible effects lined up at the red “error line” close to zero (Figure 15a).

The Pareto chart (Figure 15b) indicates the magnitude of the selected effects. The plot shows that all the selected effects are higher than Bonferroni limit = 3.46159 and t-value limit = 2.26216 (t value can be identified as a magnitude of the difference relative to the variations in the data [95]).

Analysis of variance (ANOVA) (Table 6) provides a set of formulas that enable the computation of test statistics and confidence intervals [96]. It gives the necessary evidence of the overall model significance, the importance of each coefficient, model accuracy and reliability, the possibility of model improvement and model application to navigate the design space.

Table 6. Analysis of variance table for the selected factorial model (Partial sum of squares-Type III).

Source	Sum of Squares	Df ¹	Mean Square	F-Value	p-Value Prob > F	
Model	1.89×10^{13}	6	3.15×10^{12}	50178.2	<0.0001	significant
A-pH	5.06×10^{11}	1	5.06×10^{11}	8074.3	<0.0001	
B-Temperature	2.95×10^{12}	1	2.95×10^{12}	47019.0	<0.0001	
C-MLSS	1.35×10^{13}	1	1.35×10^{13}	2.154×10^5	<0.0001	
D-D	1.16×10^{12}	1	1.16×10^{12}	18486.6	<0.0001	
AC	5.92×10^{11}	1	5.92×10^{11}	9434.2	<0.0001	
AD	1.67×10^{11}	1	1.67×10^{11}	2659.4	<0.0001	
Residual	5.64×10^8	9	6.27×10^7			
Lack of Fit	6.05×10^7	1	6.05×10^7	0.96	0.3557	not significant
Pure Error	5.04×10^8	8	6.3×10^7			
Corrected Total	1.89×10^{13}	15				

Notes: ¹ the numerator degrees of freedom.

Fisher’s value (F-value) is the ratio of the “between-group variance” (the variation as a result of the intentional experimental manipulation) to the uncontrollable “within-group or error variance” [97]. The model’s F-value is equal to 50,178.2, which indicates the significance of the derived model. There is only a 0.01% chance that an F-value this large could occur due to noise.

Besides, based on the p -values (<0.05), it can be concluded that the derived model was significant and all the selected factors, such as pH, temperature, MLSS, coagulant dose and the interaction terms pH·MLSS and pH·coagulant dose had a significant effect on the model. Otherwise, the p -values greater than 0.1 would have indicated the insignificance of the model terms.

The model was characterized by R-Squared equal to 1, which indicates its linearity.

The predicted R-Squared of 0.9999 was in reasonable agreement with the adjusted R-Squared of 1, that is, the difference was less than 0.2. "Adequate Precision," which measures the signal to noise ratio, was equal to 685.5, which is the evidence of an adequate signal. Therefore, this model can be used to navigate the design space. The "Bayes information criterion" (BIC) and the "Akaike information criterion" (AIC) determine which model from the set of models describes the dataset in the best way. The criteria take into consideration model complexity and serve as barriers to model overfitting. The distinctive feature of BIC is its consistency, which helps to select a lower dimensional model when it is the most accurate. The model, which has the highest BIC or AIC criterion, fits data best, therefore, should be selected [98,99]. In the current model, BIC and AIC criteria were equal to 342.9 and 351.5, respectively, which indicates a consistent fit of the model with the response data.

After determination of the model coefficients the final equations can be derived (Equation (5) and (6)).

Final equation in terms of coded factors:

$$(\text{Permeability})^{1.61} = 2.100 \times 10^6 - 1.779 \times 10^5 \cdot A + 4.292 \times 10^5 \cdot B - 9.187 \times 10^5 \cdot C + 2.691 \times 10^5 \cdot D - 1.923 \times 10^5 \cdot AC - 1.021 \times 10^5 \cdot AD, \quad (5)$$

where A is a coded value for pH, B is a coded value for temperature, C is a coded value for MLSS, D is a coded value for the coagulant dose, AC is a coded value for pH·MLSS and AD is a coded value for pH·coagulant dose.

It is worth noting that the equation with respect to coded or actual factors can be used to make predictions about the response for given levels of each factor. In the case of coded factors, the high levels of the factors correspond to +1 and the low levels of the factors are coded as -1. According to the derived equation, MLSS, temperature and the coagulant dose have the highest impact on the average permeability.

Final equation in terms of actual factors, which can be applied to make the predictions about the average permeability for the specified factorial levels:

$$(\text{Permeability})^{1.61} = -1.21741 \times 10^7 + 2.33256 \times 10^6 \cdot \text{pH} + 1.71694 \times 10^5 \cdot \text{Temperature} + 1.38853 \times 10^6 \cdot \text{MLSS} + 3.73531 \times 10^6 \cdot D - 3.84539 \times 10^5 \cdot \text{pH} \cdot \text{MLSS} - 5.10408 \times 10^5 \cdot \text{pH} \cdot D, \quad (6)$$

where D is a coagulant dose.

The last equation implies that the levels should be specified in the original units for each factor. This equation is not applicable for the determination of the relative impact of each factor since the coefficients are scaled to correspond to the units of each factor and the intercept is not at the centre of the design space [94].

Regression diagnostics provide the validation analysis of the derived model. In the current work, it includes a normal probability plot, which describes the distribution of model errors; a plot of the residuals against the fitted values to assess the independence of the error terms and system stability; and Cook's distance plot for the identification of the outliers (Figure 16).

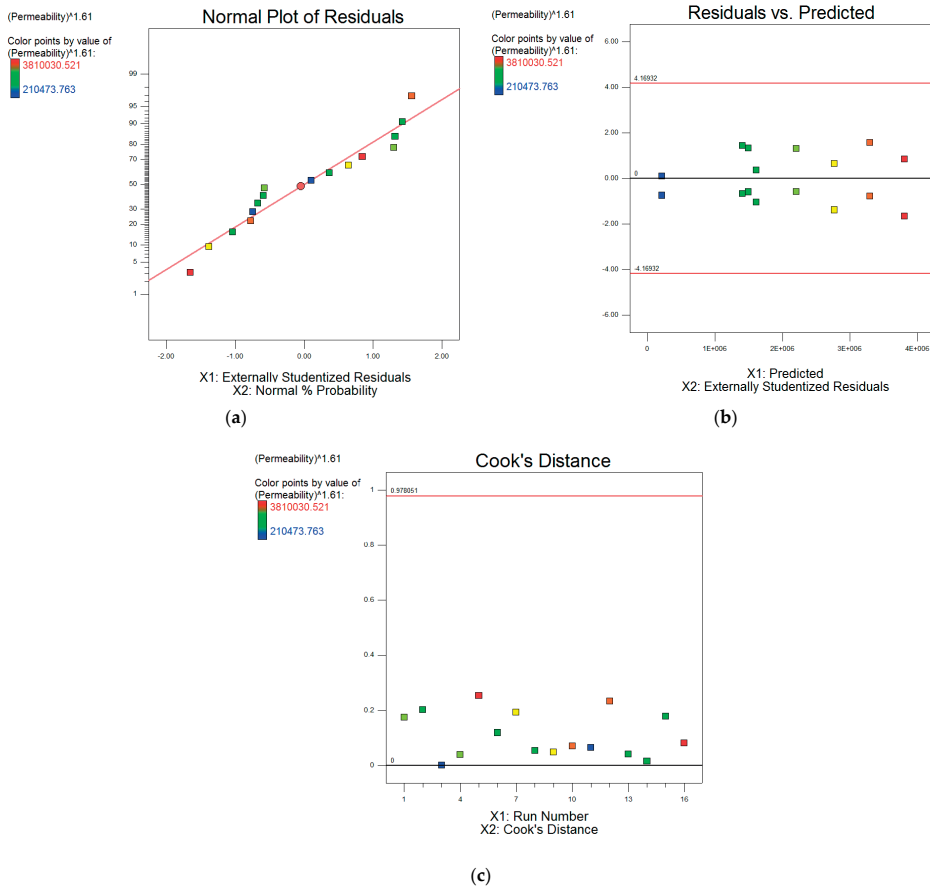


Figure 16. Model diagnostics plots: (a) normal probability plot; (b) residuals versus predicted response; (c) Cook’s distance vs. the run.

The normal probability plot demonstrates the residuals plotted against the normal scores (expected residuals values) under the assumption of normality [96]. According to the obtained results (Figure 16a), there is a clear linear trend between the residual values and normal scores in this model, indicating that the errors are normally distributed, thus the normality assumption is satisfied.

Residuals versus predicted response values plot (Figure 16b) demonstrates that all the residuals exhibit a fairly uniform spread along Y-axis, that is, no steady upward/downward trends are observed, starting from the first residual and ending with the last one. Hence, the size of the residual is independent of the predicted response value.

Cook’s distance quantifies the regression change, if needed, to exclude any of the samples from the analysis. It is an overall measure of the distances between the pairs of the regression coefficients: $\hat{\beta}_0$ and $\hat{\beta}_0^i$, $\hat{\beta}_1$ and $\hat{\beta}_1^i$ and so on. $\hat{\beta}^i$ coefficient stands for the estimate of the $\hat{\beta}$ coefficient when the i th sample is removed from the analysis. The calculation of the Cook’s distance is carried out according to the following equation [96]:

$$D_i = \frac{(y_i - \hat{y}_i)^2}{(k + 1) \cdot \text{MSE}} \cdot \left[\frac{h_i}{(1 - h_i)^2} \right], \tag{7}$$

where h_i is leverage; k is the number of β -coefficients in the model, including the intercept; $y_i - \hat{y}_i$ (a deleted residual) is a difference between the actual response and the predicted response value which is obtained when the i th sample is excluded from the analysis; MSE is the mean squared error for the fitted model [94,96].

According to the obtained graph (Figure 16c), there is no sample that shows a high value of Cook's distance: all the samples have Cook's distance substantially lower than 1. Therefore, one can conclude that all observed responses have a weak impact on the estimates of the regression coefficients, that is, neither large leverages nor large residuals can be identified, which is the evidence of the absence of the outliers in the current model.

The interpretation of the selected model can be made by analysing model graphs (Figure 17).

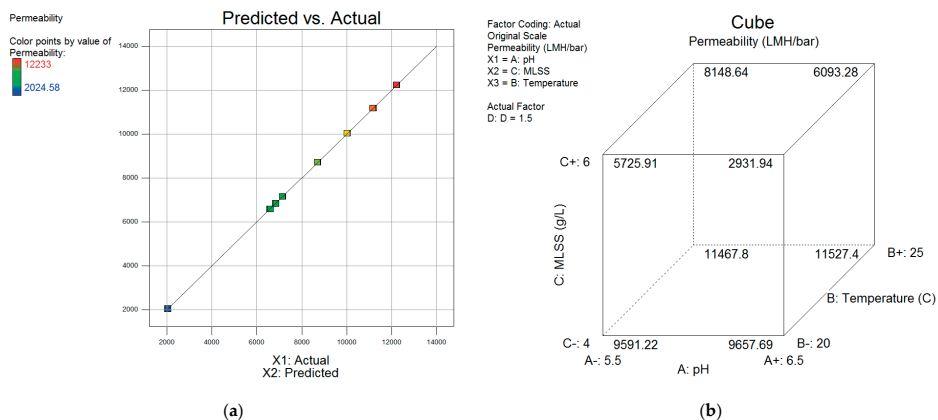


Figure 17. Model graphs of the factorial design: (a) predicted vs. reference plot; (b) cube plot, $k = 3$, $D = 1.5 \mu\text{mole Al/mgSS}$.

According to the predicted versus reference plot (Figure 17a), the predicted values fully correspond to the actual values, which indicates a high accuracy of the derived model.

The cube plot (Figure 17b), demonstrates the average predicted values of the response function superimposed on the eight corners, of the cube, at the combinations of high and low levels of the three factors, that have significant effects: MLSS, pH and temperature at the selected actual value of the coagulant dose ($1.5 \mu\text{mole Al/mgSS}$ in the represented plot) [94,100]. According to the represented graph, the highest levels of the average permeability 11467.8–11527.4 LMH/bar can be attained at minimum MLSS (4 g/L) and maximum temperature (25 °C) (values calculated at $D = 1.5 \mu\text{mole Al/mgSS}$). Meanwhile, pH has a minor positive effect at the low level of MLSS and an adverse effect at a high MLSS level.

The optimization analysis determines the settings or values of the significant factors, which provide the desired values of the response function, based on the placed criteria [100].

In the current work, the optimization is based on the maximization of the desirability function (D), which is a converted response function. In this case, the overall desirability is equal to the individual desirability function d since there is just a single response function. In the case of response maximization, D would equal 1, if the response function is at its target value; D would equal 0 if the value of the response function is undesirable [93,100].

The determination of the important factorial levels, which provided the maximum permeability yield was conducted. Two cases were tested, which differed from each other in the requirements, imposed on the values of the factors. In the first case, the goal was to maximize the response function, while varying pH, MLSS, temperature and coagulant dose in the relevant ranges, defined by high and low factorial levels, provided in Table 4. As a result, according to one of 94 possible solutions for

optimization, the maximum average permeability, equal to 12,222.8 LMH/bar, was attained at pH 5.5, temperature 25 °C, MLSS 4 g/L and coagulant dose 1.9 µmolAl/mgSS (Desirability = 0.999).

In the second case, the purpose remained the same—to maximize the average permeability. However, under harsher conditions, these parameters were imposed on the factors: temperature and coagulant dose were kept at a low level, around 20 °C and 1.1 µmolAl/mgSS, respectively, while MLSS was constrained to its maximum tested level of 6 g/L. Consequently, according to one of the 94 possible solutions for optimization, the highest average permeability was equal to 4750.9 LMH/bar at pH 5.5 (Desirability = 0.707).

Point prediction and confirmation were used to compute a single value for the response function and interval estimates, using the developed regression model. The estimation procedure establishes the weights of the regression model to minimize the difference between the predicted and actual values of the response function. Consequently, the predicted value represents the total of all effects of the regression model and turns the residuals into a validation measure for the overall model performance [101]. Confirmation is the second stage of post-analysis; of which the purpose is to confirm that the model can predict the actual dependent variable at the optimum settings of parameters determined during the optimization. The results of point prediction and confirmation are represented in Table S6.

The results of the point prediction and confirmation for the average permeability ($_{av}P$) function indicated that at pH 5.5, temperature 25 °C, MLSS 4 g/L and Dose 1.9 µmolAl/mgSS the predicted mean permeability is 12,222.8 LMH/bar with the standard deviation between the predicted and actual $_{av}P$ value equal to 15.8 LMH/bar at a 95% confidence interval. Meanwhile, (at pH 5.5; temperature 20°C; MLSS 5.92 g/L; and dose 1.1 µmole Al/mgSS) the predicted mean permeability is equal to 4750.9 LMH/bar with the standard deviation between the predicted and actual $_{av}P$ value equal to 28.1 LMH/bar at a 95% confidence interval.

The obtained values of standard deviation are the indication of high accuracy of the developed regression model.

Consequently, the developed model can be used to determine the optimum conditions of the PAX18 application, which would provide the highest yield of the average permeability in accordance with the desired factor settings.

Filtration Time

The same sequence of analysis procedures was applied to the experimental design with the filtration time as a response function for the levels of factors, defined in Table 4. During the experiment, filtration time values were in the range 5–120 min, depending on the levels of the parameters, therefore it was decided to select power family of transformations as in the case of the average permeability in order to increase the fit of the model to the data. According to the relevant Box-Cox plot (not shown), the optimum transformation parameter λ of the response function, which resulted in the minimum residual sum of squares, was equal to 3. Therefore, power transformation was chosen at the beginning of the analysis, applying $\lambda = 3$.

According to ANOVA, the overall model and every selected factor were found to be significant, having the p -values < 0.0001 . The model F-value was equal to 6.36×10^6 , indicating model significance. R-squared values > 0.9999 demonstrated model linearity and the signal to noise ratio, equal to 4627, provided evidence of an adequate signal. Consequently, this model can be used to navigate the design space.

As a result, the final equation in terms of coded factors for the filtration time was as follows:

$$\begin{aligned} (\text{Filtration time})^3 = & 8.68 \times 10^5 - 3165.47 \cdot A - 1144.71 \cdot B + 3165.47 \cdot C + 1144.71 \cdot D \\ & + 8.598 \times 10^5 \cdot AC, \end{aligned} \quad (8)$$

where A is a coded value for pH, B is a coded value for Temperature, C is a coded value for MLSS, D is a coded value for the coagulant dose, AC is a coded value for pH·MLSS.

Equation (8) demonstrates that the interaction factor pH·MLSS has the highest influence on the filtration time. The other factors have relatively identical impacts on the response function.

Final equation with respect to actual factors:

$$(\text{Filtration time})^3 = 5.25 \times 10^7 - 8.6 \times 10^6 \cdot \text{pH} - 457.9 \cdot \text{Temperature} - 1.03 \times 10^7 \cdot \text{MLSS} + 2861.8 \cdot D + 1.72 \times 10^6 \cdot \text{pH} \cdot \text{MLSS} \quad (9)$$

According to Equation (9), temperature and coagulant dose have the lowest coefficients; however, these results cannot serve as a basis for making the conclusion about the magnitudes of the model coefficients. Equation (9) is applicable merely to making the predictions about the filtration time using the provided levels of factors.

The results of diagnostics demonstrated the fulfilment of the normality assumption in the current model and the absence of the outliers.

The interpretation of the factor interactions in the derived model was provided by analysing the cube plot (Figure 18).

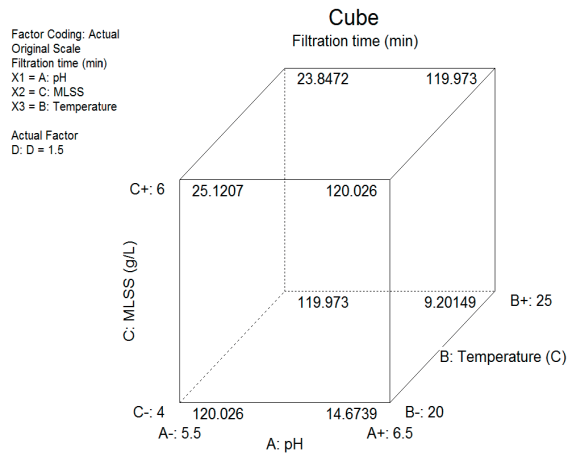


Figure 18. Cube plot of the factorial design ($k = 3$, $D = 1.5 \mu\text{mole Al/mgSS}$).

The cube plot (Figure 18) demonstrates the changes in the filtration time depending on pH, MLSS and temperature at constant coagulant dose. The obtained results show an ambiguous effect of pH on the response function, which highly depends on the MLSS. At the low MLSS level 4 g/L the increase of pH from 5.5 to 6.5 drastically reduces the filtration time from 120 to 9–15 min, whereas at the high MLSS level—6 g/L, the pH increase exhibits the opposite effect: the increase of filtration time from 23.8–25.1 to 120 min. In addition, a minor negative impact of temperature on the filtration time can be observed.

According to the represented cube plot, the filtration time is maximum (120 min) at:

- (1) A+1 (pH 6.5), B-1 - +1 (T = 20–25 °C), C+1 (MLSS 6 g/L) (values calculated at D = 1.5 $\mu\text{mole Al/mgSS}$);
- (2) A-1 (pH 5.5), B-1 - +1 (T = 20–25 °C), C-1 (MLSS 4 g/L) (values calculated at D = 1.5 $\mu\text{mole Al/mgSS}$).

The results of the numeric optimization indicated that for the provided upper and lower levels of factors with no specific requirements, imposed on the factors values, the maximum filtration time yield

equal to 120 min could be attained applying pH 6.5, temperature 20.7, MLSS 5.9, coagulant dose 1.69 (Desirability = 1). If temperature and coagulant dosage are minimized (20 °C and 1.1 $\mu\text{mole Al/mgSS}$), while MLSS is maximized 6 g/L, the maximum filtration time equal to 120 min is attained at pH 6.5 (Desirability = 1). The provided solutions represent one out of 94 possible solutions for optimization in each case of the parameter settings.

The results of the post-analysis (point prediction and confirmation) for the filtration time function indicated that at pH 6.5, temperature 20.7 °C, MLSS 5.9 g/L and Dose 1.69 $\mu\text{mole Al/mgSS}$ the predicted mean filtration time is 118 min with the standard deviation 0.0146 at a 95% confidence interval. Meanwhile, (at pH 6.5; temperature 20 °C; MLSS 6 g/L; and dose 1.1 $\mu\text{mole Al/mgSS}$) the predicted mean filtration time is equal to 120 min with the standard deviation 0.0141 at a 95% confidence interval.

Hence, the developed model can be used to determine the optimum conditions of the PAX18 application, which provide the highest yield of the filtration time in accordance with the desired factor settings.

4. Discussion

The acquired results demonstrated the importance of the electrokinetic potential, relative hydrophobicity of the flocs expressed through capillary suction time (CST), the mean particle size/particle size distribution, chemical oxygen demand (COD) and mixed liquor suspended solids (MLSS) for the characterization of the biomass fouling propensity.

The influence of MLSS, COD and relative hydrophobicity (RH) on the fouling potential of mixed liquor in the pilot scale BF-MBR agrees with the findings of our previous work [42]. According to both studies, the increase in MLSS mainly exhibited a negative influence on the average permeability. This effect could be explained by the fact that elevated MLSS content tends to induce severe reversible fouling, high ML viscosity and the production of biopolymers [102–104]. The current research together with the study by Kulesha et al. [42] also revealed that the reduction of COD positively contributes to fouling mitigation. The findings corresponded to the conclusions of different research groups [15,105–108], who identified a positive link between COD levels and irreversible fouling in MBR, which was induced by the increased production/release of soluble microbial products (SMPs). RH of the flocules was found to have a minor positive link to permeability slope [42]. However, the present study pointed out a significance of the RH for characterization of the biomass fouling propensity and its positive correlation with the permeability. These findings agree with different research works [109–111], where the increased RH had a positive contribution to membrane fouling mitigation, improved flocculation and dewaterability of activated sludge in the MBR systems. A greater fouling potential of the hydrophilic organic fractions was admitted by Johir et al. [112], Qin et al. [113], Shen et al. [114] and Pramanik et al. [115]. Mu et al. [116] used multivariate statistics to study the relationships between RH, the other physicochemical properties of the mixed liquor constituents and the fouling rate in MBR with PVDF modules. The analysed substances were classified as hydrophobic/hydrophilic based on the critical retention factor. Statistical analysis revealed a close relation of RH to the aromaticity of the organic matter and a strong correlation between the molecular weight (MW) > 10 kDa of the foulants and the fouling rate. As found out, nominally strong hydrophilic or strong hydrophobic fractions do not contribute to the membrane fouling but rather “moderately” hydrophobic/hydrophilic substances with high MW.

The CST parameter indicates the dewaterability of the sludge flocules [24,117] and has been used as a fouling indicator in MBR systems [118,119]. CST is positively linked to the concentration of biopolymers in ML and has a negative correlation with the permeability [120–122].

According to the recent findings, CST has an additional valuable property with regard to the characterization of the biomass fouling propensity, which is its relation to relative hydrophobicity of the flocs. The negative correlation between these two parameters was confirmed by the analysis of the data acquired from the previously investigated pilot plant [42] (the loadings shown in Figure S2),

where relative hydrophobicity was in the range 30.0–67.5%, while CST values were in the range 65.6–141.2 s.

According to the loadings plot (Figure S2), CST is highly negatively correlated to relative hydrophobicity. This observation can be explained by the fact that if relative hydrophobicity of the flocs is high, its free water is less firmly attached to the microstructure of the microbial flocs due to the low affinity of water for their hydrophobic surface. Consequently, less time is required for water to be released on the filter paper and to reach the outer circle during the CST measurement.

A significant impact of relative hydrophobicity on the dewaterability of the microbial flocs was also reported by Jin et al. [123]. However, their findings showed the opposite tendencies, which was, probably, due to low CST values and their low variance in the experiment (~12.5–17.5 s).

Time-to-Filter (TTF) is a parameter of ML filterability, which is correlated with CST and is occasionally used in the MBR investigation practice [117,124,125]. In a study by Gkotsis et al. [40], TTF was used as the indicator of reversible fouling and as a variable for the determination of filterability enhancement during the batch filtration tests. On the contrary, as admitted by Fan et al. [126], the static conditions, which were applied during the TTF method, involved different mechanisms of particle agglomeration on the membrane surface, than those, during the MBR filtration cycle, thus making this parameter a poor indicator of the critical flux in MBR.

In the current research, the elevated TTF levels in the overdosing regions for TRT applying the pH adjustment appeared to be a good indicator of the deterioration of the mixed liquor filterability. However, we incline to the idea that TTF is an auxiliary parameter for the characterization of biomass fouling potential, which, if necessary, can be determined based on its correlation with CST.

According to different studies [61,127,128], the surfaces of EPSs and SMPs contain ionogenic functional groups such as $-\text{OH}$; $-\text{COOH}$; $-\text{OPO}_3\text{H}_2$, $-\text{OSO}_3$, $-\text{OC}_3\text{H}_5\text{O}_3$ (glycerate), $-\text{OC}_3\text{H}_3\text{O}_2$ (pyruvate) and $\text{C}_4\text{H}_4\text{O}_4$ (succinate), which have a high affinity towards polyvalent metal ions and, at neutral and slightly alkaline pH, bear negative charges.

The decrease of the absolute value of electrokinetic potential (ζ -potential) of mixed liquor was among the central tasks of the experiments, conducted in the present study. Electrokinetic potential is a key parameter for characterization of the interaction between the ML foulants and the membrane surface, assessment of the biomass fouling propensity and efficiency of chemical flux enhancement via the charge neutralization mechanism in MBR/BF-MBR systems [15,110,129–132].

The present study assessed the flocculating ability of the flux enhancements based on the parameters of the particle size distribution. Particle size distribution/mean particle size is another important characteristic of mixed liquor in MBR/BF-MBR, which was investigated by different research teams [23,131–135]. The increase in mean particle size can play a crucial role in terms of fouling mitigation due to the potential shift of the fouling type from irrecoverable or irreversible to reversible, drastically improving the efficiency of membrane cleaning and fouling mitigation. Besides, the increase in size of the particles facilitates their back transport (shear-induced diffusion) from the membrane surface to the bulk solution and surface erosion (scouring of the membrane surface by flocs), which positively contribute to the flux enhancement [9,33,136]. The decrease in particle size over time indicates the deflocculation of the formed aggregates due to their inability to resist the shear forces [137]. Floc breakage can result in the release of SMPs to mixed liquor and, consequently, more severe membrane fouling.

Partial least squares analysis (PLS) and principal component analysis (PCA) were applied in different studies on membrane fouling in MBR [57,138–142]. Even though various fields of chemistry and industrial process control can benefit from the use of these multivariate chemometric analysis [143], its application for the analysis of the fouling development and mitigation in membrane systems, particularly in BF-MBR, is still quite limited. In the work by Kulesha et al. [42], PLS-regression analysis was used for developing the fouling prediction and control strategy based on the interrelation between the mixed liquor characteristics, fouling indicators and the operating conditions. Average normalized permeability and its slope were found to be the most reliable fouling indicators. The present study,

as well as our previous work [42], proved that multivariate chemometric approach based on (PLS), that is, PLS-regression (PLSR), is a reliable tool for characterization, prediction and control of membrane fouling in the BF-MBR.

Systematic research, demonstrated in the current work, develops the concept of chemical flux enhancement in the biofilm membrane bioreactor (BF-MBR) based on an adsorption/charge neutralization mechanism, revealed from the comparative study of prepolymerized and non-prepolymerized inorganic coagulants through the chemometric approach to membrane fouling control and optimization of membrane filtration.

The underlying hypothesis was that prepolymerized aluminium chloride (PACl) coagulants have a higher potential to improve the filtration performance of the BF-MBR system in wastewater treatment applications than the non-prepolymerized ones [35]. Neither of the currently found studies on chemical flux enhancement in BF-MBR could prove this hypothesis [22,35], despite the fact, that prepolymerized aluminium coagulants were reported to be more efficient than their non-prepolymerized counterparts in coagulation/flocculation processes with regard to removal of particulate and colloidal matter [36,144], likewise in membrane flux enhancement in MBRs [38,39].

The current research demonstrated that the general mechanisms of fouling mitigation in BF-MBR, are almost the same as in MBR systems, defined in our previous study [7], thus the observations on MBR systems could be continued for BF-MBR systems and the mechanisms of processes were studied and explained in this work.

Apart from defining the mechanisms of coagulant action, our previous work [7], reported that different bacterial solid surfaces have readily ionizable functional groups, which are pH dependent, and, a negative surface charge prevails merely at alkaline pH. The latter part of the statement was not confirmed in the current work during the analysis of the raw mixed liquor, where the zeta-potential values of the samples with no coagulant addition or pH adjustment were negative -14.01 – (-11.5) mV at acidic/neutral pH_{raw} 5.1–7.0 and temperature 17.1–23.1 °C. The negative charge of the mixed liquor system at neutral pH corresponds to the previous findings [128], while the presence of the negative biomass charge under acidic conditions still remains unclear. The potential reasons could be: (1) a complex composition of the mixed liquor, which consists not merely of the bacteria but also of the viruses, fungi, single-celled organisms, dead cells and products of their decay; (2) the release of organically bonded nitrogen from the biodegradable organics and its subsequent nitrification in the MBBR part, entailing its oxidation to nitrites (NO_2^-), which are further oxidized to nitrates (NO_3^-), influencing the charge of the system.

The current research defined the necessity of the pH adjustment before and during the coagulant addition to provide complete coagulation of the mixed liquor according to Le Chatelier's principle. The efficiency of the studied coagulants was highly improved by pH adjustment, conducting coagulation at optimum pH levels: 5.5–6.0 for prepolymerized aluminium chloride coagulants, 4.5 for aluminium sulphate and 3.8–4.1 for iron (III) sulphate.

The observations of the superior performance of prepolymerized coagulants regarding fouling mitigation in the current research agree with the studies by Wu et al. [38] and Chen and Liu [39]. However, Ivanovic and Leiknes [22,35] made the conclusions, which contradict to Wu et al. [38] and Chen and Liu [39], as well as with the results of our work.

The concept, presented in the current work, is advantageous, since it serves as a bridge between the flux enhancement mechanisms, mixed liquor fouling propensity, filtration parameters and characteristics of the tested coagulants, employing the statistical approaches, which helps to create a more comprehensive picture of fouling mitigation and prediction to solve the existing dilemma.

According to the obtained results, the extent of chemical flux enhancement in the BF-MBR system highly correlated with the resulting system charge, being strongly affected by the intrinsic charge concentration of the coagulants and their basicity. The ranking trend among the studied coagulants in decreasing order of fouling mitigation can be classified as: PACl with medium basicity (OH/Al 1.3, $0.97 \mu\text{equiv.}/\text{mg}_{\text{salt}}$) > PACl with high basicity (OH/Al 1.9, $0.65 \mu\text{equiv.}/\text{mg}_{\text{salt}}$) > $\text{Fe}_2(\text{SO}_4)_3$

(OH/Fe 0, 0.26 $\mu\text{equiv./mg}_{\text{salt}}$) \approx $\text{Al}_2(\text{SO}_4)_3$ (OH/Al 0, 0.06 $\mu\text{equiv./mg}_{\text{salt}}$). One can assume that there is a critical basicity and charge concentration level (OH/Al > 1.3, charge concentration \leq 0.26 $\mu\text{equiv./mg}_{\text{salt}}$) at which the coagulant is not able to sufficiently destabilize the disperse system in BF-MBR. Apparently, the function of filtration enhancement versus the coagulant basicity has a quadratic polynomial character with the maximum reached at the medium basicity level, which requires further investigations.

Prepolymerized aluminium chloride of medium basicity demonstrated the greatest extent of membrane fouling reduction, which can be explained by its highest bearing charge, and, hence the highest potential to neutralize the oppositely charged foulants. In addition, prepolymerized aluminium chloride of medium basicity alleviated fouling by the increase of foulant relative hydrophobicity, reduction of the concentration of soluble microbial products and the increase of the size of particulate matter. However, we attribute its outstanding efficiency mainly to the dominance of a complex adsorption/charge neutralization mechanism since, in case of non-prepolymerized aluminium or iron (III) sulphate, neither the increase of the particle size nor the combination of the SMPs removal with the increase of floc relative hydrophobicity alone could provide a sufficient level of flux enhancement.

Thus, the conclusions by Ivanovic and Leiknes [22,35], that flux enhancement occurs merely through the increase of the particle size and reduction of the content of submicron particles with practically no role of charge neutralization mechanism cannot be supported without going into the conflict. However, their results might be explained by the applied pH of coagulation, which apparently was unfavourable for coagulation (below the optimum levels). Thus, this entails the incomplete hydrolysis of $\text{Fe}(\text{H}_2\text{O})_6^{3+}$ and prepolymerized aluminium species (like $\text{Al}_{13}\text{O}_4(\text{OH})^{7+}$) and, hence, the incomplete destabilization of the disperse system. As shown in the current work, Fe-based coagulants can work at a more acidic pH, than Al-based coagulants and therefore can provide better coagulation and fouling mitigation, which was observed in the mentioned studies [22,35].

Since adsorption/charge neutralization was found to be the principal mechanism during chemical flux enhancement in BF-MBR system, no additional testing is required to evaluate the fouling alleviation propensity of the new inorganic coagulants in this system, which will help to simplify the testing procedure and bring the technology to the next level.

The optimization analysis revealed the significance of MLSS, coagulant dose, temperature and pH in the filtration processes. It is noteworthy that the developed optimization approach can be applied to predict the filtration performance, specifying the factorial levels for a single variable outside the defined factorial settings, since the valid range for coded values is -5 – $+5$. This can be very useful during the operational routine, taking into account the fluctuations in the characteristics of the incoming wastewater. While wastewater temperature is barely controllable in practice and mostly varies with the season (warm/cold) [145] and the intensity/frequency of the storm events [146], its potential impact on the BF-MBR system can be predicted, applying the derived models. The adverse effect of the low temperatures can be minimized by adjusting the levels of the other parameters in the system, according to the presented optimization analysis. As shown in our previous work [42], MLSS can be regulated by adjusting sludge retention time in the decentralized BF-MBR systems. Meanwhile, the coagulant dose and pH of mixed liquor are readily adjustable by changing the settings of the relevant dosing stations.

Different future research directions can be singled out. The developed multivariate chemometric approach can be used for the development of the sensors for fouling monitoring and prediction based on the biomass properties in BF-MBR.

In this work, mixed liquor was considered as substrate and all the mechanisms of fouling mitigation in BF-MBR were studied in relation to the substrate. However, further studies in this area can focus on the composition of the biocoenosis in BF-MBR to develop a targeting chemical influence on its fouling propensity, depending on the content.

The current research was focused on the use of individual inorganic coagulants in the separation chamber of BF-MBR; however, they can be applied in pairs with organic flocculants and the potential of their dosing in MBRR part should be checked.

If the BF-MBR is designed to biologically remove phosphorus and nitrogen in MBBR part, with the use of anaerobic and anoxic stages, it might affect fouling intensity and mitigation in the BF-MBR, which also requires further investigation.

5. Conclusions

The current research conducted the comparative study of prepolymerized and non-prepolymerized inorganic coagulants through the chemometric approach to membrane fouling control and optimization of membrane filtration, resulting in the development of the concept of chemical flux enhancement in the biofilm membrane bioreactor based on the adsorption/charge neutralization mechanism.

Introduction of prepolymerized aluminium chloride of medium and high basicity, as well as aluminium or iron (III) sulphate to the membrane separation stage of the biofilm membrane bioreactor, provides equally high turbidity removal and residual orthophosphate concentration below the allowable limits. Two prepolymerized aluminium coagulants and iron (III) sulphate provided the highest removal of dissolved organic matter. Application of prepolymerized aluminium coagulants in the optimum dosage region resulted in the residual aluminium concentrations below the allowable limits (0–0.03 mgAl/L), which is favourable for the environment.

In contrast to the non-prepolymerized coagulants, prepolymerized aluminium coagulants were much more efficient with respect to flux enhancement. They demonstrated the greatest fouling mitigation extent: 120.0 min of filtration time and the maximum increase of the average normalized permeability by 155.0–198.0%, which corresponds to a tenfold increase in filtration length of the membrane separation cycle and 30.0–56.0% increase in net flux (depending on the operational period) of the BF-MBR pilot system.

The prepolymerized aluminium chloride of medium basicity had the highest bearing positive charge and demonstrated the greatest extent of fouling alleviation, which suggests the significance of the adsorption/charge neutralization mechanism in the flux enhancement in biofilm membrane bioreactor, while in case of non-prepolymerized iron (III) or aluminium sulphate the combination of the dissolve organic matter removal with the increase of floc relative hydrophobicity or the increase in particle size were not enough.

The efficiency of the studied coagulants can be improved by applying optimum pH levels of coagulation: 5.5–6.0 for prepolymerized aluminium chloride coagulants, 4.5 for aluminium sulphate and 3.8–4.1 for iron (III) sulphate.

The developed PLS-regression model demonstrated the significance of the selected mixed liquor parameters and the response functions for estimation and prediction of fouling intensity. The cross-validation of the derived model indicated low uncertainty and negligible bias of the predictions; and hence, high reliability of the model, allowing its further implementation.

The analysis of the two-level factorial design of the experiment provided the models for estimation and prediction of the fouling intensity and the levels of the factors for optimization of membrane filtration using the prepolymerized aluminium chloride with medium basicity. The validation analysis, point prediction and confirmation for the defined factor settings proved the absence of outliers, stability and reliability of the derived optimization models.

The models can be used to adjust operational parameters of the BF-MBR pilot system according to the characteristics of biomass, which will improve filtration efficiency and stability in the system.

The results of this research will simplify the evaluation of the flux enhancers in decentralized BF-MBR systems and can serve as the basis for the automated process control of BF-MBR, which is another step towards the increase of filtration efficiency, operation improvement and the reduction of maintenance costs.

Supplementary Materials: The following are available online at <http://www.mdpi.com/2073-4441/11/3/446/s1>, Figure S1: Preliminary examination of the influence of: (a) coagulant dose; (b) pH; (c) temperature on the average permeability, coloured by MLSS, Figure S2: A negative correlation between capillary suction time (CST)

and relative hydrophobicity (RH) earlier obtained for BF-MBR mixed liquor by Kulesha et al. [42], Table S1: Characterization of particle properties by particle size distribution [48–52], Table S2: Optimum pH ranges and the corresponding parameters of the system, Table S3: Optimum dosages at the corrected pH values applying tested coagulants, Table S4: Optimum dosages and the corresponding levels of the monitored parameters during TRT with pH adjustment, Table S5: The obtained optimum concentration ranges of the added coagulants with and without the pH correction, Table S6: Point prediction and confirmation for the tested factor settings.

Author Contributions: O.K. and Z.M. conceived and designed the experiments; O.K. performed the experiments under the supervision of Z.M. and analysed the data; O.K. performed statistical and image analysis under the supervision of K.K.; K.K. contributed to the discussion of the article; H.R. contributed reagents, materials and analysis tools and contributed to the discussion of the article; O.K. wrote the paper with advice from Z.M., K.K. and H.R.

Funding: This research was co-funded by the CE-MBR project (project number: 865000006MH) and the Erasmus+ Program of the European Union (project number: 561755-EPP-1-2015-1-NOEPPKA2-CBHE-JP).

Acknowledgments: Authors express their gratitude to Stella Saliu for her input as Erasmus+ exchange student and Sven Andreas Högfeldt for his guidance on size exclusion chromatography.

Conflicts of Interest: The authors declare no conflict of interest. The founding sponsors had no role in the design of the study; in the collection, analyses or interpretation of data; in the writing of the manuscript and in the decision to publish the results.

References

1. European Commission. *Regulation of the European Parliament and the Council on Minimum Requirements for Water Reuse*; European Commission: Brussels, Belgium, 2018; Volume 169, p. 28.
2. European Commission. *Report on the Review of the European Water Scarcity and Droughts Policy*; European Commission: Brussels, Belgium, 2012.
3. Hankins, N.P.; Singh, R. *Emerging Membrane Technology for Sustainable Water Treatment*; Marinakis, K., Ed.; Elsevier: Amsterdam, The Netherlands; Oxford, UK; Cambridge, MA, USA, 2016; ISBN 978-0-444-63312-5.
4. Maletskiy, Z.; Kulesha, O.; Ratnaweera, H.C. Comparison of Al- and Fe-based Membrane Fouling Reducers for BioFilm Membrane BioReactor. In Proceedings of the Euromembrane 2018, Valencia, Spain, 9–13 July 2018.
5. United States Environmental Protection Agency Water Reuse and Recycling: Community and Environmental Benefits. Available online: <https://www3.epa.gov/region9/water/recycling/> (accessed on 22 January 2019).
6. Bernal, D.P.; Restrepo, I. Key issues for decentralization in municipal wastewater treatment. In *12th Edition of the World Wide Workshop for Young Environmental Scientists (WWW-YES-2012)—Urban Waters: Resource or Risks?* HAL-ENPC: Arcueil, France, 2012.
7. Kulesha, O.; Maletskiy, Z.; Ratnaweera, H. State-of-the-art of membrane flux enhancement in membrane bioreactor. *Cogent Eng.* **2018**, *5*, 1–30. [[CrossRef](#)]
8. Meng, F.; Zhang, S.; Oh, Y.; Zhou, Z.; Shin, H.-S.; Chae, S.-R. Fouling in membrane bioreactors: An updated review. *Water Res.* **2017**, *114*, 151–180. [[CrossRef](#)] [[PubMed](#)]
9. Jørgensen, M.K.; Nierychlo, M.; Nielsen, A.H.; Larsen, P.; Christensen, M.L.; Nielsen, P.H. Unified understanding of physico-chemical properties of activated sludge and fouling propensity. *Water Res.* **2017**, *120*, 117–132. [[CrossRef](#)] [[PubMed](#)]
10. Zhu, J.; Hou, J.; Zhang, Y.; Tian, M.; He, T.; Liu, J.; Chen, V. Polymeric antimicrobial membranes enabled by nanomaterials for water treatment. *J. Membr. Sci.* **2018**, *550*, 173–197. [[CrossRef](#)]
11. Zheng, Y.; Zhang, W.; Tang, B.; Ding, J.; Zheng, Y.; Zhang, Z. Membrane fouling mechanism of biofilm-membrane bioreactor (BF-MBR): Pore blocking model and membrane cleaning. *Bioresour. Technol.* **2018**, *250*, 398–405. [[CrossRef](#)] [[PubMed](#)]
12. Ivanovic, I.; Leiknes, T.O. The biofilm membrane bioreactor (BF-MBR)—A review. *Desalin. Water Treat.* **2012**, *37*, 288–295. [[CrossRef](#)]
13. Ødegaard, H. Innovations in wastewater treatment: The moving bed biofilm process. *Water Sci. Technol.* **2006**, *53*, 17–33. [[CrossRef](#)] [[PubMed](#)]
14. Phattaranawik, J.; Leiknes, T. Study of Hybrid Vertical Anaerobic Sludge-Aerobic Biofilm Membrane Bioreactor for Wastewater Treatment. *Water Environ. Res.* **2010**, *82*, 273–280. [[CrossRef](#)] [[PubMed](#)]
15. Sun, C.; Leiknes, T.; Fredriksen, R.H.; Riviere, E. Comparison of membrane filtration performance between biofilm-MBR and activated sludge-MBR. *Desalin. Water Treat.* **2012**, *48*, 285–293. [[CrossRef](#)]

16. Leiknes, T.; Ødegaard, H. The development of a biofilm membrane bioreactor. *Desalination* **2007**, *202*, 135–143. [[CrossRef](#)]
17. Dalmau, M.; Atanasova, N.; Gabarrón, S.; Rodriguez-Roda, I.; Comas, J. Comparison of a deterministic and a data driven model to describe MBR fouling. *Chem. Eng. J.* **2015**, *260*, 300–308. [[CrossRef](#)]
18. Deng, L.; Guo, W.; Ngo, H.H.; Zhang, H.; Wang, J.; Li, J.; Xia, S.; Wu, Y. Biofouling and control approaches in membrane bioreactors. *Bioresour. Technol.* **2016**, *221*, 656–665. [[CrossRef](#)] [[PubMed](#)]
19. Germain, E.; Stephenson, T. Biomass characteristics, aeration and oxygen transfer in membrane bioreactors: Their interrelations explained by a review of aerobic biological processes. *Rev. Environ. Sci. Biotechnol.* **2005**, *4*, 223–233. [[CrossRef](#)]
20. Sun, F.Y.; Li, P.; Li, J.; Li, H.J.; Ou, Q.M.; Sun, T.T.; Dong, Z.J. Hybrid biofilm-membrane bioreactor (Bf-MBR) for minimization of bulk liquid-phase organic substances and its positive effect on membrane permeability. *Bioresour. Technol.* **2015**, *198*, 772–780. [[CrossRef](#)] [[PubMed](#)]
21. Nouri, N.; Mehrnia, M.R.; Sarrafzadeh, M.H.; Nabizadeh, R. Performance of membrane bioreactor in presence of flocculants. *Desalin. Water Treat.* **2013**, *52*, 2933–2938. [[CrossRef](#)]
22. Ivanovic, I.; Leiknes, T.O. Improved Performance through Particle Surface Modifications by Coagulation with Inorganic Coagulants in a Biofilm Membrane Bioreactor (BF-MBR). *Sep. Sci. Technol.* **2012**, *48*, 288–294. [[CrossRef](#)]
23. Deng, L.; Guo, W.; Hao, H.; Farzana, M.; Zuthi, R.; Zhang, J.; Liang, S.; Li, J.; Wang, J.; Zhang, X. Membrane fouling reduction and improvement of sludge characteristics by biofloculant addition in submerged membrane bioreactor. *Sep. Purif. Technol.* **2015**, *156*, 450–458. [[CrossRef](#)]
24. Iversen, V.; Mehrez, R.; Horng, R.Y.; Chen, C.H.; Meng, F.; Drews, A.; Lesjean, B.; Ernst, M.; Jekel, M.; Kraume, M. Fouling mitigation through flocculants and adsorbents addition in membrane bioreactors: Comparing lab and pilot studies. *J. Membr. Sci.* **2009**. [[CrossRef](#)]
25. Wu, J.; Huang, X. Effect of dosing polymeric ferric sulfate on fouling characteristics, mixed liquor properties and performance in a long-term running membrane bioreactor. *Sep. Purif. Technol.* **2008**, *63*, 45–52. [[CrossRef](#)]
26. Wang, Z.; Wu, Z.; Mai, S.; Yang, C.; Wang, X.; An, Y.; Zhou, Z. Research and applications of membrane bioreactors in China: Progress and prospect. *Sep. Purif. Technol.* **2008**, *62*, 249–263. [[CrossRef](#)]
27. Ji, J.; Li, J.; Qiu, J.; Li, X. Polyacrylamide-starch composite flocculant as a membrane fouling reducer: Key factors of fouling reduction. *Sep. Purif. Technol.* **2014**, *131*, 1–7. [[CrossRef](#)]
28. Xiao, Y.; Waheed, H.; Xiao, K.; Hashmi, I.; Zhou, Y. In tandem effects of activated carbon and quorum quenching on fouling control and simultaneous removal of pharmaceutical compounds in membrane bioreactors. *Chem. Eng. J.* **2018**, *341*, 610–617. [[CrossRef](#)]
29. Zhang, H.; Sun, B.; Zhao, X.; Gao, Z. Effect of ferric chloride on fouling in membrane bioreactor. *Sep. Purif. Technol.* **2008**, *63*, 341–347. [[CrossRef](#)]
30. Guo, W.; Ngo, H.H.; Vigneswaran, S.; Dharmawan, F.; Nguyen, T.T.; Aryal, R. Effect of different flocculants on short-term performance of submerged membrane bioreactor. *Sep. Purif. Technol.* **2010**, *70*, 274–279. [[CrossRef](#)]
31. Liu, Y.Y.; Zhang, W.J.; Yang, X.Y.; Xiao, P.; Wang, D.S.; Song, Y. Advanced treatment of effluent from municipal WWTP with different metal salt coagulants: Contaminants treatability and floc properties. *Sep. Purif. Technol.* **2013**, *120*, 123–128. [[CrossRef](#)]
32. Holbrook, R.D.; Higgins, M.J.; Murthy, S.N.; Fonseca, A.D.; Fleischer, E.J.; Daigger, G.T.; Grizzard, T.J.; Love, N.G.; Novak, J.T. Effect of alum addition on the performance of submerged membranes for wastewater treatment. *Water Environ. Res.* **2003**, *76*, 2699–2702. [[CrossRef](#)]
33. Lee, J.C.; Kim, J.S.; Kang, I.J.; Cho, M.H.; Park, P.K.; Lee, C.H. Potential and limitations of alum or zeolite addition to improve the performance of a submerged membrane bioreactor. *Water Sci. Technol.* **2001**, *43*, 59–66. [[CrossRef](#)] [[PubMed](#)]
34. Song, K.G.; Kim, Y.; Ahn, K.H. Effect of coagulant addition on membrane fouling and nutrient removal in a submerged membrane bioreactor. *Desalination* **2008**, *221*, 467–474. [[CrossRef](#)]
35. Ivanovic, I.; Leiknes, T. Effect of addition of different additives on overall performance of biofilm-MBR (BF-MBR). *Desalin. Water Treat.* **2011**, *34*, 129–135. [[CrossRef](#)]
36. Ødegaard, H.; Fettig, J.; Ratnaweera, H.C. *Coagulation with Prepolymerized Metal Salts*; Hahn, H.H., Klute, R., Eds.; Chemical Water and Wastewater Treatment; Springer: Berlin/Heidelberg, Germany, 1990; ISBN 978-3-642-76093-8.

37. Gregory, J.; Duan, J. Hydrolyzing metal salts as coagulants. *Pure Appl. Chem.* **2001**, *73*, 2017–2026. [CrossRef]
38. Wu, J.; Chen, F.; Huang, X.; Geng, W.; Wen, X. Using inorganic coagulants to control membrane fouling in a submerged membrane bioreactor. *Desalination* **2006**, *197*, 124–136. [CrossRef]
39. Chen, W.; Liu, J. The possibility and applicability of coagulation-MBR hybrid system in reclamation of dairy wastewater. *Desalination* **2012**, *285*, 226–231. [CrossRef]
40. Gkotsis, P.K.; Batsari, E.L.; Peleka, E.N.; Tolkou, A.K.; Zouboulis, A.I. Fouling control in a lab-scale MBR system: Comparison of several commercially applied coagulants. *J. Environ. Manag.* **2017**, *203*, 838–846. [CrossRef] [PubMed]
41. Bratby, J. *Coagulation and Flocculation in Water and Wastewater Treatment*, 2nd ed.; IWA Publishing: London, UK; Seattle, WA, USA, 2006; ISBN 9781843391067.
42. Kulesha, O.; Maletskyi, Z.; Ratnaweera, H. Multivariate Chemometric Analysis of Membrane Fouling Patterns in Biofilm Ceramic Membrane Bioreactor. *Water* **2018**, *10*, 982. [CrossRef]
43. Lee, W.-N.; Chang, I.-S.; Hwang, B.-K.; Park, P.-K.; Lee, C.-H.; Huang, X. Changes in biofilm architecture with addition of membrane fouling reducer in a membrane bioreactor. *Process Biochem.* **2007**, *42*, 655–661. [CrossRef]
44. Yeon, K.-M.; Cheong, W.-S.; Oh, H.-S.; Lee, W.-N.; Hwang, B.-K.; Lee, C.-H.; Beyenal, H.; Lewandowski, Z. Quorum Sensing: A New Biofouling Control Paradigm in a Membrane Bioreactor for Advanced Wastewater Treatment. *Environ. Sci. Technol.* **2009**, *43*, 380–385. [CrossRef] [PubMed]
45. Oh, H.-S.; Yeon, K.-M.; Yang, C.-S.; Kim, S.-R.; Lee, C.-H.; Park, S.Y.; Han, J.Y.; Lee, J.-K. Control of membrane biofouling in MBR for wastewater treatment by quorum quenching bacteria encapsulated in microporous membrane. *Environ. Sci. Technol.* **2012**, *46*, 4877–4884. [CrossRef] [PubMed]
46. International Organization for Standardization. *International Standard: ISO 15705:2002. Water Quality—Determination of the Chemical Oxygen Demand Index (ST-COD)—Small-Scale Sealed-Tube Method*; International Organization for Standardization: Geneva, Switzerland, 2002; p. 18.
47. ImageJ: Image Processing and Analysis in Java. Available online: <https://imagej.nih.gov/ij/> (accessed on 1 February 2019).
48. Rawle, A. Basic Principles of Particle Size Analysis. Available online: <http://cat.inist.fr/?aModele=afficheN&cpsid=14620810> (accessed on 20 November 2018).
49. Innopharma Technology. A Guide to D-Values in Pharmaceutical Particle Characterisation. Available online: <http://www.innopharmalabs.com/tech/applications-and-processes/particle-size-distribution> (accessed on 20 November 2018).
50. Horiba Ltd. A Guidebook to Particle Size Analysis. Available online: https://www.horiba.com/fileadmin/uploads/Scientific/Documents/PSA/PSA_Guidebook.pdf (accessed on 20 November 2018).
51. Malvern Instruments Limited. A Basic Guide to Particle Characterization. Available online: https://www.cif.iastate.edu/sites/default/files/uploads/Other_Inst/ParticleSize/ParticleCharacterizationGuide.pdf (accessed on 20 November 2018).
52. Malvern Instruments Ltd. Manual 0101. Available online: Pmbrc.org/index.php/download_file/view/190 (accessed on 20 November 2018).
53. Micrometrix Corporation. *Particle Charge Analyser. Operating Manual*; Micrometrix Corporation: Suwanee, GA, USA, 2012; p. 19.
54. American Public Health Association; Water Environment Federation; American Water Works Association. *Standard Methods for the Examination of Water and Wastewater*, 22nd ed. Rice, E.W., Baird, R.B., Eaton, A.D., Clesceri, L.S., Eds.; American Public Health Association: Washington, DC, USA, 2012; ISBN 9780875530130.
55. CAMO. *The Unscrambler Tutorials. CAMO Process AS 2006*; CAMO Software AS: Oslo, Norway, 2006; p. 179.
56. Olivieri, A.C. *Introduction to Multivariate Calibration: A Practical Approach*; Springer: Cham, Switzerland, 2018; ISBN 9783319970974.
57. Van den Broeck, R.; Krzeminski, P.; Van Dierdonck, J.; Gins, G.; Lousada-Ferreira, M.; Van Impe, J.F.M.; van der Graaf, J.H.J.M.; Smets, I.Y.; van Lier, J.B. Activated sludge characteristics affecting sludge filterability in municipal and industrial MBRs: Unraveling correlations using multi-component regression analysis. *J. Membr. Sci.* **2011**, *378*, 330–338. [CrossRef]

58. Wold, S.; Sjöström, M.; Eriksson, L. PLS-regression: A basic tool of chemometrics. *Chemom. Intell. Lab. Syst.* **2001**, *58*, 109–130. [[CrossRef](#)]
59. Bratby, J. *Coagulation and Flocculation in Water and Wastewater Treatment*, 3rd ed.; IWA Publishing: London, UK, 2016; ISBN 9781780407500.
60. Ratnaweera, H.C. Influence of the Degree of Coagulant Prepolymerization on Wastewater Coagulation Mechanisms. Ph.D. Thesis, The University of Trondheim. The Norwegian Institute of Technology, Trondheim, Norway, 1991.
61. Stumm, W.; Morgan, J.J. Chemical Aspects of Coagulation. *J. Am. Water Works Assoc.* **1962**, *54*, 971–991. [[CrossRef](#)]
62. Stumm, W.; O'Melia, C. Stoichiometry of coagulation. *Am. Water Work. Assoc.* **1968**, *60*, 514–539. [[CrossRef](#)]
63. Meyn, T.; Leiknes, T.; Ødegaard, H. Coagulation/flocculation—Ceramic membrane filtration for removal of natural organic matter (NOM) under Norwegian conditions. In Proceedings of the IWA Conference on Membranes for Water and Wastewater Treatment, Harrogate, UK, 15–17 May 2007.
64. Liang, Z.; Wang, Y.; Zhou, Y.; Liu, H.; Wu, Z. Polishing treatment of molasses wastewater with iron salts: The role of counter-ions. *Water Environ. Res.* **2009**, *81*, 2293–2298. [[CrossRef](#)] [[PubMed](#)]
65. Ng, M.; Liana, A.E.; Liu, S.; Lim, M.; Chow, C.W.K.; Wang, D.; Drikas, M.; Amal, R. Preparation and characterisation of new-polyaluminum chloride-chitosan composite coagulant. *Water Res.* **2012**, *46*, 4614–4620. [[CrossRef](#)] [[PubMed](#)]
66. American Water College Zeta Potential—Coagulation and Flocculation Lecture. Available online: <https://thewaternetwork.com/article-FfV/zeta-potential-coagulation-and-flocculation-lecture-video-gUbFb9OUygf-evijymdc6g> (accessed on 29 November 2018).
67. Hall, E.S.; Packham, R.F. Coagulation of Organic Color With Hydrolyzing Coagulants. *J. Am. Water Work. Assoc.* **1965**, *57*, 1149–1166. [[CrossRef](#)]
68. Guminska, J.; Klos, M. Effect of Polyaluminium Chlorides Overdosage on Effectiveness of Coagulation and Filtration. *Environ. Prot. Eng.* **2015**, *41*, 5–14. [[CrossRef](#)]
69. Bachand, P.A.M.; Bachand, S.M.; Lopus, S.E.; Heyvaert, A.; Werner, I. Treatment with chemical coagulants at different dosing levels changes ecotoxicity of stormwater from the Tahoe basin, California, USA. *J. Environ. Sci. Heal. Part A Toxic/Hazard. Subst. Environ. Eng.* **2010**, *45*, 137–154. [[CrossRef](#)] [[PubMed](#)]
70. Wang, Z.; Wu, Z.; Tang, S. Impact of temperature seasonal change on sludge characteristics and membrane fouling in a submerged membrane bioreactor. *Sep. Sci. Technol.* **2010**, *45*, 920–927. [[CrossRef](#)]
71. Sobek, D.C.; Higgins, M.J. Examination of three theories for mechanisms of cation-induced bioflocculation. *Water Res.* **2002**, *36*, 527–538. [[CrossRef](#)]
72. Klute, R. Destabilization and Aggregation in Turbulent Pipe Flow. *Chem. Water Wastewater Treat.* **1990**, 33–54. [[CrossRef](#)]
73. Drews, A. Membrane fouling in membrane bioreactors—Characterisation, contradictions, cause and cures. *J. Membr. Sci.* **2010**, *363*, 1–28. [[CrossRef](#)]
74. Miller, D.J.; Kasemset, S.; Paul, D.R.; Freeman, B.D. Comparison of membrane fouling at constant flux and constant transmembrane pressure conditions. *J. Membr. Sci.* **2014**, *454*, 505–515. [[CrossRef](#)]
75. Council of the European Communities. *Directive Concerning Urban Waste Water Treatment (91/271/EEC)*; Urban Waste Water Directive: Brussels, Belgium, 1991; pp. 40–52.
76. Ratnaweera, H.; Ødegaard, H.; Fettig, J. Coagulation with prepolymerised aluminium salts and their influence on particle and phosphate removal. *Water Sci. Technol.* **1992**, *6*, 1229–1237. [[CrossRef](#)]
77. Zhang, X.; Fan, L.; Roddick, F.A. Feedwater coagulation to mitigate the fouling of a ceramic MF membrane caused by soluble algal organic matter. *Sep. Purif. Technol.* **2014**, *133*, 221–226. [[CrossRef](#)]
78. United States Environmental Protection Agency. *EPA Ambient Water Quality Criteria for Aluminium*; Office of Water Regulations and Standards Criteria and Standards Division: Washington, DC, USA, 1988.
79. European Commission. *EU-Level Instruments on Water Reuse: Final Report to Support the Commission's Impact Assessment*; European Commission: Brussels, Belgium, 2016.
80. Eignor, D. Draft National 304(a) Aluminum Aquatic Life Criteria. Available online: <https://www.epa.gov/sites/production/files/2017-09/documents/aluminum-webinar-9192017.pdf> (accessed on 1 December 2018).

81. Zhang, Z.; Wang, Y.; Leslie, G.L.; Waite, T.D. Effect of ferric and ferrous iron addition on phosphorus removal and fouling in submerged membrane bioreactors. *Water Res.* **2015**, *69*, 210–222. [CrossRef] [PubMed]
82. Wang, X.-M.; Waite, T.D. Role of gelling soluble and colloidal microbial products in membrane fouling. *Environ. Sci. Technol.* **2009**, *43*, 9341–9347. [CrossRef] [PubMed]
83. Dulko, J.M. Stable Concentrated Polyaluminium Chlorosilicate Solutions. US 2016/0244345 A1, issued 2016. US 2016/0244345 A1, 2016. [CrossRef]
84. Dulko, J.M. Stable Concentrated Polyaluminum Chlorosilicate Solutions. WO 2016/134277 A1, 2016. Available online: <https://patents.google.com/patent/WO2016134277A1> (accessed on 28 February 2018).
85. Zouboulis, A.I.; Tzoupanos, N.D. Polyaluminium silicate chloride-A systematic study for the preparation and application of an efficient coagulant for water or wastewater treatment. *J. Hazard. Mater.* **2009**, *162*, 1379–1389. [CrossRef] [PubMed]
86. Gao, B.Y.; Yue, Q.Y.; Wang, B.J.; Chu, Y.B. Poly-aluminum-silicate-chloride (PASiC)—A new type of composite inorganic polymer coagulant. *Colloids Surfaces A Physicochem. Eng. Asp.* **2003**, *229*, 121–127. [CrossRef]
87. Zhang, P.; Hahn, H.H.; Hoffmann, E.; Zeng, G. Influence of some additives to aluminium species distribution in aluminium coagulants. *Chemosphere* **2004**, *57*, 1489–1494. [CrossRef] [PubMed]
88. Tzoupanos, N.D.; Zouboulis, A.I.; Tsoleridis, C.A. A systematic study for the characterization of a novel coagulant (polyaluminium silicate chloride). *Colloids Surf. A Physicochem. Eng. Asp.* **2009**, *342*, 30–39. [CrossRef]
89. Ratnaweera, H.; Fetting, J. State of the art of online monitoring and control of the coagulation process. *Water (Switzerland)* **2015**, *7*, 6574–6597. [CrossRef]
90. Adgar, A.; Cox, C.S.; Jones, C.A. Enhancement of coagulation control using the streaming current detector. *Bioprocess Biosyst. Eng.* **2005**, *349*–357. [CrossRef] [PubMed]
91. Brookes, A.; Judd, S.; Reid, E.; Germain, E.; Smith, S.; Alvarez-Vazquez, H.; Le-Clech, P.; Stephenson, T.; Turra, E.; Jefferson, B. Biomass characterisation in membrane bioreactors. In Proceedings of the International Membrane Science and Technology Conference (IMSTEC), Sydney, Australia, 10–14 November 2003.
92. Striegel, A.M. Size-exclusion chromatography. In *Liquid Chromatography: Fundamentals and Instrumentation: Second Edition*; Elsevier: Gaithersburg, MD, USA, 2017; pp. 193–224. ISBN 9780128053935.
93. Montgomery, D.C. Design and Analysis of Experiments, 15th ed. John Wiley & Sons, Inc.: Scottsdale, AZ, USA, 1997.
94. Stat-Ease Inc. Design-Expert 11.1.0. Documentation. Tutorials. Available online: <https://www.statease.com/docs/v11/index.html> (accessed on 31 October 2018).
95. Ogee, A.; Ellis, M.; Stone, B.K.; Scibilia, B.; Pammer, C.; Steele, C. MiniTab 18: What Are T Values and P Values in Statistics? Available online: <https://blog.minitab.com/blog/statistics-and-quality-data-analysis/what-are-t-values-and-p-values-in-statistics> (accessed on 12 January 2019).
96. Mendenhall, W.; Sincich, T. *A Second Course in Statistics. Regression Analysis*, 7th ed.; Lynch, D., Ed.; Pearson Education, Inc.: Boston, MA, USA, 2012; ISBN 0-321-69169-5.
97. Winter, B. The F Distribution and the Basic Principle behind ANOVAs. Available online: http://www.bodowinter.com/tutorial/bw_anova_general.pdf (accessed on 1 November 2018).
98. The Bayes Information Criterion (BIC). Available online: <http://www-math.mit.edu/~rjmd/650/bic.pdf> (accessed on 1 November 2018).
99. Merisaari, H.; Jambor, I.; Jødal, L.; Oikonen, V. Akaike Information Criterion (AIC) in Model Selection. Available online: http://www.turkupetcentre.net/petanalysis/model_aic.html (accessed on 1 November 2018).
100. Montgomery, D.C. *Design and Analysis of Experiments*, 8th ed.; Ratts, L., Melhorn, A., Eds.; John Wiley & Sons, Inc.: Hoboken, NJ, USA, 2013; ISBN 9781118146927.
101. Hair, J.F.; Black, W.C.; Babin, B.J.; Anderson, R.E. *Multivariate Data Analysis. Pearson New International Edition*, 7th ed.; Pearson Education Limited: Harlow, UK, 2014; ISBN 9781292021904.
102. Azami, H.; Sarrafzadeh, M.H.; Mehrnia, M.R. Influence of sludge rheological properties on the membrane fouling in submerged membrane bioreactor. *Desalin. Water Treat.* **2011**, *34*, 117–122. [CrossRef]
103. Meng, F.; Shi, B.; Yang, F.; Zhang, H. Effect of hydraulic retention time on membrane fouling and biomass characteristics in submerged membrane bioreactors. *Bioprocess Biosyst. Eng.* **2007**, *30*, 359–367. [CrossRef] [PubMed]

104. Chang, I.S.; Kim, S.N. Wastewater treatment using membrane filtration—Effect of biosolids concentration on cake resistance. *Process Biochem.* **2005**, *40*, 1307–1314. [[CrossRef](#)]
105. Le-Clech, P.; Chen, V.; Fane, T.A.G. Fouling in membrane bioreactors used in wastewater treatment. *J. Membr. Sci.* **2006**, *284*, 17–53. [[CrossRef](#)]
106. Ji, L.; Zhou, J. Influence of aeration on microbial polymers and membrane fouling in submerged membrane bioreactors. *J. Membr. Sci.* **2006**, *276*, 168–177. [[CrossRef](#)]
107. Hernandez Rojas, M.E.; Van Kaam, R.; Schetrite, S.; Albasi, C. Role and variations of supernatant compounds in submerged membrane bioreactor fouling. *Desalination* **2005**, *179*, 95–107. [[CrossRef](#)]
108. Xie, W.M.; Ni, B.J.; Sheng, G.P.; Seviour, T.; Yu, H.Q. Quantification and kinetic characterization of soluble microbial products from municipal wastewater treatment plants. *Water Res.* **2016**, *88*, 703–710. [[CrossRef](#)] [[PubMed](#)]
109. Tu, X.; Zhang, S.; Xu, L.; Zhang, M.; Zhu, J. Performance and fouling characteristics in a membrane sequence batch reactor (MSBR) system coupled with aerobic granular sludge. *Desalination* **2010**, *261*, 191–196. [[CrossRef](#)]
110. Deng, L.; Guo, W.; Ngo, H.H.; Zhang, J.; Liang, S.; Xia, S.; Zhang, Z.; Li, J. A comparison study on membrane fouling in a sponge-submerged membrane bioreactor and a conventional membrane bioreactor. *Bioresour. Technol.* **2014**, *165*, 69–74. [[CrossRef](#)] [[PubMed](#)]
111. Zhang, H.; Yu, H.; Zhang, L.; Song, L. Bioresource Technology Stratification structure of polysaccharides and proteins in activated sludge with different aeration in membrane bioreactor. *Bioresour. Technol.* **2015**, *192*, 361–366. [[CrossRef](#)] [[PubMed](#)]
112. Johir, M.A.H.; Vigneswaran, S.; Sathasivan, A.; Kandasamy, J.; Chang, C.Y. Effect of organic loading rate on organic matter and foulant characteristics in membrane bio-reactor. *Bioresour. Technol.* **2012**, *113*, 154–160. [[CrossRef](#)] [[PubMed](#)]
113. Qin, L.; Zhang, G.; Meng, Q.; Zhang, H.; Xu, L.; Lv, B. Enhanced submerged membrane bioreactor combined with biosurfactant rhamnolipids: Performance for frying oil degradation and membrane fouling reduction. *Bioresour. Technol.* **2012**, *126*, 314–320. [[CrossRef](#)] [[PubMed](#)]
114. Shen, Y.; Zhao, W.; Xiao, K.; Huang, X. A systematic insight into fouling propensity of soluble microbial products in membrane bioreactors based on hydrophobic interaction and size exclusion. *J. Membr. Sci.* **2010**, *346*, 187–193. [[CrossRef](#)]
115. Pramanik, B.K.; Roddick, F.A.; Fan, L. Impact of biological activated carbon pre-treatment on the hydrophilic fraction of effluent organic matter for mitigating fouling in microfiltration. *Environ. Technol.* **2018**, *39*, 2243–2250. [[CrossRef](#)] [[PubMed](#)]
116. Mu, S.; Wang, S.; Liang, S.; Xiao, K.; Fan, H.; Han, B.; Liu, C.; Wang, X.; Huang, X. Effect of the relative degree of foulant “hydrophobicity” on membrane fouling. *J. Membr. Sci.* **2019**, *570–571*, 1–8. [[CrossRef](#)]
117. Ivanovic, I.; Leiknes, T.O.; Ødegaard, H. Fouling control by reduction of submicron particles in a BF-MBR with an integrated flocculation zone in the membrane reactor. *Sep. Sci. Technol.* **2008**, *43*, 1871–1883. [[CrossRef](#)]
118. Tian, Y.; Chen, L.; Zhang, S.; Cao, C.; Zhang, S. Correlating membrane fouling with sludge characteristics in membrane bioreactors: An especial interest in EPS and sludge morphology analysis. *Bioresour. Technol.* **2011**, *102*, 8820–8827. [[CrossRef](#)] [[PubMed](#)]
119. Tamacki, K.; Lyko, S.; Wintgens, T.; Melin, T.; Natau, F. Impact of extra-cellular polymeric substances on the filterability of activated sludge in membrane bioreactors for landfill leachate treatment. *Desalination* **2005**, *179*, 181–190. [[CrossRef](#)]
120. Rosenberger, S.; Evenblij, H.; Te Poele, S.; Wintgens, T.; Laabs, C. The importance of liquid phase analyses to understand fouling in membrane assisted activated sludge processes—Six case studies of different European research groups. *J. Membr. Sci.* **2005**, *263*, 113–126. [[CrossRef](#)]
121. Wu, Z.; Wang, Z.; Zhou, Z.; Yu, G.; Gu, G. Sludge rheological and physiological characteristics in a pilot-scale submerged membrane bioreactor. *Desalination* **2007**, *212*, 152–164. [[CrossRef](#)]
122. Pan, J.R.; Su, Y.C.; Huang, C.; Lee, H.C. Effect of sludge characteristics on membrane fouling in membrane bioreactors. *J. Membr. Sci.* **2010**, *349*, 287–294. [[CrossRef](#)]
123. Jin, B.; Wilén, B.M.; Lant, P. Impacts of morphological, physical and chemical properties of sludge flocs on dewaterability of activated sludge. *Chem. Eng. J.* **2004**, *98*, 115–126. [[CrossRef](#)]

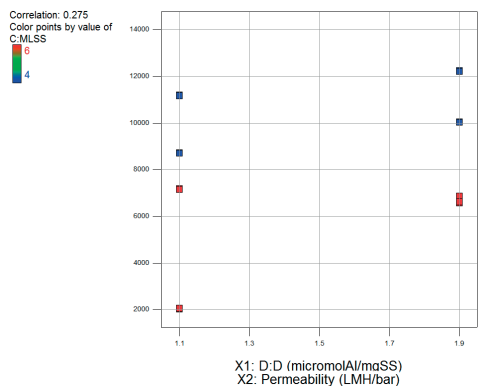
124. Niwa, R.; Yin, T.; Oo, M.H.; Noguchi, H.; Watanabe, T.; Razali, L.Y.; Png, H.Y.; Lay, W.C.L.; Ong, K.A.; Alom, M. Performance of a Full-Scale Ceramic MBR System to Treat Domestic Sewage. *Water Pract. Technol.* **2018**, *13*, 589–593. [[CrossRef](#)]
125. Gkotsis, P.K.; Mitrakas, M.M.; Tolkou, A.K.; Zouboulis, A.I. Batch and continuous dosing of conventional and composite coagulation agents for fouling control in a pilot-scale MBR. *Chem. Eng. J.* **2016**, *311*, 255–264. [[CrossRef](#)]
126. Fan, F.; Zhou, H.; Husain, H. Identification of wastewater sludge characteristics to predict critical flux for membrane bioreactor processes. *Water Res.* **2006**, *40*, 205–212. [[CrossRef](#)] [[PubMed](#)]
127. Stumm, W.; Morgan, J.J. *Aquatic Chemistry: Chemical Equilibria and Rates in Natural Waters*, 3rd ed.; Schnoor, J.J., Zehnder, A., Eds.; John Wiley & Sons, Inc.: New York, NY, USA, 1996.
128. Moran, A.P.; Holst, O.; Brennan, P.J.; von Itzstein, M. (Eds.) *Microbial Glycobiology: Structures, Relevance and Applications*; Elsevier Inc.: London, UK; Burlington: San Diego, CA, USA, 2009; ISBN 978-0-12-374546-0.
129. Chen, J.; Lin, H.; Shen, L.; He, Y.; Zhang, M.; Liao, B.Q. Realization of quantifying interfacial interactions between a randomly rough membrane surface and a foulant particle. *Bioresour. Technol.* **2017**, *226*, 220–228. [[CrossRef](#)] [[PubMed](#)]
130. Zhang, M.; Zhou, X.; Shen, L.; Cai, X.; Wang, F.; Chen, J.; Lin, H.; Li, R.; Wu, X.; Liao, B.Q. Quantitative evaluation of the interfacial interactions between a randomly rough sludge floc and membrane surface in a membrane bioreactor based on fractal geometry. *Bioresour. Technol.* **2017**, *234*, 198–207. [[CrossRef](#)] [[PubMed](#)]
131. Meng, F.; Zhang, H.; Yang, F.; Zhang, S.; Li, Y.; Zhang, X. Identification of activated sludge properties affecting membrane fouling in submerged membrane bioreactors. *Sep. Purif. Technol.* **2006**, *51*, 95–103. [[CrossRef](#)]
132. Ji, J.; Qiu, J.; Wai, N.; Wong, F.S.; Li, Y. Influence of organic and inorganic flocculants on physical-chemical properties of biomass and membrane-fouling rate. *Water Res.* **2010**, *44*, 1627–1635. [[CrossRef](#)] [[PubMed](#)]
133. Qin, L.; Fan, Z.; Xu, L.; Zhang, G.; Wang, G.; Wu, D.; Long, X.; Meng, Q. A submerged membrane bioreactor with pendulum type oscillation (PTO) for oily wastewater treatment: Membrane permeability and fouling control. *Bioresour. Technol.* **2015**, *183*, 33–41. [[CrossRef](#)] [[PubMed](#)]
134. Jang, N.; Ren, X.; Choi, K.; Kim, I.S. Comparison of membrane biofouling in nitrification and denitrification for the membrane bioreactor (MBR). *Water Sci. Technol.* **2006**, *53*, 43–49. [[CrossRef](#)] [[PubMed](#)]
135. Jin, L.; Ong, S.L.; Ng, H.Y. Fouling control mechanism by suspended biofilm carriers addition in submerged ceramic membrane bioreactors. *J. Membr. Sci.* **2013**, *427*, 250–258. [[CrossRef](#)]
136. Lykkegaard, M.; Niessen, W.; Boie, N.; Hove, S.; Koustrup, M.; Halkjær, P. Sludge fractionation as a method to study and predict fouling in MBR systems. *Sep. Purif. Technol.* **2018**, *194*, 329–337. [[CrossRef](#)]
137. Remy, M.; Potier, V.; Temmink, H.; Rulkens, W. Why low powdered activated carbon addition reduces membrane fouling in MBRs. *Water Res.* **2010**, *44*, 861–867. [[CrossRef](#)] [[PubMed](#)]
138. Philippe, N.; Racault, Y.; Stricker, A.E.; Sp, M.; Vanrolleghem, P.A. Modelling the long-term evolution of permeability in a full-scale MBR: Statistical approaches. *Desalination* **2013**, *325*, 7–15. [[CrossRef](#)]
139. Naessens, W.; Maere, T.; De Temmerman, L.; Nopens, I. Principal component analysis for monitoring membrane bioreactors: Trend detection, outlier detection and optimization. In Proceedings of the 2013 International Workshop—Membrane Bioreactor for Wastewater Reuse: Fundamental, Design and Operation, Tunis, Tunisia, 12–14 November 2013; pp. 2–5.
140. Kaneko, H.; Funatsu, K. Visualization of Models Predicting Transmembrane Pressure Jump for Membrane Bioreactor. *Ind. Eng. Chem. Res.* **2012**, *51*, 9679–9686. [[CrossRef](#)]
141. Choi, B.G.; Cho, J.; Song, K.G.; Maeng, S.K. Correlation between effluent organic matter characteristics and membrane fouling in a membrane bioreactor using advanced organic matter characterization tools. *Desalination* **2013**, *309*, 74–83. [[CrossRef](#)]
142. Jacquin, C.; Gambier, N.; Lesage, G.; Heran, M. New insight into fate and fouling behavior of bulk Dissolved Organic Matter (DOM) in a full-scale membrane bioreactor for domestic wastewater treatment. *J. Water Process Eng.* **2018**, *22*, 94–102. [[CrossRef](#)]
143. Geladi, P.; Kowalski, B.R. Partial least-squares regression: A tutorial. *Anal. Chim. Acta* **1986**, *185*, 1–17. [[CrossRef](#)]
144. Sivchenko, N. Image Analysis in Coagulation Process Control. Ph.D. Thesis, Norwegian University of Life Sciences (NMBU), Ås, Norway, 2017.

145. Wang, X.; Kvaal, K.; Ratnaweera, H. Characterization of influent wastewater with periodic variation and snow melting effect in cold climate area. *Comput. Chem. Eng.* **2017**, *106*, 202–211. [[CrossRef](#)]
146. Liltved, H.; Ratnaweera, H.; Plo, B.G. Climate change impacts on activated sludge wastewater treatment: A case study from Norway. *Water Sci. Technol. WST* **2009**, *60*, 533–541. [[CrossRef](#)]

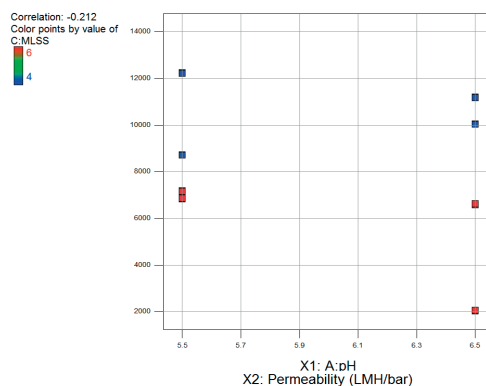


© 2019 by the authors. Licensee MDPI, Basel, Switzerland. This article is an open access article distributed under the terms and conditions of the Creative Commons Attribution (CC BY) license (<http://creativecommons.org/licenses/by/4.0/>).

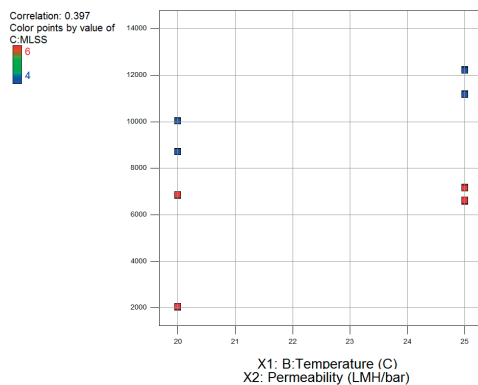
Supplementary Materials:



(a)



(b)



(c)

Figure 1. Preliminary examination of the influence of: (a) coagulant dose; (b) pH; (c) temperature on the average permeability, coloured by MLSS.

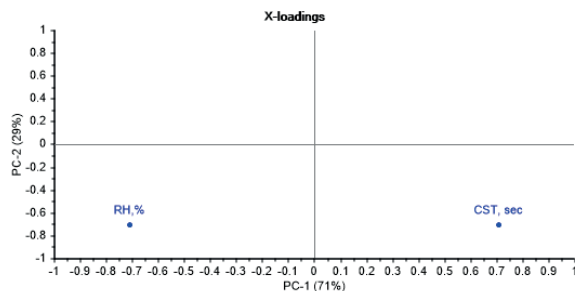


Figure 2. A negative correlation between capillary suction time (CST) and relative hydrophobicity (RH) earlier obtained for BF-MBR mixed liquor by Kulesha et al. [28].

Table 1. Characterization of particle properties by particle size distribution [48–52].

PSD parameter	Formula	Details
D[4,3], the De Broucker mean diameter	$\frac{\sum D_i^4}{\sum D_i^3}$	Volume/mass moment mean
D[3,2], the Sauter Mean diameter	$\frac{\sum D_i^3}{\sum D_i^2}$	Surface area moment mean
d10, d50, d90	- (from the cumulative distribution plot)	The diameter where 10%, 50% and 90% of the sample's population lie below this value
Uniformity	Median (d ₁ ,...d _i – Median (d ₁ ,...d _i))	The measure of the absolute deviation from the median
Span	$\frac{D90 - D10}{D50}$	The distribution width

Table 2. Optimum pH ranges and the corresponding parameters of the system.

Chemical	Parameters				Optimum pH ranges
	Zeta potential, mV	CST, sec	Turbidity, NTU	D [4,3], µm	
PAXXL61 (OH/Al 1.9)	-6.9 – (-6.3)	120.3 – 140.1	2.5 – 3.9	53.0 – 55.0	5.5 – 6.0
PAX18 (OH/Al 1.3)	-6.8 – (-6.4)	170.3 – 181.4	2.0 – 4.6	78.0 – 79.8	5.5 – 6.0
ALS (OH/Al 0)	-7.4	224.9	7.8	30.9	4.5
PIX313 (OH/Fe 0)	-5.6 – (-5.1)	107.0 – 117.5	2.7 – 3.2	31.4 – 32.5	3.8 – 4.1

Table 3. Optimum dosages at the corrected pH values applying tested coagulants.

Chemical	Maintained pH	Parameters				Optimum dosage ranges, µmole Me/mgSS
		CST, sec	Zeta potential, mV	Turbidity, NTU	D [4,3]	
PAXXL61 (OH/Al 1.9)	5.5 – 6.2	45.8 – 60.7	-1.1 – 3.7	0.5 – 1.8	25.6 – 32.6	1.1 – 2.6
PAX18 (OH/Al 1.3)	5.5 – 6.0	75.1 – 77.7	-3.7 – (-2.5)	0.5 – 1.1	37.5 – 67.4	1.3 – 2.6
ALS (OH/Al 0)	4.4 – 4.5	81.2 – 103.0	-4.6 – (-3.7)	1.8 – 2.5	21.0 – 34.3	0.5 – 1.2
PIX313 (OH/Fe 0)	4.0 – 4.1	130.0 – 150.0	-3.9 – (-3.5)	2.0 – 2.6	16.4 – 24.9	2.2 – 3.2

The highest efficiencies in respect of the average normalized permeability change ($\delta_{av}P_N$) and filtration time (F) were exhibited by the prepolymerized aluminium coagulants PAX18 and PAXXL61 (Table S3).

Table 4. Optimum dosages and the corresponding levels of the monitored parameters during TRT with pH adjustment.

Chemical	pH	Parameters						$\delta_{av}P_N$ %	F, min	Optimum Dosages, µmole Me/mgSS
		Zeta potential, mV	CST, sec	TTF, sec	Turbidity, NTU	D [4,3], µm				
PAXXL61 (OH/Al 1.9)	5.5 – 6.0	-1.1 – (-0.9)	17.9 – 18.9	209.0 – 285.0	0.6 – 0.8	21.5 – 39.3	155.4 – 198.2	120.0	1.1 – 1.9	
PAX18 (OH/Al 1.3)	5.5 – 6.0	-2.3 – (-0.8)	17.9 – 20.6	430.0 – 635.0	0.9 – 1.2	52.0 – 67.0	157.0 – 179.0	120.0	0.6 – 1.9	
ALS (OH/Al 0)	4.5	-5.2 – 0.1	20.4 – 27.5	457.0 – 1977.0	1.3 – 2.1	47.7 – 57.2	23.0 – 58.0	3.7 – 7.7	0.1 – 0.6	
PIX313 (OH/Fe 0)	3.8 – 4.1	-7.7 – (-1.0)	20.1 – 38.0	784.4 – 2017.0	0.9 – 4.4	24.0 – 39.0	-25.0 – 27.8	1.2 – 15.5	0.1 – 0.6	

Table 5. The obtained optimum concentration ranges of the added coagulants with and without the pH correction.

Coagulant	MLSS, g/L	pH _{coag}	Optimum Dose,			F, min	δ _{av} P _N , %	MLSS, g/L	pH _{coag}	Optimum Dose		F, min	δ _{av} P _N , %
			μmol Me/mg SS							μmol Me/mg SS			
			no pH adjustment							pH adjustment			
PAXXL61 (OH/Al 1.9)	5.9	4.2	1.5 – 1.9	4.7 – 10.4	76.8 – 83.0		4.5 – 5.6	5.5 – 6.0	1.1 – 1.9	120.0	155.4 – 198.2		
PAX18 (OH/Al 1.3)	4.7 – 5.2	4.1 – 4.2	1.5 – 3.7	7.0 – 49.0	5.6 – 63.0		4.5 – 5.6	5.5 – 6.0	0.6 – 1.9	120.0	157.0 – 179.0		
ALS (OH/Al 0)	3.7 – 5.2	3.7	0.1 – 0.2	1.2 – 5.0	-20.0 – 12.7		4.5 – 5.6	4.5	0.1 – 0.6	3.7 – 7.7	23.0 – 58.0		
PIX313 (OH/Fe 0)	3.2 – 5.3	2.8 – 3.2	1.3 – 3.0	3.0 – 7.7	15.7 – 19.6		4.5 – 5.6	3.8 – 4.1	0.1 – 0.6	1.2 – 15.5	-25.0 – 27.8		

Table 6. Point prediction and confirmation for the tested factor settings.

Response	Predicted Mean	Predicted Median ¹	Observed	Std Dev ⁹	SE Mean	The confidence interval for Mean		99% of the population	
						95% CI ⁵ low	95% CI high	95% TI ⁶ low	95% TI high
						I. Factor: pH 5.5; Temperature 25°C; MLSS 4.0 g/L; Dose 1.9 μmole Al/mg SS			
Permeability ²	12222.8	12222.8	-	15.8	N/A	12199.2	12246.5	12136.5	12308.8
I. Confirmation Report									
Two-sided		Confidence = 95%				n = 1			
Response	Predicted Mean	Predicted Median ⁴	Observed	Std Dev	n ⁸	SE Pred	95% PI low	Data Mean ³	95% PI high
Permeability ²	12222.8	12222.8	-	15.8	1	N/A		12179.9	12265.6
II. Factor: pH 5.5; Temperature 20°C; MLSS 5.9 g/L; Dose 1.1 μmole Al/mg SS									
Response	Predicted Mean	Predicted Median ¹	Observed	Std Dev	SE Mean	The confidence interval for Mean		99% of the population	
						95% CI ⁵ low	95% CI high	95% TI ⁶ low	95% TI high
Permeability ²	4750.9	4750.9	-	28.1	N/A	4709.9	4791.6	4597.2	4901.7
II. Confirmation Report									
Two-sided		Confidence = 95%				n = 1			
Response	Predicted Mean	Predicted Median ⁴	Observed	Std Dev	n ⁸	SE Pred	95% PI low	Data Mean ³	95% PI high
Permeability ²	4750.9	4750.9	-	28.1	1	N/A		4675.0	4826.2


Notes: ¹ For transformed responses the predicted mean and median may differ on the original scale; ² Standard error (SE) not calculated on the original scale; ³ For transformed responses the data mean is calculated on the transformed scale; ⁴ For transformed responses the predicted mean and median may differ on the original scale; ⁵ CI (confidence interval); ⁶ TI (Tolerance interval); ⁷ PI (Prediction interval); ⁸ n (the number of runs during the confirmation); Std Dev⁹ (standard deviation).

Paper IV

Kulesha, O.; Ratnaweera, H. C. Computational Thermodynamic Analysis of the Interaction between Coagulants and Monosaccharides as a Tool to Quantify the Fouling Potential Reduction in the Biofilm Membrane Bioreactor. *Water* **2019**, *11*, 1275, 1–30; DOI:10.3390/w11061275.

Article

Computational Thermodynamic Analysis of the Interaction between Coagulants and Monosaccharides as a Tool to Quantify the Fouling Potential Reduction in the Biofilm Membrane Bioreactor

Olga Kulesha ^{1,2,*}  and Harsha Ratnaweera ¹

¹ Faculty of Science and Technology (REALTEK), Norwegian University of Life Sciences, PO Box 5003, 1432 Ås, Norway; harsha.ratnaweera@nmbu.no

² Department of General and Inorganic Chemistry, Faculty of Chemical Technology, National Technical University of Ukraine "Igor Sikorsky Kyiv Polytechnic Institute", Peremohy 37, 03056 Kyiv, Ukraine

* Correspondence: olga.kulesha@nmbu.no; Tel.: +47-406-755-92

Received: 20 May 2019; Accepted: 17 June 2019; Published: 18 June 2019



Abstract: The membrane bioreactor (MBR) and the biofilm membrane bioreactor (BF-MBR) are among key solutions to water scarcity; however, membrane fouling is the major bottleneck for any expansion of these technologies. Prepolymerized aluminum coagulants tend to exhibit the greatest extent of fouling alleviation, with the reduction of soluble microbial products (SMPs) being among the governing mechanisms, which, nevertheless, has been poorly understood. This current study demonstrates that the investigation of the chemical coordination of monosaccharides, which are the major foulants in MBR and BF-MBR, to the main hydrolysis species of the prepolymerized aluminum coagulant, is among the key approaches to the comprehension of the fouling mitigation mechanisms in BF-MBR. Quantum chemical and thermodynamic calculations, together with the multivariate chemometric analysis, allowed the team to determine the principal mechanisms of the SMPs removal, understand the thermodynamic patterns of fouling mitigation, develop the model for the prediction of the fouling mitigation based on the thermodynamic stability of the inorganic-organic complexes, and classify these complexes into thermodynamically stable and less stable species. The results of the study are practically significant for the development of plant surveillance and automated process control with regard to MBR and BF-MBR systems.

Keywords: biofilm membrane bioreactor; complex; thermodynamic stability; membrane fouling mitigation; computational thermodynamic analysis; multivariate statistics

1. Introduction

Membrane bioreactor (MBR) and biofilm membrane bioreactor (BF-MBR) are advanced solutions for the problem of water scarcity, which have been recognized as highly competitive technologies when applied in water reuse schemes [1–4]. However, membrane fouling remains the major barrier for any MBR and BF-MBR expansion [5,6].

With regard to membrane fouling mechanisms, cake and gel layer formation and membrane pore blockage were identified as major contributors to any filtration resistance [7]. The formation of the cake layer is mainly attributed to the deposition of suspended solids, whose size is bigger than the membrane pores, onto the membrane surface or onto the sealed pores, with a subsequent stacking [7,8]. The gel layer is the matrix, which consists of highly concentrated solutes and macromolecular species, deposited at the membrane surface.

This gel layer is usually intertwined with the cake matrix, therefore it is highly complicated to distinguish either of them [9]. The formation of the cake layer, as well as the gel matrix at the membrane surface, are governed by the pressure-driven convective flow from the bulk mixed liquor solution to the membrane during filtration [7,9,10].

Concentration polarization (CP) is the other type of solute fouling, which accompanies every filtration system, being, however, of marginal importance in the MBR/BF-MBR operation [9,11]. This phenomenon is entailed by the tendency of the solutes, rejected by the membrane, to accumulate at the membrane-solution interface within the concentration boundary region, driven by the concentration gradients, and to form a highly concentrated zone, called a concentration polarization layer. In contrast to the cake and gel layers, the transport within the concentration polarization region is diffusion, described by the Fick's first law [7,9,10]. The solids can diffuse back to the bulk mixed liquor in the CP layer, if they are not entrapped in the gel or cake layer.

The concentration polarization model and the mechanisms and mathematical description of cake layer compaction are explained in detail by Yoon [12].

Membrane pore blockage is mainly attributed to the accumulation of the solutes and colloids in the membrane pores and on the membrane surface, which comprises complete, internal, and intermediate pore blocking mechanisms. Membrane pore blockage, altogether with the cake filtration during the dead-end membrane filtration, was comprehensively described by Hermia's pore-blocking models, represented elsewhere [5,8,13–15].

The properties of mixed liquor play a crucial role in fouling development. The soluble microbial products (SMPs) were found to be tightly linked to the fouling intensity [16–18]. Meanwhile, carbohydrates, which are one of the major components of the matrices of soluble microbial products in mixed liquor, were identified as the primary foulants in MBR and BF-MBR systems [19].

Carbohydrates were found to be principally responsible for the formation of the gel and cake layer on the membrane surface, and for complete, intermediate and internal pore blocking [20–22]. In addition, they were reported to cause concentration polarization, which entails the increased gel and cake layer thickness [23]. Complete, intermediate and internal pore blocking are associated with irreversible and irrecoverable membrane fouling [14,24,25], while gel and cake layer formation, together with concentration polarization, usually result in reversible membrane fouling [26–29]. Reversible fouling can be removed by physical cleaning, whereas irreversible fouling can only be removed by a more aggressive cleaning method—chemically enhanced backwash (CEB), cleaning in place (CIP) or “cleaning in air” (CIA). On the contrary, no techniques that could cope with the irrecoverable fouling have been developed [11,30]. Characteristic fouling types for the blocking mechanisms described by Hermia's blocking filtration laws and the best suitable cleaning methods were reviewed in detail by Kulesha et al. [8]. Based on the above-mentioned discoveries, carbohydrates are responsible for reversible, irreversible, and irrecoverable membrane fouling.

This knowledge helped to develop one of the most efficient strategies for fouling mitigation—the modification of biomass characteristics via coagulation, which has been in the center of attention of many studies [8].

During the holistic comparative assessment of the Al- and Fe-based coagulants as membrane flux enhancers for the BF-MBR system, conducted in our previous work [31], four different coagulants were experimentally and statistically evaluated: Prepolymerized aluminum chloride of medium and high basicity, non-prepolymerized aluminum and iron (III) sulfate. Based on the jar tests, the optimum pH values and the optimum dosage range for every selected coagulant were determined. These optimum conditions were maintained during the subsequent total recycle tests (TRT). The total recycle tests revealed that prepolymerized aluminum chloride coagulants provided the greatest extent of fouling inhibition among the studied compounds: The maximum filtration time (F) was equal to 120 min, and the maximum increase of the average normalized permeability ($\delta_{av}P_N$) by 155.0–198.0% at the dose 1.1–1.9 $\mu\text{molAl/mgSS}$. Meanwhile, prepolymerized aluminum chloride with the medium basicity exhibited a superior fouling mitigation behavior to its counterpart with the high basicity, demonstrated

by a higher flux enhancing efficiency at lower dosages, and a wider range of the maximum performance of the first one.

Therefore, prepolymerized aluminum chloride with medium basicity was used during the optimization of the filtration system based on the two-level factorial design of the experiment. In contrast, non-prepolymerized aluminum and iron (III) sulfate provided 58 and 28% of the maximum increase of average normalized permeability, respectively, and 12.7 and 25 min of the maximum filtration time, respectively, which indicates a much lower extent of fouling mitigation than in the case of their prepolymerized counterparts. It is worth noting that, starting from the dose 0.5 $\mu\text{molFe/mgSS}$ during the TRT at a fixed pH, iron (III) sulfate caused the decline of the normalized permeability. The potential reason could be the tendency of iron (III) coagulant at certain concentrations to trigger the formation of the Fe-rich gel matrix of polysaccharides on the membrane surface, thus increasing reversible fouling, which is reported by several studies [19,32,33]. Hence, the prepolymerized aluminum coagulant of the medium basicity is identified as the most efficient membrane flux enhancer, which entails a tenfold increase in the filtration time of the membrane separation cycle, and increases the net membrane flux by 30–56% in the BF-MBR pilot system.

Despite the extensive research work in the field of chemical flux enhancement, the processes taking place in the system after adding of the coagulants still partly remain a black box due to their complexity and rapidness [34–36]. A deeper comprehension of the influence of the flux enhancers on the mixed liquor filterability can be attained through the investigation of the physicochemical properties of the system, which can shed some light on the interaction between the carbohydrates and the hydrolysis species of the coagulants to get a better understanding of the governing mechanisms.

Thermodynamic studies, related to the membrane fouling control in MBR, were carried out by different research teams [37–41]; however, they were merely focused on the interfacial interactions between the sludge flocules and the membrane surface, and the calculation of the relevant energies according to: The XDLVO (Extended Derjaguin, Landau, Verwey, Overbeek) theory, the combined surface element integration method with the composite Simpson's rule for the calculation of the interfacial interactions, with regard to the rough membrane surface, and the quantitative definition of the hydrophilicity/hydrophobicity of the material.

Concerning the polyaluminum hydrolysis species, the computational study of the structure of the Keggin Al_{13} complex was performed by Pophristic et al. [42]. The optimized bond lengths and angles of $\text{Al}_{13}\text{O}_4(\text{OH})_{24}(\text{H}_2\text{O})_{12}\text{Cl}_7$ were determined, followed by the ab initio molecular dynamics calculations. $\text{Al}_{13}\text{O}_4(\text{OH})_{24}(\text{H}_2\text{O})_{11}^{7+}$ was identified as the most stable configuration. Armstrong et al. [43] studied the thermodynamic properties of the Keggin Al_{13} sulfate and selenate molecules in the crystal state, in order to identify the link between their structure and their reactivity. The highly exothermic enthalpies of formation of the Keggin Al_{13} clusters from the elements and oxides, and the enthalpies of the relevant 5N solutions, were reported.

The interaction between the aluminum hydrolysis species and glucose was studied by He et al. [44], who focused on the investigation of the coordination of β -D-glucopyranose to $[\text{Al}(\text{OH})(\text{H}_2\text{O})_n]^{2+}$ and $[\text{Al}(\text{OH})_2(\text{H}_2\text{O})_n]^+$ ions through the Density-functional method. The formation of the double-O-ligand coordination complex was found to be thermodynamically favorable if it was formed through two O_4 – O_6 adjacent oxygen atoms in the β -D-glucopyranose moiety.

However, no computational thermodynamic studies can be found on the chemical coordination of the monosaccharides to the polymeric hydrolysis species of the prepolymerized aluminum chloride, especially Al_{13}^{n+} , which constitute the majority of its hydrolysis species [45,46] and have the highest coagulation potential [47], thus being primarily responsible for the flux enhancing ability of the relevant coagulant.

The current work aims to fill the existing conspicuous gap in the scientific knowledge by developing a strategy, which combines the quantum chemical model and thermodynamic calculations with the multivariate chemometric approach to identify the thermodynamically favorable pathways of the formation of inorganic-organic complexes, and the thermodynamic patterns of fouling mitigation during the application of the prepolymerized aluminum coagulant of the medium basicity in BF-MBR.

2. Materials and Methods

The calculations of the thermodynamic parameters of the formation of the individual reactants and the relevant complexes were carried out, applying the semi-empirical computational molecular orbital method—Parameterized Model number 3 (PM3) using HyperChem™ 8.0.6 software (Hypercube Inc., Waterloo, ON, Canada). PM3 is based on the neglect of diatomic differential overlap approximation. This parametrization procedure enables the acquisition of fully optimized molecular geometries and the calculation of the heats of formation, dipole moments and ionization potentials. In comparison with the MNDO (Modified Neglect of Diatomic Overlap) and AM1 model (Austin Model 1), the PM3 method is characterized by lower average absolute errors when calculating standard enthalpies, and provides more precise calculations [48]. The PM3 method provides the enthalpies of formation with the weighted total mean absolute deviation ± 10.9 kJ/mol [49].

In order to simulate the interactions between the monosaccharides and Al_{13} -complex, the relevant molecules were built and solvated using 216 water molecules and the periodic solvent box of the size $18.7 \times 18.7 \times 18.7$ Å for the monosaccharides; and the periodic box of $31.3 \times 31.3 \times 31.3$ Å using 1010 water molecules for Al_{13} and Al_{13} -monosaccharide complexes. The minimum distance between the solvent and the solute atoms was kept at 2.3 Å. Full geometry optimization using a Polak-Ribiere algorithm was performed for every analyzed compound, in order to reach the conformation of the lowest potential energy. The restricted Hartree-Fock method was applied to calculate the spin interactions in every compound. The standard temperature was set in all of the simulations (298.15 K). The results of the quantum chemical calculations are reported with the accuracy of the convergence parameter, i.e., the self-consistent field energy (SCF), equal to ± 0.0418 kJ/mol.

The calculation of the main thermodynamic parameters of the reactions (i.e., standard enthalpy change (ΔH^0), standard entropy change (ΔS^0), and standard Gibbs energy change (ΔG^0)) between the selected monosaccharides and Al_{13} complex, resulting in the formation of the relevant Al_{13} -monosaccharide complexes, was performed according to Hess's law (Equation (1)), its extension to entropy (Equation (2)) and Gibbs energy (Equation (3)), and the Gibbs-Helmholtz equation (Equation (4)).

$$\Delta H^0 = \sum (n_i \cdot \Delta H_{f,i}^0)_{products} - \sum (n \cdot \Delta H_{f,i}^0)_{reactants} \quad (1)$$

$$\Delta S^0 = \sum (n_i \cdot S_{f,i}^0)_{products} - \sum (n \cdot S_{f,i}^0)_{reactants} \quad (2)$$

$$\Delta G^0 = \sum (n_i \cdot \Delta G_{f,i}^0)_{products} - \sum (n \cdot \Delta G_{f,i}^0)_{reactants} \quad (3)$$

$$\Delta G^0 = \Delta H^0 - T \cdot \Delta S^0 \quad (4)$$

where $\Delta H_{f,i}^0$ is the standard enthalpy change of formation; $S_{f,i}^0$ is the standard entropy of formation; $\Delta G_{f,i}^0$ is the standard Gibbs energy change of formation of the individual reactants and products.

The statistical investigation of the calculated thermodynamic parameters of the studied systems was conducted using PLS regression analysis and cluster analysis. The statistical software, The Unscrambler®X10.3 (CAMO Software AS, Oslo, Norway), was used for this purpose.

3. Results and Discussion

3.1. The Main Identified Fouling

Monosaccharides ($C_nH_{2n}O_n$, $n = 3-6$) and their derivatives are the main building block molecules of polysaccharides, which determine the characteristics of the latter ones. Therefore, it was decided to investigate the behavior of the monosaccharides in terms of their interaction with the selected coagulant.

Different studies investigate the presence of the monosaccharide species in the mixed liquor and the fouling layers of the membrane bioreactor (MBR) systems, as well as in the biofilm matrixes (Table 1).

Table 1. Monosaccharides and their derivatives reported in the previous studies. (MBR = membrane bioreactor).

Compound	The Open-Chain Form ¹	Source, Reference				
		Gel, Cake Layer, Mixed Liquor (MBR), Silva et al. [50,51]	Biofilms, Christensen [52]	Gel, Cake Layer (MBR), Feng et al. [53]	Mixed Liquor (MBR), Miura, Okabe [54]	Mixed Liquor, Gel, Cake Layer (MBR), Miyoshi et al. [55]
Glucose	D	+ ²	+	+	+	+
Galactose	D	+	+	+	+	+
Glucuronic acid	D	+	+			
Glucosamine	D	+	+			
Rhamnose	L	+	+	+		+
Fucose	L	+	+	+	+	+
Arabinose	L	+	+	+	+	+
Mannose	D		+	+	+	+
Galactosamine	-		+			
Galacturonic acid	D		+			
Xylose	D			+		+
Mannitol	D					+

Notes: ¹ if the OH group located at the bottom-most asymmetric centre (the carbon atom second from the bottom) is on the right side in the Fischer projection, the monosaccharide (or its derivative) belongs to D-sugars, if the OH group at the bottom-most asymmetric centre is on the left side in the Fischer projection, the compound is L-sugar [56]; ² “+” stands for the presence of the selected monosaccharide in the relevant source.

According to Table 1, such monosaccharides as glucose, galactose, glucuronic acid, glucosamine, rhamnose, fucose, arabinose, and mannose (marked with the blue rectangle) are the most typical constituents of the polysaccharides in the mixed liquor, gel, and cake layers in the MBR systems. Since the vast majority of them were also identified in the biofilm matrices [52], in the present study, it is assumed, that the highlighted monosaccharides make up the polysaccharides in the BF-MBR system.

Taking into account the above-mentioned references, a couple of nuances can be singled out. First, the relative proportions of the monosaccharide species in the structures of the polysaccharides in the gel and cake layers of the MBR system tend to vary, depending on the applied solids retention times (SRTs), which is demonstrated by Silva et al. [50]. Besides, the authors point out that the variety of monosaccharides increases with the decrease of SRT and the intensification of biofouling (all of the dominant ones at different SRTs monosaccharides lie in the blue rectangle in Table 1). Second, as reported by Miyoshi et al. [55], certain monosaccharides might have a higher affinity to the membrane surface, and can thus cause more severe irreversible fouling than others. The clear indicator was the difference in the monosaccharide content in the fouling layer and in the mixed liquor. According to the results [55], glucose, galactose, rhamnose and mannose were found to be dominant in the matrix of the fouling layer.

3.2. The Structure and Active Centers of the Studied Foulants

Different studies suggest the prevalence of the cyclic form (pyranose, furanose) of the selected monosaccharides (hexose, pentose, and their derivatives) in the aqueous solutions, which can be explained by the fact that the formed cyclic hemiacetals are strain-free and more stable than the open-chain structure [56–59]. Based on the previous research works on the determination of the characteristic anomeric forms of the selected monosaccharides [60–67] and the above-mentioned findings (Table 1), the following compounds are further considered as targeting foulants: β -D-glucopyranose (Glc), β -D-galactopyranose (Gal), β -D-mannopyranose (Man), α -D-glucopyranuronic acid (GlcUA), β -L-rhamnopyranose (Rha), β -L-fucopyranose (Fuc), α -L-arabinofuranose (Ara), and β -D-glucosamine (GlcN).

Monosaccharides in the cyclic form are characterized by an active center, which is called the glycosidic hydroxyl group. The higher reactivity of the glycosidic hydroxyl group can be explained by the influence of the ether-type oxygen atom (between C_1 and C_5) (Figure 1a), which partially shifts the electrons from the contiguous C–O bond (in the C_1 position) to its own orbitals.

Hence, the shift of electron density increases the polarity between the C_1 carbon and the –OH group, making this hydroxyl group more chemically active [68]. The shift of the electrons from the carbon atom in position 1 (atom C_1) to the ether-type oxygen atom in the structure of β -D-glucopyranose, is clearly indicated by the areas of the relatively higher electrostatic potential (around 1.25 e/a_0) and the increased net positive charge of C_1 (+0.194) in comparison to the other present carbon atoms, which is demonstrated in Figure 1b.

Figure 1b demonstrates the computationally generated electrostatic potential map of the β -D-glucopyranose molecule, which visualizes the charge/electron density distribution within the molecule, represented as the isosurface. According to the gradation of color in the electrostatic potential map, the asymmetrical distribution of the electron charge density is clearly indicated in the O–H groups. The hydrogen atoms have a low electron density, and hence a net positive charge and positive electrostatic potential, as shown by the bright green color, while the oxygen atoms have a high electron density, and thus a net negative charge and negative electrostatic potential, indicated by the deep purple color. Meanwhile, the C–O groups are characterized by the accumulation of the net positive charge and positive electrostatic potential at the carbon atoms and the negative charge and negative electrostatic potential at the oxygen atoms. The accumulation of the net negative charge at the oxygen atoms can be explained by the fact that oxygen is the element of the second highest electronegativity (χ) in the periodic table ($\chi_{O} = 3.5$, vs. $\chi_{C} = 2.5$ vs. $\chi_{H} = 2.1$ on the Pauling scale), and therefore its

atoms have the highest relative ability (after fluorine) to attract the electrons of other atoms to which it is bonded [69].

The electrostatic potential map indicates a significant part of the intermediary electrostatic potential regions, whose colors are not completely green or completely purple. This effect is explained by the nature of observed bonds in the structure of β -D-glucopyranose, as well as in the structure of the other selected monosaccharides, which is covalent polar. Meanwhile, the polarity of the O–H bonds is higher than the polarity of the C–O bonds— $\Delta\chi_{\text{OH}} = 1.4 > \Delta\chi_{\text{CO}} = 1.0$.

The electrostatic potential surfaces of the other investigated monosaccharides have the character similar to the one of β -D-glucopyranose and are demonstrated in Figure S1. The β -D-glucopyranose molecule was selected for the description since it is the most stable aldohexose, and is among the most abundant monosaccharides in MBR [50,56].

The total dipole moment of the β -D-glucopyranose molecule is 1.639 D, with the highest contribution from the X and Z vector components (Figure 1a).

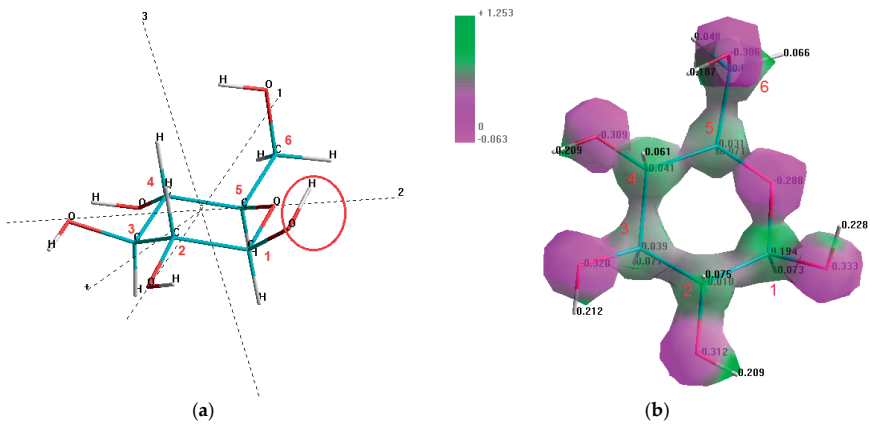


Figure 1. Molecular structure of β -D-glucopyranose with the numerated carbon atoms (based on their position in the structure): (a) The glycosidic hydroxyl group located at the C_1 atom (marked with the red oval); (b) electrostatic potential (e/a_0), mapped onto an isosurface of the total electron density of $0.13 e/a_0^3$ (Notes: the numerator stands for the electron charge “ e ” (1.6022×10^{-19} coulombs), and the denominator is the first Bohr radius “ a_0 ” (5.62918×10^{-11} m)).

3.3. Dominant Hydrolysis Species with Regard to the Medium Basicity Prepolymerized Aluminum Chloride

Prepolymerized aluminum coagulants are characterized by the dominance of the species with the charges higher than the charges of the majority of the species of non-prepolymerized inorganic coagulants. This feature enhances the coagulating ability of the prepolymerized aluminum coagulants and simplifies the operation process, thus making them more advantageous than their non-prepolymerized counterparts [35]. One of the main factors which influences the dominance of certain polyaluminum hydrolysis species is the basicity of the prepolymerized aluminum coagulant [70]. According to the previous work by Kulesha et al. [31], prepolymerized aluminum coagulant with the medium basicity (OH/Al 1.3) exhibits the best potential to mitigate fouling in the BF-MBR system at the optimum pH range 5.5–6 (acidic), which was mainly attributed to the highest bearing charge concentration among the studied species.

Al_{13}^{7+} (Figure S2) is considered the most stable aluminum complex in the prepolymerized aluminum chloride (PACl) solution [71,72], which is mainly attributed to a surface positive charge with the π -electrons delocalized in the six-member (hexagon-like) ring structures [73]. Meanwhile, the surface charge decrease makes the subsequently formed Al_{13}^{7-n} species less stable [74]. The presence of Al_{13}^{7+} complexes in polyaluminum chloride solutions is the prime contributor to their

efficiency enhancement, due to the increase in the charge concentration of the relevant PACl [71,74,75]. This polynuclear complex as the prime component of the prepolymerized aluminum chloride solutions is first introduced and described by Johansson [76].

The dominance of $[\text{Al}_{13}\text{O}_4(\text{OH})_{28}(\text{H}_2\text{O})_8]^{3+}$, (which probably originated from $[\text{Al}_{13}\text{O}_4(\text{OH})_{24}(\text{H}_2\text{O})_{12}]^{7+}$) in the medium basicity coagulant of OH/Al 1.5 at $\text{pH} \approx 3.8$ at the concentration 0.1 M Al, was reported by Bottero et al. [77], during the analysis of the nuclear magnetic resonance (NMR) spectra (~71% out of the total aluminum concentration) and computational analyses based on Glueckauf's formula and the Debye-Hückel law (~80–88% out of the total aluminum concentration). The experimental potentiometric titration analysis and the relevant model based on its results indicated the presence of the $[\text{Al}_{13}\text{O}_4(\text{OH})_{24}(\text{H}_2\text{O})_{12}]^{7+}$ complex, which consisted of the symmetrical tetrahedrally-coordinated aluminum ion at the center of the structure with the weak/non-existent electric field gradient, surrounded by twelve octahedral aluminum ions with the relatively high electric field gradient and the potentially distorted structure.

Feng et al. [78], who studied the speciation of different prepolymerized aluminum coagulants by applying electrospray ionization mass spectrometry, reported that the Al_{13}^{3+} species was one of the main components of these prepolymerized aluminum coagulants, which was assumed to be directly transformed from Keggin- $[\text{Al}_{13}\text{O}_4(\text{OH})_{24}(\text{H}_2\text{O})_{12}]^{7+}$ complex. The coexistence of Keggin- $[\text{Al}_{13}\text{O}_4(\text{OH})_{28}]^{3+}$ and the octahedral $[\text{Al}_{13}(\text{OH})_{36}]^{3+}$ structures was hypothesized; meanwhile, the Keggin- $\text{Al}_{13}^{3+}/[\text{Al}_{13}\text{O}_4(\text{OH})_{24}(\text{H}_2\text{O})_{12}]^{7+}$ form was identified as the prevailing structure.

Pernitsky and Edzwald [70], based on the experimental solubility data for the sulfated prepolymerized aluminum chloride coagulant of the medium basicity, hypothesize either the presence of the combination of monomers ($\text{Al}(\text{OH})_2^+$, $\text{Al}(\text{OH})^{2+}$) and Al_{13}^{7+} , or the occurrence of some other aluminum species in the studied system at $\text{pH} 5\text{--}7$.

In the study by Rämö et al. [79], who investigated the distribution of the polyaluminum species in the 1 μm Al solutions of prepolymerized aluminum chloride with the medium basicity (OH/Al 1.3), based on the mass spectrometry (MS) analysis, the dominance of Al_{13}^{2+} and Al_{13}^{3+} compounds, which made up 72% out of the total ion count at $\text{pH} 4.7$, is reported. No detection of $[\text{Al}_{13}\text{O}_4(\text{OH})_{24}(\text{H}_2\text{O})_{12}]^{7+}$ could be explained by any availability of the counter anions in the system and the drying droplet of the specimen. Some larger formations, for example, Al_{26} , were also observed; however, the Al_{13} complex is the dominant species in the system. On the contrary, the monomers, dimers, and trimers of aluminum were completely absent [46].

According to mass spectrometric studies, reported by Sarpola [45], the PACl with the medium basicity in the pH range 4.65–6.46 is characterized by the following protonated open form of $\text{Al}_{13}\text{—}[\text{Al}_{13}\text{O}_4(\text{OH})_{29}]^{2+}$. Due to the high stability of the $[\text{Al}_{13}\text{O}_4(\text{OH})_{24}(\text{H}_2\text{O})_{12}]^{7+}$ complex, it is suggested that the complex in its usual form is less likely to participate in any reactions. Meanwhile, it is hypothesized [46] that after the formation of $[\text{Al}_{13}\text{O}_4(\text{OH})_{24}(\text{H}_2\text{O})_{12}]^{7+}$ in the aqueous solutions, the four-coordinate oxygen atoms in each ring, which are shared with the central aluminate (Figure S2), get “over-bonded”, and thus “loose” the bond with one of the other twelve aluminum atoms that they are connected to, getting protonated and exposing the open chains or ring substructures to water. Hence, four rings with the asymmetrical charge division are produced, giving rise to the active centers, which can potentially attract the negatively charged systems and react with them [46].

Seichter et al. [80], who investigated the species of prepolymerized aluminum chloride, formed by hydrolysis and condensation, assigns the detected complex cations to the octahedral structure $[\text{Al}_{13}(\text{OH})_{24}(\text{H}_2\text{O})_{24}]^{15+}$, which is identified as the other important tridecameric cation, in addition to the Keggin (tetrahedral) type. This complex, as the complex $[\text{Al}_{13}\text{O}_4(\text{OH})_{29}]^{2+}$ introduced by Sarpola [45], has the planar core, and thus is potentially much more likely to participate in reactions with the organic matter, as well as undergo further polymerization. However, the formation of this polycation structure was expected to occur autonomously from the Keggin-type cation.

Based on the discoveries by Sarpola [45] and all above-mentioned findings, the present study assumes that during coagulation, applying the prepolymerized aluminum chloride with medium

basicity, the open structure of Al_{13} complex in the form of $[\text{Al}_{13}\text{O}_4(\text{OH})_{29}]^{2+}$ plays the most crucial role in the reactions with the oppositely charged foulants.

3.4. The Structure of Al_{13}^{2+}

The planar open structure of the Al_{13}^{3+} complex was introduced by Sarpola [45], and taken as the basis for building Al_{13}^{2+} . Meanwhile, the geometry optimization analysis conducted in the present work indicates that the minimum of potential energy can only be reached if the molecule has a non-planar conformation, as represented in Figure 2.

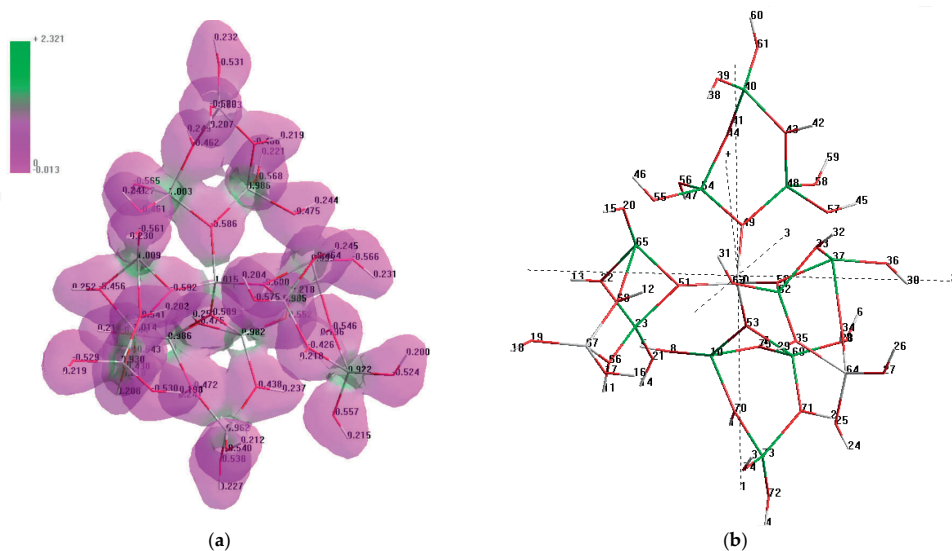


Figure 2. Molecular structure of the Al_{13}^{2+} -complex: (a) Electrostatic potential (e/a_0), mapped onto an isosurface of total electron density of $0.018 e/a_0^3$; (b) the marked aluminum atoms and their corresponding numbers, which were chosen for the simulations.

According to the charge/electron density distribution within the molecule, represented as the isosurface of the Al_{13} -complex (Figure 2a), aluminum atoms have a low electron density, a net positive charge and a positive electrostatic potential, as shown by the bright green color; meanwhile, the oxygen atoms have a high electron density, and thus a net negative charge and a negative electrostatic potential, indicated by the bright purple color. According to the represented electrostatic potential map, all aluminum atoms, except for the central tetrameric aluminum, are the potential active centers during the interaction with the foulants. Meanwhile, based on the charge balance calculations, it was identified that Al no. 64 (Figure 2b) has a slight net negative charge (-0.023), and that Al no. 67 has almost no charge (0.004); thus, both are less likely to participate in these reactions. Consequently, the aluminum atoms, highlighted with the light green color in Figure 2b, are the potential active centers of the Al_{13} -complex. The total dipole moment of the Al_{13} complex is 7.25 D . The analysis of the components of the total dipole moment demonstrates the maximum contribution from the Z vector component (Figure 2b).

The nature of the observed bonds in the structure of the Al_{13} -complex is ionic, since the polarity of the O–Al bonds ($\Delta\chi_{\text{AlO}}$) is equal to 2 ($\chi_{\text{O}} = 3.5$, $\chi_{\text{Al}} = 1.5$ on the Pauling scale). The great difference in electronegativities is also indicated by the significant differences in the electron density at the aluminum and oxygen atoms, which is demonstrated by the entirely green and entirely purple regions, respectively, with no regions of intermediary electrostatic potential.

3.5. Results of the Quantum Chemical Simulations and Calculations

It was decided to investigate the Al_{13} -monosaccharide complex formation through the double-O-ligand coordination, since the formed structure would contain an additional ring system with the delocalized π -electrons that would potentially contribute to its stabilization. Based on the findings described in Section 3.2, and the structural peculiarities of the selected monosaccharides, the formation of the Al_{13} -monosaccharide complexes can occur through the following pairs of the carbon atoms with the adjacent oxygen atoms:

- (1) C_1-C_2 , C_1-C_6 , C_4-C_6 , C_1-C_3 for the aldoses and uronic acid (β -D-glucopyranose, β -D-galactopyranose, β -D-mannopyranose, and α -D-glucopyranuronic acid);
- (2) C_1-C_2 , C_1-C_4 , C_2-C_3 , C_1-C_3 for the deoxy sugars (β -L-rhamnopyranose and β -L-fucopyranose);
- (3) C_1-C_2 , C_2-C_3 , C_3-C_5 , C_1-C_3 for the pentose (α -L-arabinofuranose);
- (4) C_1-C_6 , C_1-C_4 , C_4-C_6 , C_1-C_3 for the aminosugar (β -D-glucosamine).

The pairs of aluminum atoms in the Al_{13}^{2+} complex, which can potentially participate in the interaction with the listed active centers of the monosaccharides, are specified in Section 3.4.

It was assumed that the relevant active centers of the monosaccharides first got deprotonated, i.e., ionized, and then they participated in the chemical coordination with the Al_{13} complex. As a result of these interactions, two water molecules are dehydrated, which was taken into consideration during the relevant calculations. The enthalpy and Gibbs energy of formation of the liquid water molecule specified by Dean [81] were used in this study. The entropy change for water molecules was calculated from the reference data [81] according to Equation (2).

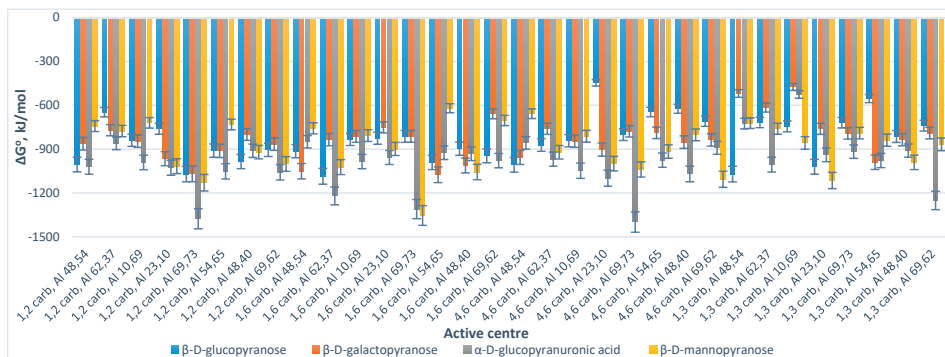
The assessment of the spontaneity of the potential interactions between the selected monosaccharides and Al_{13}^{2+} complex was performed through two steps: First, a series of quantum chemical simulations were conducted, focused on the determination of the thermodynamic parameters of the formation of the individual reactants and the relevant complexes—standard enthalpy change (ΔH°_f), standard entropy (S°_f), and standard Gibbs energy change (ΔG°_f); Second, the calculation of the main thermodynamic parameters of the reaction between the selected monosaccharides and Al_{13}^{2+} complex, i.e., the process of the formation of the Al_{13} -monosaccharide complex—standard enthalpy change (ΔH°), standard entropy change (ΔS°), and standard Gibbs energy change (ΔG°) was performed according to Equations (1)–(4).

The standard Gibbs energy change of the process of formation of Al_{13} -monosaccharide complex (interaction between the selected monosaccharides and Al_{13}^{2+} complex), which is the main indicator of the spontaneity in chemical reactions, is represented in Figure 3.

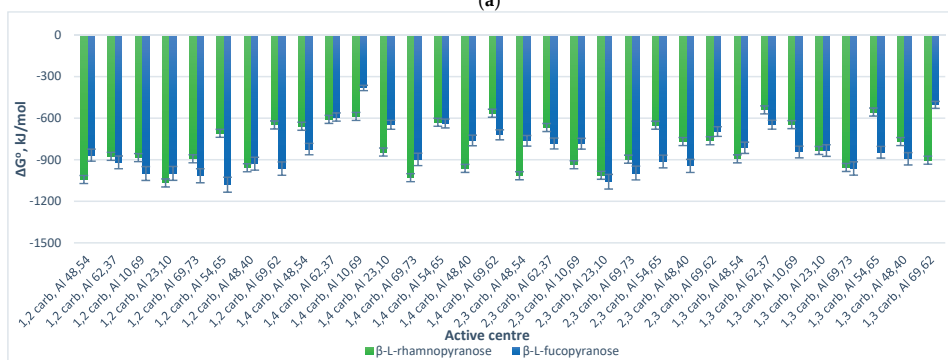
The analysis of the acquired charts (Figure 3) demonstrates that all of the processes which result in the formation of the suggested Al_{13} -monosaccharide complexes have a negative standard Gibbs energy, which indicates that the processes of their formation are spontaneous, and hence thermodynamically favorable. Meanwhile, the thermodynamic stability of the formed Al_{13} -monosaccharide complex highly depends upon the active centers of the monosaccharides and the Al_{13}^{2+} complex, which participate in the chemical coordination process, and the nature of the monosaccharide. The following complexes are identified as the most thermodynamically stable, since they exhibit the highest negative values (with regard to every considered monosaccharide as the reactant) of standard Gibbs energy change: 4,6 GlcUA, Al 69,73 ($\Delta G^\circ = -1398.87$ kJ/mol); 1,6 Glc, Al 62,37 ($\Delta G^\circ = -1085.82$ kJ/mol); 1,6 Gal, Al 54,65 ($\Delta G^\circ = -1075.71$ kJ/mol); 1,6 Man, Al 69,73 ($\Delta G^\circ = -1353.75$ kJ/mol); 1,2 Rha, Al 23,10 ($\Delta G^\circ = -1067.79$ kJ/mol); 1,2 Fuc, Al 54,65 ($\Delta G^\circ = -1080.55$ kJ/mol); 1,3 Ara, Al 69,62 ($\Delta G^\circ = -1215.10$ kJ/mol); 4,6 GlcN, Al 69,73 ($\Delta G^\circ = -1068.35$ kJ/mol).

With regard to the general tendencies, the aldoses and uronic acid exhibit similarly high (-1376.16 – -1069.30) kJ/mol negative values of the Gibbs energy change of the interaction between the oxygen atoms at the C_1-C_2 active centers of the monosaccharide skeleton and the aluminum atoms of the Al_{13}^{2+} complex no. 69, 73 (Figure 3a).

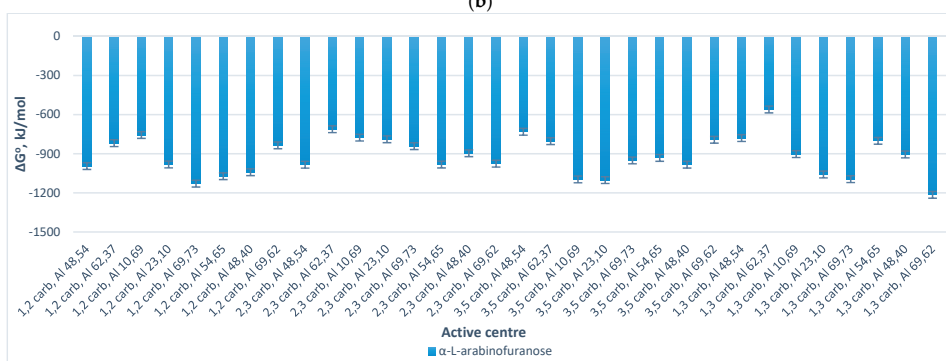
Meanwhile, the deoxy sugars demonstrated similarly high (−1067.79–(−998.74) kJ/mol) negative values of the Gibbs energy change for the interaction process between the oxygen atoms at C₁–C₂/C₂–C₃ atoms of the monosaccharide skeleton and the aluminum atoms of the Al₁₃²⁺ complex no. 23, 10 (Figure 3b).



(a)



(b)



(c)

Figure 3. Cont.

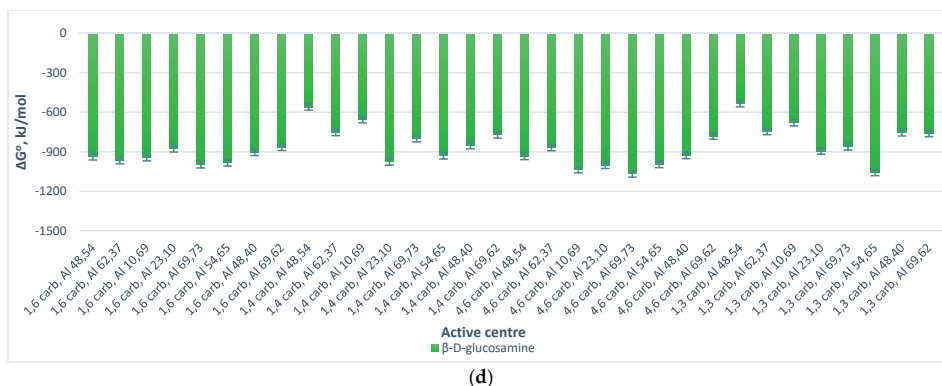


Figure 3. The development of the Gibbs energy change of formation of the Al_{13} -monosaccharide complex, depending on the active centers of the solvated Al_{13}^{2+} complex and monosaccharide for the double-O-ligand coordination of the following monosaccharides: (a) β -D-glucopyranose, β -D-galactopyranose, α -D-glucopyranuronic acid, and β -D-mannopyranose; (b) β -L-rhamnopyranose and β -L-fucopyranose; (c) α -L-arabinofuranose; (d) β -D-glucosamine. (Notes: “carb” stands for carbohydrate; the first two numbers in the name of a complex are related to the pair of the carbon atoms with the adjacent oxygen atoms in the structure of the relevant monosaccharide, which participate in the coordination, and the second two numbers stand for the numbers of the aluminum atoms (active centers) of the Al_{13} complex, which interact with the above-mentioned oxygen centers of the monosaccharide.)

Apart from 1,3 Ara, Al 69,62 complex, the pentose, represented by α -L-arabinofuranose, showed relatively high negative values of the Gibbs energy change of the process of formation of the Al_{13} -monosaccharide complexes through: (1) C_1 – C_3 / C_1 – C_2 atoms of the monosaccharide and the Al atoms of the Al_{13}^{2+} complex no. 69, 73 (–1129.30–(–1094.84) kJ/mol); (2) C_1 – C_3 / C_3 – C_5 atoms of the monosaccharide and the Al atoms of the Al_{13}^{2+} complex no. 23, 10 (–1102.18–(–1059.07) kJ/mol); (3) C_3 – C_5 atoms of the monosaccharide and the Al atoms of the Al_{13}^{2+} complex no. 10, 69 (–1096.97) kJ/mol) (Figure 3c).

Concerning the aminosugar, represented by β -D-glucosamine (Figure 3d), considerably high negative values of the Gibbs energy change of interaction of the oxygen atoms at the C_1 – C_3 atoms of the aminosugar and Al atoms of the Al_{13}^{2+} complex no. 54, 65; and the oxygen atoms at the C_4 – C_6 atoms of the aminosugar and Al atoms of the Al_{13}^{2+} complex no. 10, 69 were obtained (–1057.95–(–1036.44) kJ/mol).

The standard entropy change and enthalpy change of the processes resulting in the formation of the investigated Al_{13} -monosaccharide complexes is demonstrated in Figures S3 and S4. According to the results (Figure S3), the standard entropy change is negative for all the processes, which can be explained by the fact that the spontaneous association of such reactants as monosaccharide and the Al_{13}^{2+} complex gives the rise to a more compact/organized structure [82].

Concerning the standard enthalpy change of the interaction between the monosaccharides and the Al_{13}^{2+} complex, it is highly negative with regard to every investigated process, which results in the formation of Al_{13} -monosaccharide complex (Figure S4).

According to Equation (4), the most favorable condition for the formation of any compound is established if $\Delta H < 0$ and $\Delta S > 0$, which indicates that this process of formation can occur spontaneously at any given temperature. As shown above, the ΔS^0 of the processes of formation of all of Al_{13} -monosaccharide complexes is negative, and the processes of their formation are exothermic ($\Delta H^0 < 0$). In this case, there is a competition between the entropy (the level of the disorder of the system) and enthalpy factors: The first parameter facilitates the reversible process (complex decomposition),

while the latter one favors the forward reaction (complex formation) [83]. High negative values of ΔG° for all investigated processes result from the dominance of the enthalpy factor at the standard temperature, meaning that this temperature ($T = 298.15\text{ K}$) is low enough to facilitate the formation of the Al_{13} -monosaccharide complex ($T < \Delta H^\circ/\Delta S^\circ$). However, at very high temperatures ($T > \Delta H^\circ/\Delta S^\circ$), the process of complex formation will not occur spontaneously.

3.6. Mechanisms of the Interactions

Based on the acquired results, the optimized geometric structures of the most thermodynamically stable Al_{13} -monosaccharide complexes (with respect to every single monosaccharide considered as the reactant), and the determined mechanisms of their formation during flux enhancement in BF-MBR, applying prepolymerized aluminum chloride with the medium basicity, are demonstrated in Figure 4.

According to the determined mechanisms (Figure 4), the most thermodynamically stable complex ($\Delta G^\circ = -1398.87\text{ kJ/mol}$) is formed when the atoms of aluminum no. 69, 73 interact with the oxygen atoms in the positions $\text{C}_4\text{--C}_6$ of the $\alpha\text{-D-glucopyranuronic acid}$ (complex 4,6 GlcUA, Al 69,73). The least thermodynamically stable complex in the selected group ($\Delta G^\circ = -1067.79\text{ kJ/mol}$) is formed during the interaction of aluminum atoms no. 23, 10 of the Al_{13} -complex and the oxygen atoms of $\beta\text{-L-rhamnopyranose}$ in the positions $\text{C}_1\text{--C}_2$ (complex 1,2 Rha, Al 23,10).

Hence, the ranking trend among the studied complexes in decreasing order of thermodynamic stability can be classified as: $\text{Al}_{13}\text{-GlcUA} > \text{Al}_{13}\text{-Man} > \text{Al}_{13}\text{-Ara} > \text{Al}_{13}\text{-Glc} > \text{Al}_{13}\text{-Fuc} > \text{Al}_{13}\text{-Gal} > \text{Al}_{13}\text{-GlcN} > \text{Al}_{13}\text{-Rha}$.

The double-O-ligand coordination results in the dehydration of two H_2O molecules to comply with the requirement of four-coordinate Al atoms in Al_{13}^{2+} complex, considering two O-ligands in the monosaccharide molecule, which was taken into account during the determination of the standard Gibbs energy change of the process of the formation of every represented Al_{13} -monosaccharide complex.

The potential factors, which facilitate the described mechanisms of the interaction between the monosaccharides and Al_{13} -complex (Figure 4) by positively contributing to the stabilization of the Al_{13} -monosaccharide coordinated complexes, can be: The steric effects and the polarization of Al active centers towards the $\text{O}_i\text{--O}_n$ atoms of the monosaccharide. The polarization of the Al^{n+} center in the Al_{13} complex towards the O-ligand in the structure of the monosaccharide can originate from the transfer of the electrons from the 2p orbital of oxygen to the empty 3s/3p orbital of the Al ion (donor-acceptor mechanism), which, according to He et al. [44], has the major influence on the stabilization of the coordinated complexes, formed during the double-O-ligand coordination of $\beta\text{-D-glucopyranose}$ to $[\text{Al}(\text{OH})(\text{H}_2\text{O})_4]^{2+}$. Concerning the intramolecular hydrogen bonding, in the present work, it was only observed in the case of the complex formed by the $\text{C}_4\text{--C}_6$ atoms of $\beta\text{-D-glucosamine}$ and Al no. 69, 73 of the Al_{13} complex (the hydrogen-bonding interaction of the type $\text{O--H}\cdots\text{O}$, where the O–H group is connected to the C_3 atom of the $\beta\text{-D-GlcN}$ and the O atom is connected to Al no. 48 of the Al_{13} complex, demonstrated by the dashed line in Figure 4g). The other represented complexes did not contain the newly formed intramolecular hydrogen bonds; thus, this factor was excluded as the major contributor to the stabilization of the investigated complexes. However, the role of the stabilizing factors in the formation of Al_{13} -monosaccharide complexes should be the subject of a further investigation.

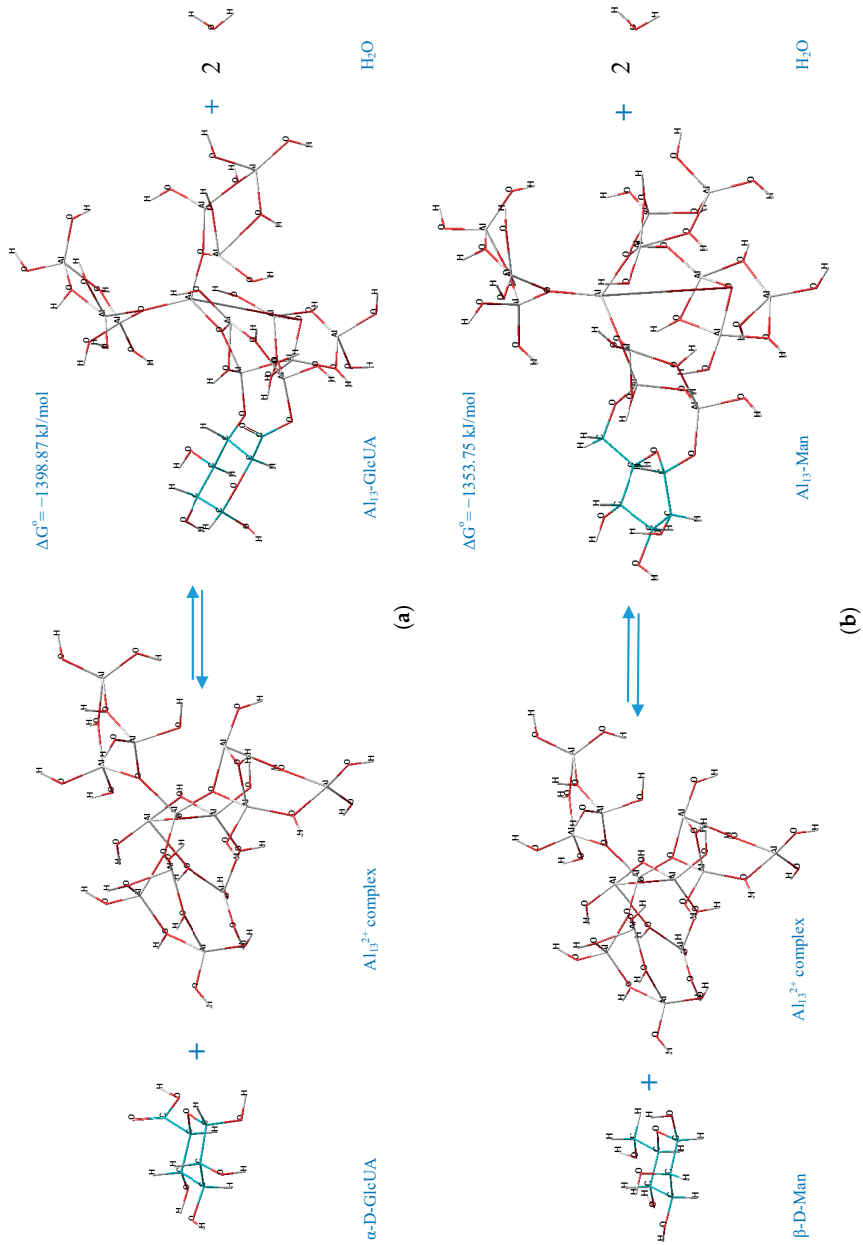


Figure 4. Cont.

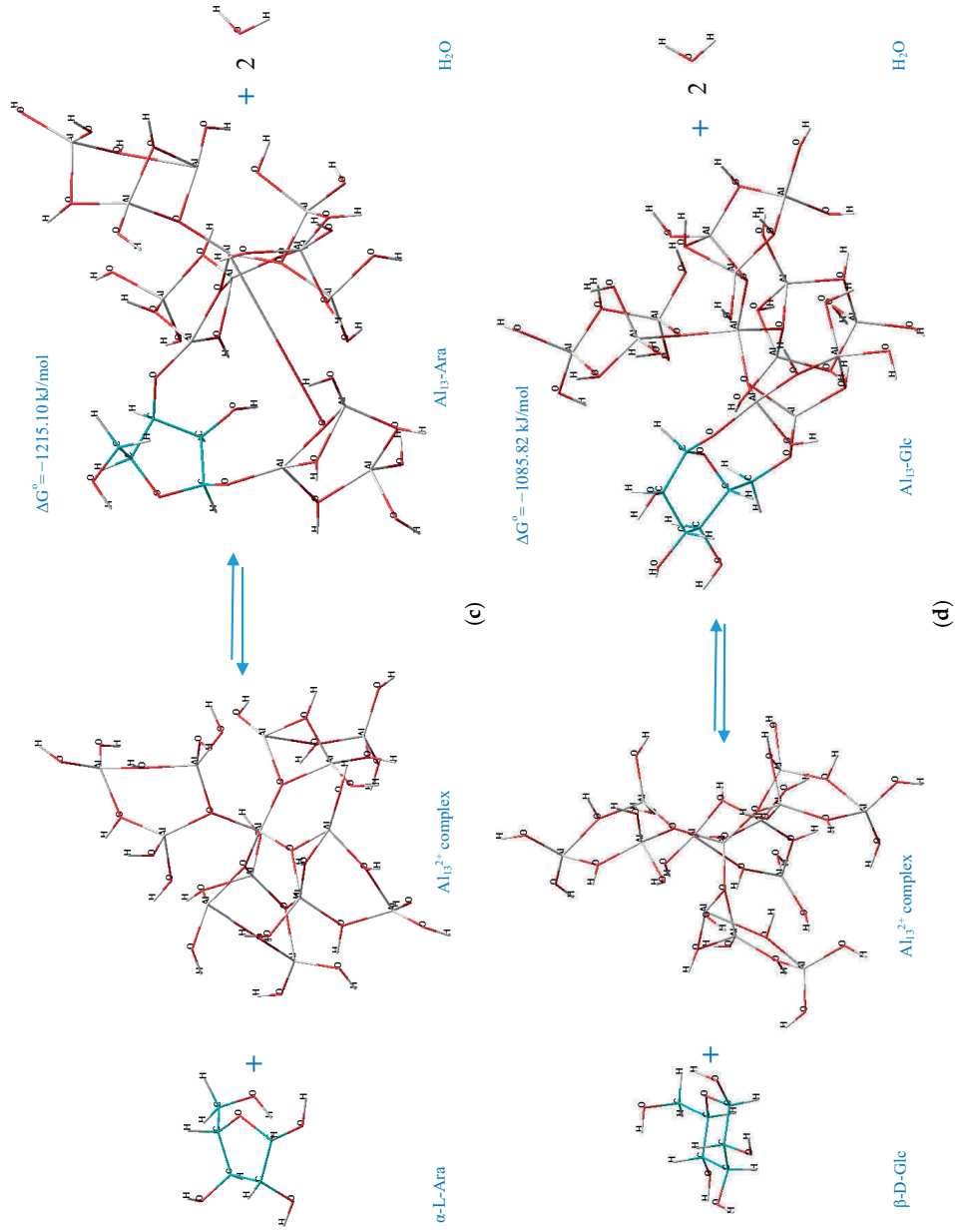
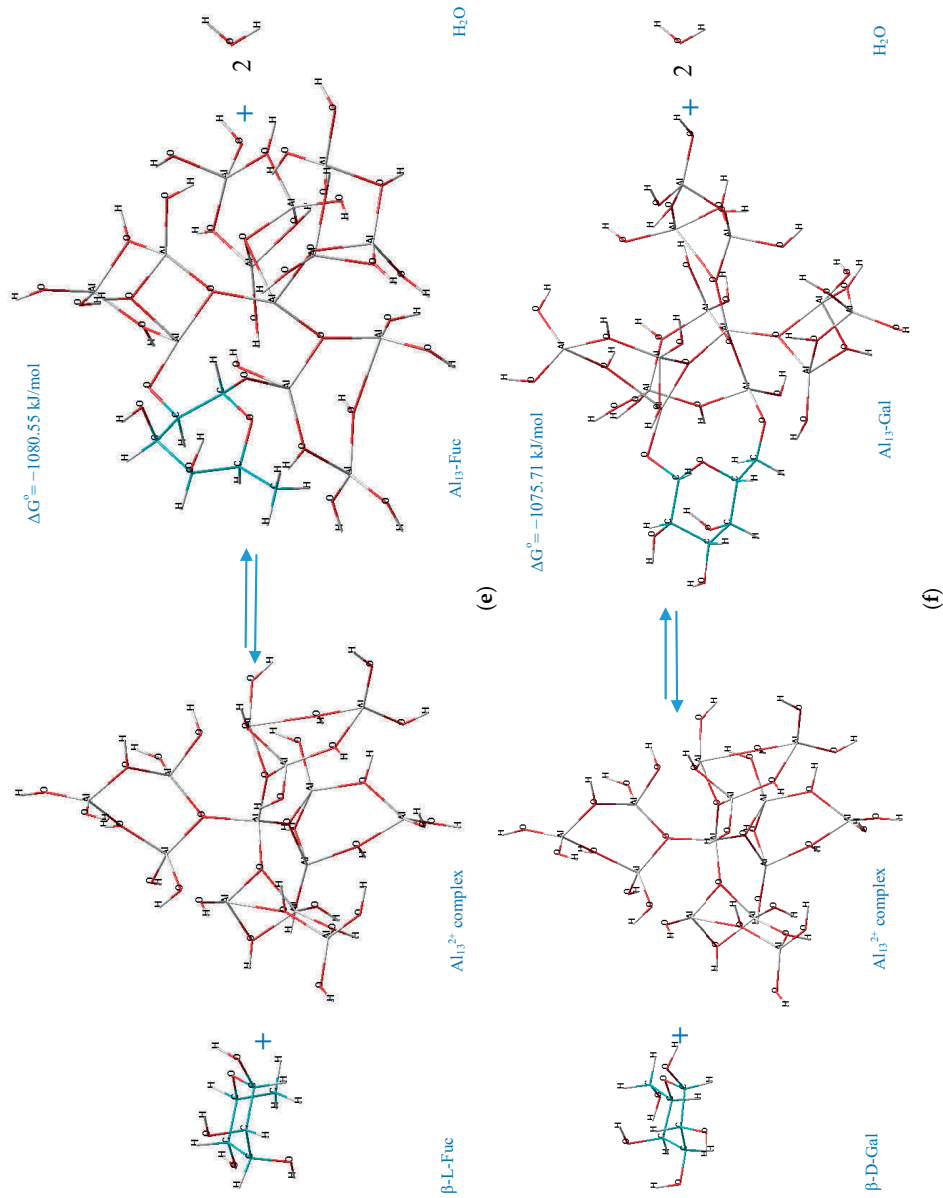
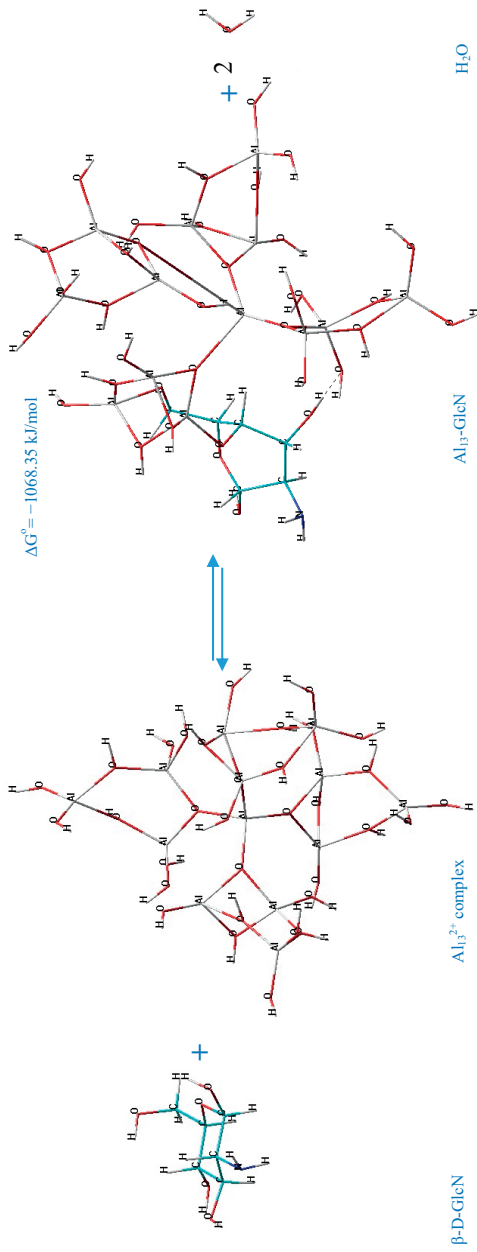


Figure 4. Cont.



(f)

Figure 4. Cont.



(g)

Figure 4. Cont.

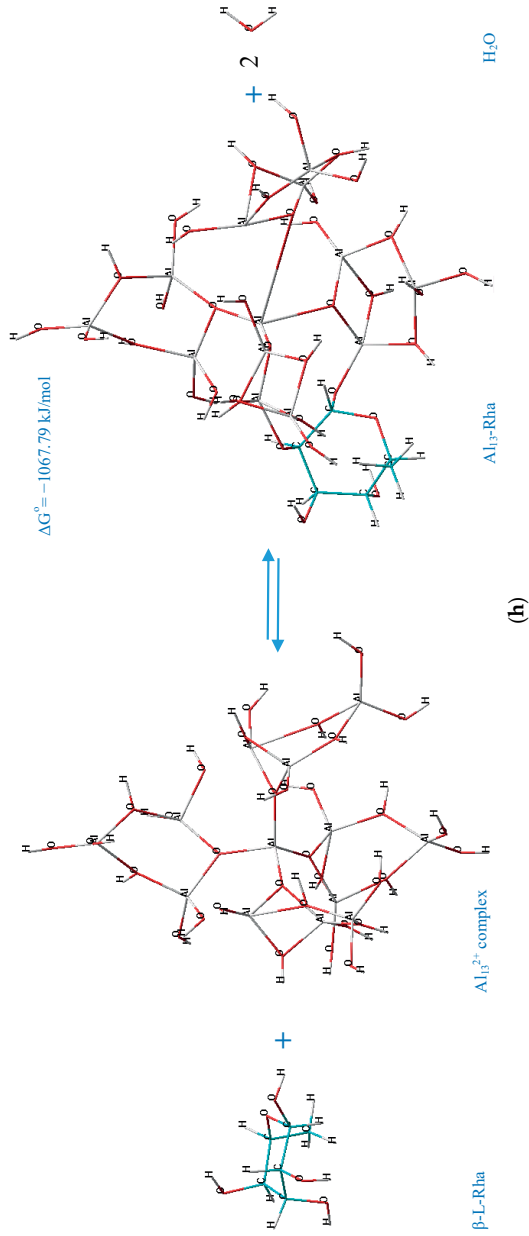


Figure 4. The determined mechanisms of formation of the most thermodynamically stable Al_{13} -monosaccharide complexes: (a) 4,6 GlcUA, Al 69,73; (b) 1,6 Man, Al 69,73; (c) 1,3 Ara, Al 69,62; (d) 1,6 Glc, Al 62,37; (e) 1,2 Fuc, Al 54,65; (f) 1,6 Gal, Al 54,65; (g) 4,6 GlcN; Al 69,73; (h) 1,2 Rha, Al 23,10.

3.7. Statistical Analysis

Partial least squares analysis (PLS) of the thermodynamic parameters acquired during all simulations was conducted according to the following variables and response function (Table 2).

Table 2. Model inputs.

Predictors (X)	Response (Y)
$\Delta H^{\circ}, \Delta S^{\circ}$	ΔG°

After the weighting at the first stage of the analysis to reduce the inherent differences of two predictor variables having the different ranges, the obtained model underwent random cross-validation in PLS, during which the dataset was divided into 20 segments, with 12–13 samples in each segment. The number of PLS factors was chosen according to the explained variance.

The output from the PLS analysis with regard to the scores and loadings plots is demonstrated in Figure 5.

According to Figure 5, the first two factors in total describe 100% of the variance in the dataset for x and y.

The scores plot demonstrates no clear clusters of similar samples (Figure S5), which can be explained by a large number of category variables. Meanwhile, the samples, marked with the dark red oval, which are located leftmost, in the third quadrant of the scores plot (Figure 5a), exhibit the highest negative standard enthalpy change (ΔH°) and Gibbs energy change (ΔG°)—1610–(–1442) kJ/mol and –1399–(–1229) kJ/mol, respectively, which was indicated by the results of the data-driven sample grouping (Figure 5b,d) and the correlation loadings plot (Figure 5e). The data-driven sample grouping was automatically conducted by equally dividing the band of the target thermodynamic parameter values in the whole range between the upper and lower limits into six groups, shown in Figure 5b–d. The lower limits of values for the standard enthalpy change and Gibbs energy change—1610–(–1442) kJ/mol and –1399–(–1229) kJ/mol, respectively, were selected as the targeting levels of interest, since they indicate the most thermodynamically stable complexes [82]. The samples, marked with the dark red oval in Figure 5a, designate the complexes with the highest negative values of the standard Gibbs energy change and enthalpy change, formed by the interaction of:

- (1) O atoms at C₁C₆ atoms of β -D-Man with the Al atoms no. 69, 73 of the Al₁₃²⁺ complex (sample no. 173, $\Delta G^{\circ} = -1353.75$ kJ/mol, $\Delta H^{\circ} = -1529.72$ kJ/mol);
- (2) O atoms at C₁C₃ atoms of α -D-GlcUA with the Al atoms no. 69, 62 of the Al₁₃²⁺ complex (sample no. 96, $\Delta G^{\circ} = -1251.41$ kJ/mol, $\Delta H^{\circ} = -1437.80$ kJ/mol);
- (3) O atoms at C₁C₆ atoms of α -D-GlcUA with the Al atoms no. 69, 73 of the Al₁₃²⁺ complex (sample no. 77, $\Delta G^{\circ} = -1310.25$ kJ/mol, $\Delta H^{\circ} = -1507.25$ kJ/mol);
- (4) O atoms at C₁C₂ atoms of α -D-GlcUA with the Al atoms no. 69, 73 of the Al₁₃²⁺ complex (sample no. 69, $\Delta G^{\circ} = -1376.16$ kJ/mol, $\Delta H^{\circ} = -1580.16$ kJ/mol);
- (5) O atoms at C₄C₆ atoms of α -D-GlcUA with the Al atoms no. 69, 73 of the Al₁₃²⁺ complex (sample no. 85, $\Delta G^{\circ} = -1398.87$ kJ/mol, $\Delta H^{\circ} = -1610.27$ kJ/mol);
- (6) O atoms at C₁C₆ atoms of α -D-GlcUA with the Al atoms no. 62, 37 of the Al₁₃²⁺ complex (sample no. 74, $\Delta G^{\circ} = -1220.22$ kJ/mol, $\Delta H^{\circ} = -1440.80$ kJ/mol);
- (7) O atoms at C₁C₃ atoms of α -L-Ara with the Al atoms no. 69, 62 of the Al₁₃²⁺ complex (sample no. 224, $\Delta G^{\circ} = -1215.10$ kJ/mol, $\Delta H^{\circ} = -1432.96$ kJ/mol).

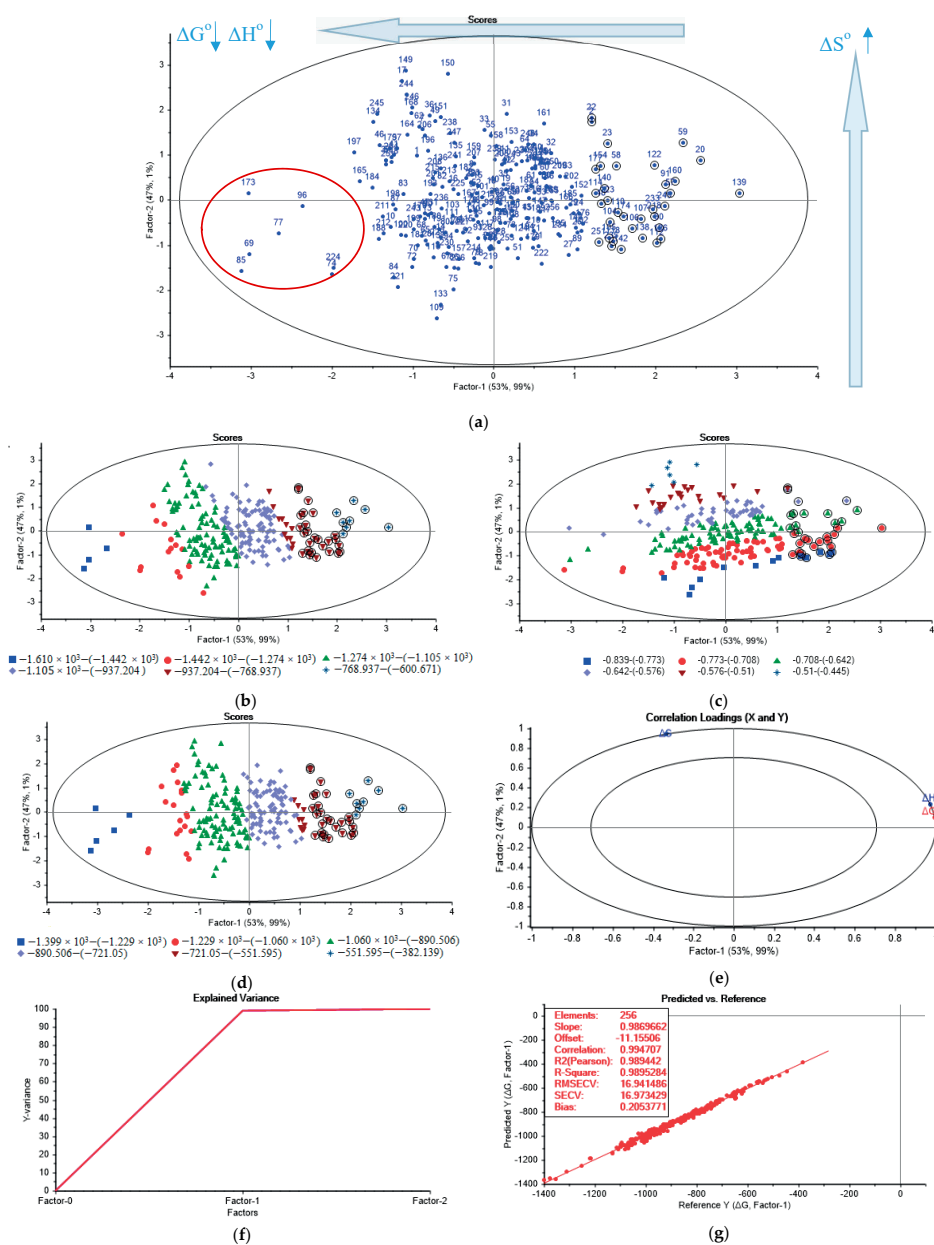


Figure 5. Results of the partial least squares analysis (PLS) using the results as the quantum chemical and thermodynamic calculations: (a) Scores plot with no sample grouping; (b) scores plot with the sample grouping according to ΔH° ; (c) scores plot with the sample grouping according to ΔS° ; (d) scores plot with the sample grouping according to ΔG° ; (e) correlation loadings plot; (f) total explained variance plot; (g) standard Gibbs energy change prediction model (validation plot).

Consequently, the complexes formed by α -D-glucopyranuronic acid and the Al atoms no. 69, 73; 62, 37; and 69, 62 of the Al_3^{2+} complex make up the majority of the most thermodynamically stable samples.

According to the PLS correlation loadings plot (Figure 5e), Factor-1 clearly accounts for the standard enthalpy change (ΔH°) and the Gibbs energy change (ΔG°), while Factor-2 mainly describes the standard entropy change (ΔS°). All of the variables explain more than 50% of the variance, and hence have high importance in relation to Factor-1 and Factor-2. ΔH° has a high positive correlation with ΔG° and both are negatively correlated with ΔS° along Factor-1.

The explained variance plot (Figure 5f) indicates that the optimum number of factors is one, which provides 98.9% of the explained Y-variance. The increase in the number of factors does not significantly influence the explained variance, which was expected due to a relatively small number of variables (i.e., two variables result in two factors at most).

The analysis of the validation plot (Figure 5g) indicates that the developed model has a linear trend (R-squared = 0.99) with a good fit for the majority of the data (slope = 0.987). The model is reliable, since the value of R-squared (Pearson) is close to the R-squared correlation (0.989 vs. 0.995). The Root Mean Square Error of Cross Validation (RMSECV) and the standard error of cross-validation (SECV) are equal to 16.94 and 16.97 kJ/mol, respectively. The obtained bias of the model is insignificant (0.21), which indicates its low tendency to any over- or underestimation of the validation values.

The stability and applicability limit of the partial least squares regression (PLSR) model was checked through the case scenarios based on the addition of the proportional and additive noise, i.e., the noise which typically affects instrument amplification and the measurement signal, respectively, to both the predictors and response function, according to Equation (5) [84]:

$$M_{new}(i, k) = M(i, k) \cdot \left[1 + \frac{PN}{100} \cdot N(0, 1) \right] + N(0, AN), \quad (5)$$

where PN is the level of proportional noise, %; AN is the level of additive noise, $AN = \frac{P\%}{100} \cdot M(i, k)$, where $P\%$ is the level of approximate additive noise in percent; $N(m, s)$ is the randomly distributed value, where m —mean standard deviation and s —standard deviation; $M(i, k)$ —the real raw value, acquired during the quantum chemical and thermodynamic calculations; $M_{new}(i, k)$ —the value with the added tested noise.

According to the performed series of calculations, the derived partial least squares regression (PLSR) model is applicable (R-squared = 0.7) for the maximum proportional noise equal to 6% and the maximum standard deviation for the additive noise equal to 14, applied for both of the predictors (ΔH° , ΔS°) and the response function (ΔG°).

Due to the scattered nature of the scores, i.e., the lack of indication of distinctive clusters, it was decided to conduct the cluster analysis of the scores to understand if any grouping of the samples can be performed based on their similarities with regard to the specified variables.

The Y-scores for the latent variables Factor-1 and Factor-2 acquired during the PLSR analysis were used as the input data for the cluster analysis. This was done in order to screen out the noise of the raw data and use the prevailing differences of the most and least thermodynamically stable complexes. The classes were generated from the scores by applying a hierarchical complete-linkage clustering method and the squared Euclidean distance as the dissimilarity function.

The obtained results are represented in Figure 6 and Figure S6.

The acquired dendrogram visualizes the clustering (Figure 6), which corresponds to the Y-scores in the four quadrants of Figure 5a–d. Six classes can be identified at a higher resolution (a relative distance of around 0.8) (Figure 6), which correspond to the six groups of the standard Gibbs energy change in the scores plot, generated during the data-driven sample grouping (Figure 5d).

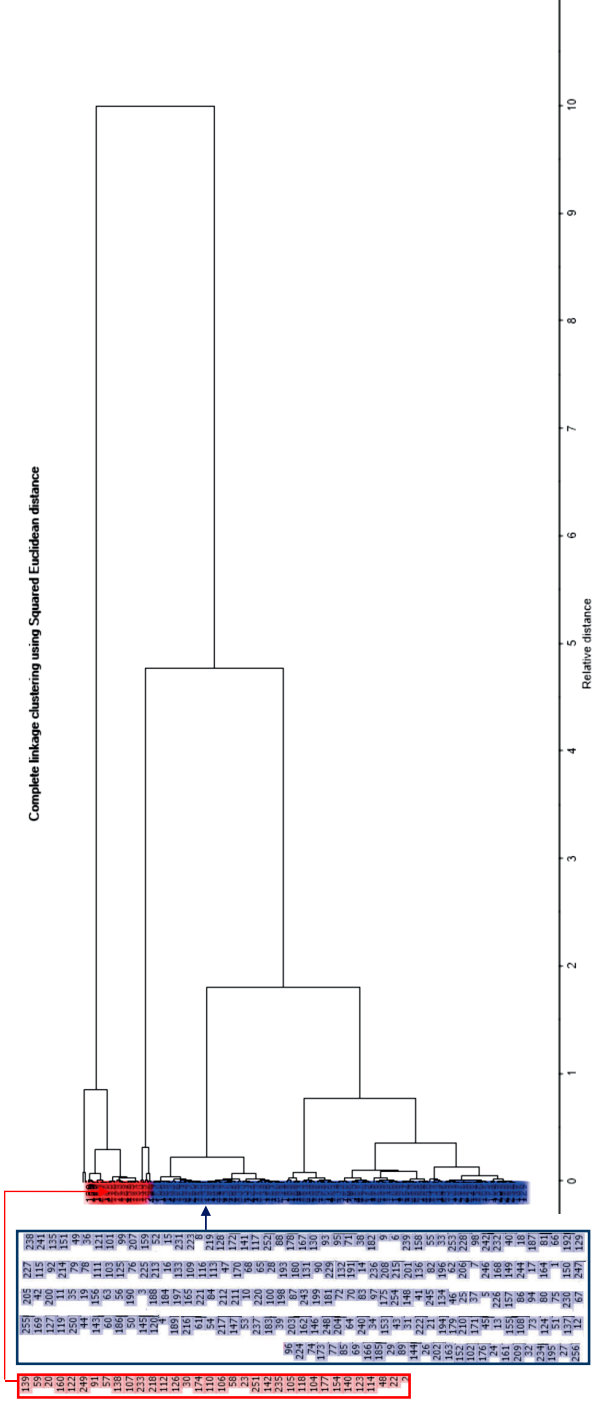


Figure 6. Dendrogram plot acquired during the cluster analysis based on the scores of PLS (the samples, highlighted with the red and blue rectangles, make up the red and blue clusters of the dendrogram, respectively; the samples are located on the y-axis of the dendrogram in the same order as in the columns in the rectangles).

Meanwhile, at a lower resolution (a relative distance of around 4.9), merely two classes can be identified (Figure 6). The red cluster is characterized by the samples with high values of Factor-1 and generally low values of Factor-2. The corresponding samples were marked with the black circles in Figure 5a–d. This position of the marked samples on the scores plot indicates that they are characterized by the low negative values of the standard enthalpy change (ΔH°) and Gibbs energy change (ΔG°) and the predominantly high negative values of the standard entropy change (ΔS°). Thus, the relevant complexes are less thermodynamically stable. The blue cluster represents the scores with low values of Factor-1, i.e., the corresponding samples are characterized by the relatively high negative values of ΔH° and ΔG° (all of the samples which do not have the black-circle mark in Figure 5a–d). Hence, the corresponding complexes are more thermodynamically stable. The location of the scores of the certain sequence numbers, which constitute each cluster shown in the dendrogram, can be found in the scores plot with no sample grouping (Figure 5a).

The described clusters, generated by cluster analysis, represented the Al-monosaccharide complexes, which are more or less liable to decompose during coagulation and can be assigned to the categories “Less stable” and “Stable”, respectively.

3.8. The Working Hypothesis, Implication of the Findings, Challenges, and Perspectives

Systematic research, conducted in the present work, develops the concept of the targeting chemical influence of the Al-based prepolymerized coagulant on the fouling propensity of mixed liquor in the MBR and BF-MBR systems. Particularly, this study focuses on the investigation of the thermodynamic patterns and the mechanisms of the removal of the carbohydrates, which were proven to be the major foulants, deteriorating the filtration performance of MBR and BF-MBR.

The need for this approach was emphasized by the latest work of this research team [31], which, as well as most of the other previous studies, dealt with the investigation of mechanisms of fouling mitigation via coagulation in MBR and BF-MBR in relation to the substrate, with no focus on the chemical fouling mitigation based on the carbohydrate composition [85–87].

Based on the analysis of zeta potential profiles and the intrinsic coagulant charges, Kulesha et al. [31] found out that the principal mechanism of chemical flux enhancement applying inorganic coagulants in BF-MBR is adsorption/charge neutralization. According to Stumm and Morgan [88], the charge neutralizing process accompanies the fixation of the multivalent cations onto the deprotonated group of macromolecular sol (carbohydrates, proteins and their derivatives). This fixation is an electrostatic or a chemical interaction. Meanwhile, the chemical coordination is of considerable significance in coagulation and flocculation reactions between multivalent cations and the macromolecular sols, producing soluble and insoluble complexes, which may have various extents of cross-linkage [88].

The underlying hypothesis of the present research is that purely chemical factors must be considered, apart from the electrostatic double-layer interactions, in order to comprehensively explain the coagulation processes occurring during the addition of the chemical flux enhancers in BF-MBR [88]. No studies on MBR/BF-MBR, which proved/refuted this hypothesis, are found.

The current study demonstrates that the investigation of the chemical coordination processes is among the key approaches to the comprehension of the fouling mitigation mechanisms in BF-MBR. The results on the reduction of the content of soluble microbial products (SMPs) after chemical dosing, acquired in our previous work [31], as well as in the studies by the other research teams [27,85,89], can be satisfactorily interpreted with regard to chemical interactions, described in the current work, while the electrostatic phenomena, described by the theories of double layer and electrostatic interactions, are not applicable to the explanation of the interactions between the solutes/macromolecular sols and the soluble hydrolyzed coagulant species.

According to Wu and Huang [90], SMPs exhibit a higher contribution to membrane fouling in MBR than the colloidal matter. Meanwhile, carbohydrates were found to be the dominant species in SMPs [91]. The carbohydrate fraction of the SMPs highly correlates with fouling in contrast to the protein fraction.

Specifically, carbohydrates were found to be responsible for the reversible, irreversible, and irrecoverable fouling, while the proteins demonstrated occasional or no quantitative relationship with the fouling extent [34,90,92–94]. On the other hand, in the studies by Choi and Ng [95] and Zhou et al. [96], the proteins exhibited a high fouling propensity in the submerged MBR. Hence, the role of the proteins in membrane fouling still remains controversial, and needs further investigation.

The general mechanisms of fouling mitigation in BF-MBR were proven to be almost the same as in the MBR systems [31], which allows for assuming that the investigated content of the mixed liquor in MBR, represented by different research groups [50,51,53–55], is also valid for the BF-MBR.

Due to the lack of the reference data on the thermodynamic parameters of formation of the Al_{13}^{7+} Keggin complex in the liquid state, it was only possible to compare the relevant characteristics of this complex with those of the investigated in the present work Al_{13}^{2+} in the crystal state. The standard enthalpy change of formation from elements of the Al_{13}^{2+} complex in the crystal state is equal to $-10,445.6 \pm 10.9$ kJ/mol, which is almost twice as low as the standard enthalpy change of formation from elements of the Al_{13}^{7+} Keggin complex in the crystal state (-20892.39 ± 70.56 kJ/mol), determined by Armstrong et al. [43]. This observation indicates the higher reactivity/lower stability of the Al_{13}^{2+} complex in comparison to Al_{13}^{7+} Keggin complex, and proves the hypothesis that the latter complex in its usual form is less likely to participate in any reactions [46].

The results acquired during the testing of different limit noises for the applicability of the derived PLSR model indicate that this model can be used, not merely for the computational results, but also for the experimentally-obtained data with the maximum noise, which affects the instrument amplification, 6%, and the maximum standard deviation for the noise, which affects the measurement signal, equal to 14, imposed on all the investigated variables (ΔH^0 , ΔS^0 , ΔG^0).

The performed PLSR and cluster analyses are the bases for developing a classifier that enables a continuous discrimination of the thermodynamically stable and less stable Al_{13} -monosaccharide complexes, based on the coagulant type and the content of the monosaccharide species in mixed liquor in the separation chamber of the MBR/BF-MBR system, which will considerably contribute to plant surveillance and process control.

The concept, presented in the current study, provides a physicochemical and statistical verification of the reasons for the observations on the SMPs removal, which were obtained during the filtration tests in BF-MBR, conducted earlier [31].

The developed approach will help to reduce the input (time and resources), required to test the coagulants as the fouling reducers in MBR and BF-MBR systems. It addresses the questions “What to expect from the mixed liquor system with the chemical dosing?” and “How to reduce the mixed liquor fouling potential?” The quantum chemical and thermodynamic calculations, followed by the multivariate chemometric analysis, allow the researcher to predict the efficiency of the coagulants with regard to SMPs removal in MBR and BF-MBR, and to select the most efficient compound without conducting numerous experiments. The thermodynamic stability of the investigated Al_{13} -monosaccharide complexes is directly related to their fouling potential, since if the complex is more liable to decompose during/after coagulation, more severe membrane fouling is expected due to the released SMPs [97]. Hence, the present study introduces the relationship—fouling as a function of the standard Gibbs energy change—which is able to provide the best solution for the selection of the chemical fouling reducer in MBR and BF-MBR at the lowest cost.

The results of the present work can be used for the development of a sensor for the prediction of the flux enhancement efficiency based on the monosaccharide content of mixed liquor in BF-MBR.

Further study is also foreseen in the investigation of the role of the stabilizing factors in the formation of Al_{13} -monosaccharide complexes.

Besides, the thermodynamic properties of the interaction of the monosaccharide-amino acid network assemblages with the polyaluminum hydrolysis species should be investigated.

4. Conclusions

The developed computational thermodynamic-multivariate chemometric approach to the assessment of the chemical flux enhancement of the coagulants with regard to MBR and BF-MBR advances the field of fouling mitigation, and provides the thermodynamic and statistical tools for the understanding of the underlying mechanisms and the prediction of the fouling mitigation efficiency.

β -D-glucopyranose, β -D-galactopyranose, β -D-mannopyranose, α -D-glucopyranuronic acid, β -L-rhamnopyranose, β -L-fucopyranose, α -L-arabinofuranose, and β -D-glucosamine are the main building blocks of SMPs of mixed liquor in the MBR/BF-MBR, and are primarily responsible for the reversible, irreversible and irrecoverable membrane fouling.

The case study, presented in the current work, focuses on the flux enhancement efficiency of the Al_{13}^{2+} complex, which is the main hydrolysis species of the medium basicity prepolymerized aluminum chloride, proven to be the most efficient coagulant with respect to fouling mitigation in BF-MBR.

The mechanisms of the formation of the most thermodynamically stable Al_{13} -monosaccharide complexes were defined based on the results of the quantum chemical and thermodynamic analyses. The thermodynamic stability of the formed Al_{13} -monosaccharide complex was found to be highly dependent upon the active centers of the monosaccharides and the Al_{13}^{2+} complex, which participate in the chemical coordination process, and the nature of the monosaccharide. The complex, formed by the interaction of the oxygen atoms at C_4 – C_6 atoms of α -D-glucopyranuronic acid with the Al atoms no. 69, 73 of the Al_{13}^{2+} complex, was identified as the most thermodynamically stable complex ($\Delta G^{\circ} = -1398.87$ kJ/mol). Meanwhile, the complex, formed by the interaction of the oxygen atoms at C_1C_2 atoms of β -L-rhamnopyranose with the Al atoms no. 23, 10 of the Al_{13}^{2+} complex, exhibited the lowest thermodynamic stability among the investigated monosaccharides ($\Delta G^{\circ} = -1067.79$ kJ/mol).

The sample grouping according to the standard Gibbs energy change, performed during the PLSR analysis, revealed that the complexes formed by α -D-glucopyranuronic acid and the Al atoms no. 69, 73; 62, 37; and 69, 62 of the Al_{13}^{2+} complex make up the majority of the most thermodynamically stable samples among all 256 investigated Al_{13} -monosaccharide complexes.

The derived PLSR model can be used for computationally and experimentally acquired thermodynamic parameters, being applicable (R -squared = 0.7) for the maximum proportional noise equal to 6%, and the maximum standard deviation for the additive noise equal to 14, applied for both the predictors (ΔH° , ΔS°) and the response function (ΔG°).

The results of the performed PLSR and cluster analyses are the basis for developing a classification model for the continuous discrimination of the thermodynamically stable and less stable Al_{13} -monosaccharide complexes, based on the coagulant type and content of the monosaccharide species in mixed liquor, which will substantially contribute to the automated process control of the MBR/BF-MBR systems.

Supplementary Materials: The following are available online at <http://www.mdpi.com/2073-4441/11/6/1275/s1>, Figure S1: Electrostatic potential maps of the selected monosaccharides with the numerated carbon atoms (based on their position in the structure): (a) β -D-galactopyranose; (b) β -D-mannopyranose; (c) α -D-glucopyranuronic acid; (d) β -L-rhamnopyranose; (e) β -L-fucopyranose; (f) α -L-arabinofuranose; (g) β -D-glucosamine, Figure S2: The optimized structure of the Keggin Al_{13}^{7+} complex with the hydrogen bond (marked with the dashed line), Figure S3: The development of the standard entropy change of formation of the Al_{13} -monosaccharide complex depending on the active centers of the solvated Al_{13}^{2+} complex and the monosaccharide for the double-O-ligand coordination of the following monosaccharides: (a) β -D-glucopyranose, β -D-galactopyranose, α -D-glucopyranuronic acid, and β -D-mannopyranose; (b) β -L-rhamnopyranose and β -L-fucopyranose; (c) α -L-arabinofuranose; (d) β -D-glucosamine, Figure S4: The development of the standard enthalpy change of formation of the Al_{13} -monosaccharide complex depending on the active centers of the solvated Al_{13}^{2+} complex and the monosaccharide for the double-O-ligand coordination of the following monosaccharides: (a) β -D-glucopyranose, β -D-galactopyranose, α -D-glucopyranuronic acid, and β -D-mannopyranose; (b) β -L-rhamnopyranose and β -L-fucopyranose; (c) α -L-arabinofuranose; (d) β -D-glucosamine, Figure S5: Scores plot with the sample grouping, computed from PLS. (Notes: "carb." stands for carbohydrate.), Figure S6: Dendrogram plot acquired during the cluster analysis based on the scores of PLS (primary view) (TIF file).

Author Contributions: Conceptualization O.K. and H.R.; methodology, O.K.; validation, O.K.; formal analysis, O.K.; investigation, O.K.; data curation, O.K.; writing—original draft preparation, O.K.; writing—review and editing, O.K., H.R.; visualization, O.K.; supervision, H.R.; project administration, H.R.

Funding: This research received no external funding.

Acknowledgments: Authors express their gratitude to Arja Sarpola for the fruitful discussions on the hydrolysis species of the prepolymerized aluminum coagulants and Knut Kvaal for his guidance on mathematical modelling and cluster analysis using the Unscrambler software.

Conflicts of Interest: The authors declare no conflict of interest.

References

- Buer, T.; Cumin, J. MBR module design and operation. *Desalination* **2010**, *250*, 1073–1077. [[CrossRef](#)]
- Holloway, R.W.; Regnery, J.; Nghiem, L.D.; Cath, T.Y. Removal of trace organic chemicals and performance of a novel hybrid ultrafiltration-osmotic membrane bioreactor. *Environ. Sci. Technol.* **2014**, *48*, 10859–10868. [[CrossRef](#)] [[PubMed](#)]
- Wen, J.; Liu, Y.; Tu, Y.; Lechevallier, M.W. Energy and chemical efficient nitrogen removal at a full-scale MBR water reuse facility. *AIMS Environ. Sci.* **2015**, *2*, 42–55. [[CrossRef](#)]
- Subtil, E.L.; Mierzwa, J.C.; Hespagnol, I. Comparison between a Conventional Membrane Bioreactor (C-MBR) and a Biofilm Membrane Bioreactor (BF-MBR) for domestic wastewater treatment. *Braz. J. Chem. Eng.* **2014**, *31*, 683–691. [[CrossRef](#)]
- Zheng, Y.; Zhang, W.; Tang, B.; Ding, J.; Zheng, Y.; Zhang, Z. Membrane fouling mechanism of biofilm-membrane bioreactor (BF-MBR): Pore blocking model and membrane cleaning. *Bioresour. Technol.* **2018**, *250*, 398–405. [[CrossRef](#)]
- Sun, C.; Leiknes, T.; Fredriksen, R.H.; Riviere, E. Comparison of membrane filtration performance between biofilm-MBR and activated sludge-MBR. *Desalin. Water Treat.* **2012**, *48*, 285–293. [[CrossRef](#)]
- Judd, S. *The MBR Book Principles and Applications of Membrane Bioreactors in Water and Wastewater Treatment*, 1st ed.; Judd, C., Ed.; Elsevier Ltd.: London, UK, 2006; ISBN 9781856174817.
- Kulesha, O.; Maletskyi, Z.; Ratnaweera, H. State-of-the-art of membrane flux enhancement in membrane bioreactor. *Cogent Eng.* **2018**, *5*, 1–30. [[CrossRef](#)]
- Park, H.-D.; Chang, I.-S.; Lee, K.-J. *Principles of Membrane Bioreactors for Wastewater Treatment*, 1st ed.; CRC Press Taylor and Francis Group: Boca Raton, FL, USA; London, UK; New York, NY, USA, 2015; ISBN 9781466590373.
- Baker, R.W. *Membrane Technology and Applications*, 2nd ed.; John Wiley & Sons, Ltd.: Chichester, UK, 2004; ISBN 0470854456.
- Geilvoet, S.P. The Delft Filtration Characterisation Method: Assessing Membrane Bioreactor Activated Sludge Filterability. Ph.D. Thesis, Delft University of Technology, Delft, The Netherlands, 2010.
- Yoon, S.-H. *Membrane Bioreactor Processes: Principles and Applications*; Forsgren, A.J., Ed.; CRP Press Taylor and Francis Group: Boca Raton, FL, USA, 2015; ISBN 978-1-4822-5584-3.
- Martini, S.; Ang, H.M.; Znad, H. Integrated Ultrafiltration Membrane Unit for Efficient Petroleum Refinery Effluent Treatment. *Clean-Soil Air Water* **2017**, *45*. [[CrossRef](#)]
- Wang, F.; Tarabara, V.V. Pore blocking mechanisms during early stages of membrane fouling by colloids. *J. Colloid Interface Sci.* **2008**, *328*, 464–469. [[CrossRef](#)]
- Mondal, S.; De, S. A fouling model for steady state crossflow membrane filtration considering sequential intermediate pore blocking and cake formation. *Sep. Purif. Technol.* **2010**, *75*, 222–228. [[CrossRef](#)]
- Shi, Y.; Huang, J.; Zeng, G.; Gu, Y.; Hu, Y.; Tang, B.; Zhou, J.; Yang, Y.; Shi, L. Evaluation of soluble microbial products (SMP) on membrane fouling in membrane bioreactors (MBRs) at the fractional and overall level: A review. *Rev. Environ. Sci. Biotechnol.* **2018**, *17*, 71–85. [[CrossRef](#)]
- Janus, T.; Ulanicki, B. A behavioural membrane fouling model for integrated simulation of membrane bioreactors for wastewater treatment. *Procedia Eng.* **2015**, *119*, 1328–1337. [[CrossRef](#)]
- Kulesha, O.; Maletskyi, Z.; Ratnaweera, H. Multivariate Chemometric Analysis of Membrane Fouling Patterns in Biofilm Ceramic Membrane Bioreactor. *Water* **2018**, *10*, 982. [[CrossRef](#)]
- Meng, F.; Zhang, S.; Oh, Y.; Zhou, Z.; Shin, H.S.; Chae, S.R. Fouling in membrane bioreactors: An updated review. *Water Res.* **2017**, *114*, 151–180. [[CrossRef](#)] [[PubMed](#)]

20. Meng, S.; Fan, W.; Li, X.; Liu, Y.; Liang, D.; Liu, X. Intermolecular interactions of polysaccharides in membrane fouling during microfiltration. *Water Res.* **2018**, *143*, 38–46. [[CrossRef](#)] [[PubMed](#)]
21. Ye, Y.; Le Clech, P.; Chen, V.; Fane, A.G.; Jefferson, B. Fouling mechanisms of alginate solutions as model extracellular polymeric substances. *Desalination* **2005**, *175*, 7–20. [[CrossRef](#)]
22. Kola, A.; Ye, Y.; Ho, A.; Le-Clech, P.; Chen, V. Application of low frequency transverse vibration on fouling limitation in submerged hollow fibre membranes. *J. Membr. Sci.* **2012**, *409–410*, 54–65. [[CrossRef](#)]
23. Sarkar, B. A combined complete pore blocking and cake filtration model during ultrafiltration of polysaccharide in a batch cell. *J. Food Eng.* **2013**, *116*, 333–343. [[CrossRef](#)]
24. Soler-Cabezas, J.L.; Torà-Grau, M.; Vincent-Vela, M.C.; Mendoza-Roca, J.A.; Martínez-Francisco, F.J. Ultrafiltration of municipal wastewater: Study on fouling models and fouling mechanisms. *Desalin. Water Treat.* **2015**, *56*, 3427–3437. [[CrossRef](#)]
25. Lee, S.J.; Dilaver, M.; Park, P.K.; Kim, J.H. Comparative analysis of fouling characteristics of ceramic and polymeric microfiltration membranes using filtration models. *J. Membr. Sci.* **2013**, *432*, 97–105. [[CrossRef](#)]
26. Kumar, R.V.; Goswami, L.; Pakshirajan, K.; Pugazhenth, G. Dairy wastewater treatment using a novel low cost tubular ceramic membrane and membrane fouling mechanism using pore blocking models. *J. Water Process Eng.* **2016**, *13*, 168–175. [[CrossRef](#)]
27. Gkotsis, P.K.; Mitrakas, M.M.; Tolkou, A.K.; Zouboulis, A.I. Batch and continuous dosing of conventional and composite coagulation agents for fouling control in a pilot-scale MBR. *Chem. Eng. J.* **2017**, *311*, 255–264. [[CrossRef](#)]
28. Van den Berg, G.B.; Smolders, C.A. Flux decline in ultrafiltration processes. *Desalination* **1990**, *77*, 101–133. [[CrossRef](#)]
29. Wibisono, Y.; Cornelissen, E.R.; Kemperman, A.J.B.; Van Der Meer, W.G.J.; Nijmeijer, K. Two-phase flow in membrane processes: A technology with a future. *J. Membr. Sci.* **2014**, *453*, 566–602. [[CrossRef](#)]
30. Judd, S. The status of membrane bioreactor technology. *Trends Biotechnol.* **2008**, *26*, 109–116. [[CrossRef](#)] [[PubMed](#)]
31. Kulesha, O.; Maletskiy, Z.; Kvaal, K.; Ratnaweera, H. Strategy for Flux Enhancement in Biofilm Ceramic Membrane Bioreactor Applying Prepolymerized and Non-Prepolymerized Inorganic Coagulants. *Water* **2019**, *11*, 446. [[CrossRef](#)]
32. Zhang, Z.; Wang, Y.; Leslie, G.L.; Waite, T.D. Effect of ferric and ferrous iron addition on phosphorus removal and fouling in submerged membrane bioreactors. *Water Res.* **2015**, *69*, 210–222. [[CrossRef](#)] [[PubMed](#)]
33. Wang, X.-M.; Waite, T.D. Role of gelling soluble and colloidal microbial products in membrane fouling. *Environ. Sci. Technol.* **2009**, *43*, 9341–9347. [[CrossRef](#)]
34. Ivanovic, I.; Leiknes, T. Effect of addition of different additives on overall performance of biofilm-MBR (BF-MBR). *Desalin. Water Treat.* **2011**, *34*, 129–135. [[CrossRef](#)]
35. Ødegaard, H.; Fettig, J.; Ratnaweera, H. Coagulation with Prepolymerized Metal Salts. In *Chemical Water and Wastewater Treatment, Proceedings of the 4th Gothenburg Symposium 1990, Madrid, Spain, 1–3 October 1990*; Springer: Gothenburg, Sweden, 1990; Volume 304, pp. 189–220.
36. Bratby, J. *Coagulation and Flocculation in Water and Wastewater Treatment*, 3rd ed.; IWA Publishing: London, UK, 2016; ISBN 9781780407500.
37. Chen, J.; Shen, L.; Zhang, M.; Hong, H.; He, Y.; Liao, B.-Q.; Lin, H. Thermodynamic analysis of effects of contact angle on interfacial interactions and its implications for membrane fouling control. *Bioresour. Technol.* **2016**, *201*, 245–252. [[CrossRef](#)]
38. Hong, H.; Peng, W.; Zhang, M.; Chen, J.; He, Y.; Wang, F.; Weng, X.; Yu, H.; Lin, H. Thermodynamic analysis of membrane fouling in a submerged membrane bioreactor and its implications. *Bioresour. Technol.* **2013**, *146*, 7–14. [[CrossRef](#)] [[PubMed](#)]
39. Cai, H.; Fan, H.; Zhao, L.; Hong, H.; Shen, L.; He, Y.; Lin, H.; Chen, J. Effects of surface charge on interfacial interactions related to membrane fouling in a submerged membrane bioreactor based on thermodynamic analysis. *J. Colloid Interface Sci.* **2016**, *465*, 33–41. [[CrossRef](#)] [[PubMed](#)]
40. Hong, H.; Zhang, M.; He, Y.; Chen, J.; Lin, H. Fouling mechanisms of gel layer in a submerged membrane bioreactor. *Bioresour. Technol.* **2014**, *166*, 295–302. [[CrossRef](#)] [[PubMed](#)]
41. Shen, L.G.; Lei, Q.; Chen, J.R.; Hong, H.C.; He, Y.M.; Lin, H.J. Membrane fouling in a submerged membrane bioreactor: Impacts of floc size. *Chem. Eng. J.* **2015**, *269*, 328–334. [[CrossRef](#)]

42. Pophristic, V.; Balagurusamy, V.S.K.; Klein, M.L. Structure and dynamics of the aluminum chlorohydrate polymer $\text{Al}_{13}\text{O}_4(\text{OH})_{24}(\text{H}_2\text{O})_{12}\text{Cl}_7$. *Phys. Chem. Chem. Phys.* **2004**, *6*, 919–923. [[CrossRef](#)]
43. Armstrong, C.R.; Casey, W.H.; Navrotsky, A. Energetics of Al_{13} Keggin cluster compounds. *Proc. Natl. Acad. Sci. USA* **2011**, *108*, 14775–14779. [[CrossRef](#)] [[PubMed](#)]
44. He, M.F.; Fu, H.Q.; Su, B.F.; Yang, H.Q.; Tang, J.Q.; Hu, C.W. Theoretical insight into the coordination of cyclic β -D-glucose to $[\text{Al}(\text{OH})(\text{aq})]^{2+}$ and $[\text{Al}(\text{OH})_2(\text{aq})]^{1+}$ ions. *J. Phys. Chem. B* **2014**, *118*, 13890–13902. [[CrossRef](#)] [[PubMed](#)]
45. Sarpola, A. The Hydrolysis of Aluminium, A Mass Spectrometric Study. Ph.D. Thesis, University of Oulu, Oulu, Finland, 2007.
46. Sarpola, A.; Postdoctoral Fellow, Faculty of Technology, Energy and Environmental Engineering Research Unit, University of Oulu, Oulu, Finland; Business Director at Eurofins Labtium Oy, Sodankylä, Finland. Personal communication, 2019.
47. Gao, B.Y.; Chu, Y.B.; Yue, Q.Y.; Wang, B.J.; Wang, S.G. Characterization and coagulation of a polyaluminum chloride (PAC) coagulant with high Al_{13} content. *J. Environ. Manag.* **2005**, *76*, 143–147. [[CrossRef](#)] [[PubMed](#)]
48. Hasanein, A.A.; Evans, M.W. *Computational Methods in Quantum Chemistry. Quantum Chemistry Vol.2*; World Scientific Publishing Co. Pte. Ltd.: Singapore; Hackensack, NJ, USA; London, UK; Hong Kong, China, 1996; Volume 2, ISBN 981-02-2611-X.
49. Wu, Y.Y.; Zhao, F.Q.; Ju, X.H. A comparison of the accuracy of semi-empirical PM3, PDDG and PM6 methods in predicting heats of formation for organic compounds. *J. Mex. Chem. Soc.* **2014**, *58*, 223–229. [[CrossRef](#)]
50. Silva, A.F.; Antunes, S.; Saunders, A.; Freitas, F.; Vieira, A.; Galinha, C.F.; Nielsen, P.H.; Barreto Crespo, M.T.; Carvalho, G. Impact of sludge retention time on MBR fouling: Role of extracellular polymeric substances determined through membrane autopsy. *Biofouling* **2017**, *33*, 556–566. [[CrossRef](#)] [[PubMed](#)]
51. Silva, A.F.; Antunes, S.; Saunders, A.; Freitas, F.; Vieira, A.; Galinha, C.F.; Nielsen, P.H.; Barreto Crespo, M.T.; Carvalho, G. Impact of sludge retention time on the fine composition of the microbial community and extracellular polymeric substances in a membrane bioreactor. *Appl. Microbiol. Biotechnol.* **2016**, *100*, 8507–8521. [[CrossRef](#)] [[PubMed](#)]
52. Christensen, B.E. The role of extracellular polysaccharides in biofilms. *J. Biotechnol.* **1989**, *10*, 181–202. [[CrossRef](#)]
53. Feng, L.; Li, X.; Song, P.; Du, G.; Chen, J. Physicochemical properties and membrane biofouling of extra-cellular polysaccharide produced by a *Micrococcus luteus* strain. *World J. Microbiol. Biotechnol.* **2014**, *30*, 2025–2031. [[CrossRef](#)] [[PubMed](#)]
54. Miura, Y.; Okabe, S. Quantification of cell specific uptake activity of microbial products by uncultured chloroflexi by microautoradiography combined with fluorescence in situ hybridization. *Environ. Sci. Technol.* **2008**, *42*, 7380–7386. [[CrossRef](#)] [[PubMed](#)]
55. Miyoshi, T.; Naruse, T.; Yamato, N.; Kimura, K.; Watanabe, Y. Influence of operating conditions on chemically reversible fouling in submerged MBRs. In *2nd IWA National Young Water Professionals Conference, Germany "Membrane Technologies for Wastewater Treatment and Reuse"*; Lesjean, B., Ed.; KompetenzZentrum Wasser Berlin gGmbH: Berlin, Germany, 2007; pp. 231–234.
56. Bruice, P.Y. *Essential Organic Chemistry*, 2nd ed.; Pearson Education Limited: Essex, UK, 2014; ISBN 9781292020815.
57. McMurry, J. *Organic Chemistry: With Biological Applications*, 2nd ed.; Cengage Learning: Boston, MA, USA, 2010; ISBN 978-0495391449.
58. Bradley, S.A.; Tinsley, C.R.; Muiry, J.A.R.; Henderson, P.J.F. Proton-linked L-fucose transport in *Escherichia coli*. *Biochem. J.* **2015**, *248*, 495–500. [[CrossRef](#)] [[PubMed](#)]
59. Moran, A.P. *Microbial Glycobiology: Structures, Relevance and Applications*; Moran, A.P., Holst, O., Brennan, P.J., von Itzstein, M., Eds.; Elsevier Inc.: London, UK; Burlington, ON, Canada; San Diego, CA, USA, 2009; ISBN 978-0-12-374546-0.
60. Takahashi, K.; Ono, S. Calorimetric studies on the mutarotation of D-galactose and D-mannose. *J. Biochem.* **1973**, *73*, 763–770. [[CrossRef](#)] [[PubMed](#)]
61. Shulami, S.; Gat, O.; Sonenshein, A.L.; Shoham, Y. The glucuronic acid utilization gene cluster from *Bacillus stearothermophilus* T-6. *J. Bacteriol.* **1999**, *181*, 3695–3704. [[PubMed](#)]

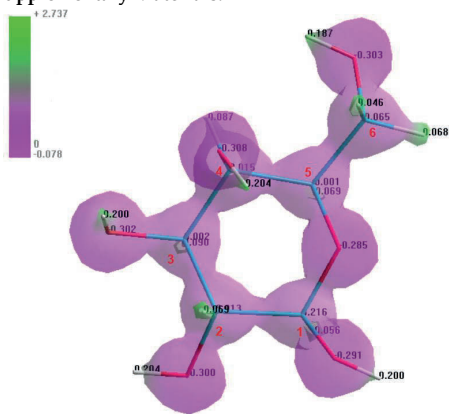
62. Yoshihara, A.; Yoshida, H.; Teraoka, M.; Kamitori, S.; Yamashita, S.; Izumori, K. Structure of L-rhamnose isomerase in complex with L-rhamnopyranose demonstrates the sugar-ring opening mechanism and the role of a substrate sub-binding site. *FEBS Open Bio* **2012**, *3*, 35–40. [\[CrossRef\]](#)
63. Antonik, P.M.; Volkov, A.N.; Broder, U.N.; Re, D.L.; Van Nuland, N.A.J.; Crowley, P.B. Anomer-Specific Recognition and Dynamics in a Fucose-Binding Lectin. *Biochemistry* **2016**, *55*, 1195–1203. [\[CrossRef\]](#)
64. Cartmell, A.; McKee, L.S.; Pena, M.J.; Larsbrink, J.; Brumer, H.; Kaneko, S.; Ichinose, H.; Lewis, R.J.; Viksø-Nielsen, A.; Gilbert, H.J.; et al. The structure and function of an arabinan-specific α -1,2-arabinofuranosidase identified from screening the activities of bacterial GH43 glycoside hydrolases. *J. Biol. Chem.* **2011**, *286*, 15483–15495. [\[CrossRef\]](#) [\[PubMed\]](#)
65. Little, D.J.; Li, G.; Ing, C.; DiFrancesco, B.R.; Bamford, N.C.; Robinson, H.; Nitz, M.; Bamford, N.C.; Pomes, R.; Howell, P.L.; et al. Modification and periplasmic translocation of the biofilm exopolysaccharide poly-1,6-N-acetyl-D-glucosamine. *Proc. Natl. Acad. Sci. USA* **2014**, *111*, 11013–11018. [\[CrossRef\]](#) [\[PubMed\]](#)
66. Korndörfer, I.P.; Fessner, W.D.; Matthews, B.W. The structure of rhamnose isomerase from *Escherichia coli* and its relation with xylose isomerase illustrates a change between inter and intra-subunit complementation during evolution. *J. Mol. Biol.* **2000**, *300*, 917–933. [\[CrossRef\]](#) [\[PubMed\]](#)
67. Seviour, T.; Lambert, L.K.; Pijuan, M.; Yuan, Z. Structural determination of a key exopolysaccharide in mixed culture aerobic sludge granules using NMR spectroscopy. *Environ. Sci. Technol.* **2010**, *44*, 8964–8970. [\[CrossRef\]](#) [\[PubMed\]](#)
68. Lastuhin, Y.; Voronov, S. *Organic Chemistry (Translated)*, 3rd ed.; Ganushchak, M., Ed.; Centre of Europe: Lviv, Ukraine, 2006; ISBN 9667022196.
69. Petrucci, R.H.; Herring, F.G.; Madura, J.D.; Bissonnette, C. *General Chemistry: Principles and Modern Applications*, 11th ed.; Pearson: Toronto, ON, Canada, 2017; ISBN 9780132931281.
70. Pernitsky, D.J.; Edzwald, J.K. Solubility of polyaluminium coagulants. *J. Water Supply Res. Technol. (AQUA)* **2003**, *52*, 395–406. [\[CrossRef\]](#)
71. Tzoupanos, N.D.; Zouboulis, A.I.; Tsoleridis, C.A. A systematic study for the characterization of a novel coagulant (polyaluminium silicate chloride). *Colloids Surf. A Physicochem. Eng. Asp.* **2009**, *342*, 30–39. [\[CrossRef\]](#)
72. Chen, Z.; Luan, Z.; Jia, Z.; Li, X. Study on the hydrolysis/precipitation behavior of Keggin Al13 and Al30 polymers in polyaluminum solutions. *J. Environ. Manag.* **2009**, *90*, 2831–2840. [\[CrossRef\]](#)
73. Gimarc, B.M. Molecular and electronic structures of planar inorganic rings. *Pure Appl. Chem.* **1990**, *62*, 423–428. [\[CrossRef\]](#)
74. Bi, Z.; Chen, Y.; Wang, S.; Wang, D. Hydrolyzed Al(III)-clusters. II: Speciation transformation and stability of Al13 aggregates. *Colloids Surf. A Physicochem. Eng. Asp.* **2014**, *440*, 59–62. [\[CrossRef\]](#)
75. Wang, D.; Wang, S.; Huang, C.; Chow, C.W.K. Hydrolyzed Al(III) clusters: Speciation stability of nano-Al13. *J. Environ. Sci.* **2011**, *23*, 705–710. [\[CrossRef\]](#)
76. Johansson, G. On the Crystal Structure of Some Basic Aluminium Salts. *Acta Chem. Scand.* **1960**, *14*, 771–773. [\[CrossRef\]](#)
77. Bottero, J.Y.; Cases, J.M.; Fiessinger, F.; Polrier, J.E. Studies of hydrolyzed aluminum chloride solutions. 1. Nature of aluminum species and composition of aqueous solutions. *J. Phys. Chem.* **1980**, *84*, 2933–2939. [\[CrossRef\]](#)
78. Feng, C.; Zhao, S.; Bi, Z.; Wang, D.; Tang, H. Speciation of prehydrolyzed Al salt coagulants with electrospray ionization time-of-flight mass spectrometry and ²⁷Al NMR spectroscopy. *Colloids Surf. A Physicochem. Eng. Asp.* **2011**, *392*, 95–102. [\[CrossRef\]](#)
79. Rämö, J.H.; Sarpola, A.T.; Hellman, A.H.; Leiviskä, T.A.; Hietapelto, V.K.; Jokela, J.T.; Laitinen, R.S. Colloidal surfaces and oligomeric species generated by water treatment chemicals. *Chem. Speciat. Bioavailab.* **2008**, *20*, 13–22. [\[CrossRef\]](#)
80. Seichter, W.; Mögel, H.-J.; Brand, P.; Salah, D. Crystal Structure and Formation of the Aluminium Hydroxide Chloride [Al13(OH)24(H2O)24]Cl15·13H2O. *Eur. J. Inorg. Chem.* **1998**, *13*, 795–797. [\[CrossRef\]](#)
81. Dean, J. *Lange's Handbook of Chemistry*, 15th ed.; McGRAW-HILL, Inc.: New York, NY, USA, 1999; ISBN 10: 0849304741.
82. Atkins, P.; de Paula, J. *Physical Chemistry for the Life Sciences*, 2nd ed.; W.H. Freeman and Company: New York, NY, USA, 2011; ISBN 9781429231145.

83. Oxtoby, D.; Gillis, H.P.; Campion, A. *Principles of Modern Chemistry*, 7th ed.; Lockwood, L., Martin, T., Eds.; Brooks/Cole, Cengage Learning: Belmont, NY, USA, 2012; ISBN 978-0-8400-4931-5.
84. CAMO. *The Unscrambler Appendices: Method References*; CAMO: Oslo, Norway, 2008; ISBN 0471930474.
85. Ivanovic, I.; Leiknes, T.O. Improved Performance through Particle Surface Modifications by Coagulation with Inorganic Coagulants in a Biofilm Membrane Bioreactor (BF-MBR). *Sep. Sci. Technol.* **2012**, *48*, 288–294. [[CrossRef](#)]
86. Chen, W.; Liu, J. The possibility and applicability of coagulation-MBR hybrid system in reclamation of dairy wastewater. *Desalination* **2012**, *285*, 226–231. [[CrossRef](#)]
87. Wu, J.; Chen, F.; Huang, X.; Geng, W.; Wen, X. Using inorganic coagulants to control membrane fouling in a submerged membrane bioreactor. *Desalination* **2006**, *197*, 124–136. [[CrossRef](#)]
88. Stumm, W.; Morgan, J.J. Chemical Aspects of Coagulation. *J. Am. Water Works Assoc.* **1962**, *54*, 971–991. [[CrossRef](#)]
89. Gkotsis, P.K.; Batsari, E.L.; Peleka, E.N.; Tolkou, A.K.; Zouboulis, A.I. Fouling control in a lab-scale MBR system: Comparison of several commercially applied coagulants. *J. Environ. Manag.* **2016**, *203*, 838–846. [[CrossRef](#)] [[PubMed](#)]
90. Wu, J.; Huang, X. Effect of mixed liquor properties on fouling propensity in membrane bioreactors. *J. Membr. Sci.* **2009**, *342*, 88–96. [[CrossRef](#)]
91. Malamis, S.; Andreadakis, A. Fractionation of proteins and carbohydrates of extracellular polymeric substances in a membrane bioreactor system. *Bioresour. Technol.* **2009**, *100*, 3350–3357. [[CrossRef](#)] [[PubMed](#)]
92. Jørgensen, M.K.; Nierychlo, M.; Nielsen, A.H.; Larsen, P.; Christensen, M.L.; Nielsen, P.H. Unified understanding of physico-chemical properties of activated sludge and fouling propensity. *Water Res.* **2017**, *120*, 117–132. [[CrossRef](#)] [[PubMed](#)]
93. Kimura, K.; Naruse, T.; Watanabe, Y. Changes in characteristics of soluble microbial products in membrane bioreactors associated with different solid retention times: Relation to membrane fouling. *Water Res.* **2009**, *43*, 1033–1039. [[CrossRef](#)] [[PubMed](#)]
94. Zhang, H.; Gao, Z.; Zhang, L.; Song, L. Performance enhancement and fouling mitigation by organic flocculant addition in membrane bioreactor at high salt shock. *Bioresour. Technol.* **2014**, *164*, 34–40. [[CrossRef](#)]
95. Choi, J.H.; Ng, H.Y. Effect of membrane type and material on performance of a submerged membrane bioreactor. *Chemosphere* **2008**, *71*, 853–859. [[CrossRef](#)]
96. Zhou, Z.; Meng, F.; He, X.; Chae, S.-R.; An, Y.; Jia, X. Metaproteomic analysis of biocake proteins to understand membrane fouling in a submerged membrane bioreactor. *Environ. Sci. Technol.* **2015**, *49*, 1068–1077. [[CrossRef](#)] [[PubMed](#)]
97. Feng, S.; Zhang, N.; Liu, H.; Du, X.; Liu, Y.; Lin, H. The effect of COD/N ratio on process performance and membrane fouling in a submerged bioreactor. *Desalination* **2012**, *285*, 232–238. [[CrossRef](#)]

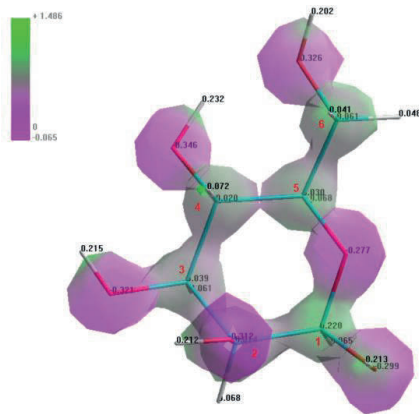


© 2019 by the authors. Licensee MDPI, Basel, Switzerland. This article is an open access article distributed under the terms and conditions of the Creative Commons Attribution (CC BY) license (<http://creativecommons.org/licenses/by/4.0/>).

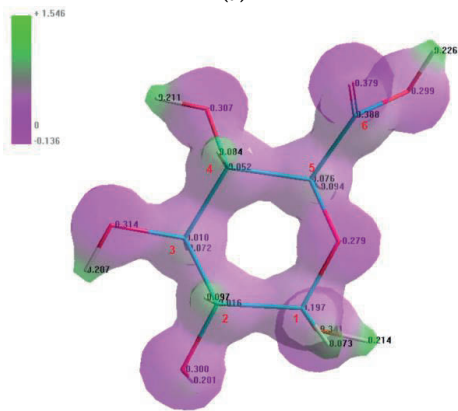
Supplementary Materials:



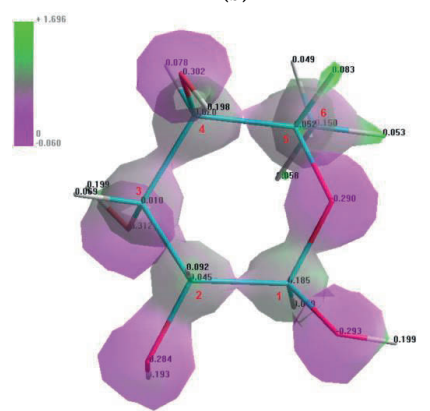
(a)



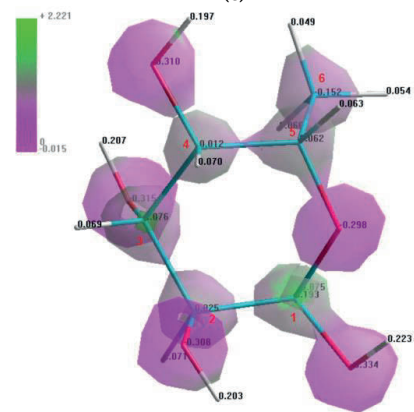
(b)



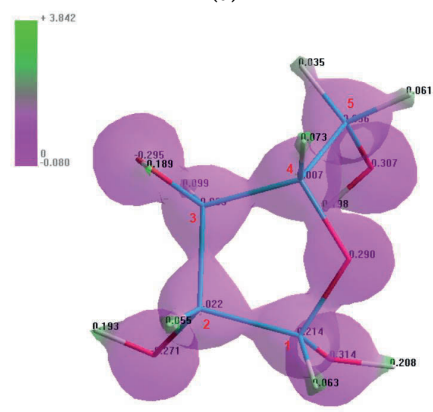
(c)



(d)



(e)



(f)

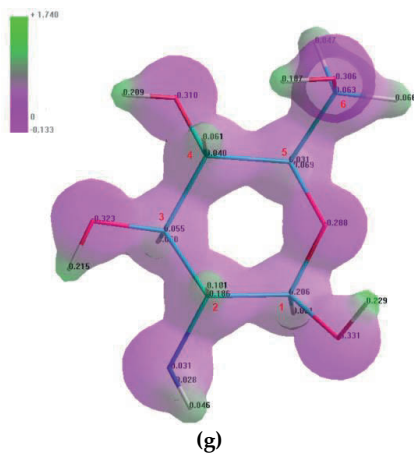


Figure S1. Electrostatic potential maps of the selected monosaccharides with the numerated carbon atoms (based on their position in the structure): **(a)** β -D-galactopyranose; **(b)** β -D-mannopyranose; **(c)** α -D-glucopyranuronic acid; **(d)** β -L-rhamnopyranose; **(e)** β -L-fucopyranose; **(f)** α -L-arabinofuranose; **(g)** β -D-glucosamine.

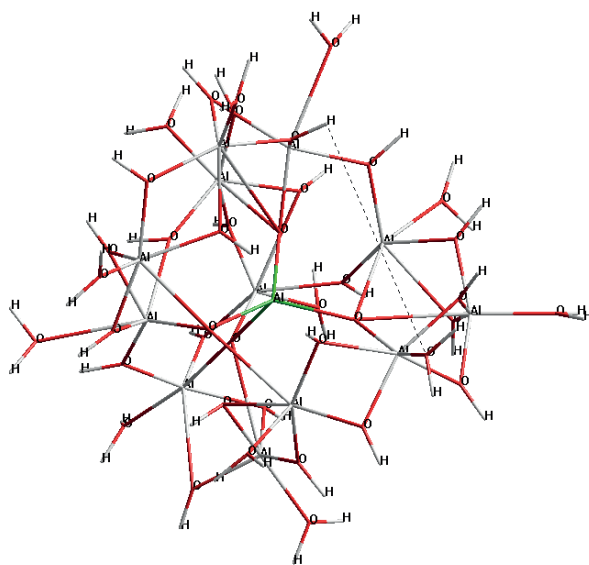
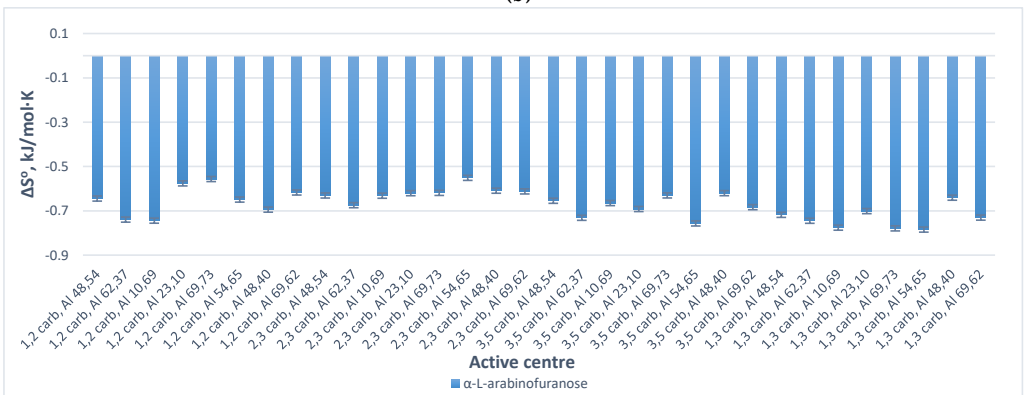
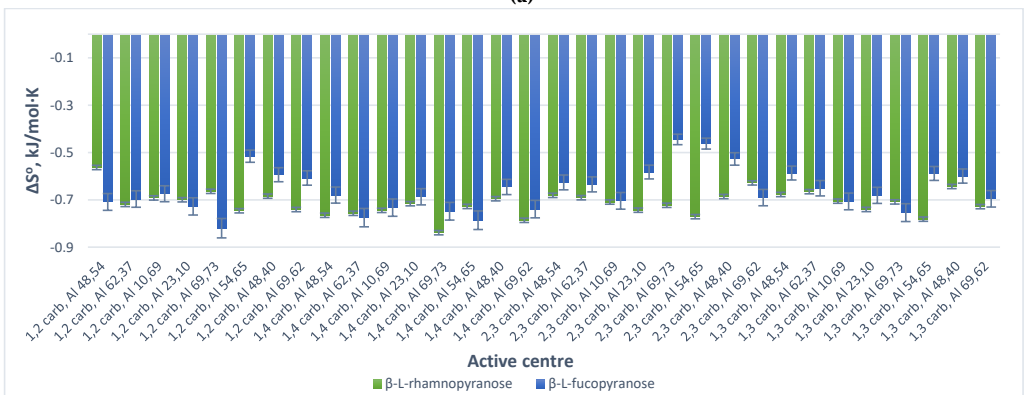
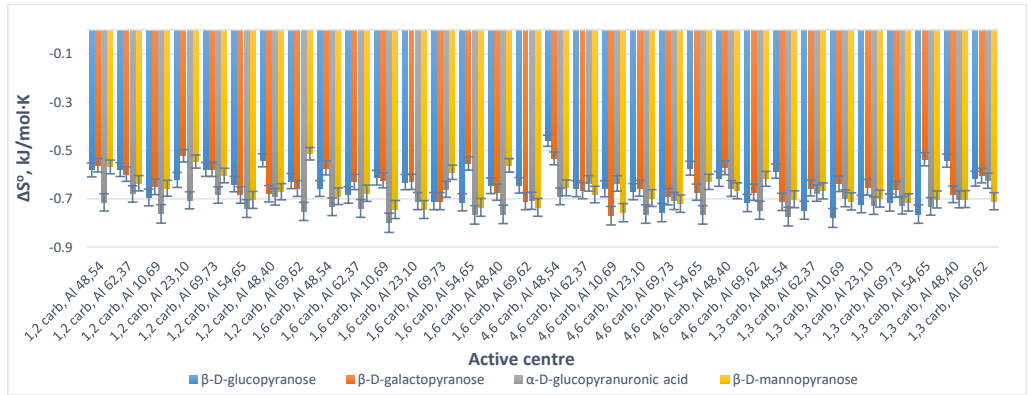
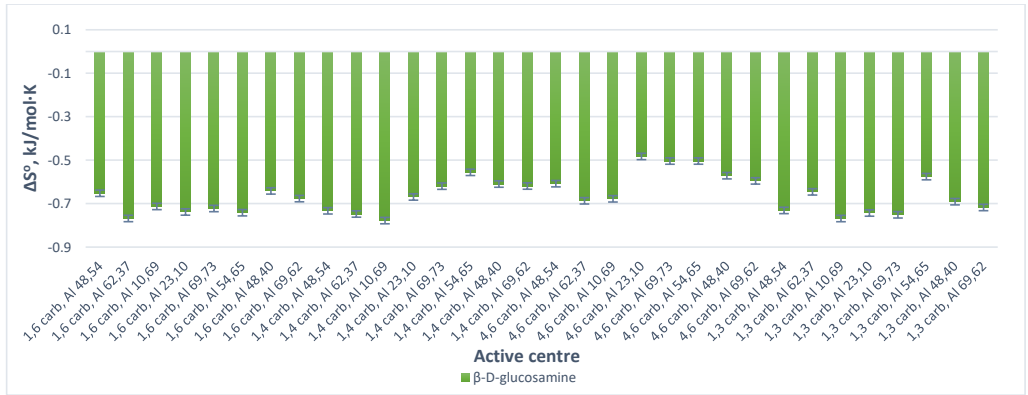


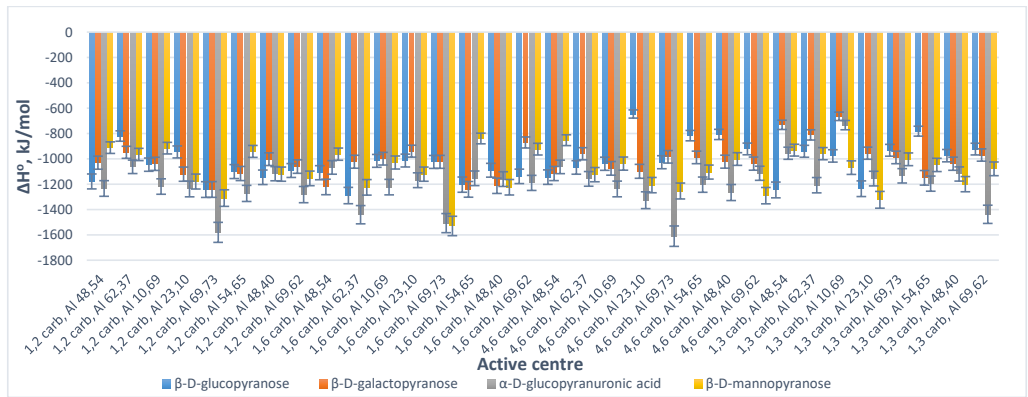
Figure S2. The optimized structure of the Keggin Al_{13}^{7+} complex with the hydrogen bond (marked with the dashed line).



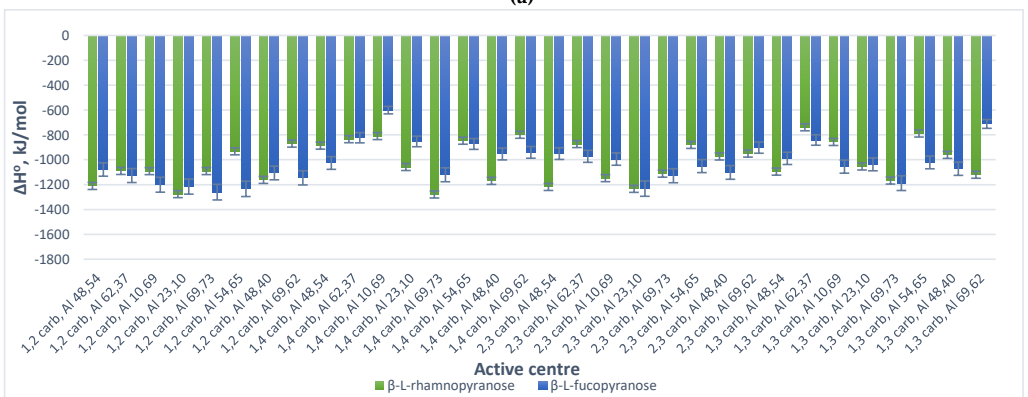


(d)

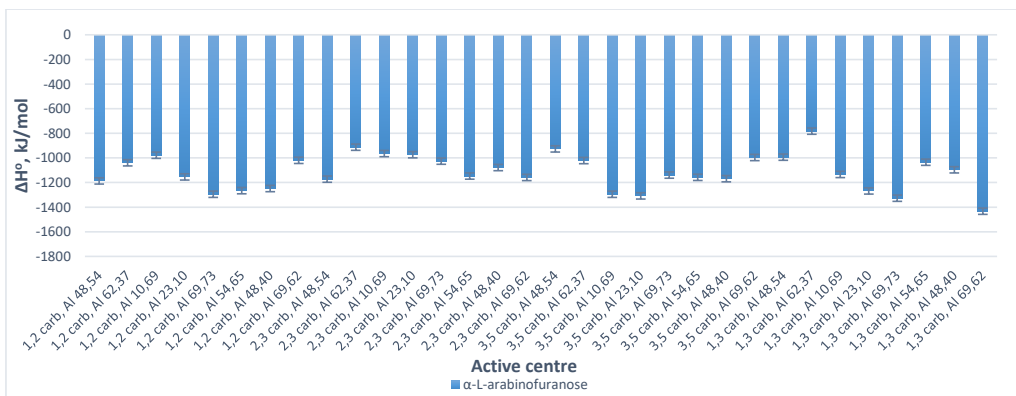
Figure S3. The development of the standard entropy change of formation of the Al_{13}^{3+} complex depending on the active centers of the solvated Al_{13}^{3+} complex and the monosaccharide for the double-O-ligand coordination of the following monosaccharides: (a) β -D-galactopyranose, α -D-glucopyranuronic acid, and β -D-mannopyranose; (b) β -L-rhamnopyranose and β -L-fucopyranose; (c) α -L-arabinofuranose; (d) β -D-glucosamine.



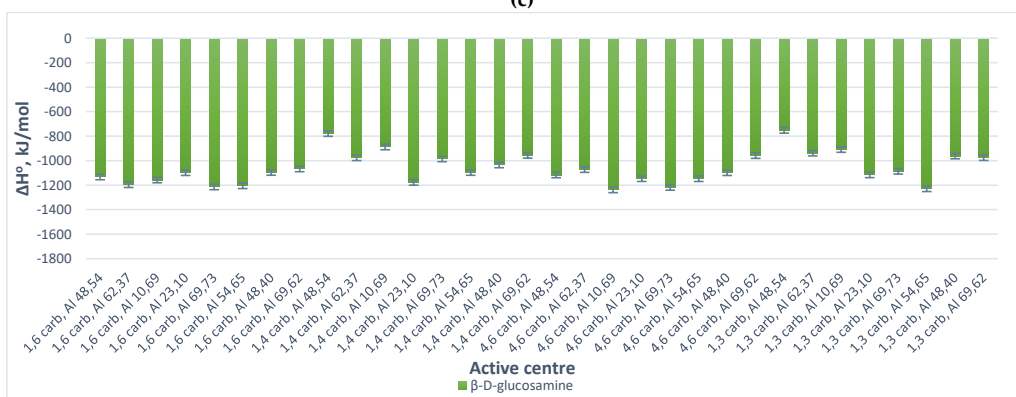
(a)



(b)



(c)



(d)

Figure S4. The development of the standard enthalpy change of formation of the Al_{13}^{2+} -monosaccharide complex depending on the active centers of the solvated Al_{13}^{2+} complex and the monosaccharide for the double-O-ligand coordination of the following monosaccharides: (a) β -D-glucopyranose, β -D-galactopyranose, α -D-glucopyranuronic acid, and β -D-mannopyranose; (b) β -L-rhamnopyranose and β -L-fucopyranose; (c) α -L-arabinofuranose; (d) β -D-glucosamine.

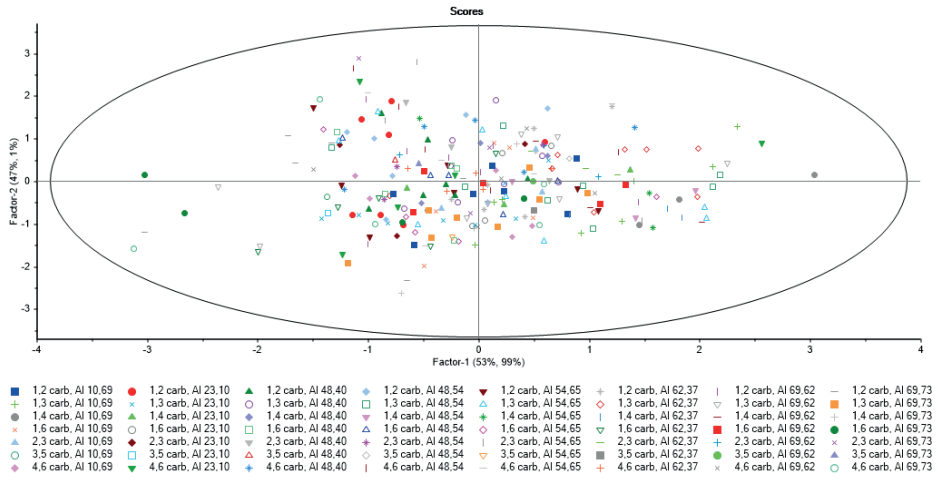


Figure S5. Scores plot with the sample grouping, computed from PLS. (Notes: “carb.” stands for carbohydrate.).

Errata list

PhD candidate: Olga Kulesha

Thesis: Flux Enhancers in Biofilm Membrane Bioreactors: Insight into Fouling Control

Date: 04.11.2019

Side	Line	Original text	Corrected text
xii	10	thermodynamically stable and lest stable	thermodynamically stable and less stable
6	4	are illustrated	is illustrated
20	12-13	a tool to data normalization	a tool for data normalization
23	9	uniformity parameter	the uniformity parameter
28	5-6	wastewater treatment plant	the wastewater treatment plant
29	14-15	while the proteins – the major component	while the proteins were found to be the major component
29	33	the majority of the identified proteins in the aerobic sludge has	the majority of the identified proteins in the aerobic sludge have
41	12	operational conditions in BF-MBR pilot system	operational conditions in the BF-MBR pilot system
41	15	fouling mitigation in BF-MBR system	fouling mitigation in the BF-MBR system
42	30-31	floc relative hydrophobicity (RH) parameter	the floc relative hydrophobicity (RH) parameter
47	18	don't comply	do not comply
61	12	might be the caused	might be caused
62	13	thermodynamically stable and lest stable	thermodynamically stable and less stable
74	8	to the machine learning	to machine learning
75	18-19	based on partial least squares-artificial neural network (PLS-ANN) hybrid model	based on the partial least squares-artificial neural network (PLS-ANN) hybrid model
75	20	has a potential	has the potential
76	16	strategies to fouling mitigation	strategies for fouling mitigation
77	10-11	in membrane separation part	in the membrane separation part
77	28	in BF-MBR system	in the BF-MBR system
78	25	Al ₁₃ ²⁺ complex	the Al ₁₃ ²⁺ complex
79	23	based on partial least squares-artificial neural network (PLS-ANN) hybrid model	based on the partial least squares-artificial neural network (PLS-ANN) hybrid model

ISBN: 978-82-575-1645-1
ISSN: 1894-6402



Norwegian University
of Life Sciences

Postboks 5003
NO-1432 Ås, Norway
+47 67 23 00 00
www.nmbu.no